Investigating the requirement of KRAS for the maintenance of pancreatic cancer

By

Pan-Yu Chen

B.A., Molecular Biology and Biochemistry
Wesleyan University, Middletown, Connecticut (2008)

Submitted to the Department of Biology in Partial Fulfillment of the Requirements for the Degree of
Doctor of Philosophy
at the Massachusetts Institute of Technology

June 2016

Signature of Author: Signature redacted

Department of Biology
May 20, 2016

Certified by: Signature redacted

Tyler Jacks
Professor of Biology
Thesis Supervisor

Accepted by: Signature redacted

Michael T. Hemann
Associate Professor of Biology
Co-Chair, Biology Graduate Committee

Investigating the requirement of KRAS for the maintenance of pancreatic cancer

By

Pan-Yu Chen

Submitted to the Department of Biology on May 20, 2016 in partial fulfillment of the requirements for the degree of Doctor of Philosophy

ABSTRACT

Pancreatic cancer, of which 85% is pancreatic ductal adenocarcinoma (PDAC), is the fourth leading cause of cancer death in the United States and a major cause of mortality and morbidity worldwide. Although recent advances in multi-agent chemotherapies have increased median survival in advanced disease, the 5-year survival rate for PDAC patients remains low at 7%, highlighting an urgent need for novel therapeutic options with improved efficacy and reduced toxicity.

Genomic studies have identified mutations in the proto-oncogene *KRAS* as a hallmark of PDAC, making KRAS an attractive therapeutic target. While the driver role of oncogenic KRAS for PDAC initiation has been well established, the degree of *KRAS* oncogene addiction in established PDAC tumors remains unclear. To facilitate the development of targeted therapies for PDAC, we sought to elucidate the requirement of endogenous KRAS for PDAC maintenance and potential resistance mechanisms that may arise in response to KRAS inhibition.

Since there is no effective pharmacological KRAS inhibitor to date, we interrogated the requirement of KRAS for PDAC cell survival using an inducible shRNA-based system that enables precise temporal control of endogenous *KRAS* expression. Surprisingly, the majority of PDAC cells analyzed tolerated acute and sustained Kras knockdown by adapting to a reversible cell state, characterized by differences in cell morphology, proliferative kinetics, and tumor-initiating capacity. While significant mutational or transcriptional changes were not observed in the KRAS-inhibited state, global phosphoproteomic profiling revealed alterations in cell signaling, including increased phosphorylation of focal adhesion pathway components. Accordingly, KRAS-inhibited cells displayed focal adhesion plaque formation, enhanced adherence properties, and increased dependency on adhesion for viability *in vitro*. Our analyses highlighted the possibility of adaptive non-genetic and non-transcriptional mechanisms of resistance to KRAS inhibition.

As most PDAC cells tolerated partial inhibition of KRAS, we explored whether the observed adaptive resistance can be overcome by CRISPR/Cas-mediated KRAS ablation. While *KRAS* knockout led to decreased *in vitro* proliferation and impaired *in vivo* tumorigenic growth, KRAS was dispensable in a subset of human and mouse PDAC cells. *KRAS* knockout cells exhibited a unique dependency on PI3K activation. Mechanistically, PI3K inhibition in *KRAS* knockout cells led to transient MAPK blockade while impeding AKT-dependent 4EBP1 phosphorylation and cap-dependent translation. Furthermore, comparison of gene expression

profiles of cells retaining or lacking KRAS revealed a novel functional role of KRAS in the suppression of metastasis-related genes.

Taken together, our data suggested that the majority of PDAC cells can tolerate sustained partial KRAS inhibition by adaptation and upregulation of focal adhesion signaling. Therefore, candidate targets from this pathway can provide a basis for rational design of combination therapeutic strategies with novel KRAS inhibitors. Importantly, KRAS is non-essential in at least a subset of human and murine PDAC cells, demonstrating the potential for resistance to even the very best of KRAS inhibitors. Finally, combination therapies with PI3K inhibitors may be a viable strategy to circumvent resistance to KRAS inhibition.

Thesis Supervisor: Tyler Jacks, Ph.D.
Title: Professor of Biology

ACKNOWLEDGEMENTS

I feel extremely fortunate for having received my graduate training in a stimulating and collegial environment at MIT. Looking back on the last six years, I am grateful not only for being able to learn from the best scientists, but also for having met the most amazing friends. The invaluable friendships I have formed here will be what I miss the most about Boston. Without the support and help from my generous mentors, talented colleagues and collaborators, and wonderful friends, this journey and the work in this thesis would not have been possible.

First and foremost, I would like to express my gratitude for my thesis advisor, Tyler Jacks. Thank you, Tyler, for training and believing in me through the twists and turns of my projects. I will always look up to you as a role model, both scientifically and as a person. The way you successfully lead an Institute, a lab, and a family, while genuinely caring for the people who work with you, never ceases to inspire me. Your integrity, rigor, generosity, and insight are qualities that I will strive to achieve throughout the rest of my career.

I would like to express my appreciation for my thesis committee members, Frank Gertler and Mike Hemann, for their academic guidance and support over the years. Frank, thank you for your enthusiasm in teaching me cell biology and thoroughly going through my data to help me move my projects forward. Mike, thank you for not only providing valuable scientific insights, but also guiding me in planning next steps and developing my career. Additionally, I would like to thank Kevin Haigis for generously agreeing to be on my thesis defense committee.

I would like to thank every single past and present member of the Jacks lab. I feel privileged to have worked with so many engaging, talented, collaborative, and fun scientists. Thank you for all the thoughtful discussions, constructive feedback, and technical assistance. All of you have mentored or helped me in some ways, which I am extremely grateful for. In particular, I would like to thank the post-docs and senior graduate students that helped me orient myself when I first joined the lab as a naïve graduate student:

...Thales, McFadden, and Wen, thank you for having trained me the basic techniques, given me the tools to explore different research projects, and encouraged me to succeed.

...Keara and Irene, you have trained me well in terms of being persistent when projects go in unexpected directions, as well as enhancing my alcohol consumption ability despite my genetic defects. I can always count on you for scientific and life advice, and for throwing awesome parties. Irene, thank you for encouraging me to pursue my goals and being a big sister to me.

Importantly, I have been very fortunate to work especially closely with several people:

...Mandar, I thought we became friends only because we had no one else to talk to in the annex when we started in lab, but you turned out to be such a patient mentor, caring friend, and a great collaborator. We are polar opposites in many ways, but we sure share the passion and curiosity for KRAS biology. I am grateful for your faith in me, and for having read every single word in this thesis.

...Kim Mercer, thank you for being so thoughtful, patient, and always encouraging me to have a positive outlook. I will miss all the group meeting grocery shopping trips we shared.

... Amy, thank you for being such a great baymate. Your passion for immunology is truly contagious. I will miss all of our snack breaks and strangely, all of our mouse infection and imaging sessions.

...Judy, you always manage to make me laugh even when I am stressed. Thank you for welcoming me to the lab from day one and being such an amazing friend over the last few years.

...Anne, thank you for welcoming me to MIT even before I joined the lab, and for being so caring and looking out for me as I am applying for jobs.

...Karen, Kate, and Margaret, thank you for being so dedicated and ensuring things run smoothly in lab. None of the research we do would be possible without your help.

I would also like to thank my fellow biograd friends, who have shared this journey with me:

...Peter, Monica, Daniel, Courtney, Mark, and Rini, who have been my buddies in the Koch. We've worked hard and had so much fun together. Especially Peter and Monica, who have been keeping me sane and taking care of me during the last month.

...Jess and Amaris, you know how important our margarita nights are to me. I will miss all the times you girls make me laugh, although more often you two are just laughing at me...

I am grateful for all my friends outside of the biology program for always being there for me:

...Erica, Jess, and Ceci, I feel so lucky that we got to be in Boston together for a few years. You girls were my family in Boston. I miss all the intellectual and silly conversations we've had over brunch and dinner. Erica, thank you for being there every time I needed a friend.

...Shu-Heng, Ann, Yuhan, Alice, and KC, thank you for exploring Boston with me. With you guys, this initially foreign city feels a lot more like home. Shu-Heng, I will miss running with you along the Charles River and learning about (but not understanding) string theory from you.

...Marcus and Sasha, you are the best dinner and shopping buddies. I will miss walking everywhere during the beautiful but short Boston summers with you guys.

...Michelle and George, my non-scientist friends who teach me all about literature and politics. I miss laughing about nothing with you guys and hope we can be in the same city again soon.

Last, but most certainly not least, I am grateful for my parents and little brother Ching-Yu, who have inspired me to be dedicated to whatever I do and to pursue my dreams. We are oceans apart, but you have never ceased to support and encourage me despite the distance. Even though you can hardly understand why I am still in school, this journey would not have been possible without your unconditional love and support.

TABLE OF CONTENTS

ABSTRACT **3**

ACKNOWLEDGEMENTS **5**

TABLE OF CONTENTS **7**

CHAPTER 1 INTRODUCTION **11**

1.1 An overview of RAS signaling and function **13**

1.1.1 The discovery of a mutant *RAS* as the first human oncogene 13

1.1.2 The RAS superfamily 15

1.1.3 The expression and structure of mammalian *Ras* genes 15

1.1.4 The biochemical properties and three-dimensional structure of RAS proteins 18

1.1.5 Post-translational modification and membrane localization of RAS proteins 22

1.1.6 Upstream regulators of RAS-mediated signal transduction 24

1.1.7 Downstream effector pathways regulated by RAS proteins 28

1.2 The role of oncogenic KRAS as a driver of pancreatic tumorigenesis **36**

1.2.1 Prevalence of oncogenic *RAS* mutations in human cancers 36

1.2.2 Activating *KRAS* mutations are the hallmark of pancreatic ductal adenocarcinoma 38

1.2.3 The spectrum of *KRAS* point mutations in PDAC 42

1.2.4 Ability of oncogenic *KRAS* to initiate transformation *in vitro* and *in vivo* 43

1.3 The requirement of oncogenic KRAS signaling for PDAC maintenance **47**

1.3.1 Oncogene addiction underlies the efficacy of molecularly targeted therapies 47

1.3.2 Early studies using non-RNAi-based approaches demonstrated the requirement of oncogenic RAS for tumor maintenance 48

1.3.3 RNAi-based studies demonstrated that human PDAC cell lines and tumors exhibit variable *KRAS* dependency 49

1.3.4 The requirement of oncogenic *Kras* for PDAC maintenance *in vivo* 52

1.3.5 Bypass mechanisms following *Kras* inhibition 55

1.4 Direct and indirect therapeutic targeting of KRAS in cancer 57

1.4.1 Direct inhibition of KRAS activity 58

1.4.2 Inhibition of downstream effector pathways of KRAS 70

1.4.3 Synthetic lethal targeting of oncogenic KRAS 78

1.5 Conclusions and aims 86

REFERENCES 88

CHAPTER 2 Adaptive and reversible resistance to Kras inhibition in pancreatic cancer cells 103

ABSTRACT 104

INTRODUCTION 105

RESULTS 107

Generation of a doxycycline-inducible shRNA *in vitro* system that enables the temporal control of endogenous *Kras* expression 107

Murine PDAC cells tolerate stable Kras knockdown *in vitro* and *in vivo* 108

Response to Kras knockdown is adaptive and reversible 112

Diminished *in vivo* tumor initiating capacity following stable Kras inhibition 116

The Kras-inhibited state does not display significant alterations in gene expression 119

Global phosphoproteomic profiling reveals enhanced focal adhesion signaling in the Kras-inhibited state 124

The Kras-inhibited state depends on cell attachment 128

Genetic or pharmacological inhibition of FAK does not impair survival of Kras-inhibited PDAC cells 131

DISCUSSION 131

SUPPLEMENTARY FIGURES AND TABLES **136**

MATERIALS AND METHODS **149**

ACKNOWLEDGEMENTS **164**

REFERENCES **165**

CHAPTER 3 Survival of pancreatic cancer cells lacking KRAS function **167**

ABSTRACT **168**

INTRODUCTION **169**

RESULTS **171**

KRAS is dispensable in a subset of PDAC cells 171

KRAS knockout cells exhibit PI3K pathway activation and dependence 178

Simultaneous MAPK and AKT blockade by PI3K inhibition in *KRAS* knockout cells 183

Identification of KRAS-regulated pathways in PDAC cells 188

KRAS-relevant signatures predict survival in PDAC patients 189

DISCUSSION **194**

SUPPLEMENTARY FIGURES AND TABLES **197**

MATERIALS AND METHODS **221**

ACKNOWLEDGEMENTS **233**

REFERENCES **234**

CHAPTER 4 CONCLUSIONS AND DISCUSSION **238**

4.1 Significant inhibition of KRAS may be required to impair PDAC cell survival **241**

4.2 Resistance mechanisms to KRAS inhibition are adaptive and reversible **249**

4.3 Emerging roles of oncogenic KRAS in PDAC progression and maintenance offer therapeutic opportunities **257**

REFERENCES **262**

APPENDIX 1 Investigating the synthetic lethal interaction between *Stk33* and oncogenic *Kras* **265**

ABSTRACT **266**

INTRODUCTION **267**

RESULTS **269**

Preliminary characterization of an $Stk33^{flox}$ allele 269

Alternatively spliced transcripts of *Stk33* are made upon Cre-mediated $Stk33^{fl}$ recombination 274

CRISPR/Cas9-mediated genome editing of *Stk33* in an autochthonous $Kras^{G12D}$-driven lung cancer mouse model 277

Isolation and characterization of 373T1 *Stk33* knockout single cell clones 279

373T1 *Stk33* knockout clones exhibited impaired ability to transplant lung tumors in immunocompromised mice 281

DISCUSSION **283**

SUPPLEMENTARY FIGURES AND TABLES **286**

MATERIALS AND METHODS **292**

ACKNOWLEDGEMENTS **297**

REFERENCES **298**

CHAPTER 1

INTRODUCTION

The discovery in 1982 that a somatic missense mutation conferred transforming ability to *RAS* has since then shaped our view of the molecular basis of cancer. Subsequent discoveries of additional proto-oncogenes and tumor suppressor genes whose functions are altered in human cancer have led to the current understanding that successive accumulation of genetic and epigenetic alterations, each conferring a unique proliferative, survival, invasive, or metabolic advantage to cancer cells, underlies the progression from normal tissue homeostasis to malignant phenotypes. While more than 500 cancer genes have been identified to date according to the Catalogue of Somatic Mutations in Cancer (COSMIC) database, *KRAS*, *HRAS*, and *NRAS* remain the most frequently mutated family of proto-oncogenes in human cancers. In particular, activating *KRAS* mutations are the most frequent and especially prevalent in some of the most lethal cancer types, including cancers of the pancreas, lung, and colon, making *KRAS* an attractive therapeutic target and its biology an intensive area of research. However, KRAS has been found to be an intractable drug target and much remains to be learned about its specific functions in tumor initiation, progression, and maintenance. The work presented in this thesis aimed to interrogate the requirement of *KRAS* for the maintenance of pancreatic ductal adenocarcinoma, as well as possible bypass mechanisms following *KRAS* inhibition in this disease. This chapter provides an overview of the current understanding of RAS signaling and function, the role of KRAS in tumor initiation and progression, and the efforts and challenges involved in the development of pharmacological inhibitors targeting KRAS for cancer therapies thus far.

1.1 An overview of RAS signaling and function

1.1.1 The discovery of a mutant *RAS* as the first human oncogene

When scientists met in London in 1958 to discuss the nature of cancer, their sentiments were reported as follows: "Some hoped that cancer can be eradicated without an understanding of its very nature; others felt that we must understand better the enigma of the cancer cell and even of life itself. If the somatic mutation theory of cancer is right, then development of cancer is an inherent property of life, and cancer research is but in its lusty infancy"[1]. This is a rather philosophical but accurate illustration of the nature of cancer. The challenge to fully understanding this disease lies in the ability to decipher the intricate regulatory mechanisms of tissue homeostasis, and how they go awry during malignant transformation. Similarly, in his Nobel lecture in 1966, Francis Peyton Rous described the biology of tumors as perplexing and daunting: "Tumors destroy man in a unique and appalling way, as flesh of his own flesh which has somehow been rendered proliferative, rampant, predatory, and ungovernable. They are the most concrete and formidable of human maladies, yet despite more than 70 years of experimental study they remain the least understood"[2]. After half a century, our understanding of the molecular basis of cancer has increased tremendously. Unfortunately, despite our rapidly expanding knowledge of the biology and vulnerabilities of cancer, the successful elimination of this complex disease remains an unresolved challenge.

Before the discovery of cellular oncogenes, cancer was once thought to be an infectious disease transmitted by tumor viruses. However, the inability to isolate tumor viruses in most human cancers as well as the accumulating experimental evidence supporting the notion that mutations in normal growth-controlling genes could be the underlying cause of cancer gradually made the link between genetic alterations and transformation a more favorable hypothesis[2-5].

While a subset of cancers, such as cervical and hepatocellular carcinomas, are associated with viral infections, cancer is now commonly viewed as a genetic disease that arises from cumulative acquisition of somatic mutations that alter or disrupt the function of proteins encoded by cellular proto-oncogenes or tumor suppressor genes.

Interestingly, the *Ras* oncogenes were first identified in the 1960s as the transforming principle of the Harvey and Kirsten strains of rat sarcoma viruses[6-8], hence they were named *Ras*. Transforming retroviruses like the Harvey and Kirsten sarcoma viruses are replication-defective, and contain exogenous genetic information transduced from a previous host genome that encodes proteins unnecessary for the viral life cycle but required for transformation. In 1982, research groups led by Robert Weinberg, Mariano Barbacid, and Michael Wigler independently discovered and successfully cloned the very first human oncogene from T24 and EJ human bladder carcinoma cell lines by serial transfection and transformation of NIH-3T3 mouse fibroblasts[9-11]. The identity of this human oncogene was soon unveiled by restriction endonuclease mapping and Southern blotting, which demonstrated homology between the cloned human oncogene and the *Ras* genes from the Harvey and Kirsten sarcoma viruses[12-14]. Further analysis by systematically substituting each restriction fragment from the non-transforming allele of *RAS* with the corresponding one from the transforming allele led to the surprising discovery that the two alleles only differed by a single amino acid change: G12V, or a glycine to valine mutation at position 12[15-17]. The isolation and characterization of the *RAS* oncogenes not only corroborated the cellular oncogene hypothesis, but also laid the foundation for rigorous research in how various genetic lesions contribute to the initiation and progression of cancer.

1.1.2 The RAS superfamily

RAS proteins are the founding members of the RAS superfamily of low molecular weight guanosine triphosphatases (GTPases). In human, the RAS superfamily comprises more than 150 RAS-like members, with evolutionarily conserved orthologues found in *Drosophila*, *C. elegans*, *S. cerevisiae*, *S. pombe*, *Dictyostelium*, and plants[18,19]. All members of this superfamily function as GDP/GTP-regulated molecular switches and share a set of conserved G box GDP/GTP-binding motif elements (G1 to G5)[20]. Interestingly, there is a large number of *RAS* superfamily pseudogenes in the human genome, for which it is unclear whether transcripts are made[18].

The RAS superfamily is divided into five major branches based on sequence and functional similarities: RAS, RHO, RAB, RAN, and ARF[18]. Members of the RAS subfamily have been the focus of intensive research since they are frequently mutated in human cancers. Members of the other subfamilies are 50% or less similar to *RAS* genes, with the highest level of conservation occurring at the protein level at the amino terminal and the CAAX (C: cysteine; A: aliphatic amino acid; X: any amino acid) domains[8]. Different subfamilies of the RAS superfamily are involved in distinct cellular processes. Whereas the RAS subfamily is known to regulate gene expression and cell proliferation, differentiation, and survival[18], the RHO subfamily is primarily known to regulate actin organization, cell cycle progression, and gene expression[21]. The RAB and ARF subfamilies are both regulators of intracellular vesicular transport[22,23]. The RAN subfamily is the most abundant small GTPase in the cell, and is best known for its function in nucleocytoplasmic transport of RNA and proteins[24].

1.1.3 The expression and structure of mammalian *Ras* genes

Ras genes are ubiquitously expressed in diverse eukaryotic organisms, including yeast, plants, insects, mollusks, birds, and mammals. Moreover, *Ras* genes are highly conserved across

species, suggesting that they are fundamentally important for key cellular functions[8]. Speaking to the degree of conservation of both the structure and biological functions of Ras, it has been shown that Ras can function in heterologous systems. The expression of an activated yeast *Ras* gene or a chimeric yeast-mammalian *Ras* can transform NIH-3T3 cells, and mammalian *Ras* expression can rescue the viability of mutant *ras1*$^{-}$ *ras2*$^{-}$ yeast cells[25,26]. Importantly, these are the first illustrations of the interchangeability of functional genes between yeast and mammalian cells.

Analysis of mammalian *Ras* gene expression indicates that they are expressed at low levels in most cell lineages, and are consistently expressed throughout mouse embryonic development[27]. Although increased levels of *Ras* expression have been reported in highly proliferative tissues such as the regenerating rat liver[28], other studies have observed higher levels of *Ras* expression in non-dividing tissues, including the rat brain or the mouse heart, compared to that of proliferating tissues[29,30]. Immunohistochemical survey of Ras expression in normal fetal and adult human tissues showed that Ras is expressed in all tissues, and is generally more highly expressed in undifferentiated than in differentiated cells[31]. However, certain terminally differentiated cells, including epithelial cells of the endocrine glands and neurons of the central nervous system, express high levels of Ras.

The mammalian genome contains three canonical and closely related *Ras* genes: *Hras*, *Kras*, and *Nras*[32]. The *H* and *K* nomenclatures correspond to Harvey and Kirsten, respectively, and *N* refers to neuroblastoma, in which *NRAS* was first identified[33,34]. These three genes reside on separate chromosomes, and encode four distinct but highly homologous 21kDa proteins: Hras, Nras, Kras4A, and Kras4B[35]. Kras4A and Kras4B result from alternative inclusion of exons 4A or 4B of *Kras*[36-38], with Kras4A being the most similar to the original retroviral Kras

and Kras4B being the predominant form expressed in most tissues and in human cells[39,40]. Mammalian *Ras* genes contain four coding exons and a 5' noncoding exon, termed exon 0, which is located immediately downstream of the promoter[36,37]. Interestingly, although their intron structures vary greatly, the splice junctions are highly conserved in all mammalian *Ras* genes, suggesting a common origin from one ancestral gene[8].

Expression analysis of the different *Ras* isoforms showed significant variations in spatial and temporal expressions. In adult mouse tissues, transcripts of all isoforms are detected in all tissues examined. However, *Hras* is most highly expressed in brain, skeletal muscle, and skin, while *Kras* is most highly expressed in the gut and thymus, and *Nras* is primarily expressed in the testis and thymus[41]. Overall, all isoforms are expressed at very low levels in the liver[41]. Furthermore, differential levels of expression have been observed for individual isoforms during mouse embryonic development. For instance, even though there is ubiquitous expression of all isoforms in the embryo throughout prenatal development, *Hras* expression remains relatively high and constant, while *Kras* expression starts to drop towards the end of gestation[27]. Differences in isoform expression suggest that the three Ras isoforms may perform distinct tissue-specific functions. Interestingly, mouse knockout studies revealed a unique requirement for *Kras* but not for *Hras* or *Nras* during embryonic development[42-45]. Whereas *Nras*$^{-/-}$, *Hras*$^{-/-}$, and *Nras*$^{-/-}$;*Hras*$^{-/-}$ mice lack any obvious phenotype, *Kras* knockout is embryonic lethal. *Kras*$^{-/-}$ mouse embryos die between E12 and E14, with fetal liver defects and evidence of anemia[43]. Taken together, these knockout mouse studies suggest that intact wild-type Kras function is uniquely indispensible and sufficient for embryonic development.

The primary structure of mammalian Ras proteins is classically defined to consist of four domains. The first domain encompasses the first 85 amino acid residues, which is identical

between all Ras proteins in human and rodents[8]. The next 80 amino acid residues comprise the second domain, which exhibits 85% homology between the human RAS proteins. The rest of the protein except for the last four amino acid residues is considered the third domain, also known as the hypervariable domain, which is the region of the greatest sequence divergence. Finally, the fourth domain consists of the very last four amino acid residues at the carboxyl terminal, and is a conserved CAAX motif found in all members of the Ras and Ras-related proteins[8,38]. The hypervariable region and CAAX motif are critical determinants of Ras localization and biological activity.

1.1.4 The biochemical properties and three-dimensional structure of RAS proteins

As early as 1979, protein products of the *v-Ras* oncogenes derived from retroviral RNA had been reported to have high affinity for guanine-containing nucleotides[46]. Additionally, the association of v-Ras with the inner side of the plasma membrane appeared to be required for its transforming ability[47,48]. These initial observations provided important insights into the possible function and localization of RAS proteins before molecular cloning of *RAS* became available. Large-scale expression of RAS proteins in biochemical assays verified the GTPase activity of RAS proteins, whose enzymatic activity is greatly reduced in the proteins encoded by their transforming alleles[49-51]. Furthermore, certain domains of RAS proteins exhibit significant sequence homology with the alpha subunit of G proteins and the bacterial elongation factor Tu (EF-Tu), which are GTPases[52]. Taken together, these observations suggest that RAS proteins are GTPases and mediators of signal transduction across the plasma membrane. It is now well understood that the primary biochemical activities of RAS proteins are the binding of guanine nucleotides and the hydrolysis of GTP to GDP. The relevance of these activities to their biological function had been demonstrated in various earlier studies: microinjection of antibodies

that inhibit guanine nucleotide binding of RAS reverts the oncogenic *RAS*-transformed phenotypes of NIH-3T3 cells[53,54]; RAS mutants that fail to bind guanine nucleotides do not transform NIH-3T3 cells[55]; and the GTPase activity of RAS is severely impaired in proteins encoded by the transforming alleles[49-51]. This section describes the basic biochemical properties and three-dimensional structure of RAS proteins, and how oncogenic mutations of *RAS* alter the biochemical properties and three-dimensional structures of RAS proteins.

The GTPase cycle of RAS proteins

Like other GTPases, RAS proteins function as conserved molecular switches in cells by cycling between the active GTP-bound state and the inactive GDP-bound state in a tightly regulated fashion[20]. The GTPase cycle generally involves three major conformational states. Release of the bound GDP converts the RAS inactive state into a transient empty state. When the intracellular level of GTP is higher than that of GDP, GTP preferentially enters the empty guanine nucleotide binding site and this binding converts RAS into an active conformation. Hydrolysis of this GTP molecule to GDP in turn reverts RAS back to its inactive state[20]. The effects of RAS proteins depend on the concentration of GTP-bound RAS. In unstimulated cells, the majority of RAS is inactive and GDP-bound, suggesting that the GTPase rate is faster than the guanine nucleotide exchange rate. However, upon stimulation by growth factors or other perturbations, GTP-bound RAS accumulates above the basal level[56]. Since the intrinsic rates of GDP release and GTP hydrolysis for RAS are rather inefficient (a dissociation constant of $\sim 10^{-11}$ M for guanine nucleotide binding and a GTP hydrolysis turnover rate of ~2 mmol/min/mol)[56], these processes are facilitated by two classes of regulatory proteins. The guanine nucleotide exchange factors (GEFs) catalyze the release of bound GDP to promote its replacement by GTP. On the other hand, GTPase-activating proteins (GAPs) speed up GTP hydrolysis, which is the

irreversible step in the GTPase cycle. Importantly, escape from this GAP-mediated hydrolysis step, resulting in inhibition of the GTPase activity of RAS, is the primary mechanism by which oncogenic forms of RAS become constitutively active[8,56].

The Switch I and Switch II regions are responsible for RAS conformational change and effector binding

The hydrophobic core of RAS protein comprises six β-sheets, which are connected by hydrophilic loops and α-helices. Five regions of the polypeptide chain, designated G1 to G5, are associated with loops on one side of the protein and are critical in GDP/GTP exchange, GTP-induced conformational change, and GTP hydrolysis[20]. Crystal structures of GDP-bound RAS and GTP-bound RAS complexes revealed prominent GTP-induced changes in two regions of the RAS protein: the G-2 loop (residues 32-38) and the G-3 loop together with the α2 helix just downstream (residues 60-76)[20]. These two regions are also known respectively as the Switch I and Switch II regions. They undergo dramatic structural changes dependent on the type of guanine nucleotide that is bound. Importantly, the Switch I region overlaps with the effector region (residues 32-40) that forms an interaction surface for effector molecules to bind when RAS is GTP-bound[57]. Moreover, the effector loop can determine the specificity of effector binding to a given GTPase.

Activating mutations alter critical biochemical properties of RAS proteins

A combination of mutagenesis studies, crystallography analysis, and comparison with related proteins with known functions and structures elucidated the RAS functional domains important for their biochemical properties and shed light on how a single point mutation of *RAS* confers its protein product oncogenic abilities. Some of the first RAS mutations identified in animal tumors occur at glycine 12, glycine 13, alanine 59, glutamine 61, and lysine 117[56], with

mutations at codons 12, 13, and 61 being the most common and thus are viewed as the canonical activating mutations. These mutations are referred to as activating because they result in oncogenic RAS activities. Mutagenesis studies demonstrated that mutations at positions 12, 13, 59, 61, and 63 result in impaired GTPase activity. On the other hand, mutations at positions 16, 17, 116, 117, 119, 144, and 146 lead to increased guanine nucleotide exchange rates[56]. More recently, previously uncharacterized and non-canonical *RAS* mutations have been identified in human colorectal tumor and leukemia cell lines as well as patient samples[58,59]. Moreover, certain *RAS* mutations appear to be associated with differential therapeutic response[60]. The specific functional alterations of individual oncogenic *RAS* variants and their roles in mediating tumor initiation and progression and response to therapies remain to be elucidated.

The guanine nucleotide binding domain of RAS has been identified to lie in regions encompassing amino acid residues 5-22 and 109-120, based on sequence homology with G proteins and EF-Tu as well as the ability of antibodies directed against these regions to inhibit GTP binding[53,54,61]. Combining analyses of the X-ray crystallography of the GDP binding domain of EF-Tu and sequence homology between EF-Tu and Ras, it has been determined that glycine 12 of mammalian RAS proteins should be located in the phosphoryl binding loop[8,61]. Thus, replacement of glycine 12 with an alternative amino acid with a bulky or charged side chain may create a protein that cannot efficiently interact with the phosphoryl region of the GTP molecule, compromising the GTPase activity of RAS proteins. Moreover, oncogenic substitutions in residues 12 or 13 prevent the proper insertion of the catalytic arginine finger of GAP into a position near the β- and γ-phosphates of GTP through steric hindrance, resulting in accumulation of GTP-bound RAS and subsequently constitutive downstream signaling[35,62,63].

The RAS protein domain encompassing residues 59-63 does not exhibit homology to other guanine nucleotide binding proteins. However, mutations at positions 59, 61, and 63 lead to impaired GTPase activity[56]. Examination of the three-dimensional structure of the active site residues revealed that the side chain of glutamine 61 is positioned to activate the water molecule that is responsible for the nucleophilic attack on the γ-phosphate of GTP during the hydrolysis reaction[56,64,65]. Substitution of glutamine 61 by alternative amino acids impairs activation of the water molecule required for GTP hydrolysis, which similarly results in accumulation of GTP-bound RAS and constitutive activation of downstream effector pathways.

1.1.5 Post-translational modification and membrane localization of RAS proteins

In order for RAS to mediate signaling and carry out its full biological functions, it must associate with the cytoplasmic surface of cellular membranes[48,66]. For a long time, the inner surface of the plasma membrane has been considered to be a unique platform for RAS and RAS-related proteins to assemble signaling complexes and regulate signaling events. Recently, however, characterizations of endosomes derived from the plasma membrane, the Golgi apparatus, and endoplasmic reticulum as platforms for RAS signaling are beginning to emerge[67]. Nevertheless, the best-characterized pathways that activate RAS signaling to date are those mediated by receptor tyrosine kinases (RTKs) that span the plasma membrane and sense extracellular stimuli.

RAS proteins are initially synthesized as cytosolic and inactive precursor proteins and are required to undergo a series of post-translational modifications to attain full biological activity. The CAAX motif is necessary and sufficient to signal three sequential steps of modifications that increase the hydrophobicity of RAS, facilitating the association of RAS with cellular membranes[40]. First, farnesyltransferase (FTase) mediates the covalent addition of a 15-carbon

farnesyl isoprenoid to the cysteine residue (cysteine 186) in the CAAX motif. Next, RAS-converting enzyme 1 (RCE1) catalyzes the proteolytic removal of the AAX peptide of the CAAX domain. Finally, isoprenylcysteine methyltransferase (ICMT) catalyzes the carboxylmethylation of the now terminal farnesylated cysteine[40,63]. These modifications, however, target RAS proteins to the endoplasmic reticulum (ER) but are insufficient to promote RAS trafficking to and association with the plasma membrane. A second membrane-targeting element located in the C-terminal hypervariable region is required for plasma membrane localization[40]. In KRAS4B, this second membrane-targeting element is a polybasic amino acid stretch (lysine residues 175-180), which stabilizes the interaction between KRAS4B and the negatively charged phospholipid head groups[68]. In contrast, in HRAS, NRAS, and KRAS4A, the second membrane-targeting element comprises cysteine residues just upstream of the farnesylated C-terminal cysteine: cysteines 181 and 184 in HRAS, and cysteine 181 in NRAS and KRAS4A[69]. These cysteine residues undergo reversible palmitoyl acyltransferase (PAT)-mediated acylation and acyl-protein thioesterase (APT)-mediated deacylation, which adds or removes a 16-carbon palmitate, respectively. This additional modification stabilizes the interaction of RAS with the plasma membrane. After palmitoylation at the ER, HRAS, NRAS, and KRAS4A can be trafficked through the classical secretory pathway via the vesicles budded from the Golgi to the plasma membrane[69,70]. KRAS4B, on the other hand, bypasses the Golgi and reaches the plasma membrane by a poorly understood mechanism, possibly diffusion or microtubule-dependent transport.

Both the amino acid sequence of the hypervariable region and post-translational modification-dependent intracellular trafficking determine the differential localizations of the different RAS isoforms, which provide an additional layer of regulation of the biological

activities of RAS. The reversible palmitoylation modification, which has a very short half-life (20-60 minutes) compared to the half-life of RAS proteins (>20 hours), allows shuttling of RAS to distinct cellular compartments[71]. For example, monopalmitoylation on cysteine 181 of HRAS is necessary and sufficient for localization to the plasma membrane, whereas monopalmitoylation on cysteine 184 confines HRAS to the Golgi[72]. Furthermore, the palmityolated and polybasic-targeted RAS isoforms are directed to different microdomains within the plasma membrane, where they form nanoclusters with components of specific effector cascades to facilitate signaling[73]. The palmitoylation of HRAS preferentially targets it to cholesterol-rich microdomains, such as the lipid rafts and caveolae, thus rendering HRAS-dependent signaling sensitive to perturbations of membrane cholesterol[74]. In contrast, KRAS is normally localized outside of lipid rafts. The polybasic domain of KRAS4B confers a unique capacity for this isoform to aggregate the anionic lipid phosphatidylinositol-4,5-bisphosphate, which is a substrate for PI3K[75]. Additionally, protein kinase C-mediated phosphorylation of S181 in the polybasic region has been shown to promote localization to the mitochondria, consequently triggering apoptosis due to association of KRAS with BCL-X_L[76]. In summary, post-translational modification-regulated subcellular localization of the different RAS isoforms is in a constant state of spatiotemporal flux, and such differences in localization underlie the isoform-specific functional outputs of RAS signaling.

1.1.6 Upstream regulators of RAS-mediated signal transduction

Other than activating mutations in RAS itself, alterations in the upstream regulators of RAS can also result in constitutive activation of RAS. Hence, the major regulators of RAS GTPase cycle, GEFs and GAPs, can be putative proto-oncogenes and tumor suppressor genes, respectively. A third class of regulators of the RAS GTPase cycle is guanine nucleotide

dissociation inhibitors (GDIs), which act as negative regulators of RAS activity by inhibiting GEFs[77]. However, they may be more critical in regulating RAS-related proteins RAB and RHO, and their direct involvement in regulating RAS activity is less studied than that of GEFs and GAPs. Biochemical studies in mammalian cells and genetic studies in *S. cerevisiae*, *C. elegans*, and *D. melanogaster* have demonstrated remarkably conserved signal transduction pathways mediated by functionally conserved components[77]. It is now well established that RAS proteins are critical mediators of mitogenic signals transmitted from stimulated receptor and non-receptor tyrosine kinases and G protein-coupled receptors. Examples of upstream regulators of RAS proteins are provided below.

Guanine nucleotide exchange factors (GEFs)

The rapid and transient elevation of RAS-GTP levels following ligand stimulation of cell surface receptors is facilitated by GEFs. Three main classes of RAS-GEFs are currently known: SOS, RAS-GRF, and RAS-GRP. They share a common CDC25 homology catalytic domain and an N-terminal RAS exchange motif[63]. Among these RAS-GEFs, the best characterized are SOS1 and SOS2. They were first identified as mammalian homologues of proteins encoded by *Drosophila* Son of sevenless, a genetically identified RAS activator[68,78]. In addition to the SOS homology domain, each SOS protein also contains a DB1 homology (DH) domain that mediates the guanine nucleotide exchange, as well as a pleckstrin homology (PH) domain responsible for membrane localization[63]. In resting cells, SOS mostly associates with the SRC homology 3 (SH3, binds proline-rich motifs) domains of the GRB2 adaptor protein in the cytoplasm. Activation of receptor tyrosine kinases (RTKs), such as the epidermal growth factor receptor (EGFR), allows binding of the dimerized and autophosphorylated RTKs to the SRC homology 2 (SH2, binds tyrosine-phosphorylated sites) domains of GRB2 and possibly SHC, an adaptor

protein that has an SH2 domain and can be tyrosine-phosphorylated[63,68,77,79]. This interaction thereby recruits GRB2-SOS to the plasma membrane, where RAS is located, allowing SOS-facilitated nucleotide exchange on RAS and thus RAS activation. It is important to note that the above model is a simplified view of the regulation of GEF-mediated RAS activation. Other non-receptor proteins can become tyrosine phosphorylated and act as anchors for GRB2 interaction as well, and RAS-GEFs other than SOS can be regulated differently[80-82].

GTPase-activating proteins (GAPs)

GAPs limit RAS signaling by rapidly inactivating RAS post-stimulation and can accelerate the rate of intrinsic RAS GTP hydrolysis by approximately 100,000-fold[83]. Several GAPs have been identified, including $p120^{GAP}$, NF1, GAP1m, GAPIII, and CAPRI[32,63]. $p120^{GAP}$ was identified both as the first RAS-GAP and the first protein found to interact with the effector domain of RAS[84]. In addition to a catalytic domain that binds the RAS effector domain, $p120^{GAP}$ also harbors N-terminal SH2, SH3, and PH domains, as well as calcium-dependent phospholipid-binding motifs (CaLB)[63]. The N-terminal is thought to regulate the catalytic activity and interact with putative RAS downstream effectors. An alternative splicing event generates a smaller variant of $p120^{GAP}$, $p100^{GAP}$, which is only expressed in the placenta and lacks the N-terminal hydrophobic sequences. The functions of $p100^{GAP}$ are unknown. In contrast to GEFs, the precise mechanism that regulates GAPs is less well understood. The importance of GAPs is highlighted by the discovery that tumor suppressor gene neurofibromatosis type I (*NF1*) exhibits sequence similarity to $p120^{GAP}$ and encodes a neurofibromin protein that negatively regulates RAS proteins with GAP activity[85-88]. Patients with germline *NF1* defects have an increased incidence of neural crest-derived tumors and sporadic neuroblastomas and melanomas, consistent with inherent tumor suppressive function of GAPs through inactivation of RAS.

Indeed, malignant tumor cell lines derived from patients with type 1 neurobiromatosis showed reduced total GAP activity and hyperactive RAS signaling[89,90]. Furthermore, somatic loss of neurofibromin expression by mutation, deletion, or by other means occurs in 14% of glioblastoma, 13-14% of melanoma, 8-10% of lung adenocarcinoma, and at single digit frequency in many other cancers[91]. These observations demonstrate that neurofibromin is a major tumor suppressor in human cancers.

Extracellular growth factors, cell surface receptors, and non-receptor tyrosine kinases

Upstream of the GEFs and GAPs, a diverse set of extracellular growth factors is known to activate RAS. Examples of such factors include those that stimulate the growth of fibroblasts (such as EGF and PDGF) or hematopoietic cells (such as IL-2 and GM-CSF)[77]. These factors are sensed by RTKs or cell surface receptors associated with non-receptor tyrosine kinases. Examples of upstream regulators include growth factor receptors, G protein-coupled receptors, and focal adhesion molecules, among others[68,77]. The first suggestion that mitogenic signals may regulate RAS activity was made by the observation that epidermal growth factor (EGF) stimulated GTP binding to RAS proteins in serum-starved *HRAS*-transformed rat kidney cells[92]. This connection between mitogenic signals and RAS activity was further solidified by subsequent studies demonstrating that microinjection of a monoclonal antibody against RAS blocked serum-induced DNA synthesis[93], and that RAS activity was required for transformation induced by membrane associated tyrosine kinase- or growth factor receptor-derived oncogenes (such as *SRC* and *FMS*) but not for transformation induced by cytoplasmic serine/threonine kinase-derived oncogenes (such as *RAF*)[94]. These studies provided the first evidence supporting RAS as a critical intermediate that transmits extracellular signals to the nucleus, elicits effector pathway activation, and ultimately regulates the activities of nuclear transcription factors.

Unsurprisingly, RAS signaling is commonly activated in tumors harboring mutations in growth factor RTKs. A classic example is the frequent activation of EGFR and ERBB2 by overexpression in various cancers, including breast, ovarian, and stomach carcinomas[68]. Furthermore, *EGFR* mutation resulting in the expression of a truncated receptor that lacks part of the extracellular domain can be constitutively associated with adaptor proteins SHC and GRB2, which can recruit and activate RAS[95]. This mutation is found in a significant proportion of glioblastomas. In summary, aberrant RAS signaling can result from alterations in the functions of RAS upstream regulators, which can contribute to oncogenesis.

1.1.7 Downstream effector pathways regulated by RAS proteins

RAS proteins regulate diverse cellular signaling pathways responsible for proliferation, migration, adhesion, cytoskeletal integrity, survival, and differentiation. Upon extracellular ligand-induced activation of upstream receptors and/or receptor-associated tyrosine kinases, RAS becomes activated and subsequently triggers effector signaling cascades. RAS facilitates effector translocation to the plasma membrane, where additional steps are required for full activation of effector interaction. The cellular functional outputs of RAS signaling are dependent on both the specific cell type in which RAS is activated and the specific effector pathways being activated. As discussed previously, the interaction between RAS and its effectors is largely dependent on the subcellular localization of RAS. At least eleven RAS effector pathways have been identified to date[40,63], but this list is by no means exhaustive. Examples of mammalian RAS effectors include RAF, PI3K, RalGDS, $p120^{GAP}$, Rin1 Abl-interacting protein, and serine/threonine kinase PKCζ[96]. Among the many effector pathways, the most widely studied and thoroughly characterized are the RAF/MAPK (mitogen-activated protein kinase, also known as ERK, extracellular signal regulated kinase) and the PI3K (phosphatidylinositol 3-kinase)

pathways, because components of these two pathways are also frequently mutationally activated in human cancer.

In theory, a RAS effector is defined as a protein with strong preferential binding to the GTP-bound form of RAS and whose binding is impaired by mutations in the core effector domain[97]. However, these biochemical properties alone do not fully validate the protein as a RAS effector. For full validation, interaction between endogenous RAS with the full-length effector must be demonstrated, the function of the effector protein should be modulated by the interaction with RAS, and the biological activity of RAS should be modulated by the effector[97]. Verified and putative RAS effectors are characterized by a RAS-binding domain (RBD), which is an approximately 100 amino acids sequence. So far, three distinct RBD sequences have been identified: the RBD of RAF or Tiam1; the RBD of PI3K; and the Ras association (RA) domains originally identified in RalGDS and are found in the majority of RAS effectors[97]. Importantly, not all RA-containing proteins are RAS effectors, as some bind to RAS-related proteins instead.

Interestingly, different RAS isoforms activate different effectors with varying potencies. For instance, KRAS4B has been shown to be the most potent activator of C-RAF, followed by KRAS4A, then NRAS, and finally HRAS[98]. In contrast, HRAS was identified to be a more potent activator of the PI3K pathway than KRAS[99]. Isoform-specific interaction with effectors and how such differences underlie distinct biological functions of individual isoforms remain to be elucidated. The best-characterized effector pathways of RAS are described below.

The RAF/MAPK pathway

The first mammalian RAS effector to be identified and the most intensively studied is the serine/threonine kinase RAF. The name *RAF* derives from the initial discovery that this oncogene acquired by the murine retrovirus 3611-MSV induced rapidly growing fibrosarcoma in

mice[100], hence the cellular homologue was named *c-RAF1*. Two related *RAF* genes, *ARAF* and *BRAF*, were subsequently cloned, with *BRAF* being the founder of this gene family[63]. Several observations identified RAF as a direct downstream target of RAS: 1) activated RAS can result in hyperphosphorylation of RAF in the absence of mitogenic stimuli[101]; 2) a dominant-negative RAF blocked both the transforming activity of oncogenic RAS and transcription activation from RAS response elements[102,103]; and 3) a dominant-negative RAS blocked the ability of activated RTKs to activate RAF[104]. GTP-bound RAS recruits RAF to the plasma membrane, which is essential for RAF activation[105,106]. Activated RAF in turn phosphorylates and activates mitogen-activated protein kinases 1 and 2 (MEK1 and MEK2), which are dual-specificity kinases that phosphorylate and activate the mitogen-activated protein kinases ERK1 and ERK2. More than 200 cytosolic and nuclear substrates have been identified for ERK1 and ERK2[40], reflecting the fact that they can be transported into the nucleus following activation[68]. In general, active ERK phosphorylates serine or threonine residues within the Ser/Thr-Pro motif in many cytoplasmic and nuclear proteins[107]. Cytoplasmic substrates of ERK include kinases (such as p90 ribosomal S6 kinase), apoptotic regulators (such as BIM), and cytoskeletal proteins (such as paxillin). Understanding the full range of effects of ERK activation is still an active area of research, with particular interests in the regulation of transcription factors in the nucleus, including the ETS family transcription factors and AP-1. Through transcriptional regulation, MAPK activation increases expression of cell cycle regulatory proteins, such as D-type cyclins, enabling the cell to progress through the G1 phase of the cell cycle[108]. This widely accepted illustration of MAPK signaling may seem linear at first, but it is now well established that the RAF-MEK-ERK cascade is at the center of a complex signaling network that dynamically regulates ERK activity. The ability of MAPK pathway signaling to control proliferation contributes to the fact that this

pathway is deregulated in approximately one-third of all human cancers, making these kinases attractive therapeutic targets.

A complex network of negative-feedback interactions is known to limit ERK activation. Negative-feedback regulation is mainly mediated through direct phosphorylation of almost all components of the RTK-RAS-MAPK cascade by ERK, including EGFR, SOS1, NF1 (to promote NF1 stability in this case), and CRAF[107]. Surprisingly, activated ERK phosphorylates CRAF at multiple residues, and some lead to decreased CRAF kinase activity while others lead to increased CRAF activation. This suggests that the degree of ERK activation may dictate the predominant effect of feedback regulation on CRAF kinase activity[107]. Additionally, activated ERK induces the expression of genes that inhibit MAPK pathway activation, including dual-specificity phosphatases (DUSPs) and Sprouty (SPRY)[109,110]. ERK induces transcriptional activation of multiple DUSPs, but DUSPs dephosphorylate ERK to limit ERK activation. An additional layer of reciprocal regulation involves ERK phosphorylation of DUSP1 to induce its degradation. On the other hand, SPRY proteins act as negative-feedback regulators of ERK signaling by inhibiting the activation of RAS by multiple RTKs[111]. Phosphorylation on a conserved N-terminal tyrosine residue of SPRY serves as a docking site for GRB2 to impair RAS activation. Moreover, SPRED, a member of the SPRY family, has been shown to recruit NF1 to the plasma membrane, leading to RAS inactivation[112]. All in all, the regulation of the RAF/MAPK signaling cascade is extremely dynamic and complex, and the positive and negative effects of inhibiting components of this pathway need to be thoroughly assessed for such inhibition to be therapeutically beneficial.

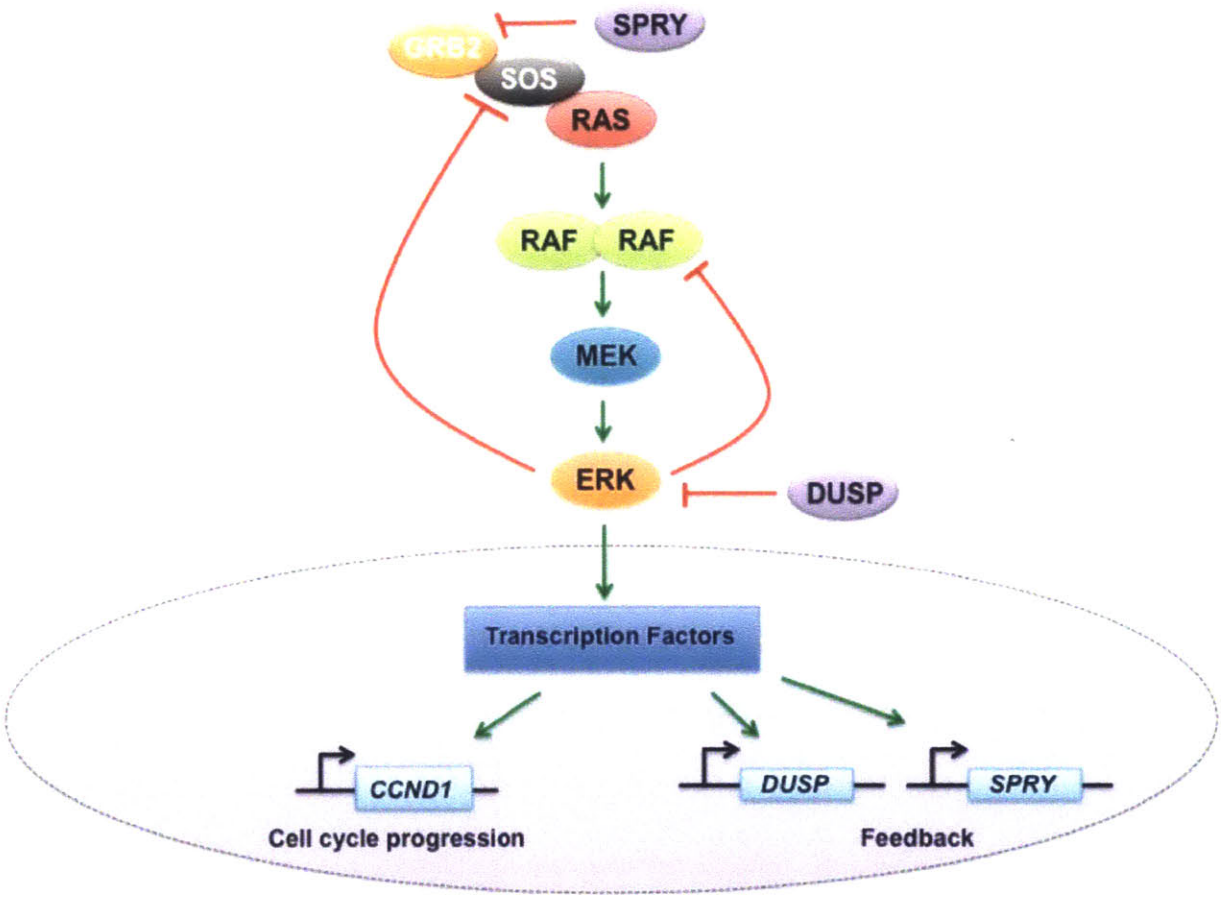

Figure 1. A simplified schematic of the RAS-RAF-MEK-ERK signaling axis.

The PI3K pathway

The second best-validated mammalian RAS effector is the p110 catalytic subunits (α-, γ-, and δ-subunits) of class I PI3K[40]. In its active form, PI3K is composed of a regulatory p85 subunit and a catalytic p110 subunit. The first evidence of direct activation of PI3K catalytic subunit by RAS was demonstrated by: a significant increase in PI3K activity bound to beads coupled to immobilized GTP-bound RAS proteins compared to that of GDP-bound RAS proteins; a dominant-negative RAS inhibits accumulation of phosphatidylinositol 3' phosphorylated lipids; and RAS overexpression elevates phosphorylated lipid levels[113]. PI3K phosphorylates phosphatidylinositol-4,5-biphosphate (PtdIns(4,5)P_2) to produce phosphatidylinositol-3,4,5-triphosphate (PtdIns(3,4,5)P_3), which is a second messenger that binds to a large number of proteins through PH and other domains. Like MAPK, PI3K controls the activity of a large number of downstream enzymes, with phosphatidylinositol-dependent kinase 1 (PDK1) being the most well studied one. PtdIns(3,4,5)P_3 recruits PDK1 and AKT (also known as PKB) to the plasma membrane, where PDK1 phosphorylates and activates AKT. AKT isoforms are implicated in modulating apoptosis and proliferation[40,68], which may be critical for the pro-survival effects observed in cancer cells harboring activating *RAS* mutations. AKT is thought to promote cell survival by phosphorylating MDM2, a negative regulator of p53, and by negatively regulating the pro-apoptotic BCL-2 family members BAD and BAX, as well as forkhead transcription factors, such as FOXO[114]. Importantly, AKT also negatively regulates TSC1 and TSC2 to activate mTORC1, a key regulator of cellular growth and protein synthesis. mTORC1 stimulates S6 kinase activity, which has multiple substrates, including the ribosomal protein S6. In addition, mTORC1 phosphorylates 4E-BP1, which releases the eukaryotic initiation factor 4E (eIF4E) to permit assembly of the cap-binding complex, initiating translation of specific

mRNAs[114]. Furthermore, PI3K activation leads to stimulation of RAC, which is a RHO family protein that is involved in regulating the actin cytoskeleton and NFκB activation. The frequent mutational activation of *PIK3CA* (mutated in 12% of human tumors), which encodes p110α, and inactivation of the phosphatase and tensin homologue (*PTEN*, now considered the second most commonly mutated tumor suppressor after p53), which catalyzes the removal of the D3 phosphate from PtdIns(3,4,5)P_3 to terminate downstream signaling, supports a critical role of PI3K in malignant transformation[40,68].

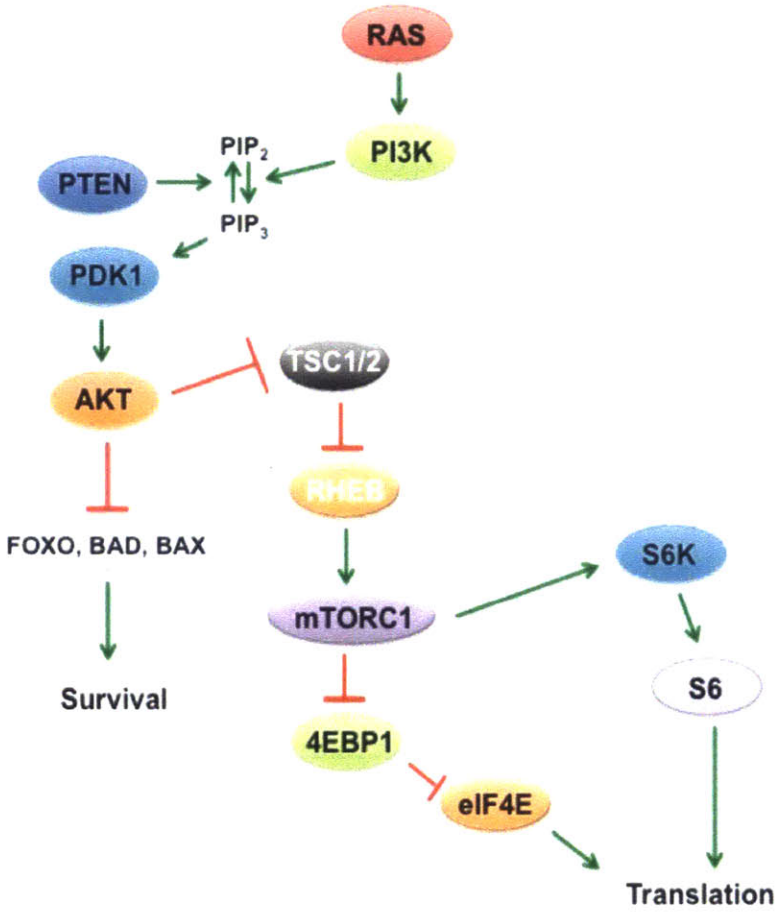

Figure 2. A simplified schematic of the RAS-PI3K-AKT signaling axis.

The RalGDS pathway

The third best-validated RAS effector is RalGDS (Ral guanine nucleotide dissociation stimulator), which is a RAS-like GTPase. RalGDS serves as a link that allows RAS to stimulate RALA and RALB GTPases, resulting in activation of phospholipase D1 and the CDC42/RAC-GAP-RAL binding protein 1 (RALBP1). RalGDS is a member of the highly related mammalian RalGEF protein family. Other RalGEFs that are also identified as Ras effectors are RGL, RGL2, and RGL3. The RalGDS pathway contributes, in conjunction with AKT, to the inhibition of the forkhead transcription factors of the FOXO family, which are thought to promote cell cycle arrest and apoptosis[68]. To date, there has been no report of RalGEF or RAL mutations in human tumors[97]. However, RGL2 expression has been found in *KRAS*-mutant colorectal cancer cell lines, and RNAi-mediated suppression of RGL2 in pancreatic cancer cell lines reduces anchorage-independent growth and matrigel invasion *in vitro*[40,115]. Interestingly, RALA and RALB may have distinct roles in cancer. RALA but not RALB appears to be necessary for anchorage-independent growth of human pancreatic cancer cell lines, whereas RALB is required for invasion *in vitro* and metastasis *in vivo*[116]. Overall, the connection between RalGDS and human cancer is not well understood. Moreover, RalGDS is considered an intractable drug target like RAS itself, and thus this pathway is not as amenable as the MAPK and PI3K pathways are for cancer drug target discovery.

1.2 The role of oncogenic KRAS as a driver of pancreatic tumorigenesis

1.2.1 Prevalence of oncogenic *RAS* mutations in human cancers

Approximately 30% of all human tumors harbor activating *RAS* mutations, with *KRAS* mutations being the most frequent (about 85% of total), followed by *NRAS* mutations (about 15% of total) and then *HRAS* mutations (less than 1% of total)[68]. *KRAS* mutations are most

prevalent in pancreatic, colorectal, and lung (mostly in non-small cell lung cancer) cancers, whereas *NRAS* mutations are common in hematopoietic malignancies and melanoma, and *HRAS* mutations are frequently associated with tumors of the bladder and of the head and neck[35,117]. In particular, activating *KRAS* mutations are found in more than 90% of human pancreatic ductal adenocarcinoma, in almost 50% of colorectal adenocarcinoma, and approximately 30% of lung adenocarcinoma[40], which are three of the most lethal cancers in the United States.

Evidently, the mutational frequency of individual *RAS* isoforms varies greatly in the different cancer types. The underlying rationale for why activation of specific RAS isoforms associates with cancers originating from distinct tissue types remains to be resolved. Interestingly, it has been suggested that oncogenic *KRAS* may confer unique stem-like properties to endodermal cell lineages whereas oncogenic *HRAS* promotes differentiation and growth arrest[118], which partially explains the difference between the isoform-specific mutational frequencies in different types of cancer. Another intriguing mechanism that may underlie the isoform-specific differences is that *KRAS* favors the usage of rare codons and thus is poorly translated, which allows more efficient oncogenesis by preventing oncogene-induced senescence[119].

Despite its lower prevalence in human cancer compared to the other *RAS* isoforms, *HRAS* has been the most intensively studied *RAS* isoform historically. This is due to the availability of laboratory reagents to study *HRAS* and the earlier assumption that the functions of different RAS isoforms are largely equivalent in normal cellular and disease contexts. However, it is now well established that there are important isoform-specific functional differences between the individual isoforms in both development and cancer. Given the high prevalence of activating *KRAS* mutations in human cancer, much of the research focus has shifted to *KRAS*. For the

scope of this thesis, the discussion here places a special emphasis on the role of *KRAS* in pancreatic ductal adenocarcinoma.

1.2.2 Activating *KRAS* mutations are the hallmark of pancreatic ductal adenocarcinoma

Pancreatic ductal adenocarcinoma (PDAC) is a devastating disease that is highly invasive and extremely refractory to current standard of care therapeutic options. The worldwide incidence of all types of pancreatic cancer, of which 85% are PDAC, ranges from 1 to 10 cases per 100,000 people, with higher incidence in developed countries and among men[120]. In the United States, 53,070 new pancreatic cancer cases and 41,780 pancreatic cancer-associated deaths are estimated to occur in 2016, making it the fourth leading cause of cancer deaths in this country[121]. The risk factors of this disease include smoking, diabetes, chronic pancreatitis, and obesity. Approximately 10% of pancreatic cancers are due to inherited predispositions with germline mutations in *CDKN2A*, *BRCA2*, *LKB1*, and *MLH1*, but these predispositions have a low penetrance[120,122], suggesting that these mutations may be more critical for malignant progression than disease initiation. Despite recent advances in multi-agent chemotherapies, the 5-year survival rate for PDAC patients remains low at 7%[121]. The poor prognosis for this disease is in part due to the lack of specific symptoms and reliable detection tools for asymptomatic premalignant or early malignant tumors, resulting in clinical presentation of predominantly late-stage disease, which is not surgically resectable in most patients. However, even for the small percentage of patients diagnosed with local disease (15-20%), the 5-year survival rate is only 25-30%[121]. Approximately 70% of all deaths result from extensive metastatic disease. Currently, surgical resection is the only potentially curative therapy for pancreatic cancer. The standard of care for metastatic pancreatic cancer is multi-agent chemotherapy regimens, including FOLFIRINOX (combination of fluorouracil, irinotecan, oxaliplatin, and leucovorin) and

gemcitabine plus albumin-bound paclitaxel particles (nab-paclitaxel)[120]. While combination chemotherapies increase median survival by several months (5 months for FOLFIRINOX and 2 months for gemcitabine plus nab-paclitaxel) compared to single agent gemcitabine treatment, they show limited long-term survival benefit[123,124]. Collectively, the statistics presented here underscore an urgent need for developing novel therapeutic strategies with improved efficacy and reduced toxicity for this disease.

The key genetic alterations in PDAC appear to occur in a temporal sequence and associate with the defined histopathological progression from precursor lesions to invasive PDAC, but how these alterations mechanistically contribute to disease progression remain to be determined. Moreover, the presence of these genetic alterations is not correlated with the acquisition of specific histopathological features. PDAC is generally thought to arise from pancreatic ductal epithelial cells, although the precise cell of origin of this disease is still an outstanding question. The best-characterized precursor lesions of PDAC, pancreatic intraepithelial neoplasias (PanINs), are neoplastic growths that originate from intralobular ducts and progress with increasing degrees of architectural and nuclear atypia in a stepwise manner from low-grade to high-grade in types 1, 2, and 3 (also referred to as PanIN-1A, PanIN-1B, PanIN-2, and PanIN-3)[122,125]. PanINs are frequently associated with acinar-to-ductal metaplasia (ADM) structures that are thought to be precursors of PanIN lesions. Advancing PanIN stages correlate with an increase in cell proliferation rates as well as the accumulation of genetic lesions, and advanced PanINs eventually progress to form PDAC. This disease progression model has been corroborated by mutation profiling of PanINs and associated PDACs, which exhibit similar mutation patterns[126-128]. Two other types of ductal preneoplastic lesions that might be precursors for PDAC are intraductal papillary mucinous neoplasms (IPMNs),

originating from the main pancreatic duct, and mucinous cystic neoplasms (MCN), which are mucin-producing epithelial neoplasms with an ovarian-type stroma[125].

KRAS activation is thought to be both the earliest and the initiating genetic alteration in pancreatic cancer. It is considered to be the defining feature of this disease. Activating *KRAS* mutations are the first genetic changes that are detected, occurring occasionally in histologically normal pancreas and in 30% of the earliest neoplasias[122]. Moreover, the frequency of *KRAS* mutations increases with disease progression, and is nearly 100% in human PDACs[129,130]. The reason for the increasing frequency that correlates with disease progression is not yet clear. It is possible that *KRAS* mutations, being the initiating event, occur in 100% of early lesions, but diagnostic technology at the time is not sensitive enough to reliably detect all mutations. As described in the previous section, constitutive *KRAS* activation is postulated to induce an array of cellular effects, such as increased proliferation, survival, and invasion, through activation of effector pathways. The roles of specific *KRAS* effector pathways in PDAC tumorigenesis and progression are not yet elucidated. It has been suggested that $p21^{WAF1/CIP1}$ can be coordinately induced with the onset of *KRAS* mutations, likely through activation of the MAPK pathway[131]. Additionally, there may be an important contribution of autocrine EGF signaling starting at early stages of pancreatic neoplasia. First of all, EGF-family ligands (such as EGF and transforming growth factor alpha, TGF-α) and EGFR are overexpressed in human pancreatic cancer tumor samples and cell lines[132-134]. Secondly, EGF-family receptors (such as EGFR and ERBB2) are overexpressed in low-grade PanINs[135]. Third, functional importance of this pathway is illustrated by the growth inhibition of PDAC cell line xenografts following EGFR signaling inhibition[136-138]. Additionally, the combination of gemcitabine with EGFR inhibitor erlotinib was superior to gemcitabine alone in terms of overall survival by ~10 days in advanced PDAC

patients, and patients who exhibited a pharmacodynamics effect of EGFR inhibition (i.e. rash) also showed the best survival[139]. It is hypothesized that this EGF autocrine loop and the resulting PI3K activation are required for transformation mediated by oncogenic *KRAS*, as EGFR loss prevents *Kras*-induced PanIN formation in mice[140,141]. However, many pathways possibly contribute to the *KRAS*-mediated tumorigenesis, and a deeper understanding of which pathways are the most critical in PDAC initiation and progression will be essential for developing better and hopefully more targeted therapies for this disease.

Other than activating *KRAS* mutations, deletion, mutation, or epigenetic inactivation of *CDKN2A* (which encodes two tumor suppressors, INK4A and ARF, via distinct first exons and alternative reading frames), *TP53*, and *SMAD4* tumor suppressors are detected with increasing frequency in type 2 and type 3 PanINs, suggesting that subsequent inactivation of these tumor suppressors contribute to the progression of neoplastic transformation[120,122,125]. *CDKN2A* inactivation is observed in 30-70% of PanIN lesions, and up to 95% in full-blown PDAC. *TP53* and *SMAD4* mutations, on the other hand, are associated with the progression of type 3 PanIN lesions to invasive PDAC tumors in 50-75% of the cases. Mutations of *BRCA2* are found in less than 10% of pancreatic cancers and more frequently in familial cases. Inactivating mutations in transforming growth factor TGF-β receptors I and II are found with low frequency. Additional alterations frequently found in higher grade PanINs and PDAC include overexpression of growth factors and growth factor receptors, and activation of signaling pathways driven by NFκB, STAT3, and SRC[125]. The complexity of the PDAC mutational landscape is evident from exome sequencing analysis of human PDAC samples, which demonstrated that PDAC tumors harbor up to 50 mutations involving at least 12 distinct core signaling pathways[129].

Beyond mutational events, PDAC genome is often characterized by diverse, large-scale chromosomal changes, including amplifications, deletions, and rearrangements[122]. Telomere shortening in PDAC is thought to be responsible for inducing genomic instability[125]. Additionally, recent exome sequencing studies have identified additional loss-of-function mutations encoding components of the SWI/SNF nucleosome-remodeling complex, which were detected in approximately 10-15% of PDAC[142]. Whole genome sequencing and copy number variation analysis of 100 human PDAC samples verified near ubiquitous activating *KRAS* mutations (mostly missense single nucleotide variants, some amplifications, some structural variants, and a few had combinations of the above), as well as >50% inactivating mutational frequencies of *CDKN2A*, *TP53*, and *SMAD4*[130]. These recent sequencing studies confirmed that despite the complexity of the PDAC genome, the most frequently mutated genes in PDAC have already been identified, and aberrant KRAS function remains to be the key feature and is likely a critical target for this disease.

1.2.3 The spectrum of *KRAS* point mutations in PDAC

The frequency of specific *KRAS* activating mutations that occur is crucial to understand for developing targeted therapeutic strategies for PDAC. Similar to how different *RAS* isoforms are not functionally equivalent in human cancer, distinct point mutations also occur at varying frequencies in different cancer types and may have important functional differences. A study that curated the COSMIC database and surveyed the types of *RAS* mutations in cancer by large-scale tumor profiling revealed isoform-specific codon and point mutation biases[117]. Across cancers, 80% of *KRAS* mutations occurred at codon 12, whereas very few mutations were observed at codon 61. In contrast, nearly 60% of *NRAS* mutations occurred at codon 61, while 35% occurred at codon 12. *HRAS*, on the other hand, displayed approximately a 50% to 40%

split between mutations at codons 12 and 61. Furthermore, 43% of *KRAS* mutations were G12D or G13D, and G12V accounted for the bulk of the remaining mutations. Interestingly, a special case was observed in lung cancer, in which G12C predominated. Part of this mutational bias could be explained by the source of mutagen, DNA primary sequence, and three-dimensional structural effects. For example, the G12C mutation in lung cancer is thought to be a hallmark of exposure to tobacco smoke[91]. Among the 2,661 PDAC tumors surveyed[117], 1,312 tumors harbored the *KRAS* G12D mutation, followed by 812 tumors with G12V mutation, 312 tumors with G12R mutation, and fewer than 100 tumors harboring each of the G12C, G12S, or G12A mutations. A very small number of PDAC tumors harbored the rare G13D and Q61H mutations. In summary, G12D and G12V are the predominant mutations in PDAC, which is important for the design of mutant-specific inhibitors for this disease.

1.2.4 Ability of oncogenic *KRAS* to initiate transformation *in vitro* and *in vivo*

KRAS mutations typically occur early in tumor progression, suggesting that they have a critical role in tumor initiation. While ectopic expression of *RAS* oncogenes readily transformed immortalized fibroblasts *in vitro*, expression of additional oncogenes, such as *MYC* or adenovirus *E1A*, were required to successfully transform primary cells and circumvent oncogene-induced premature senescence[143-146]. In contrast to the effect of ectopic *RAS* overexpression, endogenous levels of $Kras^{G12D}$ expression led to partial transformation of primary murine embryonic fibroblasts *in vitro* without triggering p19ARF/p53-mediated growth arrest or apoptosis[146]. This finding highlighted the sensitivity of cells to the level of oncogene expression, and underscored the importance of expressing oncogenes at physiological levels to study cancer cell biology in a clinically relevant setting. On the other hand, results from numerous *in vivo* studies strongly suggested that oncogenic *KRAS* is a driver of tumor initiation and progression[40]. Additionally,

mouse models of different cancer types have demonstrated that loss of tumor suppressor function, such as p53, Lkb1 or APC, could enhance and accelerate progression of oncogenic *Kras*-driven tumors[147-149]. Collectively, these observations suggested that additional genetic lesions are necessary to cooperate with oncogenic *KRAS* to result in full malignant transformation, as cancer is a multi-step process that requires successive protein function-altering events for initiation and progression.

Previous work in our lab using genetically engineered mouse models has demonstrated the tumor-initiating ability of activating *Kras* mutations *in vivo*. Somatic activation of $Kras^{G12D}$ via spontaneous recombination (using $Kras^{LA1}$ and $Kras^{LA2}$, or latent alleles of $Kras^{G12D}$) in the whole animal has been shown to lead to a range of tumor types in adult mice, including lung tumors, thymic lymphoma, and skin papilloma[150]. While all of the mice developed multiple early onset lung tumors, metastases from the lung to the thoracic lymph nodes and kidney were only infrequently observed in older mice. Additionally, many mice had multiple aberrant crypt foci (ACF) of the colon, which are often found in patients with colon cancer. Importantly, some lung tumors and thymic lymphomas from these mice displayed a greater than 1-to-1 ratio of mutant-to-wild-type *Kras* alleles, indicating amplification of mutant *Kras* or loss of wild-type *Kras* alleles. This observation, along with a separate study that showed that heterozygous loss of wild-type *Kras* predisposed mice to chemically induced (by urethane or N-methyl-N-nitrosourea) lung cancer[151], suggested that while activated Kras is tumorigenic, wild-type Kras may actually be tumor suppressive. Furthermore, cooperation between inactivation of *p53* and $Kras^{LA}$ led to a broader tumor spectrum and decreased survival[150]. Overall, analysis of the $Kras^{LA}$ mice demonstrated that somatic activation of *Kras* alone is sufficient to initiate neoplastic progression, which can be enhanced by additional genetic alterations. Additional studies restricting $Kras^{G12D}$

expression to the mouse lung supported the tumorigenic ability of mutant *Kras in vivo*, and inactivated or mutant forms of *p53* further promoted the progression to more advanced lung tumors and metastases[152,153]. Similarly, in the mouse colonic epithelium, $Kras^{G12D}$ expression alone was also sufficient to initiate hyperplastic growth[147]. However, it is thought that oncogenic *Kras* may play a bigger role in accelerating tumor progression in the colon, as APC inactivation typically precedes Kras activation in human colon cancer.

In the pancreas, expression of mutant *Kras* from the endogenous locus or a transgene has exhibited oncogenic ability in various PDAC mouse models. The cell of origin for PDAC is not well defined due to possible transdifferentiation and cell plasticity that occur during the tumorigenic process. Therefore, mouse models for PDAC were engineered to restrict mutant *Kras* expression to different pancreatic cell lineages via distinct pancreas-specific promoters, the most commonly used ones being *Pdx1*, *Ptf1a* (or *p48*), and *Elastase*[125]. Both *Pdx1* and *p48* are expressed in pancreatic progenitor cells during embryonic development, so they target multiple pancreatic cell lineages, including acinar, centroacinar, ductal, and endocrine cells[125]. Whereas *Pdx1* is expressed around E8.5, *p48* is expressed slightly later and is required to commit cells to a pancreatic fate[154]. On the other hand, *Elastase* expression is limited to acinar cells[125]. In these mouse models, mutant *Kras* expression could initiate PanINs, which then spontaneously progressed to PDAC with long latency and at low frequency. Interestingly, acinar-cell specific $Kras^{G12V}$ expression induced development of PanIN lesions with similar latencies and penetrance to mice expressing the $Kras^{G12D}$ oncogene in all pancreatic cell lineages, suggesting that the cell of origin might be an acinar cell or an acinar precursor[155]. Importantly, the ability of mutant *Kras* to initiate transformation was highly context-dependent[125,156]. Specifically, expression of mutant *Kras* in the embryo and younger mice or in multiple pancreatic cell lineages via *Pdx1* or

p48 promoters invariably led to neoplastic development[125,154,156,157]. However, mutant *Kras* expression in older animals or expression restricted to a single cell type (such as acinar cells via the *Elastase* promoter or islet cells via the rat insulin promoter) was insufficient to induce transformation unless chronic pancreatitis was induced[125,155,156,158]. These observations suggested that cell plasticity, which might be diminished in older animals, might be essential for PanINs and PDAC initiation and progression. It is possible that inflammation and tissue damage can alter the fate of differentiated cells that are normally refractory to oncogenic stimulation.

Similar to what has been observed in mouse models of other cancer types, additional genetic alterations could enhance the ability of mutant *Kras* to initiate transformation as well as accelerate malignant progression. When Kras was activated in conjunction with the loss of tumor suppressor function, such as that of p53, Smad4, or Ink4a/Arf, the requirement for pancreatitis to induce neoplastic growth in adult animals could be bypassed[148,156,159,160]. Moreover, loss of tumor suppressor function accelerated the progression to high-grade PanINs, invasive PDAC, and metastases. In particular, two inducible $Kras^{G12D}$ transgenic models exhibited a requirement for additional genetic events to facilitate disease progression. Inducible expression of $Kras^{G12D}$ from an artificial transgene in the pancreas was sufficient to induce acinar-ductal metaplasia (ADM, the replacement of pancreatic acinar cells with duct-like structures) and low-grade PanINs in adult mice (4-6 weeks of age) within one week of induction, and prolonged $Kras^{G12D}$ expression (23 weeks) led to PanINs of different grades and occasionally adenocarcinomas[161]. Transgenic $Kras^{G12D}$ expression combined with cerulein-induced pancreatitis accelerated the appearance of PanINs in this model. Inactivation of tumor suppressor p53 was required for the development of full-blown invasive PDAC. The second inducible transgenic $Kras^{G12D}$ expression mouse model reported similar results, in which the

induction of *Kras*^{G12D} transgene led to infrequent occurrence of invasive PDAC after long latency (35-70 weeks) but cooperation with complete inactivation of p53 (*p53*$^{-/-}$) led to rapid progression to PDAC[157]. These results supported the notion that oncogenic *Kras* alone inefficiently drives PDAC. It has been postulated that the loss of tumor suppressor function enhances mutant *Kras*-driven PDAC initiation and progression because of increased chromosomal instability, which can facilitate the amplification of mutant *Kras* and acquisition of additional alterations, as well as inactivation of the cellular senescence pathway that may be induced by oncogene expression[148,159].

1.3 The requirement of oncogenic KRAS signaling for PDAC maintenance

1.3.1 Oncogene addiction underlies the efficacy of molecularly targeted therapies

As driver genetic alterations and key signaling pathway aberrations in different types of cancers are being characterized, a shift away from conventional chemotherapies towards molecularly targeted therapies has emerged. It is thought that molecularly targeted therapies, which selectively inhibit key oncogenes required for initiating and maintaining the proliferation and survival of cancer cells, can achieve higher efficacy and lower toxicity than conventional chemotherapies for cancer treatment. A partial list of successful molecularly targeted therapies in the clinic include the BRAF^{V600E} inhibitors (vemurafenib and dabrafenib) for the treatment of late-stage melanoma, BCR-ABL inhibitors (imatinib and dasatinib) for the treatment of chronic myeloid leukemia (CML), and mutant EGFR inhibitors (erlotinib, gefitinib, and afatinib) for the treatment of non-small cell lung cancer (NSCLC). The efficacy of these targeted therapies is dependent on oncogene addiction, which is the phenomenon that despite the accumulation of multiple genetic alterations, cancer cells remain sensitive to the inhibition of a single driver oncogene[162,163]. On average, established human tumors harbor 30-60 protein function-altering

mutations, with highly mutagenic cancers such as melanoma harboring nearly 200 protein function-altering mutations per tumor[162,164]. Therefore, it is critical to identify the key oncogenic alteration necessary for tumor maintenance in order to devise an effective therapeutic strategy. This section describes research studies to date that aimed to elucidate whether cancer cells exhibit *KRAS* oncogene addiction and the possible bypass mechanisms that may arise following *KRAS* inhibition.

1.3.2 Early studies using non-RNAi-based approaches demonstrated the requirement of oncogenic RAS for tumor maintenance

Unlike its well-established role in tumor initiation, the absolute requirement of oncogenic *KRAS* for tumor maintenance has been a longstanding question in the field. Activating *KRAS* mutations typically occur as an early event in tumor development, and cancer cells continue to acquire additional genetic and epigenetic alterations as well as respond to microenvironmental factors during cancer progression. Therefore, whether targeting KRAS is a useful therapeutic approach in late stage tumors and what aspects of the malignant phenotype are promoted by oncogenic KRAS remain unresolved.

Given the lack of suitable RAS inhibitors for analyzing the requirement of oncogenic *RAS* for cancer cell viability, early evidence for the requirement of oncogenic RAS function for tumor maintenance has come from studies of a mouse model harboring doxycycline-inducible transgenes of mutant *Ras*. In a mouse model using doxycycline-inducible mutant $Hras^{G12V}$ transgene that induced melanomas in an *INK4a*-null background[165], withdrawal of $Hras^{G12V}$ expression resulted in clinical and histological regression of primary and explanted tumors, whereas re-expression of $Hras^{G12V}$ led to recurrence of tumors at previous tumor sites. Moreover, marked apoptosis was observed in explanted tumor cells and host-derived endothelial

cells upon $Hras^{G12V}$ withdrawal, suggesting that $Hras^{G12V}$ is required not only for tumor cell survival but also for angiogenic support. Similarly, in a doxycycline-inducible $Kras4b^{G12D}$ transgenic mouse model of lung adenocarcinoma, removal of mutant *Kras* expression led to apoptotic regression of lung tumors in the absence or presence of tumor suppressor genes[166]. Additional evidence has come from the use of *in vitro* homologous recombination to specifically disrupt the expression of the oncogenic *KRAS* allele in two human colorectal carcinoma cell lines, DLD-1 and HCT116 (DLD-1 harbors one $KRAS^{G13D}$ allele, one wild-type *KRAS* allele, and point mutant $p53^{S241F}$; HCT116 harbors a $KRAS^{G13D}$ allele and mutations in *DCC* tumor suppressor gene)[167]. Disruption of oncogenic KRAS function in both cell lines led to impaired anchorage-independent growth and tumorigenic growth in nude mice. These initial studies supported the functional importance of oncogenic RAS in tumor maintenance.

1.3.3 RNAi-based studies demonstrated that human PDAC cell lines and tumors exhibit variable *KRAS* dependency

As it became feasible to stably knockdown the expression of endogenous genes in mammalian cells with RNA interference (RNAi), several research groups sought to interrogate the requirement of endogenous *KRAS* expression for maintaining cancer cell proliferation and survival by leveraging this tool[168-171]. Agami and colleagues selectively suppressed the expression of $KRAS^{G12V}$ in a human pancreatic cancer cell line, Capan-1 (harbors two $KRAS^{G12V}$ alleles), with retrovirus-based RNAi[171]. This study demonstrated that while stable $KRAS^{G12V}$ knockdown did not affect Capan-1 proliferation in standard adherent tissue culture conditions, it led to impaired anchorage-independent growth and tumorigenic ability in nude mice. Adrienne Cox and colleagues adopted this retrovirus-based $KRAS^{G12V}$-specific RNAi system and made it into an inducible system to analyze the effect of mutant *KRAS* knockdown that mimicked *KRAS*

inhibition in established tumors more closely[169]. They observed that both anchorage-dependent and anchorage-independent growth were impaired in Capan-1 cells upon $KRAS^{G12V}$ knockdown, underscoring the importance of selecting an appropriate system that accurately recapitulates the therapeutic setting in order to thoroughly understand oncogenic KRAS function. The discrepancy between the effects of stable versus inducible $KRAS^{G12V}$ knockdown on adherent growth might have been caused by massive cell death or growth arrest upon the loss of oncogenic *KRAS* expression, and the subsequent selection for subpopulations of cells that could overcome the loss of mutant KRAS function in the stable knockdown condition. Similarly, a more recent study using an encapsulated RNAi delivery system achieved mutant-specific knockdown of *KRAS* and subsequently increased survival by delaying the growth of established Panc-1 (harbors $KRAS^{G12D}$) and Capan-1 xenograft tumors as well as syngeneic mouse transplant tumors[172]. Finally, in a separate study, a thorough analysis was done on the molecular consequences of mutant-specific *KRAS* knockdown in human pancreatic cancer cell lines, Panc-1 and MiaPaca-2 (harbors $KRAS^{G12C}$)[170]. Interestingly, while *KRAS* knockdown consistently impaired proliferation, migration, and angiogenic potential *in vitro* between the two cell lines, only MiaPaca-2 showed an increase in apoptosis. Taken together, RNAi-mediated *KRAS* knockdown studies in a limited number of human pancreatic cancer cell lines confirmed the functional importance of activated KRAS in supporting the proliferation and survival of PDAC cells. However, it is difficult to understand the generalizability of the observed effects without expanding these analyses to a larger panel of cell lines harboring distinct mutant *KRAS* alleles and diverse genomic backgrounds.

In order to eliminate cell line-specific and mutant-specific effects in clarifying whether human cancer cells exhibit oncogenic *KRAS* addiction, Jeff Settleman and colleagues

interrogated the requirement of *KRAS* expression for maintaining the viability of an expanded panel of human *KRAS* mutant pancreatic and lung adenocarcinoma cell lines[168]. In this study, *KRAS* dependency for each cell line was determined quantitatively by assessing cell viability before and after acute short hairpin RNA (shRNA)-mediated *KRAS* knockdown. RAS dependency indices (RDIs) were calculated as the inverse of the relative cell densities following *KRAS* ablation, thus a greater RDI correlated with a higher *KRAS* dependency for a given cell line. Importantly, induction of apoptosis was specifically seen in cell lines demonstrating RDIs greater than 2.0, which was therefore defined as the "dependency threshold". Based on this definition, human cancer cell lines were classified as *KRAS*-dependent or *KRAS*-independent. Whereas *KRAS*-dependent cells exhibited decreased viability and induction of apoptosis upon *KRAS* knockdown, *KRAS*-independent lines did not. This finding has important clinical implications, as it suggested that KRAS-directed therapies may be more effective for certain patients while other patients may show limited response. Additionally, *KRAS* dependency appeared to correlate with an increase in *KRAS* copy number due to focal amplification, which could potentially serve as a biomarker to predict therapeutic response. Furthermore, morphological and gene expression analyses of *KRAS*-dependent and *KRAS*-independent cells revealed that *KRAS*-dependent cells associated with an epithelial differentiation state, whereas *KRAS*-independent cells might have undergone epithelial-mesenchymal transition (EMT), suggesting a possible mechanism of resistance to *KRAS* inhibition.

Consistent with the above observations that human cancer cell lines exhibit variable dependency on *KRAS* for survival, whole exome and genome sequencing studies of human PDAC tumors have revealed that PDAC is indeed an extremely heterogeneous disease with diverse molecular subtypes[129,142,173,174]. A detailed classification of the different molecular

subtypes of human PDAC was performed by Joe Gray and colleagues[173]. In this study, gene expression profiling of 63 PDAC tumor samples allowed the stratification of these samples into three distinct subtypes: classical, quasimesenchymal, and exocrine-like. In accordance with human cell line analysis reported by Settleman's group, the classical subtype exhibited high expression of adhesion-associated and epithelial genes and was highly dependent on *KRAS* expression for survival. In contrast, the quasimesenchymal subtype showed high expression of mesenchyme-associated genes and was less sensitive to *KRAS* knockdown. Collectively, human PDAC cell line and tumor studies revealed a high level of genetic heterogeneity and consequently variability for *KRAS* dependency, suggesting that oncogenic KRAS signaling is essential for at least a subset but not all of PDAC tumors.

1.3.4 The requirement of oncogenic *Kras* for PDAC maintenance *in vivo*

Recently developed mouse models that allowed pancreas-specific doxycycline-inducible expression of an oncogenic $Kras^{G12D}$ transgene demonstrated the requirement of sustained $Kras^{G12D}$ expression for the maintenance and progression of established murine PanINs and PDAC[157,161]. In addition to providing strong evidence for the functional importance of oncogenic Kras signaling in PDAC maintenance, these mouse models also allowed the characterization of how activated Kras might contribute to pancreatic cancer progression and how resistance could emerge following Kras inhibition. However, caution must be taken when interpreting these results, as the overexpression of an oncogene might have differential effects compared to the endogenous expression of an oncogene.

One pancreas-specific inducible-$Kras^{G12D}$ mouse model, a triple transgenic *p48-Cre; R26-rtTA-IRES-EGFP; TetO-*$Kras^{G12D}$ strain with or without inactivation of one allele of the tumor suppressor *p53*, was developed by Marina Pasca di Magliano and colleagues[161]. The *p48*

promoter allowed expression of Cre broadly in the pancreatic epithelium. This model required cerulein-induced pancreatitis prior to $Kras^{G12D}$ transgene expression to facilitate tissue-wide PanIN formation. Careful analysis of the induction and withdrawal of $Kras^{G12D}$ expression at different time points in $p53^{+/+}$ as well as $p53^{+/-}$ backgrounds demonstrated that the inactivation of $Kras^{G12D}$ in ADM and early PanIN lesions fully reverted the neoplastic phenotype, whereas inactivation of $Kras^{G12D}$ in advanced PanINs and PDAC induced apoptosis but led to incomplete pancreatic parenchymal remodeling. The restoration of ADM and low-grade PanINs to normal pancreatic architecture upon $Kras^{G12D}$ inactivation suggested that oncogenic Kras might prevent tissue repair following acute pancreatitis, which facilitated the ductal differentiation of acinar cells that is thought to be required for neoplastic progression. Interestingly, $Kras^{G12D}$ inactivation resulted in the involution of the fibroinflammatory stroma and decreased expression of cytokines and matrix metalloproteinases, suggesting that oncogenic Kras is required for the maintenance of the reactive stroma as well. A follow-up study performed by the same group investigated the importance of oncogenic Kras in metastatic PDAC *in vivo* by inducing and subsequently withdrawing $Kras^{G12D}$ expression in a $p53^{R172H/+}$ background[158], as expression of the mutant *p53* allele promoted liver metastasis and occasionally lung and duodenal invasion. This study showed that $Kras^{G12D}$ is required for the maintenance of not only primary tumors but also metastatic lesions. However, individual tumor cells remained dormant and led to tumor recurrence upon re-expression of $Kras^{G12D}$. Collectively, these observations demonstrated that oncogenic Kras signaling is necessary for both the progression and maintenance of PDAC, although resistance may develop.

Another pancreas-specific inducible-$Kras^{G12D}$ mouse model, with *tetO-LSL-*$Kras^{G12D}$*; ROSA26-LSL-rtTA-IRES-GFP; p48-Cre* in a $p53^{L/L}$ or $p53^{+/L}$ background, was developed by

Ronald DePinho and colleagues[157]. In this model, rapid tumor regression accompanied by decreased tumor cell proliferation assayed by BrdU incorporation and increased apoptosis was observed within 2 to 3 days of doxycycline withdrawal, and complete regression of established PDAC was observed approximately one week after $Kras^{G12D}$ extinction. A reduction in pancreatic stellate cells, a major component of the reactive stroma, also occurred. These observations again provided strong evidence for the requirement of oncogenic Kras signaling for tumor and stromal maintenance. Furthermore, transcriptomic and metabolomic analyses of orthotopic tumors derived from this model before and after $Kras^{G12D}$ withdrawal demonstrated that $Kras^{G12D}$ might play a role in stimulating glucose uptake and channeling glucose intermediates into the hexosamine biosynthesis and pentose phosphate pathways. This finding suggested that the requirement of oncogenic Kras for PDAC maintenance might in part be due to its ability to reprogram glucose metabolism to support cancer cell proliferation and survival.

In summary, *in vivo* analyses of the induction and subsequent removal of oncogenic *Kras* transgene expression in various p53 genetic backgrounds demonstrated that oncogenic Kras not only is a driver for ADM, PanIN and PDAC initiation and progression, but also is essential for PanIN, PDAC, and metastatic lesion maintenance. Examination of neoplastic tissues, tumors, and stroma in these mouse models revealed possible functions of oncogenic Kras signaling in this disease. Other than promoting cancer cell proliferation and survival, oncogenic Kras appeared to also mediate stromal remodeling and metabolic reprogramming. Importantly, although $Kras^{G12D}$ inactivation led to rapid regression of PDAC, some dormant tumor cells possibly remained in the primary tumor sites, as evident by the rapid recurrence of tumors from the primary sites upon re-expression of the $Kras^{G12D}$ transgene. This observation suggested that

even though PDAC tumors were initially sensitive to oncogenic Kras inhibition, resistant cells could lead to tumor relapse given time.

1.3.5 Bypass mechanisms following *Kras* inhibition

Even though kinase inhibitors have shown promising clinical results in inhibiting cancer progression, resistance often emerges by upregulation of canonical signaling pathways regulated by the target kinase, selection for cancer cells that have acquired a resistance-conferring mutation, or activation of alternative pro-survival and proliferation-promoting pathways. The last mode of resistance is also known as bypass mechanism. As Kras itself is currently not a viable therapeutic target and *in vivo* studies suggest that residual dormant tumor cells may be left behind following oncogenic Kras inhibition, several research groups sought to uncover alternative pathways required for oncogenic *Kras*-driven cancers using different *in vitro* and *in vivo* systems. Surprisingly, results from three independent studies converged on a link between Yes-associated protein 1 (Yap1) activity and oncogenic Kras. Yap1 is a transcriptional coactivator that partners with the TEAD family of transcription actors to promote the expression of pro-proliferative and anti-apoptotic genes. Results from these studies are discussed below.

Despite an initial rapid tumor regression following $Kras^{G12D}$ suppression *in vivo*, prolonged period of $Kras^{G12D}$ loss led to tumor relapse in the model developed by DePinho and colleagues[175]. While half of the relapse tumors exhibited re-expression of and thus addiction to the $Kras^{G12D}$ transgene, the remaining relapse tumors did not show an increased expression of the transgene or endogenous *Kras*. Moreover, these $Kras^{G12D}$-independent relapse tumors did not upregulate canonical Kras effector pathway signaling. Array-based comparative genomic hybridization revealed that a subset of the $Kras^{G12D}$-independent tumors harbor amplification of a chromosomal region encompassing *Yap1*. The interaction between Yap1 and TEAD2 appeared

to be crucial for tumor growth in the absence of $Kras^{G12D}$, and promoted transcription of genes that mediate proliferation. Interestingly, the transcription profiles of the $Kras^{G12D}$-independent mouse tumors clustered with human quasimesenchymal subtype of PDAC, and human PDAC cell lines of the quasimesenchymal subtype also seemed to depend on *YAP1* expression for proliferation.

In order to identify alternative therapeutic targets in *Kras*-driven PDAC, Chunling Yi and colleagues curated and surveyed published human PDAC miacroarray datasets and noticed that there was often an elevated level of *YAP* mRNA in human PDAC[176]. Subsequently, they determined whether Yap1 was required for PDAC progression *in vivo* by crossing $Yap1^{flox/flox}$ mice with mice that were $Kras^{G12D/+}$;*p48-Cre* or $Kras^{G12D/+}$;$p53^{R172H/+}$;*p48-Cre*. It became apparent that although Yap1 was dispensable for ADM development, it was required for the progression to PDAC. Further analysis demonstrated that Yap1 was a critical transcriptional switch downstream of Kras, promoting the expression of genes that encode secretory factors, which mediated neoplastic proliferation and stromal response in the tumor microenvironment.

In accordance with the *in vivo* PDAC studies, a study done by William Hahn and colleagues aimed to identify genes that maintain oncogenic *KRAS*-driven cancer cell survival reported *YAP1* expression as a bypass mechanism to KRAS inhibition[177]. They conducted a cDNA rescue screen in a human colon cancer cell line, HCT116, which was *KRAS*-dependent and was engineered to express an inducible *KRAS*-specific shRNA. The screen revealed *YAP1* as the highest scoring gene and exogenous *YAP1* expression rescued the loss of KRAS in additional human colon and pancreatic cancer cell lines. However, unlike results from murine PDAC model, this study reported that TEAD transcription factors were not required to

circumvent KRAS loss. In contrast, the activator protein 1 family member FOS interacted with YAP1 to activate a transcriptional program that regulates EMT.

Collectively, these studies suggested that YAP1 might be a viable therapeutic target in oncogenic *KRAS*-driven cancers like PDAC. Interestingly, a recent study suggested that YAP1 might mediate resistance to MEK- and BRAF-targeted cancer therapies in a wide spectrum of *RAS*-mutated (melanoma, non-small cell lung cancer, pancreatic cancer) or *BRAF*-mutated (melanoma, non-small cell lung cancer, thyroid, colon) tumors[178]. Currently, a YAP inhibitor, verteporfin, is prescribed in the clinic for treatment of abnormal growth of leaky blood vessels in the eye and other eye-related indications. A Phase I/II clinical trial to assess the safety of verteporfin as a photosensitizer for photodynamic therapy in locally advanced pancreatic cancer has been completed in the United Kingdom[179,180]. However, it is yet unclear whether this will be an effective therapeutic option for PDAC. Moreover, given the genetic heterogeneity of human PDAC tumors, it is highly likely that tumor cells can bypass the requirement for oncogenic *KRAS* in *YAP*-independent manners. For instance, alternative mechanisms of resistance to *KRAS* inhibition have been reported by a study that analyzed the surviving cells responsible for tumor relapse in the inducible $Kras^{G12D}$ transgene model developed by DePinho and colleagues[181]. In this system, upregulation of genes that promoted mitochondrial function and autophagy could support cell survival in the absence of oncogenic Kras[181]. It is therefore critical to gain a deeper understanding of the key effector pathways downstream of oncogenic KRAS as well as alternative pro-survival pathways that can support KRAS-independent tumor growth.

1.4 Direct and indirect therapeutic targeting of KRAS in cancer

Due to the high prevalence of oncogenic *KRAS* mutations in human cancer and abundant experimental data suggesting at least a partial requirement of sustained KRAS activation for

tumor initiation and maintenance, KRAS has remained an attractive therapeutic target for cancer. Moreover, the presence of activating *KRAS* mutations in tumors has been associated with worse prognosis and poorer response to treatment in NSCLC and colorectal cancer patients, highlighting the potential value of developing a KRAS-specific inhibitor[182-185]. Unfortunately, early efforts to develop pharmacological inhibitors targeting KRAS and other RAS proteins were largely unsuccessful, leading to the prevailing viewpoint that RAS proteins are "undruggable". However, given the important implications of oncogenic RAS in human cancer, improved technology and research tools, and a deeper understanding of RAS biology, there is now renewed interest in pursuing the development of a drug that directly or indirectly inhibits RAS, described as a "RAS renaissance"[186]. In 2013, the National Cancer Institute launched the RAS Initiative, which is a 10-million-dollars-a-year effort to find new ways to tackle *RAS*-driven cancers. This section presents the past and present efforts, challenges, and future directions of developing a direct or indirect inhibitor against KRAS.

1.4.1 Direct inhibition of KRAS activity

Key steps to successful cancer drug development

There are several essential steps involved in the successful development of a drug for cancer therapy[187]. First, a distinct aberration that exhibits strong molecular epidemiology for a given disease needs to be identified. Then, the molecular mechanisms of the defective pathway need to be elucidated to uncover potentially targetable, or druggable, proteins. Characterization of the structure of these key proteins often helps determine which chemical entities are likely to bind to these proteins with high affinity. A high-throughput screening method of combinatorial chemistry compound libraries can then be utilized to identify the lead inhibitory compound. Once the lead compound is identified and subsequently optimized, antitumor activity,

biochemical effects on the target protein, absorption/distribution/metabolism/excretion (ADME) profiles, toxicity, and pharmacodynamic properties of the compound can be assessed *in vitro* and *in vivo* before moving into clinical trials. Based on these criteria, it is not hard to see why KRAS proteins are not ideal drug targets. While there is compelling *in vitro* and *in vivo* evidence that support the causal relationship between activating *KRAS* mutations and human cancer, some inherent properties of KRAS proteins make it impossible to identify compounds that will potently bind to KRAS proteins to inhibit their activities. Furthermore, it is still unclear which biological pathways are most critical for oncogenic KRAS function in the development and progression of cancer. It appears that aberrant KRAS signaling contributes to different aspects of the transformed and malignant phenotype in different tumors, making the identification of alternative targets involved in oncogenic KRAS signaling challenging. In this section, attempts to design inhibitors that directly bind KRAS or impair the oncogenic activity of KRAS are discussed.

GTP-competitive inhibitors

RAS is inherently a difficult drug target for being a small GTPase. Currently, most of the successful small molecule inhibitors with specificity in the clinic are ATP-competitive inhibitors that target protein kinases. In an attempt to replicate the success of ATP-competitive inhibitors, GTP-competitive inhibitors of RAS have been pursued. However, whereas ATP binds kinases with low micromolar affinity and ATP-competitive inhibitors bind kinases with potent nanomolar affinity, GTP binds RAS proteins with picomolar affinity[40,91,188]. This tight binding makes it difficult to compete off GTP with any small molecule inhibitor. Moreover, the intracellular concentration of GTP is relatively high in the millimolar range. Therefore, development of an effective GTP-competitive inhibitor for RAS has been unsuccessful so far.

Low-affinity inhibitors

A few low-affinity inhibitors of RAS nucleotide exchange activity have been reported using a combination of mass spectrometry, nuclear magnetic resonance (NMR) spectroscopy, and molecular modeling techniques. The first compound was SCH-53239, which was originally designed to compete with GDP for the nucleotide-binding site of RAS[189]. However, a water-soluble analogue of this compound, SCH-54292, was later found to bind not to the nucleotide binding site but instead to a hydrophobic pocket near the RAS Switch II region. Further modification based on these original compounds led to the development of additional compounds that were shown to inhibit nucleotide exchange and $Kras^{G12D}$-dependent NIH-3T3 cell proliferation[190]. However, all of these compounds contain a hydroxylamine, which is critical for their inhibitory activity but leads to high toxicity and poor metabolic stability.

Another group of compounds has been reported to non-covalently and reversibly bind to RAS to inhibit the formation of the RAS-RAF complex[191]. These compounds are analogues of sulindac sulfide, a non-steroidal anti-inflammatory drug, which has been suggested to impair nucleotide exchange on RAS as well as to accelerate $p120^{GAP}$-mediated GTP hydrolysis[191]. Sulindac analogues bind to RAS at the RAF-binding site, resulting in decreased MAPK signaling *in vitro*[192]. Furthermore, the sulindac derivative IND12 selectively inhibited the proliferation of *RAS*-transformed MDCK-F3 cells, and increased E-cadherin expression as well as the level of E-cadherin-bound-β-catenin to impair invasion[193]. However, none of these compounds are potent enough for clinical use, and their off-target activities are unknown.

RAS protein lacks a deep hydrophobic pocket

A protein's shape typically provides insight into the likelihood of identifying a compound that would bind to a critical site to inhibit the protein's function. In general, deep hydrophobic

pockets allow drugs to slip into them and bind with multiple points of contact[186]. However, RAS proteins are relatively smooth in terms of their three-dimensional structure. The lack of a deep hydrophobic pocket makes it difficult to screen for compounds that can bind to RAS with high affinity. A possibility that has been considered is to target the interacting surface between RAS and its effectors. However, small molecule drugs that are able to get inside cells are often too small to block the wide surface area involved in protein-protein interactions[186]. While antibodies are ideal for masking large areas on their targets, it is difficult for antibodies to penetrate cell membranes, where actively signaling RAS proteins are localized.

Fortunately, recent advances in computer modeling and in the strategies to screen for drug compounds have offered new opportunities of synthesizing compounds that would bind to RAS. Instead of the conventional method of screening for a pre-existing compound that tightly binds RAS, it is now more favorable to tailor an inhibitor to bind to RAS by piecing together fragments of compounds that are capable of weakly interacting with RAS. The resulting inhibitor is likely to be a large novel compound that typically does not exist in standard chemical libraries. This technique is called fragment-based screening[186]. Additionally, the identified weakly interacting compounds can possibly induce a change in the structure of RAS, which may open up a binding pocket in the process. These recent developments in chemical biology and protein dynamic modeling definitely enhance the probability of developing a potent pharmacological inhibitor that can directly target RAS.

Inhibiting the membrane association and post-translational modifications of RAS proteins

Since a compound that would directly bind to and inhibit RAS proteins has not yet been developed, preventing the association of RAS proteins with the inner surface of the plasma membrane to inhibit the signal transduction ability of RAS proteins seems to be a compelling

alternative therapeutic strategy. As discussed previously, membrane association requires a series of post-translational modifications on the C-terminal domain of RAS. Although each additional modification increases the hydrophobicity of RAS proteins and contributes to membrane association, the initial farnesylation step alone is sufficient to promote significant membrane association and transforming potential[194,195].

The finding that farnesylation is critical for RAS function was encouraging because the farnesyl pyrophosphate (FPP) contributing the lipid group to proteins is a necessary intermediate component of the mevalonate-cholesterol biosynthetic pathway, whose synthesis can be blocked by the FDA-approved cholesterol-lowering drugs, such as lovastatin[196]. However, it was soon demonstrated that the clinically effective concentration of statins sufficient for lowering cholesterol biosynthesis was significantly lower than the concentration needed to block RAS farnesylation[197]. The research efforts then shifted towards the identification and development of inhibitors targeting farnesyltransferase (FTase), the enzyme responsible for adding the farnesyl modification to RAS proteins. Early approaches to identify farnesyltransferase inhibitors (FTIs) included high throughput random screens of chemical library compounds that would inhibit farnesylation of HRAS *in vitro*, random screening of microbial and natural products using yeast genetic screens for cell-permeable farnesylation inhibitors, and the search for cell-permeable CAAX peptidomimetics that could act as competitive inhibitors of RAS farnesylation[187,195,196,198-200]. These diverse screening approaches led to the discovery of a wide variety of natural and synthetic compounds, which could be divided into three classes based on their mechanisms of action: FPP analogs, peptidomimetic and non-peptide peptidomimetic CAAX competitive inhibitors, and bisubstrate compounds that combine both features[187,195]. Among these three classes, compounds competitive with CAAX in particular showed promising results in multiple

in vitro and *in vivo* models. Since reagents to study HRAS were more accessible and it was previously thought that all RAS isoforms are functionally identical, the preclinical models that showed impressive antitumor activities of FTIs were mostly *HRAS*-based. The first demonstrations of specific inhibition of RAS processing in whole cells were reported in rodent fibroblast model systems, such as NIH-3T3 cells transformed by oncogenic *HRAS*[201,202]. *In vivo*, FTIs displayed strong anti-*HRAS* and antitumor activities in subcutaneous xenograft tumors and in a viral *Hras*-driven salivary and mammary tumor mouse model[203,204].

Promising preclinical data led to at least six FTIs entering clinical trials, with two non-peptide peptidomimetics, tipifarnib (R115777) and lonafarnib (SCH66336), receiving the most significant clinical evaluation[187,195,196]. Both of these FTIs advanced to Phase III clinical trials. Disappointingly, these FTIs showed no antitumor activity in patients with colorectal and pancreatic cancer, which are associated with mutations in *NRAS* or *KRAS* rather than *HRAS*[40,187]. In fact, while FTIs effectively blocked HRAS farnesylation, membrane association, and transformation, they did not have the same effects on NRAS and KRAS. This was due to the fact that when FTase activity is blocked, NRAS and KRAS are able to be alternatively prenylated by an enzyme called geranylgeranyltransferase type I (GGTase I). GGTase I catalyzes the addition of a C20 geranylgeranyl isoprenoid group, which can substitute for the farnesyl group and support NRAS and KRAS membrane association and transforming ability[205-209]. Like FTase, GGTase I recognizes C-terminal CAAX motifs. Whereas FTase preferentially recognizes CAAX motifs where X is methionine, alanine, serine, or glutamine, GGTase I preferentially recognizes CAAX motifs where X is leucine[205,206]. There are approximately 50 mammalian protein substrates of FTase, and a far greater number of proteins are known to be substrates for GGTase I[195]. The large number of substrates is thought to be an additional

confounding factor that contributes to the preclinical antitumor activities of FTIs, which may not be entirely RAS-specific. Concurrent inhibition of both FTase and GGTase I have been considered, although toxicity may be an issue. Although FTIs turned out to be ineffective in treating *KRAS*-driven colorectal and pancreatic cancers, it is possible that *HRAS* mutant tumors, like bladder, thyroid, skin, and head and neck cancers, are susceptible to FTase inhibition. However, *HRAS* mutation frequency is quite low in these cancers, and whether *HRAS* is a driver of these cancers remains to be determined.

In addition to FTases, the other two CAAX-signaled modifications (proteolytic cleavage by RCE1 and carboxymethylation by ICMT) have also been considered as targets for RAS inhibition. However, the effects of blocking these two enzymes appeared to be context-dependent. While some studies provided evidence for the potential value of RCE1 and ICMT inhibition in suppressing RAS oncogenecity, others showed that inhibition of either enzyme could actually lead to increased RAS-mediated tumorigenesis[210-213]. Other possibilities of disrupting RAS localization to cellular membranes are actively being explored. One example is salirasib, which is a farnesylcysteine mimetic that competes with RAS for binding to membrane-associated RAS escort proteins, galectins, leading to degradation of cytoplasmic RAS[196,214]. This competition displaces all RAS isoforms from the plasma membrane. Although combination of salirasib and gemcitabine showed promising antitumor activity in patient-derived xenografts of PDAC, a Phase II clinical trial of salirasib showed that lung cancer patients with *KRAS* mutations did not benefit from salirasib treatment[214,215]. Another example is deltarasin, which is a small molecule inhibitor that targets PDE6δ[216]. PDE6δ acts as a solubilizing factor that modulates RAS proteins by sustaining their dynamic distribution in cellular membranes, and augments KRAS and HRAS signaling by enriching RAS at the plasma membrane[217]. There have been

encouraging results showing that deltarasin effectively inhibited PDE6δ binding to farnesylated RAS and suppressed proliferation of human *KRAS*-dependent pancreatic cancer cell lines *in vitro* and *in vivo*[216]. However, whether deltarasin will be a clinically effective inhibitor for *KRAS*-driven tumors requires further investigation. One concern is the unforeseen consequences of off-target effects of PDE6δ, which can interact with other farnesylated and possibly geranylgeranylated proteins, including farnesylated RAS-family proteins that act as tumor suppressors, such as NOEY2[218,219]. Furthermore, it is so far unclear how dependent RAS proteins are on PDE6δ for proper localization. It has been demonstrated that KRAS4B, which binds membrane phospholipids with high affinity by electrostatic interactions, could bind to cell membranes in the absence of PDE6δ[217]. Additionally, while KRAS deficiency is embryonic lethal, PDE6δ deficiency is not, suggesting that there are PDE6δ-independent functions of KRAS[220].

Recently described post-translational modifications of RAS that regulate its subcellular localization provide novel directions for RAS-targeted drug discovery. It has been shown that PKCα catalyzes phosphorylation of KRAS4B at S181 within the C-terminal polybasic sequence. This phosphorylation causes KRAS4B to be trafficked to endomembranes, where it interacts with inositol triphosphate receptors on the ER[221], and this interaction converts KRAS4B from a growth promoting to a growth suppressing protein in a mitochondrial BCL-X_L-dependent manner[76]. Additionally, bryostatin-1, a PKC agonist, suppressed the growth of $Kras^{G12V}$-transformed fibroblast xenograft tumors in mice[76]. However, these results have been contradicted by similar analyses performed by a different group[222], and the reason behind this discrepancy has not been elucidated so far.

Additional post-translational modifications that fine-tune the activities of KRAS have been reported recently. Mono-ubiquitination at Lys147 appeared to enhance GTP loading and effector-binding affinity of KRAS[223], suggesting that inhibiting ubiquitin pathway enzymes may be a useful therapeutic strategy. On the other hand, acetylation of Lys104 has been shown to decrease GEF-induced nucleotide exchange, leading to decreased transforming ability of KRAS *in vitro*[224]. Since the deacetylases HDAC6 and SIRT2 were found to regulate the level of aceylation of KRAS, inhibitors of these deacetylases might be useful for suppressing the oncogenic potential of mutant KRAS[225]. Another interesting target is the endothelial nitric oxide synthase (ENOS)-catalyzed nitrosylation at C118, which is thought to activate endogenous wild-type HRAS and NRAS, but not KRAS, by enhancing nucleotide dissociation[226]. The ENOS protein appeared to be a promising therapeutic target, as genetic ablation of the gene encoding ENOS led to prolonged survival in a *Pdx1-Cre; Kras*$^{G12D/+}$*; p53*$^{R172H/+}$ pancreatic cancer mouse model[227]. Similarly, treatment of a small molecule inhibitor of ENOS impaired the growth of human pancreatic cell line xenografts[227].

Even though targeting the membrane association of KRAS proteins has not proven to be clinically beneficial yet, there are many therapeutic opportunities related to interfering with KRAS trafficking and localization. As our understanding of the distinct functions of KRAS differential endomembrane localization emerges, additional factors and chaperones involved in the trafficking of KRAS proteins could serve as potential targets for small molecule inhibitors. Furthermore, recent studies revealed additional post-translational modifications that could modulate the activities of KRAS, providing novel enzymes and pathways for target discovery.

GEF inhibitors

It is surprisingly challenging to decipher whether oncogenic RAS proteins are regulated at all by GEFs, partly due to the fact that there are many types of mammalian GEFs. Additionally, the most well studied RAS-GEF, SOS1, is known to have multiple allosteric sites for RAS binding and GDP/GTP exchange, which makes it difficult to measure GTP loading on individual RAS isoforms in cells[40,91]. Therefore, whether inhibiting the interactions between RAS and GEF is a useful therapeutic strategy remains unresolved. Nevertheless, by fragment-based screening, two groups have reported compounds that could bind KRAS to weakly inhibit SOS1-mediated nucleotide exchange by blocking RAS-SOS1 complex formation[228,229]. The inhibitory compounds were shown to bind to a pocket located between the α2 helix and the β-sheet of KRAS that was not readily observed in the ligand-free form of KRAS. In fact, compound binding actually induced a conformational change in the protein to create a primary binding pocket and a second nearby cleft. Although the reported compounds were not very potent, these discoveries provided important insights into how the conformation of RAS changes upon ligand binding.

Restoring GTP hydrolysis

Impaired GAP-facilitated GTPase activity has been found to be the main biochemical mechanism underlying the oncogenicity of mutant RAS proteins. Therefore, identification of small molecules that could function as GAPs for mutant RAS has been pursued but has been mostly unsuccessful. One interesting observation made by Scheffzek and colleagues showed that $HRAS^{G12V}$ could hydrolyze a GTP analogue that contained an exocyclic aromatic amino group, which mimicked the catalytic effects of GAP's arginine finger[230]. This observation suggested that a small molecule providing a local charge might trick mutant RAS into GTP

hydrolysis. However, further attempts to develop molecules that would stimulate or accelerate intrinsic GTP hydrolysis have not been reported.

Allele-specific inhibitors

One of the most exciting recent developments in the search for *KRAS*-specific inhibitors has been the identification of *KRAS* mutant G12C-specific inhibitors. Since glycine lacks a side chain, the charged and reactive side chain of the amino acid that substitutes for glycine in mutant *KRAS* provides a selective therapeutic targeting opportunity. The first examples of G12C-specific inhibitors were identified by Kevan Shokat and colleagues[231]. Taking advantage of the unique nucleophilic property of cysteine thiols, Shokat and colleagues screened for electrophilic compounds that covalently binded to the mutant cysteine. These compounds interacted selectively with the GDP-bound form of $KRAS^{G12C}$ by binding at a newly discovered allosteric pocket beneath the Switch II region. This binding disrupted both Switch I and Switch II regions, favoring GDP-binding over GTP-binding and impairing RAS-RAF binding. Based on the discovery of this allosteric binding site, Neal Rosen and colleagues reported a compound, ARS853, which could bind $KRAS^{G12C}$ with high affinity[232,233]. ARS853 was shown to bind to the GDP-bound form of $KRAS^{G12C}$ and trap it in this inactive state, leading to inhibition of RAS-RAF interaction, MAPK signaling, and proliferation as well as induction of apoptosis in lung cancer cell lines that harbor the $KRAS^{G12C}$ mutation. Addition of RTK inhibition further enhanced the effect of ARS853, suggesting a possible combination therapeutic strategy for $KRAS^{G12C}$-driven cancer. Another compound, SML-8-73-1, has been developed by Nathanael Gray and colleagues. SML-8-73-1 is a GDP analogue with an attached electrophile that covalently and specifically binds the cysteine of $KRAS^{G12C}$ to render it inactive[234]. Importantly, SML-8-73-1 is capable of binding $KRAS^{G12C}$ even in the presence of 1mM concentrations of

GDP and GTP. Furthermore, a cell-permeable analogue of this compound attenuated AKT and ERK signaling to inhibit proliferation of multiple cell lines. Despite showing promising anti-proliferative effects *in vitro*, the compounds described so far need to be markedly improved to be effective drugs in the clinic. Since the $KRAS^{G12C}$ mutation is found in approximately 13% of lung adenocarcinoma[235], development of G12C-specific inhibitors can be particularly useful for treating lung cancer patients. However, G12D and G12V are the predominant mutations in PDAC, and thus PDAC therapies will require a different set of allele-specific inhibitors.

The development of G12C-specific inhibitors highlight the fact that the dynamic conformational states of RAS proteins may present more targeting opportunities than was previously realized. In fact, it is now established that GTP-bound HRAS actually exists in two states, only one of which is active and each with distinct binding properties for effectors, GAPs, and guanine nucleotides[236]. Furthermore, oncogenic RAS proteins are not 100% GTP-bound, but instead retain intrinsic, although inefficient, GTPase activities. This residual GTPase activity provides a useful therapeutic opportunity to stabilize the GDP-bound form rather than having to compete off the tightly bound GTP. As an alternative to targeting specific mutant variants, development of an isoform-specific inhibitor can also increase specificity and reduce toxicity. This can be achieved by targeting the distinct C-terminal hypervariable regions of individual RAS isoforms. Moreover, this method may be particularly useful for targeting KRAS4B, which has a unique polybasic sequence. A deeper understanding of the possible conformations that RAS may adopt as they bind effectors, nucleotides, GAPs, and small molecules can facilitate the development of isoform-specific or mutant-specific inhibitors.

1.4.2 Inhibition of downstream effector pathways of KRAS

As direct inhibition of KRAS itself has proven to be technically challenging, intensive investigations have focused on developing effective inhibitors that target critical effector pathways that mediate the oncogenic effects of activated KRAS. Unfortunately, the indirect inhibition of KRAS by targeting its downstream effectors appears to be equally difficult, mainly because KRAS regulates diverse signaling pathways and it is yet unclear which of these pathways are the most essential for its oncogenecity. As many of these pathways regulate key cellular functions in normal cells, the therapeutic window for inhibition of a single or multiple effector pathways is quite small. Additionally, these pathways are often not linear, but have multiple inputs and outputs and feed-forward and feedback mechanisms, making the identification of an ideal target especially challenging. Inhibition of a target may even lead to unexpectedly detrimental consequences due to the complex signaling network. Moreover, oncogenic KRAS is responsible for multiple facets of malignant transformation, including morphological transformation, uncontrolled proliferation, and anchorage-independent growth *in vitro* and tumor initiation, progression, and metastasis *in vivo*. These different aspects of oncogenic KRAS function likely depend on activation of distinct or multiple effector pathways. Further complexity arises as different KRAS mutant proteins appear to possess differential biological properties, possibly due to varying conformations imposed by different mutations leading to altered association with effectors. For instance, based on a combination of gene expression analysis of tumor samples, signaling analysis in cell lines, and molecular modeling, it has been suggested that G12C and G12V mutations of KRAS in lung adenocarcinoma preferentially activate the RalGDS pathway, whereas G12D activates the RAF/MAPK and PI3K pathways[237]. A crystal structure analysis suggested that mutations at codon 61 could have a

more profound effect on intrinsic GTPase activity when RAS is bound to RAF, which may account for the higher frequency of NRAS position 61 mutations in melanoma, a disease frequently driven by RAF hyperactivation[91,238]. Therefore, it is possible that therapeutic inhibition of distinct effector pathways will have to be tailored based on the type of *KRAS* mutation present in the individual tumor. Since pharmacological inhibitors designed to target the MAPK and the PI3K signaling cascades have received the most significant clinical development so far, the discussion here focuses on the inhibition of these two pathways.

Inhibition of the RAF-MAPK cascade

Among the many effectors of KRAS, RAF kinases are the most sought after therapeutic targets because they have a key driver role in RAS-mediated oncogenesis. It has been shown that expression of $BRAF^{V600E}$ in the mouse pancreas was sufficient to initiate PanIN formation[239]. Moreover, concomitant expression of $p53^{R270H}$ and $BRAF^{V600E}$ resulted in PDAC, suggesting that $BRAF^{V600E}$ recapitulates the effect of oncogenic *KRAS* expression in the pancreas[239]. The same study showed that human PDAC cell lines and orthotopically transplanted tumors were sensitive to MEK inhibition, suggesting that the RAF/MAPK signaling axis is critical for the initiation and maintenance of PDAC[239]. Similarly, it has been shown that CRAF is required for $Kras^{G12V}$-driven NSCLC *in vivo*[240]. Importantly, while ablation of MEK1/2 or ERK1/2 prevented tumor development, it also led to lethality in adult mice. In contrast, ablation of CRAF alone or in combination with BRAF was not deleterious for adult mouse tissues, indicating that CRAF can be an ideal drug target for *KRAS*-driven tumors[240]. Furthermore, BRAF is frequently mutationally activated in cancer, with a particularly high mutation frequency in melanomas (nearly 70%)[241]. Ironically, most of the early work that characterized the function of RAF kinases has focused on CRAF, while the most frequently mutated isoform is actually *BRAF*. A

better understanding of RAF isoform differences has clarified that BRAF has a higher basal kinase activity than CRAF, which allows a single mutation in the BRAF kinase domain to confer constitutive kinase activation[107]. Over 30 somatic mutations of *BRAF* have been identified in human cancer, with the majority being the V600E mutation that is known to enhance kinase activity and confer transforming ability in rodent fibroblasts and melanocytes[242]. Additionally, *BRAF* mutations and *RAS* mutations often exhibit mutual exclusivity in melanoma, colorectal carcinomas, papillary thyroid carcinomas, and serous ovarian carcinomas, which provides compelling evidence for the driver role of RAF in *RAS*-mutant cancers[40,97]. However, it is a misconception to view *RAF* mutations as equivalent to RAS activation. Combined inhibition of additional RAS effector pathways along with the RAF/MAPK pathway often exhibits synergistic effect in killing *RAS*-mutant cancer cells. The loss of the *PTEN* tumor suppressor, which results in PI3K/AKT activation, also co-occurs with *BRAF* mutations in melanoma[97]. Additionally, mutant *BRAF* exhibited significantly lower transforming potency than mutant *RAS* in fibroblasts, and conditional expression of endogenous activated *Kras* in mouse embryonic fibroblasts did not lead to ERK activation[146,242]. In summary, the RAF/MAPK signaling axis appears to be important for oncogenic *RAS*-driven cancers and thus is a valuable therapeutic target, but inhibition of this axis alone is likely insufficient to fully suppress *RAS*-mediated oncogenesis.

To date, at least 11 pharmacological inhibitors of RAF are under clinical evaluation, with four approved by the FDA for clinical use[40]. Interestingly, the ATP-competitive inhibitor sorafenib was first developed as a RAF inhibitor, but the antitumor efficacy of this multikinase inhibitor mainly lies in its ability to block tyrosine kinases that are involved in mediating angiogenesis[243,244]. Vemurafenib and dabrafenib are ATP-competitive RAF inhibitors that are approved for the treatment of *BRAF*-mutant melanoma[107]. A notable property of these RAF

inhibitors is that they inhibit ERK signaling only in tumors with *BRAF* mutations, which gives them a greater therapeutic window than the MEK inhibitors that suppress ERK signaling in both normal cells and tumor cells irrespective of *BRAF* mutational status. Surprisingly, when the effects of these RAF inhibitors were evaluated in *RAS*-mutant cancer cells, it was found that they paradoxically resulted in the activation, rather than the inactivation, of ERK[40,107]. The mechanistic basis for this paradox is the transactivation of RAF dimers, which accounts for the RAF inhibitor-induced benign skin tumors in individuals with mutant *RAS*[245-247]. Normally, active RAS mediates RAF dimerization, which leads to RAF activation. When RAF dimers are exposed to RAF inhibitors like vemurafenib, binding of the drug to one protomer induces a conformational change that results in the transactivation of the other non-drug-bound RAF. Even though the drug-bound RAF protomer is inactive, the non-drug-bound RAF is allosterically activated, resulting in increased ERK signaling. This implies that first-generation RAF inhibitors are probably most effective in cells with low levels of active RAS, in which most RAF proteins exist as monomers. Since $BRAF^{V600E}$ activity bypasses the requirement for RAF dimerization and $BRAF^{V600E}$ melanomas have low levels of active RAS, first-generation RAF inhibitors exhibit potent efficacy in suppressing $BRAF^{V600E}$ melanomas[107]. Importantly, a recently developed type II RAF inhibitor, LY3009120, which inhibits all RAF isoforms, homodimers, and heterodimers, showed promising growth suppressive effects in human cell lines and xenograft tumors that harbored $BRAF^{V600E}$ or *RAS* mutations[248]. It is optimistic that such second-generation RAF inhibitors may exhibit enhanced potency and be applied to broader tumor types than the first-generation inhibitors in the clinic.

At least 15 MEK inhibitors have reached clinical evaluation, with trametinib recently approved for *BRAF*-mutant metastatic melanoma[40]. Most of the existing MEK inhibitors are

non-ATP competitive inhibitors of MEK1 and MEK2, and are highly selective. However, although MEK inhibitors are effective against *BRAF*-mutant melanoma, they are only partially effective in *RAS*-mutant cancers and oncogenic *RAS*-driven mouse models[249,250]. Furthermore, as MEK inhibitors inhibit ERK signaling in normal tissues, they have substantial toxicity that may limit their clinical efficacy. Since resistance to RAF and MEK inhibitors are often due to reactivation of ERK, ERK inhibitors are also currently under clinical evaluation. However, similar to MEK inhibitors, ERK inhibitors can block ERK feedback phosphorylation and inactivation of RAF, which leads to increased MEK activation[40]. In sum, due to intricate feedback mechanisms in the RAS-RAF-MAPK signaling pathway, it is critical to evaluate the consequences of inhibiting single or multiple nodes of this pathway. Moreover, in order to avoid potentially detrimental consequences, it is necessary to assess how the mechanisms of action of individual inhibitors can differentially impact signaling in tumors harboring distinct mutations.

Inhibition of PI3K signaling

Frequent mutational activation of *PIK3CA* and inactivation of *PTEN* tumor suppressor suggest that PI3K signaling has a driver role in oncogenic *RAS*-dependent cancer development. Although PI3K activity can be modulated by upstream regulators other than RAS, *in vivo* experiments have suggested the importance of RAS-dependent PI3K signaling in cancer. A *Pik3ca* allele encoding a p110α mutant that has a defective Ras-binding domain, which specifically abolishes the interaction between p110α and Ras but retains non-Ras-dependent activities, was engineered by Julian Downward and colleagues[251]. It was reported that expression of this *Pik3ca* mutant allele in $Kras^{LA2}$ mice, which typically developed lung adenocarcinomas at high frequency and died by 200 days of age due to tumor burden, led to massively reduced tumor burden and prolonged survival of $Kras^{LA2}$ mice. Moreover, when the

interaction between Ras and p110α was abolished in established tumors in $Kras^{LA2}$ mice, partial tumor regression is observed[252]. These observations suggested that p110α is partially required for the initiation and maintenance of oncogenic *Kras*-driven lung cancer. Similarly, in the pancreas, it has been demonstrated that inactivation of PDK1 or p110α, but not p110β, blocked oncogenic *Kras*-induced ADM[253,254]. Additionally, expression of $p110\alpha^{H1047R}$ in the pancreas phenocopied $Kras^{G12D}$-induced metastatic PDAC[240]. Collectively, these studies provided compelling evidence that PI3K inhibition can be an effective therapeutic strategy in certain oncogenic *KRAS*-driven tumors. However, this requirement for PI3K signaling is not believed to be universal to all *KRAS*-mutant tumors. For instance, pharmacological inhibition of PI3K in oncogenic *Kras*-driven lung cancer did not block *in vivo* tumor growth[250]. Furthermore, in contrast to the non-overlapping *BRAF* and *RAS* mutations seen in human cancers, *PIK3CA* and *RAS* mutations often co-occur[40]. Although this relationship is only correlative, it suggests that oncogenic RAS alone may not potently activate PI3K signaling. Nevertheless, targeting PI3K signaling in combination with other effectors can be valuable for treating mutant *KRAS*-driven cancers.

Currently, numerous PI3K, AKT, and mTOR inhibitors are being clinically evaluated. In general, mTOR inhibitors, including the first-generation agent rapamycin and second-generation agents everolimus and temsirolimus, allosterically inhibit the mTORC1 complex by interacting with FKBP12. It is postulated that the limited efficacy in several tumor types of these mTOR inhibitors is due to their inability to inhibit mTORC2, which activates AKT[114]. In contrast, most PI3K inhibitors bind to the ATP-binding pocket of the catalytic domain of PI3K. Since mTOR and PI3K share structural similarities, many PI3K inhibitors are actually able to inhibit PI3K and mTOR simultaneously[114]. These dual inhibitors may offer therapeutic advantages by blocking

the whole signaling axis more completely. However, due to toxicity concerns, selective isoform-specific PI3K inhibitors have also recently emerged[114]. Overall, as monotherapies, inhibitors targeting the PI3K-AKT-mTOR pathway have shown largely disappointing activity against *RAS*-mutant cancers in preclinical and clinical settings. However, potent synergistic activity of PI3K inhibition with MEK inhibition has been reported in a mouse model of $Kras^{G12D}$-induced lung tumors[250]. Since both the MAPK and PI3K pathways are frequently deregulated in cancer, and are often involved in resistance to cancer therapies, the combined inhibition of both pathways can be an effective strategy for suppressing *KRAS*-mutant tumor growth. However, the toxicity associated with simultaneously inhibiting two major signaling pathways that regulate normal tissue homeostasis may limit the therapeutic window and thus the clinical efficacy of such combined treatment.

Crosstalk between MAPK and PI3K pathways and rationale for combined inhibition

The MAPK and PI3K pathways are known to interact at multiple nodes, resulting in cross-activation, cross-inhibition, and pathway convergence. For example, cross-activation can occur through ERK, which phosphorylates TSC2 at sites distinct from those phosphorylated by AKT[114,255]. Phosphorylation by either ERK or TSC2 negatively regulates TSC2 to promote mTORC1 activation. On the other hand, cross-inhibition can occur when AKT phosphorylates the regulatory domain of RAF after strong insulin-like growth factor (IGF1) stimulation, which leads to inhibition of RAF activity[256]. The relative importance of each point of convergence under physiological conditions may be dependent on the tissue type, cancer type, and the relative strengths of growth factor stimulation or other pathway inputs. Importantly, such redundancies between the two major RAS effector pathways provide means for tumors to develop resistance

by compensatory mechanisms against inhibition of upstream RTKs or components within a single pathway.

Since RAS signals through both MAPK and PI3K pathways, combined inhibition of MAPK and PI3K pathways is being accessed in several preclinical models of oncogenic *RAS*-driven cancers. Other than the $Kras^{G12D}$-driven lung tumor model previously discussed[250], results of additional preclinical studies are described here. In *NRAS*-mutant melanoma, which accounts for 15-20% of human cutaneous melanomas, whereas selumetinib (MEK inhibitor) or BEZ235 (PI3K and mTORC1/2 inhibitor) monotherapy alone allowed resistance to develop, combination of the two inhibitors led to tumor regression and increased survival in a genetically engineered mouse model[257]. In colorectal cancer, *PIK3CA* and *KRAS* mutations co-occur in a fraction of colorectal cancer patients[114]. Whereas *KRAS/PIK3CA*-double mutant HCT116 colorectal cancer cell line exhibited sensitivity to combined treatment of the pan-PI3K inhibitor GDC-0941 with either selumetinib or PD0325901 (MEK inhibitor), the combined treatment of BEZ235 and selumetinib only resulted in disease stabilization rather than tumor regression in patient-derived xenografts of metastatic colorectal cancer[258,259]. These findings suggest that dual inhibition of MEK and PI3K may not be sufficient to induce durable therapeutic response in patients with *KRAS*-mutant colorectal cancer, and additional biomarkers may be required to identify the subpopulation of patients that will benefit. Furthermore, *in vitro* analysis of human pancreatic cancer cell lines demonstrated that dual inhibition of AKT and MEK could lead to FOXO-mediated cell cycle arrest and apoptosis[260]. An *in vivo* pancreatic xenograft study also demonstrated that while MEK inhibition induced a more pronounced tumor suppressive effect than PI3K inhibition, combined MEK and PI3K inhibition significantly enhanced the tumor suppressive effect exerted by MEK inhibiton alone[261]. Similarly, combined inhibition of MEK

and PI3K led to prolonged survival of *Pdx1-Cre; LSL-Kras*^{G12D}*; p53*$^{Lox/+}$ mice[262]. Since single-agent MEK inhibitors have mostly showed partial response in pancreatic cancer patients so far, dual inhibition may be a useful strategy if toxicity can be appropriately limited. A recently developed inhibitor rigosertib, which can act as a RAS-mimetic and bind to the RAS-binding domains of RAF, PI3K, and RalGDS, showed promising growth inhibitory effects on xenograft tumors[263]. This inhibitor is appealing because it simultaneously targets multiple effectors of RAS, but its potentially high toxicity has to be evaluated before it can be applied clinically.

In sum, promising preclinical results indicate that dual inhibition of the MAPK and PI3K signaling cascades may be viable therapeutic options for treating oncogenic *RAS*-driven cancers, which are extremely refractory to existing therapies. Simultaneous inhibition of multiple RAS effectors can increase therapeutic efficacy by preventing compensatory mechanisms from developing. However, it is critical to identify the inhibitor combinations that are well tolerated and can be administered at effective therapeutic doses. Furthermore, identification of additional biomarkers may help classify patients and tumor types that will show the best response to such combined therapies.

1.4.3 Synthetic lethal targeting of oncogenic KRAS

As direct inhibition of KRAS is challenging and simultaneous inhibition of multiple effectors may have a narrow therapeutic window, an alternative and favorable therapeutic approach to increase selectivity and reduce toxicity is to inhibit synthetic lethal interactions with oncogenic *KRAS*. Ideally, targeting genes whose loss of function is lethal only in the presence of mutant *KRAS* will specifically eliminate *KRAS*-mutant cancer cells and spare *KRAS* wild-type normal cells. Classically, two genes are synthetic lethal if mutation of either alone is compatible with viability in an otherwise wild-type background, but simultaneous mutation of both leads to

death[264,265]. Synthetic lethality is commonly observed in lower organisms, and genetic screens for synthetic lethality has been useful for elucidating biochemical and developmental pathways in *S. cerevisiae*, *D. melanogaster*, and *C. elegans*[265]. In cancer, synthetic lethality provides an important conceptual framework for the development of cancer-specific drugs. Specifically, the protein products of genes synthetic lethal to a known cancer-causing mutation, like oncogenic *KRAS* mutations, may be more amenable to pharmacological attack than the cancer-causing mutation itself and present excellent targets for anti-cancer therapy[264]. Oncogene-specific synthetic lethal interactions stem from the fact that oncogenic mutations lead to phenotypic changes in cancer cells, which require cellular pathways to be altered to support malignant growth[40]. For example, elevated cellular stress caused by oncogenic transformation requires cancer cells to activate cellular stress-relief pathways for survival. Additionally, cancer cells often rewire their signaling pathways and metabolic flux to support proliferation, which results in compensatory changes in pathways not directly downstream of the driver oncogene. In the past, this oncogene-specific synthetic lethality has not been widely exploited mainly due to the lack of robust methods for systematically identifying synthetically lethal genes in mammalian cells[264]. However, this is rapidly changing with the increased availability of chemical and genetic tools, such as RNAi and CRISPR/Cas (clustered regularly-interspaced short palindromic repeats and CRISPR-associated proteins), which allow the perturbation of gene function in somatic cells.

The use of isogenic cell line pairs to identify compounds that selectively kill cancer cells as a result of synthetic interactions is a powerful approach for drug discovery. As an example, Kinzler and colleagues performed a chemical screen with 30,000 compounds to discover chemical entities that selectively killed *KRAS*-mutant cancer cells[266]. In this study, they co-cultured human colon cancer cells, derived from DLD-1, engineered to express a blue

fluorescent protein (BFP) with a subclone in which the mutant *KRAS* allele was knocked out by homologous recombination and engineered to express a yellow fluorescent protein (YFP). The two cell populations were co-cultured in multiwell plates to which different chemicals were added, and the ratio of blue to yellow fluorescence was monitored to identify differential killing between the two cell populations. Several chemical entities, including a novel cytidine nucleoside, were found to selectively kill cells containing mutant *KRAS*. The benefit of chemical screens is that it often yields a high number of hits. It is common for ~1% of the compounds in a chemical library to inhibit proliferation of cancer cells at the concentrations used in typical high-throughput screens[264]. Therefore, a screen conducted with 10^5 to 10^6 compounds, such as libraries created by large pharmaceutical companies or public consortiums, can generate thousands of potential anticancer drugs. By applying differential killing as a filter, compounds that are likely to have high therapeutic indices can efficiently be identified. The major disadvantage of cell-based screening of chemical libraries, however, is the challenge of and extensive additional work required for protein target identification[264].

In contrast with chemical screens, genetic screens using RNAi and CRISPR libraries are extremely powerful for the discovery of specific gene targets, which can then be aggressively pursued for drug development. Genome-wide unbiased functional screens are likely to uncover targets that will lead to unexpected and novel directions for KRAS-specific drug development. Alternatively, to efficiently identify targets that are likely to be ideal for drug development, limited and focused screens can be performed using druggable or epigenetic libraries. Taking advantage of *KRAS* oncogene addiction, several studies have applied RNAi screens in human cancer cell lines to identify genes that exhibited synthetic lethal interactions with mutant *KRAS*. Employing a variety of siRNA and shRNA libraries, both in a well-by-well or a pooled format, a

wide range of candidate genes have been identified[40]. These candidate genes encode proteins that can be classified into diverse cellular processes, including those associated with cell cycle and mitosis (such as survivin/BIRC5 and APC/C)[267,268], senescence and apoptosis (such as BCL-X_L and WT1; WT1 was identified using mouse *Kras*^{G12D}-driven lung tumor-derived cell lines)[269,270], regulation of transcriptional programs (such as SNAIL2)[271], and parallel growth and survival signals (such as TBK1 and TAK1)[272,273]. Identification of these candidates suggest that even though mutant *KRAS* plays a role in promoting cancer cell proliferation, survival, and genomic instability, additional cellular pathways are involved in supporting the survival of *KRAS*-mutant cancer cells. Importantly, none of the targets identified to date is superior to *KRAS* itself in discriminating *KRAS*-mutant and *KRAS*-wild-type cells[40]. Overall, the overlap between targets from individual synthetic lethal screens has been small, although proteasome subunits have been identified in three screens[267,272,274]. This lack of considerable overlap can be due to differences in oncogenic and secondary mutations and differences in tissue types of the cells selected for the individual screens. Most likely, synthetic lethal interactions are context-dependent and there is not one universal synthetic lethal target for all *RAS*-driven cancers.

From a therapeutic standpoint, the main purpose of uncovering synthetic lethal interactions with oncogenic *KRAS* is to identify drug targets that are likely to be therapeutically tractable, as opposed to the undruggable oncogenic KRAS itself. Inhibiting components of the cell cycle machinery like APC/C can lead to considerable toxicity in normal tissues, whereas transcription factors like WT1 and SNAIL2 are difficult to directly target. In 2009, three unbiased and functional shRNA-based synthetic lethal screens performed in human cancer cell lines to identify potential targets for indirect KRAS inhibition elicited great enthusiasm for drug

development, because candidate targets that were protein kinases were reported[267,272,275]. These candidate targets were: STK33, PLK1, and TBK1.

Serine/threonine protein kinase 33 (STK33)

Gary Gilliland and colleagues designed a limited lentiviral shRNA library targeting 1,011 genes that were cancer-related or encoded protein kinases[275]. Using human cancer cell lines that were either *KRAS*-wild-type or *KRAS*-mutant, it was found that cells dependent on mutant *KRAS* expression were also dependent on *STK33* (which encodes serine/threonine protein kinase 33), irrespective of the tissue of origin. Reciprocally, *KRAS*-independent cells also were not dependent on *STK33* expression for survival. Furthermore, this study reported that STK33 promoted cancer cell viability in a kinase activity-dependent manner by suppressing mitochondrial apoptosis mediated through S6K1-induced inactivation of pro-apoptotic BAD selectively in mutant *KRAS*-dependent cells. Importantly, no alteration in *STK33* expression or *STK33* mutations were detected, demonstrating that the specific requirement for STK33 activity would not have been discovered if it were not for this synthetic lethal screen. Unfortunately, subsequent studies found that neither genetic nor pharmacological inhibition of STK33 selectively inhibited the growth of *KRAS*-mutant cancer cells[276-278]. Further complication arose when it was demonstrated that STK33 kinase activity was not required for *KRAS*-dependent cancer cell viability[278]. Whether STK33 is actually a synthetic lethal target of oncogenic KRAS remains controversial[279,280].

Polo-like kinase 1 (PLK1)

Stephen Elledge and colleagues employed a genome-wide retroviral shRNA library targeting 32,293 unique human transcripts to reveal genes selectively required for the viability of $KRAS^{G13D}$ DLD-1 colorectal cancer cells[267]. The candidate genes encode a functionally diverse

set of proteins that regulate multiple biological processes, but there was a particular enrichment of genes associated with mitotic functions. Among these genes, *PLK1*, which encodes a serine/threonine kinase that regulates mitosis, was identified. PLK1 plays a key role in mitosis, and is frequently deregulated in cancer cells. In this study, it was found that *KRAS*-mutant cells were particularly dependent on key mitotic proteins for survival. Therefore, inhibition of the pathway involving PLK1, the anaphase-promoting complex/cyclosome (APC/C), and the proteasome led to prometaphase accumulation and the subsequent death of *KRAS*-mutant cells. Components of this pathway are tractable drug targets. Whereas the proteasome inhibitor bortezomib has been approved for treatment of various cancers, PLK1 inhibitors such as volasertib and BI-2536 are being evaluated in clinical trials. Whether these drugs exhibit selective efficacy for the treatment of oncogenic *KRAS*-driven cancers remains to be determined.

TANK-binding kinase 1 (TBK1)

William Hahn and colleagues utilized a limited lentiviral shRNA library targeting 957 genes that were known oncogenes or encoded kinases and phosphatases to identify selectively required genes in a panel of human cancer cell lines[272]. They found that the non-canonical IκB kinase, TBK1, was selectively essential in cells that harbored mutant *KRAS*. TBK1 is a serine/threonine kinase that can activate the NFκB transcription factor to support cell survival, and has been found to be overexpressed in lung, breast, and colon tumors[281]. Mechanistically, TBK1 was found to activate NFκB anti-apoptotic signals involving c-Rel and BCL-X_L in *KRAS*-dependent cancer cells[272]. Interestingly, TBK1 was previously identified to be a key downstream effector of RalB-dependent tumor cell survival[282]. However, genetic and pharmacological inhibition of TBK1 did not show a consistent requirement of TBK1 for the proliferation of *KRAS*-mutant lung, pancreatic, or colorectal cancer cell lines *in vitro*[281]. In contrast, combined

pharmacological inhibition of TBK1 and MEK (by CYT387 and selumetinib, respectively) led to synergistic partial regression of murine lung tumors driven by $Kras^{G12D}$ and *p53* loss, suggesting that inhibition of TBK1 might be a useful therapeutic strategy in *KRAS*-driven tumors[283].

Taken together, high-throughput genetic screening for synthetic lethal partners of oncogenic *KRAS* is a valuable approach for novel target discovery, but rigorous validation is required to verify that the inhibition of these candidate targets will be clinically beneficial. Currently, major caveats of shRNA libraries include off-target effects, which result in high false-positive rates, and low library penetrance (the number of shRNAs that effectively knockdown a given gene), which results in high false-negative rates. Designing improved and validated libraries will greatly facilitate target discovery. With exciting recent advances in adapting bacterial CRISPR/Cas for high-throughput genome editing of mammalian cells[284-287], sgRNA libraries can be utilized to uncover synthetic lethal targets in *KRAS*-mutant cancer cells. It is possible that CRISPR/Cas may have fewer off-target effects than RNAi. Furthermore, when properly designed, CRISPR/Cas can more reliably generate true loss-of-function phenotypes, providing higher library penetrance compared to existing RNAi libraries. Another caveat associated with some of the candidate synthetic lethal targets identified to date is the use of isogenic cell lines. While isogenic cell line pairs are valuable tools, introduction of mutant *KRAS* into wild-type cells does not necessarily confer *KRAS* oncogene addiction, and loss of mutant *KRAS* may force *KRAS*-dependent cells to upregulate compensatory pathways[40]. These caveats may partially explain the challenges associated with validating the essentiality of some of the current candidate targets for *KRAS*-mutant cancer cell viability.

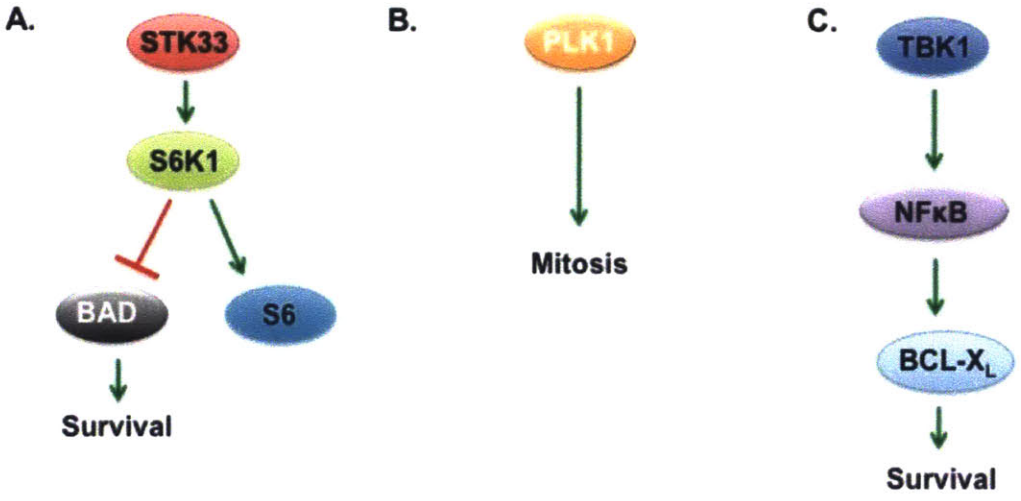

Figure 3. Proposed mechanisms of how kinases that exhibit *KRAS* synthetic lethality support *KRAS*-dependent cancer cell proliferation and survival. A. STK33. B. PLK1. C. TBK1.

1.5 Conclusions and aims

Despite the limited success in development of therapeutic inhibition of oncogenic KRAS in the last three decades, many valuable lessons have been learned about this currently intractable target. It is now well established that early views of the biological functions of RAS proteins in normal tissues and malignancies have been oversimplified, resulting in the unsuccessful attempts to target mutant *KRAS*-driven cancers. Although the clinical development of farnesyltransferase inhibitors has been disappointing, it highlights the important fact that the three canonical *RAS* genes do not encode functionally equivalent proteins. Cancers driven by different oncogenic RAS isoforms and varying mutant alleles will require distinct therapeutic approaches, which are tailored to target the specific biochemical properties that are altered and the direct or distal effectors that are most critical for maintaining cancer cell viability. Additionally, the paradoxical effect of first-generation BRAF inhibitors in *KRAS*-mutant cancer cells unraveled the complexity of signaling network downstream of KRAS. The once thought to be linear signaling pathways are actually dynamically regulated by multiple inputs and outputs, as well as intricate positive and negative feedback mechanisms. What first appeared to be parallel signaling cascades actually cross-activate and cross-inhibit with various nodes of convergence, allowing cancer cells to adapt and rewire signaling flux in response to pharmacological interventions. Importantly, discrepancies between observations made in the many flavors of *in vitro* and *in vivo* models underscore the essentiality of choosing an appropriate system that most accurately recapitulates the physiological setting to study clinically relevant phenotypes. Finally, recent advances in the development of genome editing tools and genome-wide functional screens will accelerate the discovery of drug targets and reveal novel directions for the development of oncogenic KRAS-directed therapies.

A deeper understanding of the biology of KRAS and its role in cancer may make KRAS a more tractable drug target in the future. Currently, there remain many unresolved questions in the field. The work presented in this thesis aimed to address some of these outstanding questions. In order to investigate whether KRAS inhibition can be a useful therapeutic approach for PDAC, a disease for which activating *KRAS* mutations are the defining features, we interrogated both the partial and the absolute requirements of oncogenic *KRAS* for maintaining human and murine PDAC cell survival. Leveraging RNAi- and CRISPR/Cas-based genome editing tools, we analyzed the essentiality of endogenous levels of oncogenic *KRAS* for cancer cell viability and the degree of inhibition necessary to impair *KRAS*-mutant cell survival. Thorough analyses of signaling differences, sensitivity to pharmacological inhibitors, and gene expression profiling of PDAC cells prior to and following *KRAS* inhibition revealed bypass mechanisms that allowed PDAC cells to circumvent *KRAS* oncogene addiction. Additionally, we investigated the *in vivo* requirement of *Stk33*, a putative synthetic lethal target of oncogenic *Kras*, in autochthonous *Kras*-driven mouse models of pancreatic and lung adenocarcinomas using conditional Cre/loxP- and CRISPR/Cas-based approaches. As the characterization of KRAS functions is still work in progress, we hoped to provide further insights into the biology of KRAS in oncogenic *KRAS*-driven cancers to facilitate the development of KRAS-directed therapeutic strategies.

REFERENCES

1. Rous, P. Surmise and fact on the nature of cancer. *Nature* **183**, 1357-1361 (1959).
2. Weinberg, R.A. *The Biology of Cancer*, (Garland Science, Taylor & Francis Group, LLC, 2014).
3. Shih, C., Shilo, B.Z., Goldfarb, M.P., Dannenberg, A. & Weinberg, R.A. Passage of phenotypes of chemically transformed cells via transfection of DNA and chromatin. *Proc Natl Acad Sci U S A* **76**, 5714-5718 (1979).
4. Stehelin, D., Varmus, H.E., Bishop, J.M. & Vogt, P.K. DNA related to the transforming gene(s) of avian sarcoma viruses is present in normal avian DNA. *Nature* **260**, 170-173 (1976).
5. Cooper, G.M., Okenquist, S. & Silverman, L. Transforming activity of DNA of chemically transformed and normal cells. *Nature* **284**, 418-421 (1980).
6. Harvey, J.J. An Unidentified Virus Which Causes the Rapid Production of Tumours in Mice. *Nature* **204**, 1104-1105 (1964).
7. Kirsten, W.H. & Mayer, L.A. Morphologic responses to a murine erythroblastosis virus. *J Natl Cancer Inst* **39**, 311-335 (1967).
8. Barbacid, M. ras genes. *Annual Review of Biochemistry* **56**, 779-827 (1987).
9. Goldfarb, M., Shimizu, K., Perucho, M. & Wigler, M. Isolation and preliminary characterization of a human transforming gene from T24 bladder carcinoma cells. *Nature* **296**, 404-409 (1982).
10. Shih, C. & Weinberg, R.A. Isolation of a transforming sequence from a human bladder carcinoma cell line. *Cell* **29**, 161-169 (1982).
11. Pulciani, S., *et al.* Oncogenes in human tumor cell lines: molecular cloning of a transforming gene from human bladder carcinoma cells. *Proc Natl Acad Sci U S A* **79**, 2845-2849 (1982).
12. Der, C.J., Krontiris, T.G. & Cooper, G.M. Transforming genes of human bladder and lung carcinoma cell lines are homologous to the ras genes of Harvey and Kirsten sarcoma viruses. *Proc Natl Acad Sci U S A* **79**, 3637-3640 (1982).
13. Parada, L.F., Tabin, C.J., Shih, C. & Weinberg, R.A. Human EJ bladder carcinoma oncogene is homologue of Harvey sarcoma virus ras gene. *Nature* **297**, 474-478 (1982).
14. Santos, E., Tronick, S.R., Aaronson, S.A., Pulciani, S. & Barbacid, M. T24 human bladder carcinoma oncogene is an activated form of the normal human homologue of BALB- and Harvey-MSV transforming genes. *Nature* **298**, 343-347 (1982).
15. Reddy, E.P., Reynolds, R.K., Santos, E. & Barbacid, M. A point mutation is responsible for the acquisition of transforming properties by the T24 human bladder carcinoma oncogene. *Nature* **300**, 149-152 (1982).
16. Tabin, C.J., *et al.* Mechanism of activation of a human oncogene. *Nature* **300**, 143-149 (1982).
17. Taparowsky, E., *et al.* Activation of the T24 bladder carcinoma transforming gene is linked to a single amino acid change. *Nature* **300**, 762-765 (1982).
18. Wennerberg, K., Rossman, K.L. & Der, C.J. The Ras superfamily at a glance. *J Cell Sci* **118**, 843-846 (2005).
19. Colicelli, J. Human RAS superfamily proteins and related GTPases. *Sci STKE* **2004**, RE13 (2004).

20. Bourne, H.R., Sanders, D.A. & McCormick, F. The GTPase superfamily: conserved structure and molecular mechanism. *Nature* **349**, 117-127 (1991).
21. Etienne-Manneville, S. & Hall, A. Rho GTPases in cell biology. *Nature* **420**, 629-635 (2002).
22. Pereira-Leal, J.B. & Seabra, M.C. Evolution of the Rab family of small GTP-binding proteins. *J Mol Biol* **313**, 889-901 (2001).
23. Memon, A.R. The role of ADP-ribosylation factor and SAR1 in vesicular trafficking in plants. *Biochim Biophys Acta* **1664**, 9-30 (2004).
24. Sibler, A.P., *et al.* Nucleocytoplasmic shuttling of antigen in mammalian cells conferred by a soluble versus insoluble single-chain antibody fragment equipped with import/export signals. *Experimental Cell Research* **286**, 276-287 (2003).
25. DeFeo-Jones, D., *et al.* Mammalian and yeast ras gene products: biological function in their heterologous systems. *Science* **228**, 179-184 (1985).
26. Kataoka, T., *et al.* Functional homology of mammalian and yeast RAS genes. *Cell* **40**, 19-26 (1985).
27. Muller, R., *et al.* Transcription of c-onc genes c-rasKi and c-fms during mouse development. *Mol Cell Biol* **3**, 1062-1069 (1983).
28. Goyette, M., Petropoulos, C.J., Shank, P.R. & Fausto, N. Expression of a cellular oncogene during liver regeneration. *Science* **219**, 510-512 (1983).
29. Tanaka, T., *et al.* Organ specific expression of ras oncoproteins during growth and development of the rat. *Mol Cell Biochem* **70**, 97-104 (1986).
30. Slamon, D.J. & Cline, M.J. Expression of cellular oncogenes during embryonic and fetal development of the mouse. *Proc Natl Acad Sci U S A* **81**, 7141-7145 (1984).
31. Furth, M.E., Aldrich, T.H. & Cordon-Cardo, C. Expression of ras proto-oncogene proteins in normal human tissues. *Oncogene* **1**, 47-58 (1987).
32. Malumbres, M. & Barbacid, M. RAS oncogenes: the first 30 years. *Nat Rev Cancer* **3**, 459-465 (2003).
33. Hall, A., Marshall, C.J., Spurr, N.K. & Weiss, R.A. Identification of transforming gene in two human sarcoma cell lines as a new member of the ras gene family located on chromosome 1. *Nature* **303**, 396-400 (1983).
34. Shimizu, K., Goldfarb, M., Perucho, M. & Wigler, M. Isolation and preliminary characterization of the transforming gene of a human neuroblastoma cell line. *Proc Natl Acad Sci U S A* **80**, 383-387 (1983).
35. Pylayeva-Gupta, Y., Grabocka, E. & Bar-Sagi, D. RAS oncogenes: weaving a tumorigenic web. *Nat Rev Cancer* **11**, 761-774 (2011).
36. McGrath, J.P., *et al.* Structure and organization of the human Ki-ras proto-oncogene and a related processed pseudogene. *Nature* **304**, 501-506 (1983).
37. Nakano, H., *et al.* Isolation of transforming sequences of two human lung carcinomas: structural and functional analysis of the activated c-K-ras oncogenes. *Proc Natl Acad Sci U S A* **81**, 71-75 (1984).
38. Santos, E. & Nebreda, A.R. Structural and functional properties of ras proteins. *Faseb J* **3**, 2151-2163 (1989).
39. George, D.L., *et al.* Structure and expression of amplified cKi-ras gene sequences in Y1 mouse adrenal tumor cells. *Embo J* **4**, 1199-1203 (1985).
40. Cox, A.D., Fesik, S.W., Kimmelman, A.C., Luo, J. & Der, C.J. Drugging the undruggable RAS: Mission possible? *Nat Rev Drug Discov* **13**, 828-851 (2014).

41. Leon, J., Guerrero, I. & Pellicer, A. Differential expression of the ras gene family in mice. *Mol Cell Biol* **7**, 1535-1540 (1987).
42. Umanoff, H., Edelmann, W., Pellicer, A. & Kucherlapati, R. The murine N-ras gene is not essential for growth and development. *Proc Natl Acad Sci U S A* **92**, 1709-1713 (1995).
43. Johnson, L., *et al.* K-ras is an essential gene in the mouse with partial functional overlap with N-ras. *Genes & Development* **11**, 2468-2481 (1997).
44. Koera, K., *et al.* K-ras is essential for the development of the mouse embryo. *Oncogene* **15**, 1151-1159 (1997).
45. Esteban, L.M., *et al.* Targeted genomic disruption of H-ras and N-ras, individually or in combination, reveals the dispensability of both loci for mouse growth and development. *Mol Cell Biol* **21**, 1444-1452 (2001).
46. Scolnick, E.M., Papageorge, A.G. & Shih, T.Y. Guanine nucleotide-binding activity as an assay for src protein of rat-derived murine sarcoma viruses. *Proc Natl Acad Sci U S A* **76**, 5355-5359 (1979).
47. Willingham, M.C., Pastan, I., Shih, T.Y. & Scolnick, E.M. Localization of the src gene product of the Harvey strain of MSV to plasma membrane of transformed cells by electron microscopic immunocytochemistry. *Cell* **19**, 1005-1014 (1980).
48. Willumsen, B.M., Christensen, A., Hubbert, N.L., Papageorge, A.G. & Lowy, D.R. The p21 ras C-terminus is required for transformation and membrane association. *Nature* **310**, 583-586 (1984).
49. Gibbs, J.B., Sigal, I.S., Poe, M. & Scolnick, E.M. Intrinsic GTPase activity distinguishes normal and oncogenic ras p21 molecules. *Proc Natl Acad Sci U S A* **81**, 5704-5708 (1984).
50. McGrath, J.P., Capon, D.J., Goeddel, D.V. & Levinson, A.D. Comparative biochemical properties of normal and activated human ras p21 protein. *Nature* **310**, 644-649 (1984).
51. Sweet, R.W., *et al.* The product of ras is a GTPase and the T24 oncogenic mutant is deficient in this activity. *Nature* **311**, 273-275 (1984).
52. Hurley, J.B., Simon, M.I., Teplow, D.B., Robishaw, J.D. & Gilman, A.G. Homologies between signal transducing G proteins and ras gene products. *Science* **226**, 860-862 (1984).
53. Clark, R., Wong, G., Arnheim, N., Nitecki, D. & McCormick, F. Antibodies specific for amino acid 12 of the ras oncogene product inhibit GTP binding. *Proc Natl Acad Sci U S A* **82**, 5280-5284 (1985).
54. Feramisco, J.R., *et al.* Transient reversion of ras oncogene-induced cell transformation by antibodies specific for amino acid 12 of ras protein. *Nature* **314**, 639-642 (1985).
55. Willumsen, B.M., *et al.* Mutational analysis of a ras catalytic domain. *Mol Cell Biol* **6**, 2646-2654 (1986).
56. Bollag, G. & McCormick, F. Regulators and effectors of ras proteins. *Annu Rev Cell Biol* **7**, 601-632 (1991).
57. McCormick, F. & Wittinghofer, A. Interactions between Ras proteins and their effectors. *Curr Opin Biotechnol* **7**, 449-456 (1996).
58. Edkins, S., *et al.* Recurrent KRAS codon 146 mutations in human colorectal cancer. *Cancer Biol Ther* **5**, 928-932 (2006).
59. Tyner, J.W., *et al.* High-throughput sequencing screen reveals novel, transforming RAS mutations in myeloid leukemia patients. *Blood* **113**, 1749-1755 (2009).

60. De Roock W, J.D., Di Nicolantonio F, Sartore-Bianchi A, Tu D, Siena S, Lamba S, Arena S, Frattini M, Piessevaux H, Van Cutsem E, O'Callaghan CJ, Khambata-Ford S, Zalcberg JR, Simes J, Karapetis CS, Bardelli A, Tejpar S. Association of KRAS p.G13D mutation with outcome in patients with chemotherapy-refractory metastatic colorectal cancer treated with cetuximab. *Jama* **304**, 1812-1820 (2010).
61. Jurnak, F. Structure of the GDP domain of EF-Tu and location of the amino acids homologous to ras oncogene proteins. *Science* **230**, 32-36 (1985).
62. Scheffzek, K., *et al.* The Ras-RasGAP complex: structural basis for GTPase activation and its loss in oncogenic Ras mutants. *Science* **277**, 333-338 (1997).
63. Rajalingam, K., Schreck, R., Rapp, U.R. & Albert, S. Ras oncogenes and their downstream targets. *Biochim Biophys Acta* **1773**, 1177-1195 (2007).
64. Pai, E.F., *et al.* Structure of the guanine-nucleotide-binding domain of the Ha-ras oncogene product p21 in the triphosphate conformation. *Nature* **341**, 209-214 (1989).
65. Pai, E.F., *et al.* Refined crystal structure of the triphosphate conformation of H-ras p21 at 1.35 A resolution: implications for the mechanism of GTP hydrolysis. *Embo J* **9**, 2351-2359 (1990).
66. Hancock, J.F., Paterson, H. & Marshall, C.J. A polybasic domain or palmitoylation is required in addition to the CAAX motif to localize p21ras to the plasma membrane. *Cell* **63**, 133-139 (1990).
67. Bivona, T.G. & Philips, M.R. Ras pathway signaling on endomembranes. *Curr Opin Cell Biol* **15**, 136-142 (2003).
68. Downward, J. Targeting RAS signalling pathways in cancer therapy. *Nature Reviews Cancer* **3**, 11-22 (2003).
69. Jaumot, M., Yan, J., Clyde-Smith, J., Sluimer, J. & Hancock, J.F. The linker domain of the Ha-Ras hypervariable region regulates interactions with exchange factors, Raf-1 and phosphoinositide 3-kinase. *J Biol Chem* **277**, 272-278 (2002).
70. Castellano, E. & Santos, E. Functional specificity of ras isoforms: so similar but so different. *Genes Cancer* **2**, 216-231 (2011).
71. Rocks, O., *et al.* An acylation cycle regulates localization and activity of palmitoylated Ras isoforms. *Science* **307**, 1746-1752 (2005).
72. Roy, S., *et al.* Individual palmitoyl residues serve distinct roles in H-ras trafficking, microlocalization, and signaling. *Mol Cell Biol* **25**, 6722-6733 (2005).
73. Omerovic, J. & Prior, I.A. Compartmentalized signalling: Ras proteins and signalling nanoclusters. *Febs J* **276**, 1817-1825 (2009).
74. Roy, S., *et al.* Dominant-negative caveolin inhibits H-Ras function by disrupting cholesterol-rich plasma membrane domains. *Nature Cell Biology* **1**, 98-105 (1999).
75. McLaughlin, S., Hangyas-Mihalyne, G., Zaitseva, I. & Golebiewska, U. Reversible - through calmodulin - electrostatic interactions between basic residues on proteins and acidic lipids in the plasma membrane. *Biochem Soc Symp*, 189-198 (2005).
76. Bivona, T.G., *et al.* PKC regulates a farnesyl-electrostatic switch on K-Ras that promotes its association with Bcl-XL on mitochondria and induces apoptosis. *Molecular Cell* **21**, 481-493 (2006).
77. Khosravi-Far, R. & Der, C.J. The Ras signal transduction pathway. *Cancer Metastasis Rev* **13**, 67-89 (1994).

78. Bowtell, D., Fu, P., Simon, M. & Senior, P. Identification of murine homologues of the Drosophila son of sevenless gene: potential activators of ras. *Proc Natl Acad Sci U S A* **89**, 6511-6515 (1992).
79. McCormick, F. Signal transduction. How receptors turn Ras on. *Nature* **363**, 15-16 (1993).
80. Cullen, P.J. & Lockyer, P.J. Integration of calcium and Ras signalling. *Nat Rev Mol Cell Biol* **3**, 339-348 (2002).
81. Chiu, V.K., *et al.* Ras signalling on the endoplasmic reticulum and the Golgi. *Nature Cell Biology* **4**, 343-350 (2002).
82. Ebinu, J.O., *et al.* RasGRP, a Ras guanyl nucleotide- releasing protein with calcium- and diacylglycerol-binding motifs. *Science* **280**, 1082-1086 (1998).
83. Gideon, P., *et al.* Mutational and kinetic analyses of the GTPase-activating protein (GAP)-p21 interaction: the C-terminal domain of GAP is not sufficient for full activity. *Mol Cell Biol* **12**, 2050-2056 (1992).
84. Adari, H., Lowy, D.R., Willumsen, B.M., Der, C.J. & McCormick, F. Guanosine triphosphatase activating protein (GAP) interacts with the p21 ras effector binding domain. *Science* **240**, 518-521 (1988).
85. Ballester, R., *et al.* The NF1 locus encodes a protein functionally related to mammalian GAP and yeast IRA proteins. *Cell* **63**, 851-859 (1990).
86. Martin, G.A., *et al.* The GAP-related domain of the neurofibromatosis type 1 gene product interacts with ras p21. *Cell* **63**, 843-849 (1990).
87. Wallace, M.R., *et al.* Type 1 neurofibromatosis gene: identification of a large transcript disrupted in three NF1 patients. *Science* **249**, 181-186 (1990).
88. Xu, G.F., *et al.* The neurofibromatosis type 1 gene encodes a protein related to GAP. *Cell* **62**, 599-608 (1990).
89. Basu, T.N., *et al.* Aberrant regulation of ras proteins in malignant tumour cells from type 1 neurofibromatosis patients. *Nature* **356**, 713-715 (1992).
90. Kalra, R., Paderanga, D.C., Olson, K. & Shannon, K.M. Genetic analysis is consistent with the hypothesis that NF1 limits myeloid cell growth through p21ras. *Blood* **84**, 3435-3439 (1994).
91. Stephen, A.G., Esposito, D., Bagni, R.K. & McCormick, F. Dragging ras back in the ring. *Cancer Cell* **25**, 272-281 (2014).
92. Kamata, T. & Feramisco, J.R. Epidermal growth factor stimulates guanine nucleotide binding activity and phosphorylation of ras oncogene proteins. *Nature* **310**, 147-150 (1984).
93. Mulcahy, L.S., Smith, M.R. & Stacey, D.W. Requirement for ras proto-oncogene function during serum-stimulated growth of NIH 3T3 cells. *Nature* **313**, 241-243 (1985).
94. Smith, M.R., DeGudicibus, S.J. & Stacey, D.W. Requirement for c-ras proteins during viral oncogene transformation. *Nature* **320**, 540-543 (1986).
95. Kuan, C.T., Wikstrand, C.J. & Bigner, D.D. EGF mutant receptor vIII as a molecular target in cancer therapy. *Endocr Relat Cancer* **8**, 83-96 (2001).
96. Shields, J.M., Pruitt, K., McFall, A., Shaub, A. & Der, C.J. Understanding Ras: 'it ain't over 'til it's over'. *Trends in Cell Biology* **10**, 147-154 (2000).
97. Repasky, G.A., Chenette, E.J. & Der, C.J. Renewing the conspiracy theory debate: does Raf function alone to mediate Ras oncogenesis? *Trends in Cell Biology* **14**, 639-647 (2004).

98. Voice, J.K., Klemke, R.L., Le, A. & Jackson, J.H. Four human ras homologs differ in their abilities to activate Raf-1, induce transformation, and stimulate cell motility. *J Biol Chem* **274**, 17164-17170 (1999).
99. Yan, J., Roy, S., Apolloni, A., Lane, A. & Hancock, J.F. Ras isoforms vary in their ability to activate Raf-1 and phosphoinositide 3-kinase. *J Biol Chem* **273**, 24052-24056 (1998).
100. Rapp, U.R., *et al.* Structure and biological activity of v-raf, a unique oncogene transduced by a retrovirus. *Proc Natl Acad Sci U S A* **80**, 4218-4222 (1983).
101. Morrison, D.K., Kaplan, D.R., Rapp, U. & Roberts, T.M. Signal transduction from membrane to cytoplasm: growth factors and membrane-bound oncogene products increase Raf-1 phosphorylation and associated protein kinase activity. *Proc Natl Acad Sci U S A* **85**, 8855-8859 (1988).
102. Bruder, J.T., Heidecker, G. & Rapp, U.R. Serum-, TPA-, and Ras-induced expression from Ap-1/Ets-driven promoters requires Raf-1 kinase. *Genes & Development* **6**, 545-556 (1992).
103. Heidecker, G., Kolch, W., Morrison, D.K. & Rapp, U.R. The role of Raf-1 phosphorylation in signal transduction. *Adv Cancer Res* **58**, 53-73 (1992).
104. Wood, K.W., Sarnecki, C., Roberts, T.M. & Blenis, J. ras mediates nerve growth factor receptor modulation of three signal-transducing protein kinases: MAP kinase, Raf-1, and RSK. *Cell* **68**, 1041-1050 (1992).
105. Leevers, S.J., Paterson, H.F. & Marshall, C.J. Requirement for Ras in Raf activation is overcome by targeting Raf to the plasma membrane. *Nature* **369**, 411-414 (1994).
106. Marais, R., Light, Y., Paterson, H.F. & Marshall, C.J. Ras recruits Raf-1 to the plasma membrane for activation by tyrosine phosphorylation. *Embo J* **14**, 3136-3145 (1995).
107. Lito, P., Rosen, N. & Solit, D.B. Tumor adaptation and resistance to RAF inhibitors. *Nature Medicine* **19**, 1401-1409 (2013).
108. Pruitt, K. & Der, C.J. Ras and Rho regulation of the cell cycle and oncogenesis. *Cancer Lett* **171**, 1-10 (2001).
109. Brondello, J.M., Brunet, A., Pouyssegur, J. & McKenzie, F.R. The dual specificity mitogen-activated protein kinase phosphatase-1 and -2 are induced by the p42/p44MAPK cascade. *J Biol Chem* **272**, 1368-1376 (1997).
110. Kim, H.J. & Bar-Sagi, D. Modulation of signalling by Sprouty: a developing story. *Nat Rev Mol Cell Biol* **5**, 441-450 (2004).
111. Hanafusa, H., Torii, S., Yasunaga, T. & Nishida, E. Sprouty1 and Sprouty2 provide a control mechanism for the Ras/MAPK signalling pathway. *Nature Cell Biology* **4**, 850-858 (2002).
112. Stowe, I.B., *et al.* A shared molecular mechanism underlies the human rasopathies Legius syndrome and Neurofibromatosis-1. *Genes & Development* **26**, 1421-1426 (2012).
113. Rodriguez-Viciana, P., *et al.* Phosphatidylinositol-3-OH kinase as a direct target of Ras. *Nature* **370**, 527-532 (1994).
114. Britten, C.D. PI3K and MEK inhibitor combinations: examining the evidence in selected tumor types. *Cancer Chemother Pharmacol* **71**, 1395-1409 (2013).
115. Vigil, D., *et al.* Aberrant overexpression of the Rgl2 Ral small GTPase-specific guanine nucleotide exchange factor promotes pancreatic cancer growth through Ral-dependent and Ral-independent mechanisms. *J Biol Chem* **285**, 34729-34740 (2010).
116. Lim, K.H., *et al.* Divergent roles for RalA and RalB in malignant growth of human pancreatic carcinoma cells. *Curr Biol* **16**, 2385-2394 (2006).

117. Prior, I.A., Lewis, P.D. & Mattos, C. A comprehensive survey of Ras mutations in cancer. *Cancer Research* **72**, 2457-2467 (2012).
118. Quinlan, M.P., Quatela, S.E., Philips, M.R. & Settleman, J. Activated Kras, but not Hras or Nras, may initiate tumors of endodermal origin via stem cell expansion. *Mol Cell Biol* **28**, 2659-2674 (2008).
119. Lampson, B.L., *et al.* Rare codons regulate KRas oncogenesis. *Curr Biol* **23**, 70-75 (2013).
120. Ryan, D.P., Hong, T.S. & Bardeesy, N. Pancreatic adenocarcinoma. *N Engl J Med* **371**, 2140-2141 (2014).
121. Cancer Facts & Figures 2016. (American Cancer Society, Atlanta, 2016).
122. Bardeesy, N. & DePinho, R.A. Pancreatic cancer biology and genetics. *Nat Rev Cancer* **2**, 897-909 (2002).
123. Conroy, T., *et al.* FOLFIRINOX versus gemcitabine for metastatic pancreatic cancer. *N Engl J Med* **364**, 1817-1825 (2011).
124. Von Hoff, D.D., *et al.* Increased survival in pancreatic cancer with nab-paclitaxel plus gemcitabine. *N Engl J Med* **369**, 1691-1703 (2013).
125. Guerra, C. & Barbacid, M. Genetically engineered mouse models of pancreatic adenocarcinoma. *Molecular Oncology* **7**, 232-247 (2013).
126. Moskaluk, C.A., Hruban, R.H. & Kern, S.E. p16 and K-ras gene mutations in the intraductal precursors of human pancreatic adenocarcinoma. *Cancer Research* **57**, 2140-2143 (1997).
127. Yamano, M., *et al.* Genetic progression and divergence in pancreatic carcinoma. *The American Journal of Pathology* **156**, 2123-2133 (2000).
128. Luttges, J., *et al.* Allelic loss is often the first hit in the biallelic inactivation of the p53 and DPC4 genes during pancreatic carcinogenesis. *The American Journal of Pathology* **158**, 1677-1683 (2001).
129. Jones, S., *et al.* Core signaling pathways in human pancreatic cancers revealed by global genomic analyses. *Science* **321**, 1801-1806 (2008).
130. Waddell, N., *et al.* Whole genomes redefine the mutational landscape of pancreatic cancer. *Nature* **518**, 495-501 (2015).
131. Biankin, A.V., *et al.* Overexpression of p21(WAF1/CIP1) is an early event in the development of pancreatic intraepithelial neoplasia. *Cancer Research* **61**, 8830-8837 (2001).
132. Korc, M., *et al.* Overexpression of the epidermal growth factor receptor in human pancreatic cancer is associated with concomitant increases in the levels of epidermal growth factor and transforming growth factor alpha. *J Clin Invest* **90**, 1352-1360 (1992).
133. Friess, H., *et al.* Pancreatic cancer: the potential clinical relevance of alterations in growth factors and their receptors. *J Mol Med (Berl)* **74**, 35-42 (1996).
134. Sibilia, M., *et al.* The EGF receptor provides an essential survival signal for SOS-dependent skin tumor development. *Cell* **102**, 211-220 (2000).
135. Day, J.D., *et al.* Immunohistochemical evaluation of HER-2/neu expression in pancreatic adenocarcinoma and pancreatic intraepithelial neoplasms. *Hum Pathol* **27**, 119-124 (1996).
136. Watanabe, M., Nobuta, A., Tanaka, J. & Asaka, M. An effect of K-ras gene mutation on epidermal growth factor receptor signal transduction in PANC-1 pancreatic carcinoma cells. *International Journal of Cancer* **67**, 264-268 (1996).

137. Wagner, M., *et al.* Expression of a truncated EGF receptor is associated with inhibition of pancreatic cancer cell growth and enhanced sensitivity to cisplatinum. *International Journal of Cancer* **68**, 782-787 (1996).
138. Overholser, J.P., Prewett, M.C., Hooper, A.T., Waksal, H.W. & Hicklin, D.J. Epidermal growth factor receptor blockade by antibody IMC-C225 inhibits growth of a human pancreatic carcinoma xenograft in nude mice. *Cancer-Am Cancer Soc* **89**, 74-82 (2000).
139. Moore, M.J., *et al.* Erlotinib plus gemcitabine compared with gemcitabine alone in patients with advanced pancreatic cancer: a phase III trial of the National Cancer Institute of Canada Clinical Trials Group. *J Clin Oncol* **25**, 1960-1966 (2007).
140. Navas, C., *et al.* EGF Receptor Signaling Is Essential for K-Ras Oncogene-Driven Pancreatic Ductal Adenocarcinoma. *Cancer Cell* **22**, 318-330 (2012).
141. Ardito, Christine M., *et al.* EGF Receptor Is Required for KRAS-Induced Pancreatic Tumorigenesis. *Cancer Cell* **22**, 304-317 (2012).
142. Biankin, A.V., *et al.* Pancreatic cancer genomes reveal aberrations in axon guidance pathway genes. *Nature* **491**, 399-405 (2012).
143. Land, H., Parada, L.F. & Weinberg, R.A. Tumorigenic conversion of primary embryo fibroblasts requires at least two cooperating oncogenes. *Nature* **304**, 596-602 (1983).
144. Ruley, H.E. Adenovirus early region 1A enables viral and cellular transforming genes to transform primary cells in culture. *Nature* **304**, 602-606 (1983).
145. Serrano, M., Lin, A.W., McCurrach, M.E., Beach, D. & Lowe, S.W. Oncogenic ras provokes premature cell senescence associated with accumulation of p53 and p16INK4a. *Cell* **88**, 593-602 (1997).
146. Tuveson, D.A., *et al.* Endogenous oncogenic K-ras(G12D) stimulates proliferation and widespread neoplastic and developmental defects. *Cancer Cell* **5**, 375-387 (2004).
147. Haigis, K.M., *et al.* Differential effects of oncogenic K-Ras and N-Ras on proliferation, differentiation and tumor progression in the colon. *Nature Genetics* **40**, 600-608 (2008).
148. Hingorani, S.R., *et al.* Trp53R172H and KrasG12D cooperate to promote chromosomal instability and widely metastatic pancreatic ductal adenocarcinoma in mice. *Cancer Cell* **7**, 469-483 (2005).
149. Ji, H., *et al.* LKB1 modulates lung cancer differentiation and metastasis. *Nature* **448**, 807-810 (2007).
150. Johnson, L., *et al.* Somatic activation of the K-ras oncogene causes early onset lung cancer in mice. *Nature* **410**, 1111-1116 (2001).
151. Zhang, Z., *et al.* Wildtype Kras2 can inhibit lung carcinogenesis in mice. *Nature Genetics* **29**, 25-33 (2001).
152. Jackson, E.L., *et al.* The differential effects of mutant p53 alleles on advanced murine lung cancer. *Cancer Research* **65**, 10280-10288 (2005).
153. Jackson, E.L., *et al.* Analysis of lung tumor initiation and progression using conditional expression of oncogenic K-ras. *Genes & Development* **15**, 3243-3248 (2001).
154. Hingorani, S.R., *et al.* Preinvasive and invasive ductal pancreatic cancer and its early detection in the mouse. *Cancer Cell* **4**, 437-450 (2003).
155. Guerra, C., *et al.* Chronic pancreatitis is essential for induction of pancreatic ductal adenocarcinoma by K-Ras oncogenes in adult mice. *Cancer Cell* **11**, 291-302 (2007).
156. Gidekel Friedlander, S.Y., *et al.* Context-dependent transformation of adult pancreatic cells by oncogenic K-Ras. *Cancer Cell* **16**, 379-389 (2009).

157. Ying, H., *et al.* Oncogenic Kras maintains pancreatic tumors through regulation of anabolic glucose metabolism. *Cell* **149**, 656-670 (2012).
158. Collins, M.A., *et al.* Metastatic pancreatic cancer is dependent on oncogenic Kras in mice. *PLoS ONE* **7**, e49707 (2012).
159. Bardeesy, N., *et al.* Both p16(Ink4a) and the p19(Arf)-p53 pathway constrain progression of pancreatic adenocarcinoma in the mouse. *Proc Natl Acad Sci U S A* **103**, 5947-5952 (2006).
160. Bardeesy, N., *et al.* Smad4 is dispensable for normal pancreas development yet critical in progression and tumor biology of pancreas cancer. *Genes & Development* **20**, 3130-3146 (2006).
161. Collins, M.A., *et al.* Oncogenic Kras is required for both the initiation and maintenance of pancreatic cancer in mice. *J Clin Invest* **122**, 639-653 (2012).
162. Pagliarini, R., Shao, W. & Sellers, W.R. Oncogene addiction: pathways of therapeutic response, resistance, and road maps toward a cure. *EMBO Rep* **16**, 280-296 (2015).
163. Weinstein, I.B. Cancer. Addiction to oncogenes--the Achilles heal of cancer. *Science* **297**, 63-64 (2002).
164. Vogelstein, B., *et al.* Cancer genome landscapes. *Science* **339**, 1546-1558 (2013).
165. Chin, L., *et al.* Essential role for oncogenic Ras in tumour maintenance. *Nature* **400**, 468-472 (1999).
166. Fisher, G.H. Induction and apoptotic regression of lung adenocarcinomas by regulation of a K-Ras transgene in the presence and absence of tumor suppressor genes. *Genes & Development* **15**, 3249-3262 (2001).
167. Shirasawa, S., Furuse, M., Yokoyama, N. & Sasazuki, T. Altered growth of human colon cancer cell lines disrupted at activated Ki-ras. *Science* **260**, 85-88 (1993).
168. Singh, A., *et al.* A gene expression signature associated with "K-Ras addiction" reveals regulators of EMT and tumor cell survival. *Cancer Cell* **15**, 489-500 (2009).
169. Baines, A.T., *et al.* Use of retrovirus expression of interfering RNA to determine the contribution of activated K-Ras and ras effector expression to human tumor cell growth. *Methods Enzymol* **407**, 556-574 (2006).
170. Fleming, J.B., Shen, G.L., Holloway, S.E., Davis, M. & Brekken, R.A. Molecular consequences of silencing mutant K-ras in pancreatic cancer cells: justification for K-ras-directed therapy. *Mol Cancer Res* **3**, 413-423 (2005).
171. Brummelkamp, T.R., Bernards, R. & Agami, R. Stable suppression of tumorigenicity by virus-mediated RNA interference. *Cancer Cell* **2**, 243-247 (2002).
172. Zorde Khvalevsky, E., *et al.* Mutant KRAS is a druggable target for pancreatic cancer. *Proc Natl Acad Sci U S A* **110**, 20723-20728 (2013).
173. Collisson, E.A., *et al.* Subtypes of pancreatic ductal adenocarcinoma and their differing responses to therapy. *Nature Medicine* **17**, 500-503 (2011).
174. Cowley, M.J., *et al.* Understanding pancreatic cancer genomes. *J Hepatobiliary Pancreat Sci* **20**, 549-556 (2013).
175. Kapoor, A., *et al.* Yap1 activation enables bypass of oncogenic Kras addiction in pancreatic cancer. *Cell* **158**, 185-197 (2014).
176. Zhang, W., *et al.* Downstream of mutant KRAS, the transcription regulator YAP is essential for neoplastic progression to pancreatic ductal adenocarcinoma. *Science Signaling* **7**, ra42 (2014).

177. Shao, D.D., *et al.* KRAS and YAP1 converge to regulate EMT and tumor survival. *Cell* **158**, 171-184 (2014).
178. Lin, L., *et al.* The Hippo effector YAP promotes resistance to RAF- and MEK-targeted cancer therapies. *Nature Genetics* **47**, 250-256 (2015).
179. Huggett, M.T., *et al.* Phase I/II study of verteporfin photodynamic therapy in locally advanced pancreatic cancer. *Br J Cancer* **110**, 1698-1704 (2014).
180. Jermyn, M., *et al.* CT contrast predicts pancreatic cancer treatment response to verteporfin-based photodynamic therapy. *Phys Med Biol* **59**, 1911-1921 (2014).
181. Viale, A., *et al.* Oncogene ablation-resistant pancreatic cancer cells depend on mitochondrial function. *Nature* **514**, 628-632 (2014).
182. Slebos, R.J., *et al.* K-ras oncogene activation as a prognostic marker in adenocarcinoma of the lung. *N Engl J Med* **323**, 561-565 (1990).
183. Mitsudomi, T., *et al.* ras gene mutations in non-small cell lung cancers are associated with shortened survival irrespective of treatment intent. *Cancer Research* **51**, 4999-5002 (1991).
184. Andreyev, H.J., *et al.* Kirsten ras mutations in patients with colorectal cancer: the 'RASCAL II' study. *Br J Cancer* **85**, 692-696 (2001).
185. Zlobec, I., *et al.* Combined analysis of specific KRAS mutation, BRAF and microsatellite instability identifies prognostic subgroups of sporadic and hereditary colorectal cancer. *International Journal of Cancer* **127**, 2569-2575 (2010).
186. Ledford, H. Cancer: The Ras renaissance. *Nature* **520**, 278-280 (2015).
187. Appels, N.M., Beijnen, J.H. & Schellens, J.H. Development of farnesyl transferase inhibitors: a review. *The oncologist* **10**, 565-578 (2005).
188. Vigil, D., Cherfils, J., Rossman, K.L. & Der, C.J. Ras superfamily GEFs and GAPs: validated and tractable targets for cancer therapy? *Nat Rev Cancer* **10**, 842-857 (2010).
189. Taveras, A.G., *et al.* Ras oncoprotein inhibitors: the discovery of potent, ras nucleotide exchange inhibitors and the structural determination of a drug-protein complex. *Bioorg Med Chem* **5**, 125-133 (1997).
190. Peri, F., *et al.* Design, synthesis and biological evaluation of sugar-derived Ras inhibitors. *Chembiochem* **6**, 1839-1848 (2005).
191. Herrmann, C., *et al.* Sulindac sulfide inhibits Ras signaling. *Oncogene* **17**, 1769-1776 (1998).
192. Waldmann, H., *et al.* Sulindac-derived Ras pathway inhibitors target the Ras-Raf interaction and downstream effectors in the Ras pathway. *Angew Chem Int Ed Engl* **43**, 454-458 (2004).
193. Karaguni, I.M., *et al.* New indene-derivatives with anti-proliferative properties. *Bioorg Med Chem Lett* **12**, 709-713 (2002).
194. Kato, K., *et al.* Isoprenoid addition to Ras protein is the critical modification for its membrane association and transforming activity. *Proc Natl Acad Sci U S A* **89**, 6403-6407 (1992).
195. Cox, A.D. & Der, C.J. Farnesyltransferase inhibitors and cancer treatment: targeting simply Ras? *Biochim Biophys Acta* **1333**, F51-71 (1997).
196. Baines, A.T., Xu, D. & Der, C.J. Inhibition of Ras for cancer treatment: the search continues. *Future Med Chem* **3**, 1787-1808 (2011).

197. Sinensky, M., Beck, L.A., Leonard, S. & Evans, R. Differential inhibitory effects of lovastatin on protein isoprenylation and sterol synthesis. *J Biol Chem* **265**, 19937-19941 (1990).
198. Tamanoi, F. & Mitsuzawa, H. Use of yeast for identification of farnesyltransferase inhibitors and for generation of mutant farnesyltransferases. *Methods Enzymol* **255**, 82-91 (1995).
199. Reiss, Y., Goldstein, J.L., Seabra, M.C., Casey, P.J. & Brown, M.S. Inhibition of purified p21ras farnesyl:protein transferase by Cys-AAX tetrapeptides. *Cell* **62**, 81-88 (1990).
200. Moores, S.L., *et al.* Sequence dependence of protein isoprenylation. *J Biol Chem* **266**, 14603-14610 (1991).
201. James, G.L., *et al.* Benzodiazepine peptidomimetics: potent inhibitors of Ras farnesylation in animal cells. *Science* **260**, 1937-1942 (1993).
202. Kohl, N.E., *et al.* Selective inhibition of ras-dependent transformation by a farnesyltransferase inhibitor. *Science* **260**, 1934-1937 (1993).
203. Kohl, N.E., *et al.* Inhibition of farnesyltransferase induces regression of mammary and salivary carcinomas in ras transgenic mice. *Nature Medicine* **1**, 792-797 (1995).
204. Kohl, N.E., *et al.* Protein farnesyltransferase inhibitors block the growth of ras-dependent tumors in nude mice. *Proc Natl Acad Sci U S A* **91**, 9141-9145 (1994).
205. Cox, A.D., Hisaka, M.M., Buss, J.E. & Der, C.J. Specific isoprenoid modification is required for function of normal, but not oncogenic, Ras protein. *Mol Cell Biol* **12**, 2606-2615 (1992).
206. Hancock, J.F., Cadwallader, K. & Marshall, C.J. Methylation and proteolysis are essential for efficient membrane binding of prenylated p21K-ras(B). *Embo J* **10**, 641-646 (1991).
207. James, G.L., Goldstein, J.L. & Brown, M.S. Polylysine and CVIM sequences of K-RasB dictate specificity of prenylation and confer resistance to benzodiazepine peptidomimetic in vitro. *J Biol Chem* **270**, 6221-6226 (1995).
208. Whyte, D.B., *et al.* K- and N-Ras are geranylgeranylated in cells treated with farnesyl protein transferase inhibitors. *J Biol Chem* **272**, 14459-14464 (1997).
209. Rowell, C.A., Kowalczyk, J.J., Lewis, M.D. & Garcia, A.M. Direct demonstration of geranylgeranylation and farnesylation of Ki-Ras in vivo. *J Biol Chem* **272**, 14093-14097 (1997).
210. Court, H., *et al.* Isoprenylcysteine carboxylmethyltransferase deficiency exacerbates KRAS-driven pancreatic neoplasia via Notch suppression. *J Clin Invest* **123**, 4681-4694 (2013).
211. Wahlstrom, A.M., *et al.* Rce1 deficiency accelerates the development of K-RAS-induced myeloproliferative disease. *Blood* **109**, 763-768 (2007).
212. Bergo, M.O., *et al.* Targeted inactivation of the isoprenylcysteine carboxyl methyltransferase gene causes mislocalization of K-Ras in mammalian cells. *J Biol Chem* **275**, 17605-17610 (2000).
213. Wahlstrom, A.M., *et al.* Inactivating Icmt ameliorates K-RAS-induced myeloproliferative disease. *Blood* **112**, 1357-1365 (2008).
214. Laheru, D., *et al.* Integrated preclinical and clinical development of S-trans, trans-Farnesylthiosalicylic Acid (FTS, Salirasib) in pancreatic cancer. *Invest New Drugs* **30**, 2391-2399 (2012).

215. Riely, G.J., *et al.* A phase II trial of Salirasib in patients with lung adenocarcinomas with KRAS mutations. *J Thorac Oncol* **6**, 1435-1437 (2011).
216. Zimmermann, G., *et al.* Small molecule inhibition of the KRAS-PDEdelta interaction impairs oncogenic KRAS signalling. *Nature* **497**, 638-642 (2013).
217. Chandra, A., *et al.* The GDI-like solubilizing factor PDE δ sustains the spatial organization and signalling of Ras family proteins. *Nature Cell Biology* **14**, 148-148 (2012).
218. Nancy, V., Callebaut, I., El Marjou, A. & de Gunzburg, J. The delta subunit of retinal rod cGMP phosphodiesterase regulates the membrane association of Ras and Rap GTPases. *J Biol Chem* **277**, 15076-15084 (2002).
219. Baker, N.M. & Der, C.J. Cancer: Drug for an 'undruggable' protein. *Nature* **497**, 577-578 (2013).
220. Zhang, H., *et al.* Deletion of PrBP/delta impedes transport of GRK1 and PDE6 catalytic subunits to photoreceptor outer segments. *Proc Natl Acad Sci U S A* **104**, 8857-8862 (2007).
221. Sung, P.J., *et al.* Phosphorylated K-Ras limits cell survival by blocking Bcl-xL sensitization of inositol trisphosphate receptors. *Proc Natl Acad Sci U S A* **110**, 20593-20598 (2013).
222. Barcelo, C., *et al.* Phosphorylation at Ser-181 of oncogenic KRAS is required for tumor growth. *Cancer Research* **74**, 1190-1199 (2014).
223. Sasaki, A.T., *et al.* Ubiquitination of K-Ras enhances activation and facilitates binding to select downstream effectors. *Science Signaling* **4**, ra13 (2011).
224. Yang, M.H., *et al.* Regulation of RAS oncogenicity by acetylation. *Proc Natl Acad Sci U S A* **109**, 10843-10848 (2012).
225. Yang, M.H., *et al.* HDAC6 and SIRT2 regulate the acetylation state and oncogenic activity of mutant K-RAS. *Mol Cancer Res* **11**, 1072-1077 (2013).
226. Lim, K.H., Ancrile, B.B., Kashatus, D.F. & Counter, C.M. Tumour maintenance is mediated by eNOS. *Nature* **452**, 646-649 (2008).
227. Lampson, B.L., *et al.* Targeting eNOS in pancreatic cancer. *Cancer Research* **72**, 4472-4482 (2012).
228. Maurer, T., *et al.* Small-molecule ligands bind to a distinct pocket in Ras and inhibit SOS-mediated nucleotide exchange activity. *Proc Natl Acad Sci U S A* **109**, 5299-5304 (2012).
229. Sun, Q., *et al.* Discovery of small molecules that bind to K-Ras and inhibit Sos-mediated activation. *Angew Chem Int Ed Engl* **51**, 6140-6143 (2012).
230. Ahmadian, M.R., *et al.* Guanosine triphosphatase stimulation of oncogenic Ras mutants. *Proc Natl Acad Sci U S A* **96**, 7065-7070 (1999).
231. Ostrem, J.M., Peters, U., Sos, M.L., Wells, J.A. & Shokat, K.M. K-Ras(G12C) inhibitors allosterically control GTP affinity and effector interactions. *Nature* **503**, 548-551 (2013).
232. Lito, P., Solomon, M., Li, L.S., Hansen, R. & Rosen, N. Allele-specific inhibitors inactivate mutant KRAS G12C by a trapping mechanism. *Science* **351**, 604-608 (2016).
233. Patricelli, M.P., *et al.* Selective Inhibition of Oncogenic KRAS Output with Small Molecules Targeting the Inactive State. *Cancer Discovery* **6**, 316-329 (2016).
234. Lim, S.M., *et al.* Therapeutic targeting of oncogenic K-Ras by a covalent catalytic site inhibitor. *Angew Chem Int Ed Engl* **53**, 199-204 (2014).

235. Comprehensive molecular profiling of lung adenocarcinoma. *Nature* **511**, 543-550 (2014).
236. Liao, J., *et al.* Two conformational states of Ras GTPase exhibit differential GTP-binding kinetics. *Biochem Biophys Res Commun* **369**, 327-332 (2008).
237. Ihle, N.T., *et al.* Effect of KRAS oncogene substitutions on protein behavior: implications for signaling and clinical outcome. *J Natl Cancer Inst* **104**, 228-239 (2012).
238. Buhrman, G., Holzapfel, G., Fetics, S. & Mattos, C. Allosteric modulation of Ras positions Q61 for a direct role in catalysis. *Proc Natl Acad Sci U S A* **107**, 4931-4936 (2010).
239. Collisson, E.A., *et al.* A central role for RAF-->MEK-->ERK signaling in the genesis of pancreatic ductal adenocarcinoma. *Cancer Discovery* **2**, 685-693 (2012).
240. Blasco, R.B., *et al.* c-Raf, but not B-Raf, is essential for development of K-Ras oncogene-driven non-small cell lung carcinoma. *Cancer Cell* **19**, 652-663 (2011).
241. Davies, H., *et al.* Mutations of the BRAF gene in human cancer. *Nature* **417**, 949-954 (2002).
242. Wellbrock, C., *et al.* V599EB-RAF is an oncogene in melanocytes. *Cancer Research* **64**, 2338-2342 (2004).
243. Lyons, J.F., Wilhelm, S., Hibner, B. & Bollag, G. Discovery of a novel Raf kinase inhibitor. *Endocr Relat Cancer* **8**, 219-225 (2001).
244. Wilhelm, S.M., *et al.* BAY 43-9006 exhibits broad spectrum oral antitumor activity and targets the RAF/MEK/ERK pathway and receptor tyrosine kinases involved in tumor progression and angiogenesis. *Cancer Research* **64**, 7099-7109 (2004).
245. Poulikakos, P.I., Zhang, C., Bollag, G., Shokat, K.M. & Rosen, N. RAF inhibitors transactivate RAF dimers and ERK signalling in cells with wild-type BRAF. *Nature* **464**, 427-430 (2010).
246. Hatzivassiliou, G., *et al.* RAF inhibitors prime wild-type RAF to activate the MAPK pathway and enhance growth. *Nature* **464**, 431-435 (2010).
247. Heidorn, S.J., *et al.* Kinase-dead BRAF and oncogenic RAS cooperate to drive tumor progression through CRAF. *Cell* **140**, 209-221 (2010).
248. Peng, S.B., *et al.* Inhibition of RAF Isoforms and Active Dimers by LY3009120 Leads to Anti-tumor Activities in RAS or BRAF Mutant Cancers. *Cancer Cell* **28**, 384-398 (2015).
249. Gilmartin, A.G., *et al.* GSK1120212 (JTP-74057) is an inhibitor of MEK activity and activation with favorable pharmacokinetic properties for sustained in vivo pathway inhibition. *Clin Cancer Res* **17**, 989-1000 (2011).
250. Engelman, J.A., *et al.* Effective use of PI3K and MEK inhibitors to treat mutant Kras G12D and PIK3CA H1047R murine lung cancers. *Nature Medicine* **14**, 1351-1356 (2008).
251. Gupta, S., *et al.* Binding of ras to phosphoinositide 3-kinase p110alpha is required for ras-driven tumorigenesis in mice. *Cell* **129**, 957-968 (2007).
252. Castellano, E., *et al.* Requirement for interaction of PI3-kinase p110alpha with RAS in lung tumor maintenance. *Cancer Cell* **24**, 617-630 (2013).
253. Baer, R., *et al.* Pancreatic cell plasticity and cancer initiation induced by oncogenic Kras is completely dependent on wild-type PI 3-kinase p110alpha. *Genes & Development* **28**, 2621-2635 (2014).

254. Eser, S., *et al.* Selective requirement of PI3K/PDK1 signaling for Kras oncogene-driven pancreatic cell plasticity and cancer. *Cancer Cell* **23**, 406-420 (2013).
255. Ma, L., *et al.* Identification of S664 TSC2 phosphorylation as a marker for extracellular signal-regulated kinase mediated mTOR activation in tuberous sclerosis and human cancer. *Cancer Research* **67**, 7106-7112 (2007).
256. Zimmermann, S. & Moelling, K. Phosphorylation and regulation of Raf by Akt (protein kinase B). *Science* **286**, 1741-1744 (1999).
257. Roberts, P.J., *et al.* Combined PI3K/mTOR and MEK inhibition provides broad antitumor activity in faithful murine cancer models. *Clin Cancer Res* **18**, 5290-5303 (2012).
258. Migliardi, G., *et al.* Inhibition of MEK and PI3K/mTOR suppresses tumor growth but does not cause tumor regression in patient-derived xenografts of RAS-mutant colorectal carcinomas. *Clin Cancer Res* **18**, 2515-2525 (2012).
259. Haagensen, E.J., Kyle, S., Beale, G.S., Maxwell, R.J. & Newell, D.R. The synergistic interaction of MEK and PI3K inhibitors is modulated by mTOR inhibition. *Br J Cancer* **106**, 1386-1394 (2012).
260. Roy, S.K., Srivastava, R.K. & Shankar, S. Inhibition of PI3K/AKT and MAPK/ERK pathways causes activation of FOXO transcription factor, leading to cell cycle arrest and apoptosis in pancreatic cancer. *J Mol Signal* **5**, 10 (2010).
261. Hofmann, I., *et al.* K-RAS mutant pancreatic tumors show higher sensitivity to MEK than to PI3K inhibition in vivo. *PLoS ONE* **7**, e44146 (2012).
262. Alagesan, B., *et al.* Combined MEK and PI3K inhibition in a mouse model of pancreatic cancer. *Clin Cancer Res* **21**, 396-404 (2015).
263. Athuluri-Divakar, S.K., *et al.* A Small Molecule RAS-Mimetic Disrupts RAS Association with Effector Proteins to Block Signaling. *Cell* **165**, 643-655 (2016).
264. Kaelin, W.G., Jr. The concept of synthetic lethality in the context of anticancer therapy. *Nat Rev Cancer* **5**, 689-698 (2005).
265. Hartman, J.L.t., Garvik, B. & Hartwell, L. Principles for the buffering of genetic variation. *Science* **291**, 1001-1004 (2001).
266. Torrance, C.J., Agrawal, V., Vogelstein, B. & Kinzler, K.W. Use of isogenic human cancer cells for high-throughput screening and drug discovery. *Nature Biotechnology* **19**, 940-945 (2001).
267. Luo, J., *et al.* A genome-wide RNAi screen identifies multiple synthetic lethal interactions with the Ras oncogene. *Cell* **137**, 835-848 (2009).
268. Sarthy, A.V., *et al.* Survivin depletion preferentially reduces the survival of activated K-Ras-transformed cells. *Mol Cancer Ther* **6**, 269-276 (2007).
269. Vicent, S., *et al.* Wilms tumor 1 (WT1) regulates KRAS-driven oncogenesis and senescence in mouse and human models. *J Clin Invest* **120**, 3940-3952 (2010).
270. Corcoran, R.B., *et al.* Synthetic lethal interaction of combined BCL-XL and MEK inhibition promotes tumor regressions in KRAS mutant cancer models. *Cancer Cell* **23**, 121-128 (2013).
271. Wang, Y., *et al.* Critical role for transcriptional repressor Snail2 in transformation by oncogenic RAS in colorectal carcinoma cells. *Oncogene* **29**, 4658-4670 (2010).
272. Barbie, D.A., *et al.* Systematic RNA interference reveals that oncogenic KRAS-driven cancers require TBK1. *Nature* **462**, 108-112 (2009).

273. Singh, A., *et al.* TAK1 inhibition promotes apoptosis in KRAS-dependent colon cancers. *Cell* **148**, 639-650 (2012).
274. Steckel, M., *et al.* Determination of synthetic lethal interactions in KRAS oncogene-dependent cancer cells reveals novel therapeutic targeting strategies. *Cell Res* **22**, 1227-1245 (2012).
275. Scholl, C., *et al.* Synthetic lethal interaction between oncogenic KRAS dependency and STK33 suppression in human cancer cells. *Cell* **137**, 821-834 (2009).
276. Babij, C., *et al.* STK33 kinase activity is nonessential in KRAS-dependent cancer cells. *Cancer Research* **71**, 5818-5826 (2011).
277. Weiwer, M., *et al.* A Potent and Selective Quinoxalinone-Based STK33 Inhibitor Does Not Show Synthetic Lethality in KRAS-Dependent Cells. *ACS Med Chem Lett* **3**, 1034-1038 (2012).
278. Luo, T., *et al.* STK33 kinase inhibitor BRD-8899 has no effect on KRAS-dependent cancer cell viability. *Proc Natl Acad Sci U S A* **109**, 2860-2865 (2012).
279. Azoitei, N., *et al.* Targeting of KRAS mutant tumors by HSP90 inhibitors involves degradation of STK33. *J Exp Med* **209**, 697-711 (2012).
280. Frohling, S. & Scholl, C. STK33 kinase is not essential in KRAS-dependent cells--letter. *Cancer Research* **71**, 7716; author reply 7717 (2011).
281. Muvaffak, A., *et al.* Evaluating TBK1 as a therapeutic target in cancers with activated IRF3. *Mol Cancer Res* **12**, 1055-1066 (2014).
282. Chien, Y., *et al.* RalB GTPase-mediated activation of the IkappaB family kinase TBK1 couples innate immune signaling to tumor cell survival. *Cell* **127**, 157-170 (2006).
283. Zhu, Z., *et al.* Inhibition of KRAS-driven tumorigenicity by interruption of an autocrine cytokine circuit. *Cancer Discovery* **4**, 452-465 (2014).
284. Ran, F.A., *et al.* Genome engineering using the CRISPR-Cas9 system. *Nature Protocols* **8**, 2281-2308 (2013).
285. Wang, T., Wei, J.J., Sabatini, D.M. & Lander, E.S. Genetic screens in human cells using the CRISPR-Cas9 system. *Science* **343**, 80-84 (2014).
286. Shalem, O., *et al.* Genome-scale CRISPR-Cas9 knockout screening in human cells. *Science* **343**, 84-87 (2014).
287. Shi, J., *et al.* Discovery of cancer drug targets by CRISPR-Cas9 screening of protein domains. *Nature Biotechnology* **33**, 661-667 (2015).

CHAPTER 2

Adaptive and reversible resistance to Kras inhibition in pancreatic cancer cells

Pan-Yu Chen[1, 2*], Mandar Deepak Muzumdar[1, 3, 4*], Kimberly Judith Dorans[1], Rebecca Robbins[1], Arjun Bhutkar[1], Amanda del Rosario[1], Philipp Mertins[5], Jana Qiao[5], Steven Carr[5], and Tyler Jacks[1, 2, 6]

Author Affiliations:
[1] David H. Koch Institute for Integrative Cancer Research, Massachusetts Institute of Technology, 500 Main Street, Cambridge, MA 02139, USA
[2] Department of Biology, Massachusetts Institute of Technology, 77 Massachusetts Avenue, Cambridge, MA 02139, USA
[3] Harvard Medical School, 25 Shattuck Street, Boston, MA 02115, USA
[4] Dana-Farber Cancer Institute, 450 Brookline Avenue, Boston, MA 02115, USA
[5] Broad Institute of MIT and Harvard, 415 Main Street, Cambridge, MA 02142, USA
[6]Howard Hughes Medical Institute, Massachusetts Institute of Technology, Cambridge, MA 02139, USA

[*]P-Y.C. and M.D.M. contributed equally to this work.

P-Y.C., M.D.M., and T.J. designed the study; P-Y.C., M.D.M., K.J.D., and R.R. performed all of the molecular biology, *in vitro*, and *in vivo* experiments in the laboratory of T.J.; A.B. conducted bioinformatics analyses on the RNA-sequencing data; P-Y.C. and A.R. conducted the iTRAQ experiments and analyses in the Biopolymers and Proteomics Core Facility at the Koch Institute; P.M. and J.Q. conducted the SILAC experiments and analyses in the laboratory of S.C.; a large part of this chapter is adapted from a manuscript that was written by P-Y.C., M.D.M., and T.J., with comments from other co-authors.

ABSTRACT

Activating *KRAS* mutations are the hallmark genetic alterations in pancreatic ductal adenocarcinoma (PDAC) and key drivers of PDAC initiation and progression. Despite increased efforts to develop novel KRAS inhibitors, the degree of *KRAS* oncogene addiction in PDAC cells remains unclear. Here, we analyzed the requirement of endogenous Kras for the maintenance of murine PDAC cells using an inducible shRNA-based system that enables precise temporal control of endogenous *Kras* expression. Surprisingly, the majority of murine PDAC cells analyzed tolerated acute and sustained Kras knockdown by adapting to a reversible cell state, characterized by differences in cell morphology, proliferative kinetics, and tumor-initiating capacity. While significant mutational or transcriptional changes were not observed in the Kras-inhibited state, global phosphoproteomic profiling revealed alterations in cell signaling, including increased phosphorylation of focal adhesion pathway components. Accordingly, Kras-inhibited cells displayed prominent focal adhesion plaque structures, enhanced adherence properties, and increased dependency on adhesion for viability *in vitro*. Our analyses highlight the possibility of adaptive non-genetic and non-transcriptional mechanisms of resistance to Kras inhibition. Furthermore, we have identified candidate proteins whose signaling activities are altered in the Kras-inhibited state, providing a basis for rational design of combination therapeutic strategies with novel Kras inhibitors.

INTRODUCTION

Pancreatic cancer, of which 85% is pancreatic ductal adenocarcinoma (PDAC), is an aggressive and devastating disease that is largely refractory to current standard of care therapies[1]. In the United States, 53,070 new pancreatic cancer cases and 41,780 pancreatic cancer-associated deaths are estimated to occur in 2016, making it the fourth leading cause of cancer death[2]. Although recent advances in multi-agent chemotherapy have increased median survival in advanced disease by several months compared to conventional single-agent gemcitabine treatment, the 5-year survival rate for PDAC patients remains low at 7%[2-4]. Furthermore, the vast majority of patients who undergo potentially curative surgical resection relapse with advanced disease. Together, these statistics underscore an urgent need for novel therapeutic options with improved efficacy and reduced toxicity for this disease.

Genomic studies have revealed that activating mutations of the proto-oncogene *KRAS* are the hallmark of PDAC, occurring in >90% of advanced PDACs[5-7]. *KRAS* encodes a small GTPase that regulates a diverse set of cellular processes, including proliferation, differentiation, adhesion, and survival. In cancer cells, somatic missense mutations, occurring predominantly in codons 12, 13, and 61 of KRAS, abolish the interaction between KRAS and GTPase-activating proteins, resulting in the accumulation of active GTP-bound KRAS and constitutive effector signaling[8]. As oncogenic KRAS signaling potentially contributes to multiple facets of malignant transformation, its precise biological functions in distinct cancer types appear context-dependent and remain to be fully elucidated[9-12].

The high frequency of activating *KRAS* mutations implies that oncogenic KRAS may be a driver of PDAC initiation and progression. Various mouse models have demonstrated that the expression of mutant *Kras* in the mouse pancreas leads to the development of precursor

pancreatic intraepithelial neoplasia (PanINs) and PDAC, confirming the role of oncogenic KRAS in tumor initiation[9,13,14]. In contrast, the requirement of KRAS for PDAC progression and maintenance remains unresolved. RNA interference-mediated knockdown of endogenous *KRAS* in human cell lines demonstrates variable dependencies of PDAC cells on *KRAS* for survival[15]. In accordance with this observation, gene expression profiling of human PDAC tumors reveals distinct molecular subtypes that are associated with varying *KRAS* dependencies[16]. In established *Kras*-driven mouse PDAC tumors, the withdrawal of oncogenic *Kras* transgene expression results in rapid tumor regression, suggesting that sustained expression of oncogenic *Kras* is essential for PDAC maintenance[9,12]. Although the removal of oncogenic *Kras* is initially detrimental, tumor relapse via Kras-dependent and -independent bypass mechanisms is observed in these mouse models[17,18].

Since at least a subset of PDAC cells and tumors exhibit *KRAS* oncogene addiction, KRAS inhibition may be a useful therapeutic approach for PDAC treatment. Unfortunately, effective pharmacological KRAS inhibitors have not been developed to date[8]. A deeper understanding of the essentiality of KRAS for tumor maintenance and the degree of KRAS inhibition required to impair PDAC cell survival can provide important insights into the role of KRAS in PDAC and facilitate the development of KRAS-directed therapies. Furthermore, given that resistance against single-agent targeted therapies frequently emerges after prolonged periods of treatment[19,20], it is critical to preemptively strategize effective treatment methods to circumvent possible resistance. Elucidation of the molecular basis for cancer therapy resistance has led to the general conception that resistance often arises from the selection of pre-existing rare cells that have acquired resistance-conferring genetic alterations[19,21,22]. In this case, combined inhibition of multiple nodes of a single pathway or simultaneous targeting of distinct

pathways can be effective in overcoming resistance. However, recent studies have suggested that non-mutational mechanisms of drug resistance are also possible[19,20,23,24], for which the intermittent dosing of the same inhibitor can prevent resistance from developing and induce a re-treatment response[25,26].

In this study, we sought to assess the requirement of oncogenic *Kras* for PDAC maintenance and potential resistance mechanisms that may arise in response to Kras inhibition. We examined the consequence of acute and sustained Kras knockdown in murine PDAC cells *in vitro* and *in vivo*. Additionally, we conducted global gene expression and phosphoproteomic profiling of PDAC cells before and after *Kras* knockdown to decipher the precise mechanisms that mediate escape from *Kras* oncogene addiction. Through these studies, we defined an adaptive and reversible state of Kras inhibition marked by prominent alterations in cell morphology, proliferative kinetics, and cell signaling, shedding light on resistance mechanisms to Kras inhibition in PDAC cells. Furthermore, candidate targets revealed by these analyses offer the potential for the design of rational combination therapies with novel KRAS inhibitors for clinical application in PDAC.

RESULTS

Generation of a doxycycline-inducible shRNA *in vitro* system that enables the temporal control of endogenous *Kras* expression

In order to elucidate the consequence of inhibiting endogenous *Kras* in PDAC cells, we first derived stable cell lines from three distinct primary tumors (A, B, and D) from an autochthonous PDAC mouse model (*Pdx1-CreER; $Kras^{LSL\text{-}G12D/+}$; $p53^{flox/flox}$*), which faithfully recapitulates the progression and histology of human PDAC upon the induction of Cre

recombinase expression[13]. We used murine cells with defined genetic alterations frequently observed in human PDACs (*Kras* and *p53*)[7,27] to minimize genetic variability between tumor cell lines in our analyses. We transduced these cell lines with a doxycycline-inducible shRNA-mediated knockdown system that enables the temporal control of endogenous *Kras* expression (**Fig. 1A**). In this system, partial inhibition and the subsequent reactivation of endogenous *Kras* are achieved by simple administration and withdrawal of doxycycline (DOX) treatment. We employed two DOX-inducible miR30-based hairpins targeting the 3' UTR of *Kras* (shKras.1442 or shKras.923) or a control hairpin targeting *luciferase* (shLuc). Importantly, the Kras hairpins do not distinguish between wild-type and mutant alleles of *Kras* due to 3' UTR targeting. Following retroviral transduction, we selected for cells with robust hairpin expression by 24-48 hours of DOX treatment (prior to visible phenotypic consequences of Kras knockdown) to induce concomitant expression of a GFP reporter and the hairpin, and isolated single cell clones that express GFP at the highest levels by FACS. Finally, we confirmed stable and effective on-target Kras protein and mRNA knockdown at >70% in these cell clones under DOX treatment (**Figs. 1B-C, Supplementary Figs. 1A-C**).

Murine PDAC cells tolerate stable Kras knockdown *in vitro* and *in vivo*

Rather than undergoing permanent growth arrest or apoptosis, all PDAC cells analyzed were able to tolerate both acute and sustained Kras knockdown and continued to proliferate *in vitro*. Short-term DOX treatment for 3-5 days ("ST DOX") of shKras-expressing cells, but not shLuc-expressing cells, resulted in significantly altered cell morphology and decreased proliferation, consistent with a partial requirement of endogenous *Kras* expression for PDAC maintenance (**Figs. 1D and F**). Under prolonged DOX treatment for >21 days ("LT DOX"),

shKras-expressing cells retained GFP expression, indicative of sustained shKras expression, and demonstrated persistent Kras mRNA and protein knockdown (**Figs. 1B-C**). Interestingly, these LT DOX cells continued to proliferate with slower kinetics than untreated cells ("No DOX") and maintained the morphological changes (**Figs. 1E-F**).

To further examine the requirement of endogenous *Kras* for PDAC maintenance *in vivo*, we transplanted untreated shKras-transduced cells subcutaneously into nude mice, allowed tumors to form, and induced hairpin expression with DOX feed. Acute *Kras* knockdown following short-term DOX treatment (4 days) in established tumors resulted in decreased tumor growth and even tumor regression, attributable in part to decreased proliferation as evident by reduced BrdU incorporation (**Supplementary Figs. 2A-C**). Despite long-term DOX treatment of mice (>6 weeks; LT DOX), tumors grew at decreased rates compared to untreated tumors and retained GFP expression, indicative of stable knockdown (**Supplementary Fig. 2D**). Taken together, these observations suggest that endogenous levels of *Kras* expression are not absolutely essential for maintaining murine PDAC cell proliferation and survival *in vitro* or *in vivo*.

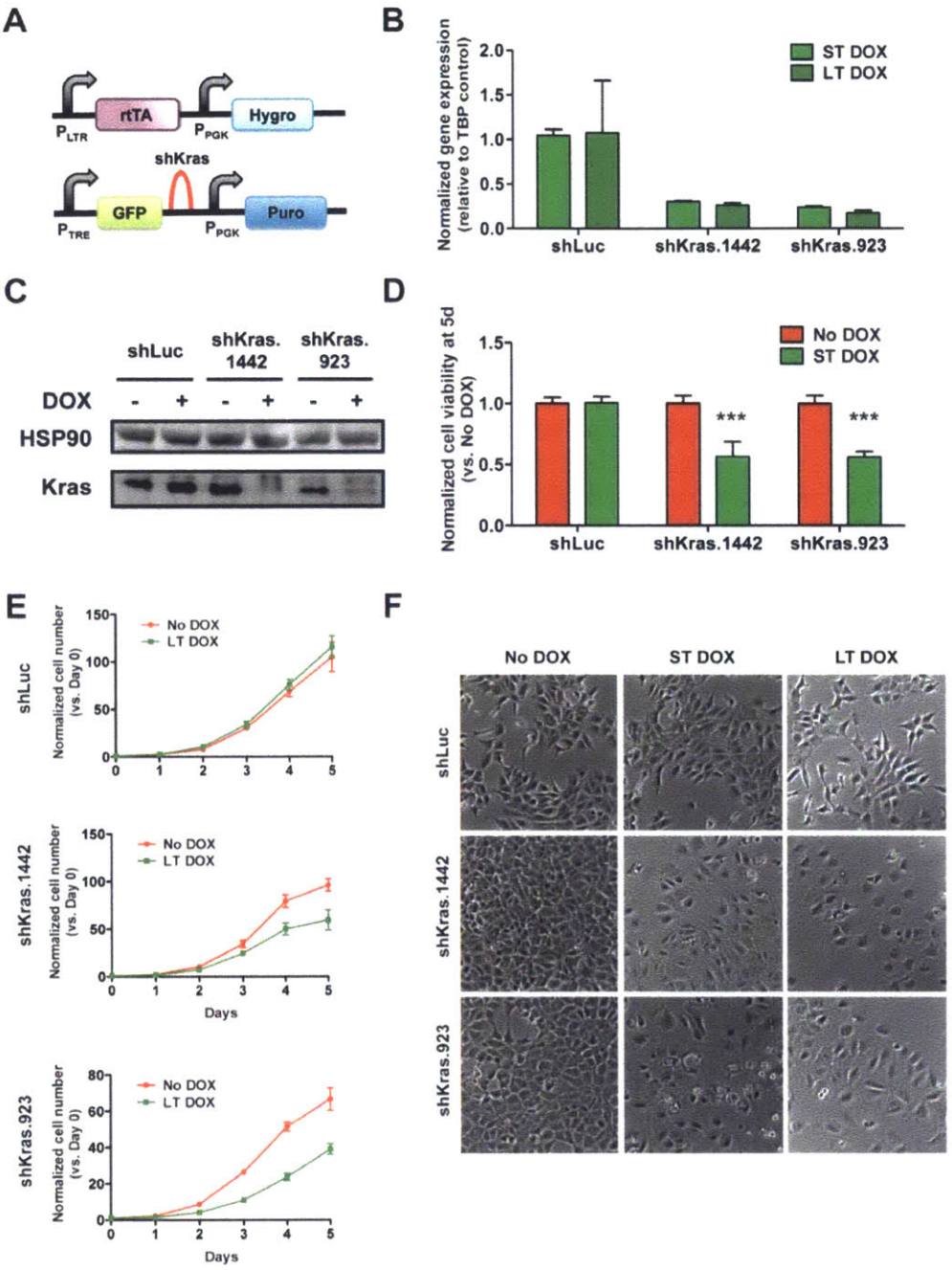

Figure 1: Sustained Kras knockdown in murine PDAC cells *in vitro*.

A. Schematic of lentiviral constructs used to express the reverse tetracycline transactivator (rtTA) and doxycycline-inducible shRNA system. P_{LTR} = 5'-Long Terminal Repeat promoter from MSCV backbone. P_{PGK} = mouse phosphoglycerate kinase promoter. Hygro = hygromycin resistance gene. P_{TRE} = tetracycline-response element minimal promoter. GFP = green fluorescent protein. Puro = puromycin resistance gene. GFP mRNA and hairpins are on the same transcript, permitting GFP expression to serve as a readout of hairpin expression.

B. *Kras* mRNA levels following short-term (ST DOX, 4 days) or long-term (LT DOX, 21 days) DOX treatment of shLuc- or shKras-transduced cells. Gene expression is normalized to untreated condition and TATA binding protein (TBP) is employed as relative control. Average normalized Kras

expression +/- 95% confidence intervals (n=3 replicates per condition) of three independent clones from D parental cell line, using two independent Kras hairpins and shLuc as control, is shown.

C. Western blot shows sustained Kras protein knockdown following LT DOX treatment of shKras-transduced cells.
D. Cell viability following short-term (5 days) Kras knockdown normalized to untreated (No DOX) condition. Average cell viability +/- SD (n=4 replicates per condition) is shown. *** $p<0.001$, unpaired student t-test comparing to No DOX condition.
E. Growth curves of untreated (No DOX) and LT DOX cells transduced with shKras or shLuc. Average cell viability (normalized to day 0) +/- SD (n=4 replicates per cell line per time point) is plotted.
F. Phase-contrast images reveal uniform morphological changes associated with ST and LT DOX treatment (by visual inspection but not quantitation). The Kras-inhibited cells appear larger, more translucent, and have smoother edges.

Response to Kras knockdown is adaptive and reversible

It is generally thought that cancer cells gain resistance to oncogene inhibition through elimination of a sensitive cell population and outgrowth of a resistant, oncogene-independent population. Given the lack of significant apoptosis with acute and sustained Kras knockdown and the rapid conversion of cell morphology that occurred within 3-5 days, we hypothesized that murine PDAC cells have undergone adaptation to a state tolerant to Kras inhibition rather than a selection of rare cells intrinsically resistant to Kras knockdown. To distinguish between these two possibilities, we analyzed the number of single cell clones that could grow from shKras-transduced cell lines in the absence and presence of sustained DOX treatment. The rationale is that if there were a selection process, we would expect to see a marked decrease in the number of clones that formed under prolonged DOX treatment. Alternatively, if adaptation occurred, then the same number of clones should form regardless of DOX treatment condition. While we observed differences between parental cell lines, the vast majority of clones were able to expand despite sustained Kras knockdown (**Fig. 2A**), suggesting adaptation to a state tolerant to Kras inhibition (Kras-inhibited state). All colonies that did form in the presence of DOX were smaller in size, consistent with the expected decreased proliferative rate following Kras knockdown (**Fig. 2B**). Indeed, when we removed DOX to restore endogenous Kras levels (**Fig. 2C**), cells rapidly reverted back to baseline morphology with restored proliferative kinetics (**Figs. 2D-E**). Finally, the cells were re-sensitized to DOX treatment in terms of proliferative and morphological phenotypes (**Fig. 2F** and data not shown). Collectively, these observations indicate that upon partial Kras inhibition, murine PDAC cells respond by undergoing a reversible cell state change rather than selecting for rare cells harboring resistance-conferring mutations. This adaptive Kras-inhibited state is unlikely to be dependent on additional mutational events, as RNA-

sequencing did not reveal recurrent mutations in expressed genes in knockdown cells compared to Kras-uninhibited cells.

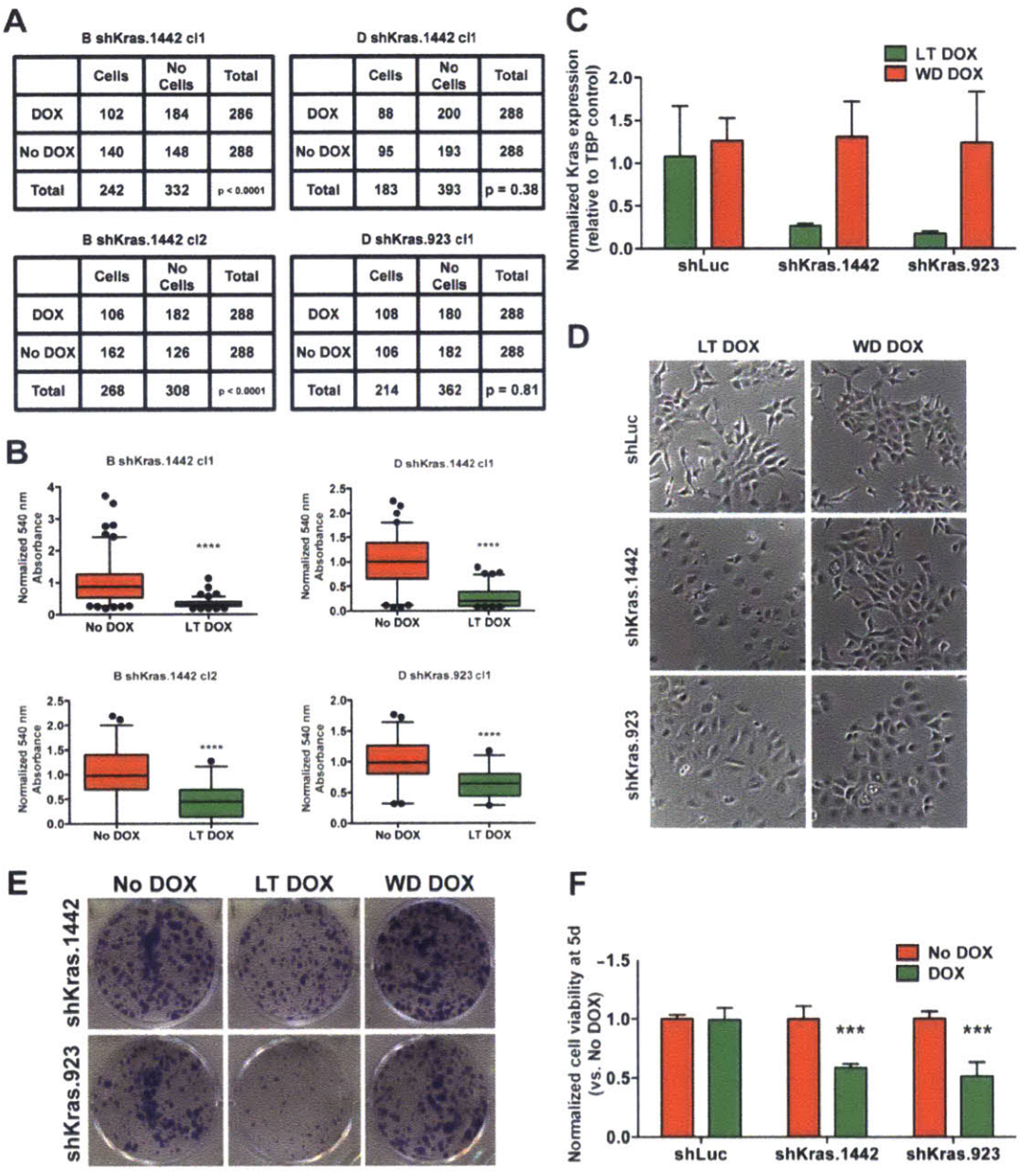

Figure 2: The Kras-inhibited state is adaptive and reversible.

A. Clonal efficiency of Kras knockdown in four independent shKras clones (two from B parental line, two from D parental line, of which one harbors shKras.923 and the other harbors shKras.1442). Clonal efficiency appears to be parental line- but not clone- or hairpin-dependent. D line shows no difference in clonal efficiency in the presence or absence of DOX. B line shows a 25-35% decrease under DOX treatment. The majority of cells appear to survive Kras knockdown. p-values are calculated based on a chi-square test.

B. Quantitation of clone size 21 days after clonal expansion shows decreased clone size in LT DOX cells, consistent with decreased proliferative kinetics described in Figure 1. Quantitation is based on solubilizaton of crystal violet stain and measurement of absorbance at 540 nm shown as box plots

with 5-95% confidence. **** $p<0.0001$, two-tailed unpaired student's t-test with Welch correction for unequal variance.

C. *Kras* mRNA levels following DOX withdrawal (DOX WD) from LT DOX cells. Gene expression is normalized to untreated condition and TBP is employed as relative control. Average normalized *Kras* expression +/- 95% confidence intervals (n=3 replicates per condition) of three independent clones from D parental cell line, using two independent Kras hairpins and shLuc as control, is shown.
D. Reversal of cell morphology following DOX WD.
E. Reversal of proliferative rates following DOX WD as shown by colony forming assay.
F. Re-induced sensitivity to Kras knockdown with DOX treatment in reverted cells. Cell viability following short-term (5 days) Kras re-knockdown normalized to untreated (No DOX) condition. Average cell viability +/- SD (n=4 replicates per condition) is shown. *** $p<0.001$, unpaired student t-test comparing to No DOX condition.

Diminished *in vivo* tumor initiating capacity following stable Kras inhibition

While Kras inhibition did not significantly block the ability of PDAC clones to form in 2D cultures (**Fig. 2A**), we also interrogated the tumorigenic ability of Kras-inhibited cells in 3D culture *in vitro* and in immunocompromised mice *in vivo*, as Kras has recently been implicated in maintaining tumor-initiating cells (TICs) or stemness in various contexts[28]. Interestingly, Kras-inhibited cells retained the ability to form 3D tumorspheres in matrigel *in vitro* (**Fig. 3A**) in similar relative frequencies to 2D clonal cultures (**Fig. 2A**), though the spheres that formed were also smaller, consistent with a proliferative defect (**Fig. 3B**). In contrast, Kras-inhibited cells exhibited reduced TICs in forming subcutaneous tumors in immunocompromised mice *in vivo* (**Fig. 3C-D**). Consistent with tumor initiation and survival despite persistent Kras knockdown, tumors did form from LT DOX-treated shKras-expressing cells. Sustained Kras inhibition was maintained even in secondary cell lines (**Fig. 3E**), which exhibited comparable levels of Kras protein and mRNA knockdown to that of the primary cell lines (**Fig. 3F-G**). Collectively, these data suggest that sustained Kras inhibition can reduce cell proliferation *in vitro* and *in vivo* and impair TICs *in vivo*, confirming the value of Kras as a therapeutic target. Nonetheless, Kras inhibition does not completely ablate the tumorigenic ability of murine PDAC cells when sufficient TICs and a favorable environment (e.g. abundant growth factors and extracellular matrix substrates) are present.

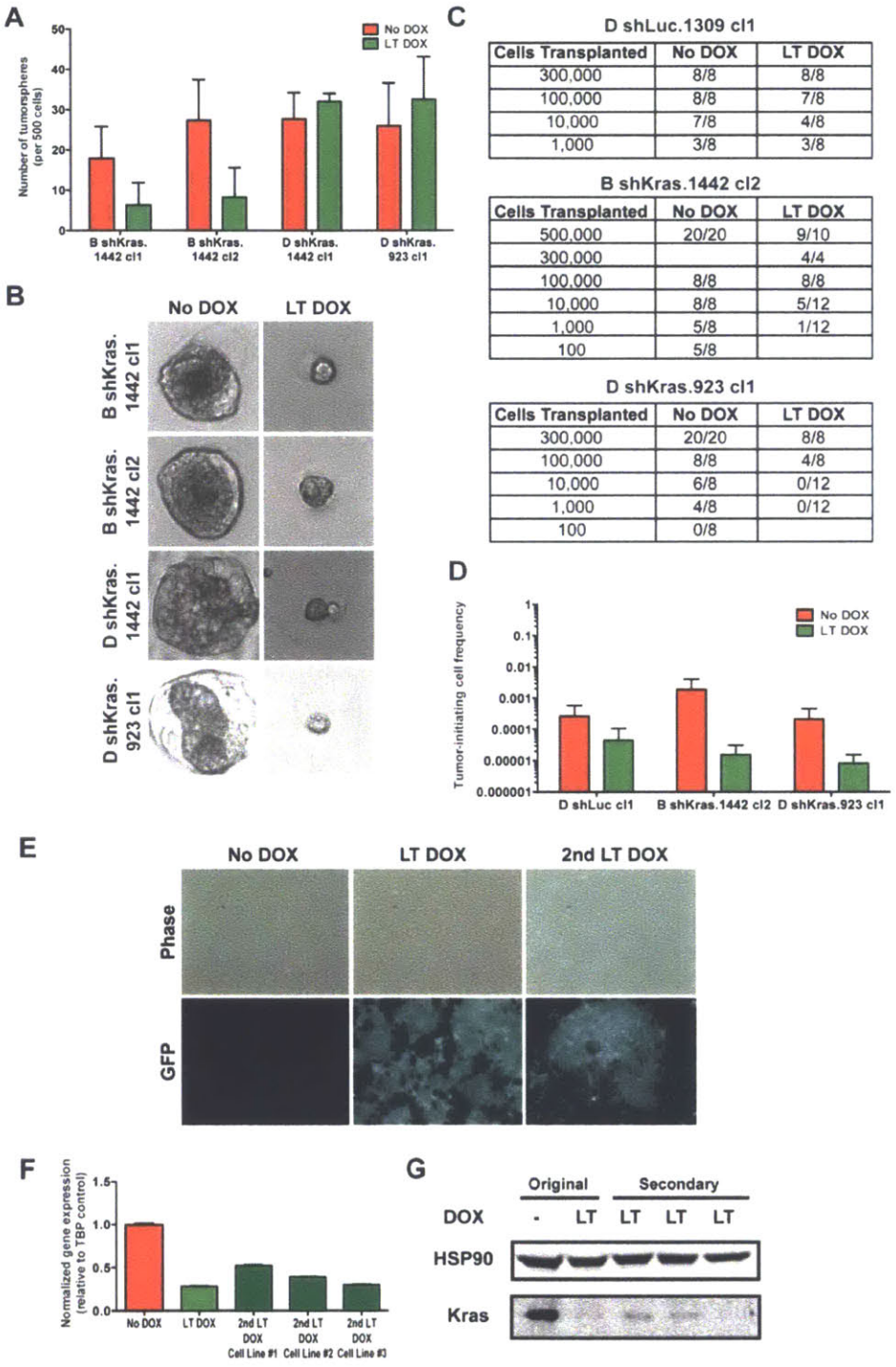

Figure 3: Characterization of tumor-initiating properties of Kras-inhibited PDAC cells.

A. Quantitation showing parental line variation in the efficiency of tumorsphere formation in matrigel-based 3D cultures with Kras knockdown. Average number of tumorspheres formed +/- SD (n=3 replicates per condition) per 500 cells plated is shown.

B. Tumorspheres imaged 12 days after plating demonstrate decreased size of LT DOX spheres, consistent with a decrease in proliferation rate.

C. Tumor-initiating frequency of varying numbers of transplanted cells per subcutaneous injection of shLuc- and shKras-transduced clones.
D. Quantitation of tumor-initiating cell (TIC) number shows decreased TIC in LT DOX shKras-expressing cell lines.
E. Secondary cell lines derived from LT DOX-treated shKras-expressing tumors retain GFP expression long-term. Phase-contrast and fluorescence images of representative secondary cell line at 18 days post-tumor dissociation (2^{nd} LT DOX) are shown compared to the original cell line either untreated (No DOX) or treated DOX for >21 days (LT DOX) *in vitro*.
F. *Kras* mRNA levels of pre-transplant and secondary cell lines derived from LT DOX-transplanted cells. Gene expression is normalized to untreated (No DOX) condition and TBP is employed as relative control. Average normalized *Kras* expression +/- 95% confidence intervals (n=3 replicates per condition) is shown.
G. Western blot of cell lines in (F) demonstrates decreased Kras protein levels in secondary cell lines comparable to original cell line treated with DOX *in vitro* prior to transplant.

The Kras-inhibited state does not display significant alterations in gene expression

We next sought to better understand the molecular and biochemical changes associated with the Kras-inhibited state, which may reveal targetable mechanisms of adaptive resistance to Kras inhibition. To identify transcriptional changes associated with adaptation to a Kras-inhibited state, we performed RNA-sequencing on polyA-selected RNA from seven shKras-transduced Kras-inhibited and -uninhibited subclone pairs (2-3 per primary cell line A, B, and D) and a control shLuc-transduced pair. We verified data quality by confirming *Kras* knockdown and identifying the engineered C→T *G12D Kras* gene mutation in our transcript sequencing reads (data not shown). Additionally, we did not observe recurrent non-synonymous mutations in exonic regions in the Kras-inhibited cells based on RNA-sequencing (data not shown). Surprisingly, we also did not observe significant differences in gene expression between the baseline and Kras-inhibited states. Indeed, unsupervised hierarchical clustering demonstrated that gene expression differences were driven more strongly by parental cell line and subclonal identifies (except for one outlier clone pair) than alterations in the *Kras* expression state (**Fig. 4A**).

To account for clonal variability and to derive a robust gene signature associated with the Kras-inhibited state using an unbiased approach, we performed a blind-source separation method called independent component analysis (ICA; see **Materials and Methods**). ICA not only derived gene expression signatures associated with individual parental cell lines or clones, it also identified signature profiles that distinguished the independent gene expression changes associated with Kras knockdown and DOX treatment (using the shLuc control cell line treated with DOX) (**Figs. 4B-D**). Indeed, it became readily apparent that DOX treatment alone could have significant effects on gene expression independent of Kras knockdown in our cell lines.

For example, the G-protein coupled receptor *Gpr56* was strongly upregulated by DOX treatment (**Supplementary Fig. 3A**) and was significantly associated with the DOX signature but not the Kras knockdown signature (*Z*-scores of 7.32 and -0.51, respectively). We confirmed that the expression of *Gpr56* was not associated with Kras status, but instead, *Gpr56* represented an endogenous eukaryotic target of the prokaryotic protein rtTA in the presence of DOX (**Supplementary Figs. 3B-C**). Indeed, knockdown of *Gpr56* did not functionally impact the proliferative or morphological phenotypes of Kras-inhibited cells (**Supplementary Figs. 3D-E**). This ability to distinguish a DOX-regulated gene from a Kras-regulated gene demonstrates the power of ICA to reliably identify meaningful and functionally important gene signatures. Furthermore, genes in the Kras knockdown signature were specifically and significantly, although not strongly, enriched in Kras-inhibited cells (**Fig. 4D**). Comparison of the degree of transcriptional alterations associated with either DOX treatment or Kras knockdown suggested that stable Kras inhibition does not lead to striking gene expression changes (**Figs. 4C-D**), contrary to what one might expect as Kras-mediated signal transduction ultimately regulates nuclear transcriptional activity. These observations suggest that the Kras-inhibited state is not strongly dependent on mutational or transcriptional alterations.

To elucidate potential Kras-regulated transcriptional pathways or functionally important pathways that maintain cell viability in the Kras-inhibited state, we performed gene set enrichment analysis (GSEA) on the Kras knockdown signature. While few genes sets in MSigDB were significantly associated with the Kras knockdown signature, network correlation analysis revealed enrichment of gene sets associated with receptor tyrosine kinase (RTK), integrin, NFκB, and IL1 signaling pathways in Kras-inhibited cells (**Fig. 4E**), possibly because compensatory pathways are upregulated in response to Kras inhibition to support the steady-state

proliferation of PDAC cells. Additionally, tubulin-folding genes, which are crucial for cell cycle progression, and previously defined cancer-related genes are also upregulated (**Fig. 4E**). In contrast, genes associated with ribosome functions are downregulated (**Fig. 4E**), implying a reduction in translational activity in the Kras-inhibited state.

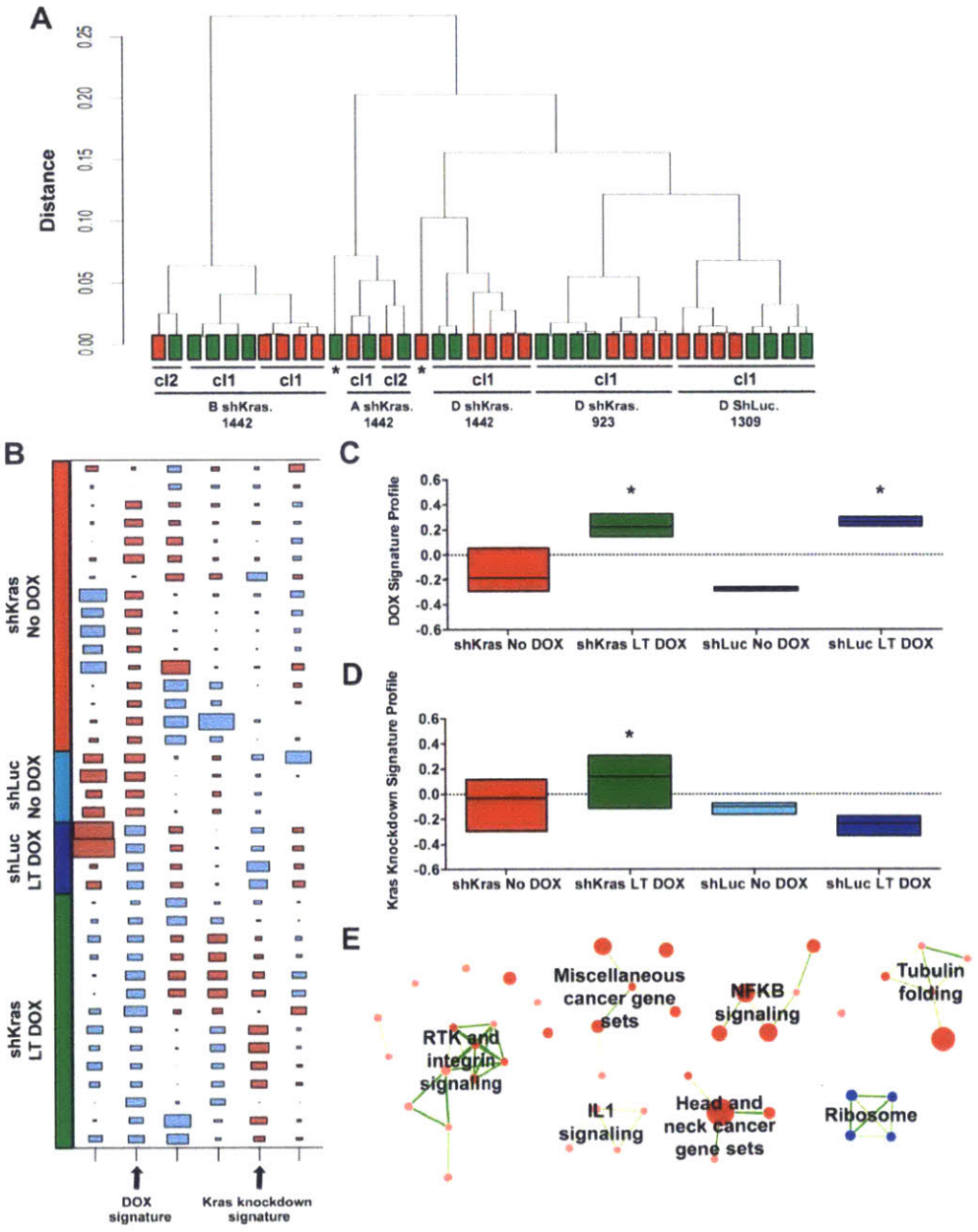

Figure 4: Gene expression analysis of Kras-inhibited cells shows minimal transcriptional changes.

A. Unsupervised hierarchical clustering across all expressed genes from RNA-sequencing data demonstrates segregation based on parental cell line and clone rather than Kras knockdown status (red box = no DOX, uninhibited; green box = LT DOX, Kras inhibited), suggesting that clonal differences are stronger than transcriptional changes in response to Kras inhibition. Multiple boxes of same DOX condition for same clone are replicates, which cluster together. * marks an outlier pair (D shKras.1442 cl2) that does not cluster based on parental cell line and clone.

B. Hinton diagrams of independent component analysis of clone pairs in (A). Columns represent distinct gene expression patterns (signatures), where colors encode directionality of gene expression (red upregulated, green downregulated). Sizes of individual boxes correlate with strength of association between each signature and a given sample (row). DOX and Kras knockdown components are shown.

C. DOX signature profile of individual cell line groups based on hairpin (shKras vs. shLuc) and DOX treatment conditions. Higher scores indicate greater correlation of individual cell lines with DOX signature. *$p<0.05$, Mann-Whitney U-test, comparing shKras/shLuc LT DOX vs. shKras/shLuc No DOX.
D. Kras knockdown signature profile of individual cell line groups based on hairpin (shKras vs. shLuc) and DOX treatment condition. Higher scores indicate greater correlation of individual cell lines with DOX signature. *$p<0.05$, Mann-Whitney U-test, comparing shKras LT DOX vs. other groups.
E. Network representation of overlapping enriched GSEA/MSigDB gene sets in the Kras knockdown signature ($p<0.05$, FDR<0.25). Each circle represents a gene set with circle size corresponding to gene set size and intensity corresponding to enrichment significance. Red is upregulated and blue is downregulated. Each line corresponds to a minimum 50% mutual overlap with line thickness corresponding to degree of overlap. Cellular processes associated with related gene sets are listed.

Global phosphoproteomic profiling reveals enhanced focal adhesion signaling in the Kras-inhibited state

As visible morphological conversion between the Kras-uninhibited and -inhibited states occurs rapidly (3-5 days) without strong mutational or transcriptional alterations, we hypothesized that signaling flux through alternative pro-proliferation and pro-survival pathways may instead underlie the adaptive state. Importantly, identification of compensatory signaling pathways that confer *Kras* independence to PDAC cells could uncover potentially druggable protein targets for PDAC therapies. We first examined signaling differences between the Kras-uninhibited and -inhibited states in a tyrosine-focused fashion, because the best-characterized upstream regulators of Kras-mediated signal transduction are RTKs and genes associated with RTK signaling are enriched in the Kras knockdown signature (**Fig. 4E**). Assessment of global tyrosine phosphorylation levels with a pan-specific anti-phosphotyrosine antibody (**Fig. 5A**) showed an overall increase in the levels of tyrosine phosphorylation in Kras-inhibited cells, suggestive of increased activation of tyrosine kinase-mediated pathways that may compensate for the decrease of Kras levels. However, a limited phospho-RTK array (**Supplementary Table 1**) did not reveal candidate upstream kinase regulators that may be responsible for mediating the adaptive state change (**Supplementary Fig. 4A**). We therefore employed two distinct approaches of unbiased global phosphoproteomic analysis: stable isotope labeling by amino acids in cell culture (SILAC) and isobaric tag for relative and absolute quantitation (iTRAQ). These two complementary approaches offer distinct advantages. The SILAC approach[29] enables the simultaneous analysis of serine-, threonine-, and tyrosine-phosphorylated peptides (pS, pT, and pY, respectively) as well as total proteome changes, and thus is high-throughput and comprehensive (**Supplementary Figs. 5A**). However, this approach captures a significantly

larger representation of highly abundant serine- and threonine-phosphorylated peptides than lowly abundant tyrosine-phosphorylated peptides. Therefore, we adopted an optimized iTRAQ protocol to enrich specifically for tyrosine-phosphorylated peptides[30], enhancing the resolution of tyrosine kinase signaling analysis of the Kras-inhibited state (**Supplementary Fig. 4B**). Combining these two approaches, we were able to cross-compare candidate signaling pathways specifically activated or inhibited in the Kras-inhibited state.

We first validated the quality of our proteomic and phosphoproteomic data. For SILAC, we examined total proteome differences between Kras-uninhibited and Kras-inhibited states, which showed minimal overall protein abundance alterations (**Supplementary Fig. 5B**), consistent with the paucity of transcriptional changes observed. Importantly, one of the few proteins whose abundance was significantly altered in the Kras-inhibited state was Kras itself (reduced by 60%). Conversely, the highest upregulated protein was Gpr56. Interestingly, pathways associated with the proteins that exhibited significant alterations in overall abundance or phosphorylation in the Kras-inhibited state were similar to pathways identified by our gene expression analysis in *KRAS* knockout cells (**Supplementary Tables 3-5**; details of these pathways and the *KRAS* knockout cells will be described in **Chapter 3** of this thesis). For iTRAQ, each experimental replicate identified a robust number of pY peptides (200-300 pY). We then examined the overlap between the peptides called with stringent criteria in three independent iTRAQ experimental replicates (**Fig. 5B**), which showed at least 230 overlapping pY peptides identified in more than two experimental replicates. Additionally, we verified that the signaling changes that occurred in the two independent evaluated clones, B (B shKras.1442 cl2) and D (D shKras.923 cl1), are highly correlative in both SILAC and iTRAQ datasets (**Figs.**

5C-D), suggesting that the clonal and parental cell line differences are small. Taken together, we have high confidence in the quality and validity of our SILAC and iTRAQ data.

We next performed combined analysis of phosphoprotein abundance from SILAC and iTRAQ data. To ensure the identification of critical pathways that mediate the response to Kras inhibition with minimal clonal or technical confounding effects, we only included peptides that were called in at least two replicates of iTRAQ experiments and showed significant and correlative up- or down-regulation (≥2-fold for SILAC, ≥1.2-fold for iTRAQ) in the Kras-inhibited cells in both clones. With these stringent filtering criteria, we found that multiple sites on focal adhesion-associated proteins showed increased phosphorylation (**Fig. 5C**). Examples included Src, focal adhesion kinase (FAK), tensin, paxillin, talin, and vinculin, among many others (**Fig. 5C**). Furthermore, despite the low abundance of pY residues in the total phosphoproteome, our SILAC analysis identified 20-30 pY peptides that overlapped with our iTRAQ analysis (**Supplementary Fig. 5C**). More importantly, phosphosites on proteins associated with adhesion pathways also exhibited significant upregulation in the SILAC analysis (**Fig. 5D**). Collectively, these signaling changes suggest that the Kras-inhibited state is characterized by enhanced focal adhesion-associated signaling. To confirm that increased signaling is actually associated with enhanced focal adhesion structures, we performed immunofluorescent staining of focal adhesion proteins paxillin (**Fig. 6A**) and vinculin (data not shown), which exhibited strikingly enhanced focal adhesion plaque formation in Kras-inhibited cells (**Figs. 6A-B**). Therefore, we conclude that a major feature of the Kras-inhibited state is the upregulation of focal adhesion pathway signaling.

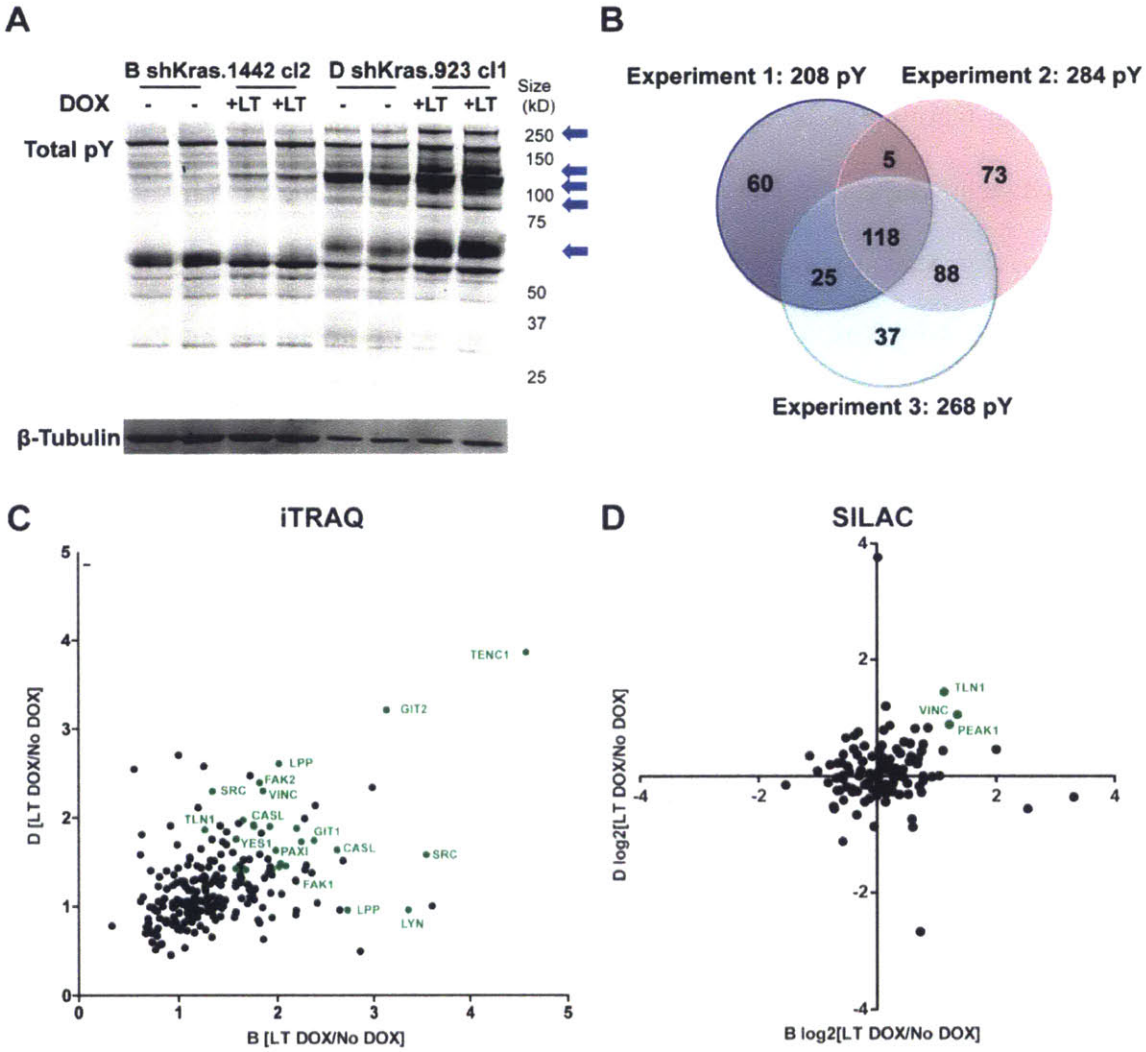

Figure 5: Unbiased phosphoproteomic analysis of signaling alterations in Kras-inhibited cells.

A. Western blot of total phospho-tyrosine levels (total pY) shows increased total pY in Kras-inhibited cells.

B. Overlap of quantified and identified pY peptides between 3 technical replicates of iTRAQ experiments. Criteria for such peptides are that they are unambiguously assigned, can be unique or not unique to a protein, phosphorylated, with an isolation interference ≤25 (low chance of contaminating or co-eluting peptides), and have a Mascot score of ≥25 (high confidence in the identification of the peptide).

C. Scatter plot of the ratio (LT DOX/No DOX) of the abundance of pY sites identified in at least 2 iTRAQ experiments. The changes in peptide abundance positively correlate between the two subclones analyzed. The names of focal adhesion-associated proteins containing upregulated pY sites in the LT DOX state in both B (B shKras.923 cl1) and D (D shKras.1442 cl2) lines are labeled (green).

D. Scatter plot of the log2 ratio (LT DOX/No DOX) of the abundance of pY sites identified in SILAC. The names of focal adhesion-associated proteins containing upregulated pY sites in the LT DOX state in both B (B shKras.923 cl1) and D (D shKras.1442 cl2) lines are labeled (green).

The Kras-inhibited state depends on cell attachment

Given the enhanced focal adhesion signaling and prominent focal adhesion plaque formation in Kras-inhibited cells, we hypothesized that Kras-inhibited cells may be more dependent on attachment for survival. Interestingly, Kras-inhibited cells exhibited enhanced cell attachment capacity, demonstrated by faster adherence to culture dishes than uninhibited cells (**Fig. 6C**). This enhanced adherence property likely underlies the greater resistance of Kras-inhibited cells to actin polymerization inhibitor latrunculin B-induced detachment (**Fig. 6D**). Moreover, Kras-inhibited cells were more sensitive than uninhibited cells to anoikis, as evident by increased induction of apoptosis in non-adherent culture conditions (**Fig. 6E**). Conversely, Kras-inhibited cells exhibited significantly enhanced viability in suspension when the media was supplemented with extracellular matrix proteins (**Fig. 6F**). Overall, analyses of the cell biological features of Kras-inhibited cells reveal uniquely enhanced adherence properties and an increased dependency on adhesion for cell viability *in vitro*.

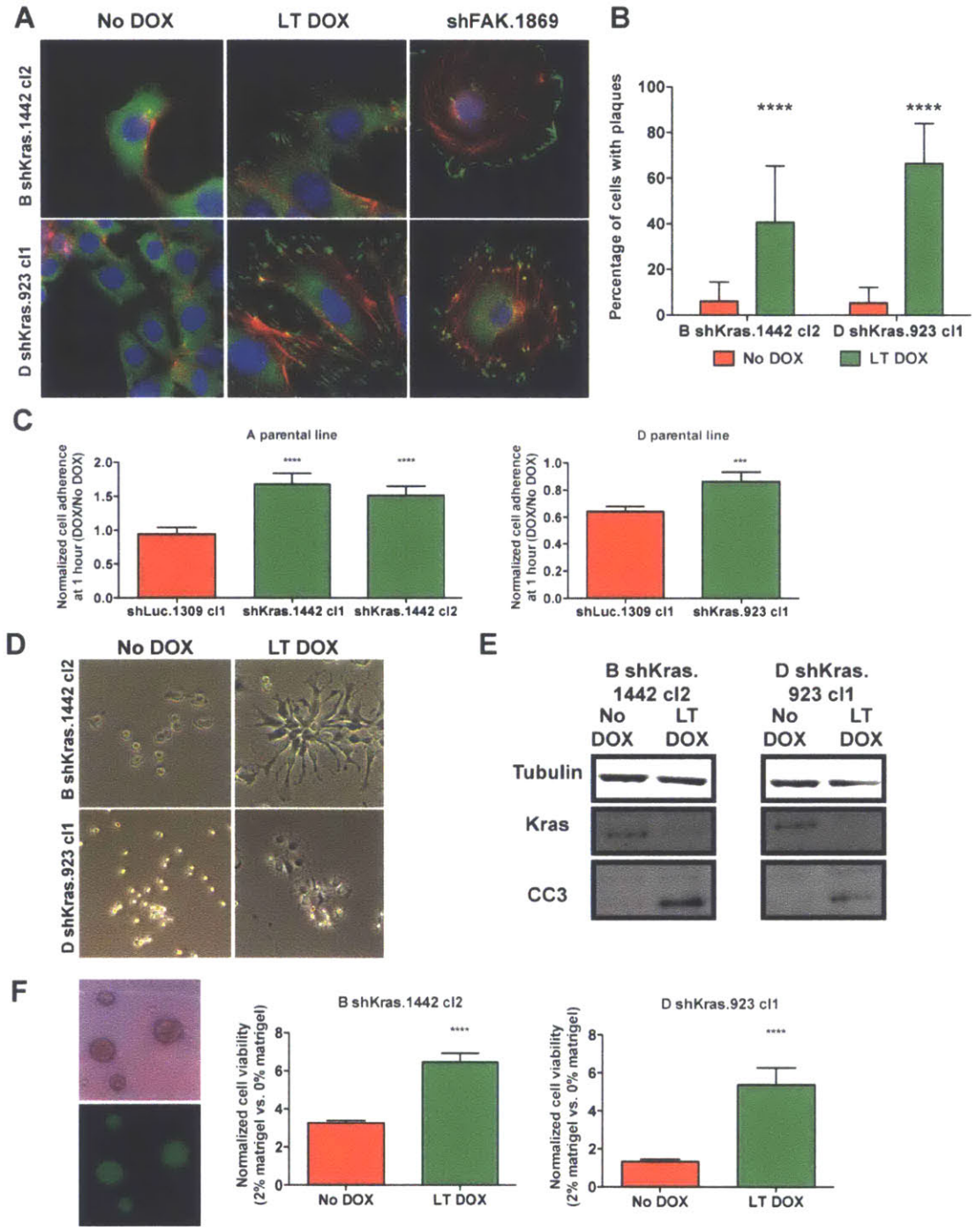

Figure 6: Kras-inhibited cells exhibit enhanced adherence properties and dependence.

A. Immunofluorescence staining of paxillin demonstrates the distribution and morphology of focal adhesion plaques of No DOX and LT DOX cells. shRNA-mediated knockdown of FAK disrupts the polarity of focal adhesion structures. Green: paxillin (focal adhesion), red: phalloidin (F-actin), and blue: DAPI (nuclei).

B. Quantitation of the percentage of cells that contain focal adhesion plaques. Average % +/-SD (per high power field (hpf), n = 6-14). **** $p<0.0001$, two-tailed student's t-test, LT DOX vs. DOX.

C. Quantitation of normalized cell number (LT DOX vs. No DOX condition) +/- SD (n=5 replicates) of adherent cells one hour after plating of single-cell suspension for shLuc and shKras-transduced clones derived from A and B parental cell lines. *** $p<0.001$, **** $p<0.0001$, two-tailed student's t-test.
D. Phase-contrast images of two Kras-uninhibited (No DOX) and –inhibited (LT DOX) clone pairs 1 hour after treatment with the actin disrupting agent latrunculin B.
E. Western blot shows increased expression of the apoptotic marker cleaved-caspase 3 (CC3) in Kras-inhibited cells after forced suspension growth for 48 hours.
F. Normalized cell viability +/- SEM (n=6 replicates per condition) of cells grown in suspension with or without 2% matrigel. Brightfield and fluorescence images of LT DOX tumorspheres maintaining GFP expression are shown.

Genetic or pharmacological inhibition of FAK does not impair survival of Kras-inhibited PDAC cells

Given the phosphoproteomic data and adherence properties of Kras-inhibited cells, we hypothesized that direct inhibition of focal adhesion kinase (FAK) may target a unique vulnerability in the context of Kras inhibition. We therefore interrogated the requirement of FAK-mediated signaling in maintaining Kras-inhibited cell viability. Interestingly, Kras-inhibited cells did not show increased sensitivity to pharmacological inhibition of FAK compared to uninhibited cells (**Supplementary Fig. 6A**). As off-target effects of these pharmacological inhibitors could mask differential sensitivity, we performed more-specific shRNA-mediated knockdown of FAK (**Supplementary Fig. 6B**). Surprisingly, FAK knockdown did not synergize with Kras knockdown to further impair proliferation *in vitro* or subcutaneously transplanted tumor growth *in vivo* (**Supplementary Fig. 6C and Supplementary Figs. 7A-E**). Importantly, even though FAK knockdown disrupted the polarity and organization of focal adhesion plaques, it did not fully ablate the formation of these structures in Kras-inhibited cells (**Fig. 6A**). This suggests that there may be compensatory mechanisms to maintain focal adhesions in the context of FAK inhibition. While inhibition of FAK was insufficient to impair Kras-inhibited cell survival, blockade of the cell adhesion phenotype through alternative means may still offer a tractable therapeutic strategy.

DISCUSSION

In this study, we interrogated the requirement of endogenous *Kras* for maintaining murine PDAC cell survival with an inducible shRNA-based knockdown system. Surprisingly, our results demonstrate only a partial requirement of *Kras* for PDAC maintenance. Not only are

PDAC cells able to proliferate under sustained *Kras* knockdown, but they also retain oncogenic abilities *in vitro* and *in vivo*. Furthermore, the majority of murine PDAC cells tolerate both acute and sustained Kras inhibition by adapting to a reversible cell state. The lack of significant mutational and gene expression changes indicates that such resistance to Kras inhibition is non-genetic and non-transcriptional. Accordingly, global phosphoproteomic analyses confirm that the Kras-inhibited state is a result of rewiring of signaling flux through alternative pro-proliferation and pro-survival pathways. Specifically, PDAC cells exhibit upregulation of focal adhesion signaling, formation of prominent focal adhesion plaque structures, enhanced adherence properties, and increased adherence dependency in response to Kras inhibition. However, due to the complexity of focal adhesion signaling and possible compensatory mechanisms, inhibition of FAK alone is insufficient to impair the survival of Kras-inhibited cells. Nevertheless, components of this pathway can be novel drug targets for rational combination therapeutic strategies with Kras inhibition.

Unlike its well-established role as the driver of PDAC initiation, whether endogenous oncogenic *Kras* is required for PDAC maintenance has remained a longstanding question. To further elucidate the function of Kras-mediated signaling in malignant transformation and the dependency of PDAC cells on Kras for survival, we employed an *in vitro* system that allows reversible partial inhibition of Kras to mimic the effect of pharmacological inhibitors. Although the Kras hairpins described here do not distinguish between wild-type and mutant *Kras* alleles, they model the physiological effects of a non-specific pharmacological inhibitor of Kras, which represents the vast majority of Kras targeting approaches under investigation[8]. Moreover, this *in vitro* inducible shKras system can easily be introduced into other types of cancer cells to analyze

the function of Kras in lung and colon cancer, in which oncogenic *Kras* mutations are also highly prevalent.

Our approach has several advantages over previous studies to understand the requirement of Kras for PDAC maintenance and potential mechanisms of resistance to Kras inhibition. Early studies used constitutive lentiviral RNAi to knockdown Kras in human PDAC cell lines and correlate dependency with gene expression. These experiments defined human PDAC cell lines with variable dependencies on *KRAS* for survival following short-term inhibition, but the effects of sustained knockdown, as would more closely mimic prolonged drug treatment of patients, were undefined[15,16]. More recent work used a similar doxycycline-inducible RNAi approach to knockdown KRAS in human PDAC cell lines *in vitro* and established human tumor xenotransplants. While comparable decreased *in vitro* proliferation and slower tumor growth *in vivo* were observed[31], signaling studies were limited to the study of well-defined MAPK and PI3K pathways and resistance mechanisms were not explored. Finally, recent *in vivo* studies aimed to characterize the requirement of sustained oncogenic *Kras* expression for pancreatic cancer maintenance have employed elegant mouse models engineered to express an inducible oncogenic *Kras* transgene[9,10,12]. Because oncogenic *Kras* alone induces PDAC with low frequency and long latency, these models require additional tumor suppressor inactivation or pancreatitis induction along with transgene expression to increase cell plasticity and facilitate PDAC development. In these mouse models, withdrawal of oncogenic *Kras* transgene in established PDAC tumors led to an initial tumor regression due to massive apoptosis, but tumor relapse via Kras-dependent and –independent mechanisms was observed after a period of dormancy[9,10,12,17,18]. Although observations from these studies provide invaluable insights into the requirement of oncogenic Kras functions for tumor maintenance, care must be taken into

extrapolating the effects of the overexpression of a transgenic form of oncogenic *Kras* and its complete withdrawal to explain its endogenous functions and model inhibition.

Consistent with results from these previous studies, murine PDAC cells can bypass *Kras* oncogene addiction in response to partial inhibition of Kras. Importantly, we found that a large fraction of murine PDAC cells can adapt to the Kras-inhibited state in a reversible manner. Conventionally, it is thought that resistance to cancer therapies is dependent on the selection of rare cells that harbor resistance-conferring mutations. In contrary, our observations support the emerging view that non-genetic and non-transcriptional response to oncogene inhibition can be equally important resistance mechanisms[19,20]. Given the significant public and private investments into the development of KRAS inhibitors, advanced knowledge of these resistance mechanisms will facilitate the clinical translation of novel inhibitors and circumvent the limitations of single-agent therapy.

Unbiased phosphoproteomic analysis of the Kras-inhibited state uncovered increased focal adhesion signaling as a possible resistance mechanism to sustained Kras inhibition. This intriguing finding led us to explore the potential benefit of targeting FAK in Kras-inhibited PDAC cells. FAK is the central kinase of the focal adhesion signaling pathway, and is known to integrate and transduce adhesion- and growth factor-dependent signals to regulate cell shape, adhesion, motility, and survival[32]. Interestingly, *FAK* is overexpressed in multiple human cancers, including PDAC, and its overexpression is often associated with worse prognosis and metastatic disease[33-35]. Furthermore, FAK directly and indirectly interacts with multiple regulators and effectors of KRAS, including GEFs, GAPs, RTKs, and components of the MAPK and PI3K pathways. In fact, it has been suggested that KRAS-mediated activation of MEK1 results in phosphorylation of FAK at Ser910, which leads to suppression of FAK kinase

activity[36]. Moreover, inhibition of FAK has been shown to synergistically suppress the growth of xenograft PDAC tumors with gemcitabine treatment[37]. Together, the connection between FAK and KRAS-mediated signaling as well as its implication in human cancers made FAK an appealing target. Unfortunately, as focal adhesion signaling involves multiple inputs and outputs, FAK inhibition alone was insufficient to impair Kras-inhibited cell survival. Nevertheless, there is still merit to identify the critical nodes of the focal adhesion signaling pathway that underlie the resistance to Kras inhibition.

In sum, we have employed a conditional system of RNAi to study the requirement of endogenous *Kras* in PDAC maintenance, and performed unbiased gene expression and phosphoproteomic analyses to characterize the adaptive and reversible Kras-inhibited state. Our observations have important therapeutic implications. First, by showing that the majority of cells can tolerate an approximately 70% inhibition of Kras, it is possible that a Kras-directed inhibitor needs to achieve near-complete inhibition of Kras function to exhibit a significant clinical impact. Alternatively, multiple nodes of Kras signaling may need to be inhibited to achieve greater efficacy. Second, even if an effective Kras inhibitor is successfully developed, resistance may develop. Based on our observation that PDAC cells likely circumvent Kras inhibition via an adaptive and reversible state change, intermittent dosing of a Kras-directed inhibitor to allow for re-treatment response could prevent PDAC cells from becoming resistant to single-agent targeted therapy. Third, the Kras-inhibited state is not characterized by mutational or significant transcriptional changes, but rather alterations in signaling. Targeting these compensatory signaling pathways together with Kras inhibition could be a useful therapeutic strategy for PDAC.

SUPPLEMENTARY FIGURES AND TABLES

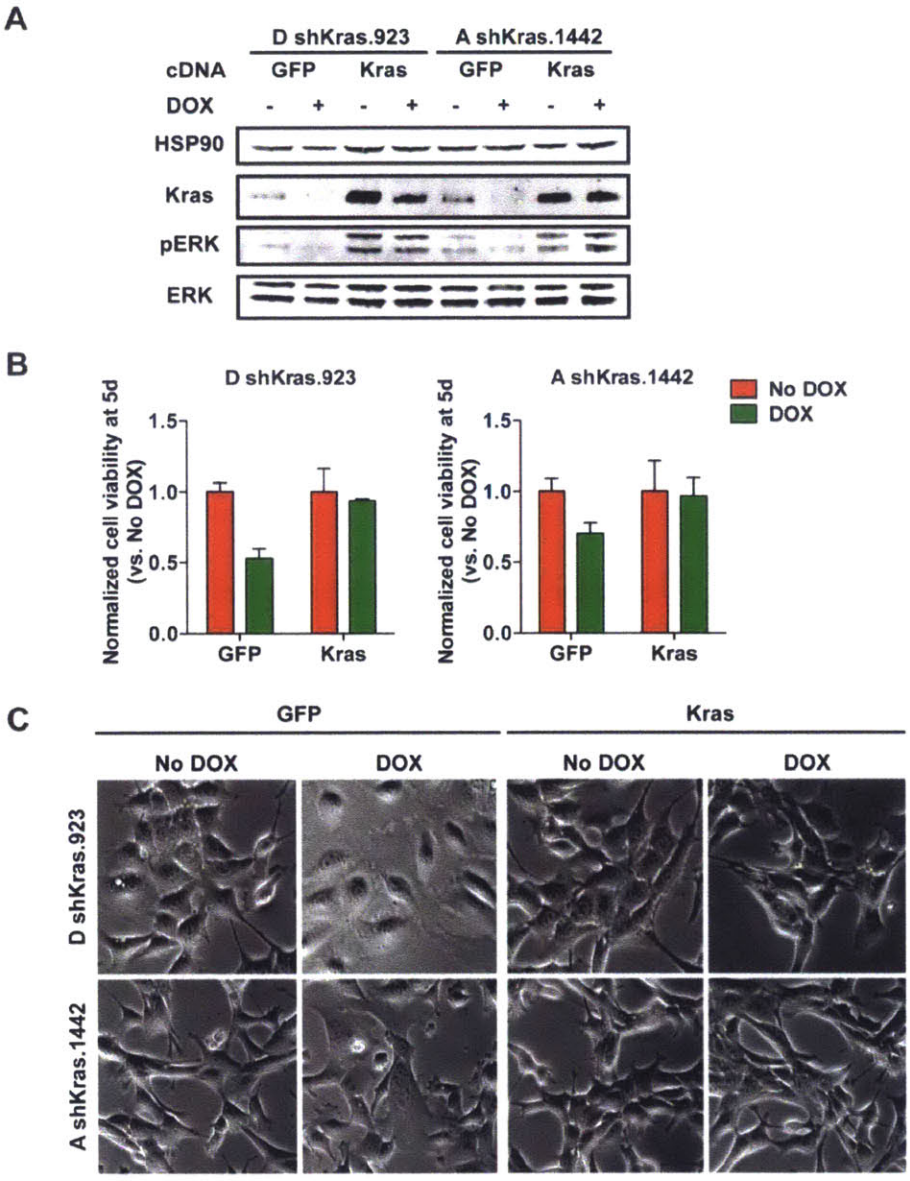

Supplementary Figure 1: On-target effects of Kras short hairpins on murine PDAC cells.

A. Western blot shows Kras and pERK levels in cell lines subject to endogenous Kras knockdown (+DOX) following overexpression of *GFP* or *KrasG12D* cDNA. *KrasG12D* cDNA-expressing cell retain Kras expression following DOX treatment. The effects of two different hairpins in two different parental cell lines are shown.

B. Cell viability following short-term (5 days) endogenous Kras knockdown normalized to untreated (No DOX) condition. Average cell viability +/- SD (n=4 replicates per condition) is shown and demonstrates that *KrasG12D* overexpression prevents decrease in cell viability associated with endogenous Kras knockdown.

C. Phase-contrast images reveal that the effects on morphology following ST DOX treatment are rescued by *KrasG12D* cDNA expression.

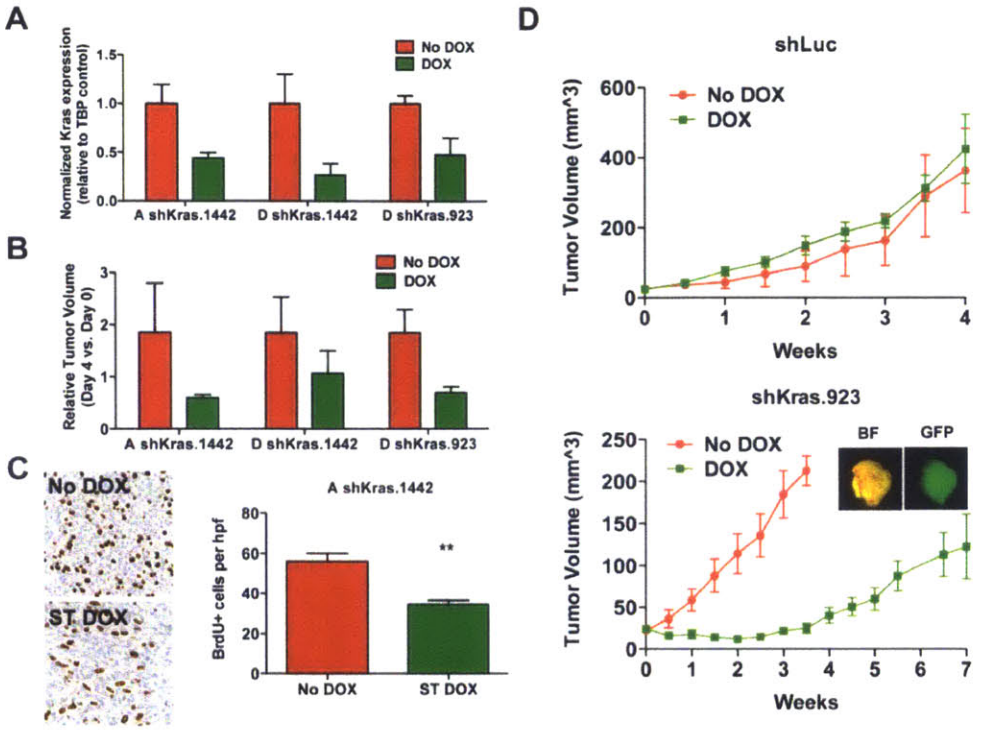

Supplementary Figure 2: Effects of short-term and sustained Kras knockdown *in vivo*.

A. *Kras* mRNA levels of subcutaneous tumors derived from transplanted shKras-transduced cells following short-term DOX (4 days) treatment. Gene expression is normalized to untreated condition and TBP is employed as relative control. Average normalized *Kras* expression +/- 95% confidence intervals (n=2-4 tumors per cell line).

B. Relative tumor volumes +/- SD (n=2-5 tumors per condition) 4 days after DOX treatment (normalized to day 0).

C. Tumors demonstrate decreased proliferation after 4 days of DOX treatment. Shown is example BrdU staining of subcutaneous tumors from A shKras.1442 tumors treated with or without DOX. Quantitation shows average number of BrdU-positive cells per high-power field (hpf) (No DOX n=4 tumors, DOX n=5 tumors). ** $p<0.01$, two-tailed unpaired student's t-test.

D. Tumor growth following LT DOX treatment of nude mice transplanted with D shLuc.1309 cl1 or D shKras.923 cl1 cells. Tumor volumes +/- SD (n=5-10 tumors per group) at each time point are shown. Brightfield (BF) and GFP fluorescence images show LT DOX-treated D shKras.923 cl1 tumors retain GFP expression, which is a surrogate for Kras hairpin expression.

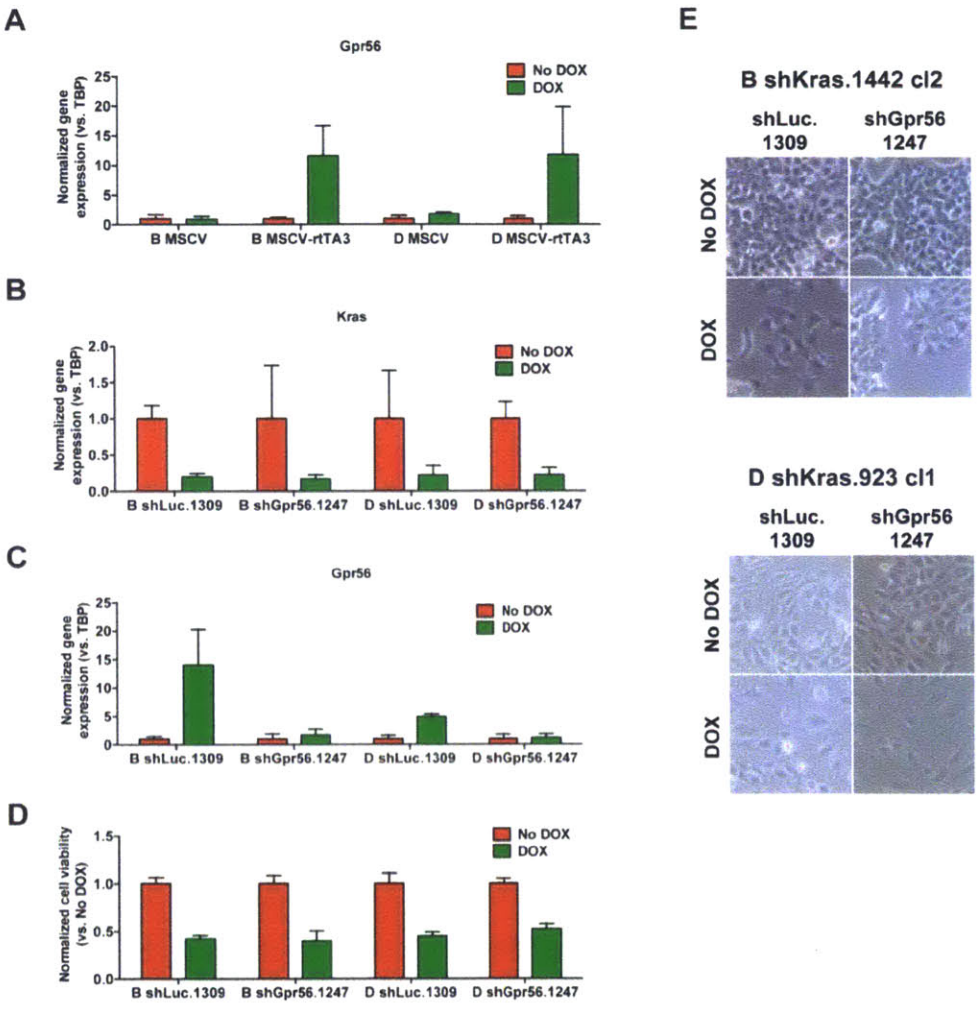

Supplementary Figure 3: Expression of *Gpr56* is strongly induced by DOX treatment irrespective of Kras status.

A. *Gpr56* mRNA levels (relative to TBP) are significantly increased in mPDAC parental cells harboring rtTA3 when treated by DOX in absence of Kras hairpins. Average normalized *Kras* expression +/- 95% confidence intervals (n=3 replicates per cell line).

B. *Kras* mRNA levels are decreased in B shKras.1442 cl2 and D shKras.923 cl1 cells following short-term DOX treatment in both cells co-transduced with shGpr56.1247 or shLuc.1309 control. Average normalized *Kras* expression +/- 95% confidence intervals (n=3 replicates per cell line).

C. *Gpr56* mRNA levels are induced by DOX treatment in cell lines from (B) but induction is repressed by shGpr56.1247. Average normalized *Gpr56* expression +/- 95% confidence intervals (n=3 replicates per cell line).

D. Cell viability following short-term (5 days) DOX treatment compared to No DOX condition of cell lines in (B). Average cell viability +/- SD (n=4 replicates per condition) is shown and demonstrates that Gpr56 knockdown does not impact the effect of Kras knockdown on cell viability.

E. Phase-contrast images reveal that Gpr56 knockdown does not affect morphological phenotypes of Kras-inhibited cells.

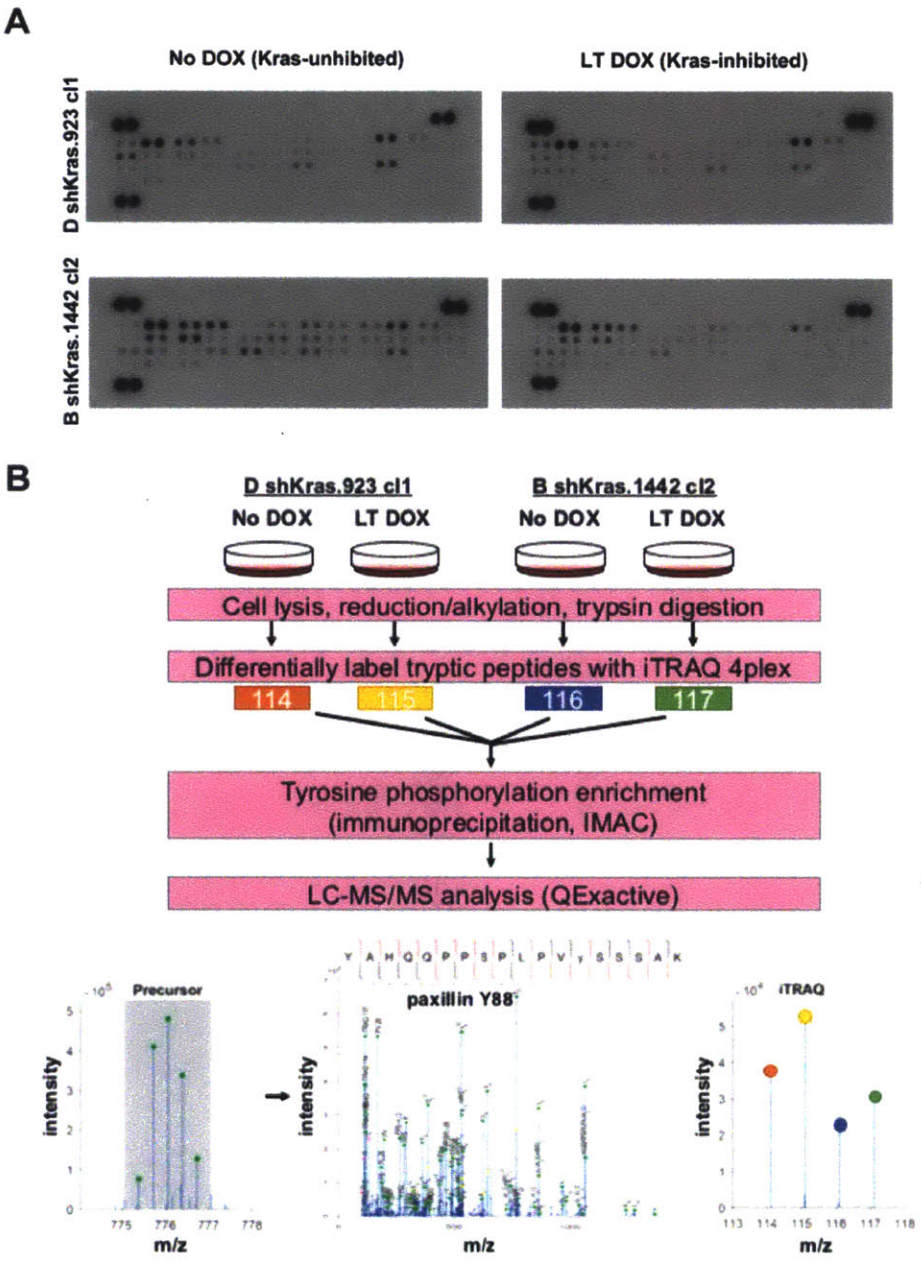

Supplementary Figure 4: Phospho-tyrosine profiling of Kras-inhibited cells.

A. Phospho-RTK array shows no obvious candidate RTK that is upregulated in LT DOX cells. The key for the RTK array can be found in Supplementary Table 1.

B. Schematic of iTRAQ workflow and data analysis. Following lysis and protein digestion, peptides from each sample were labeled with a different iTRAQ 4plex reagent for relative quantitation. Tyrosine phosphorylated peptides were enriched with pan anti-phosphotyrosine antibodies followed by IMAC, then peptides were analyzed by LC-MS/MS analysis. Peptides were identified using Mascot (Matrix Science) and quantified using Proteome Discoverer (Thermo). A precursor mass from the MS1 scan was selected for fragmentation. The fragment ions in the MS/MS scan were used to determine the amino acid sequence and localization of the tyrosine phosphorylation site. Additionally, the iTRAQ reporter ions (114-117 m/z) generated in the MS/MS scan were used for relative quantification.

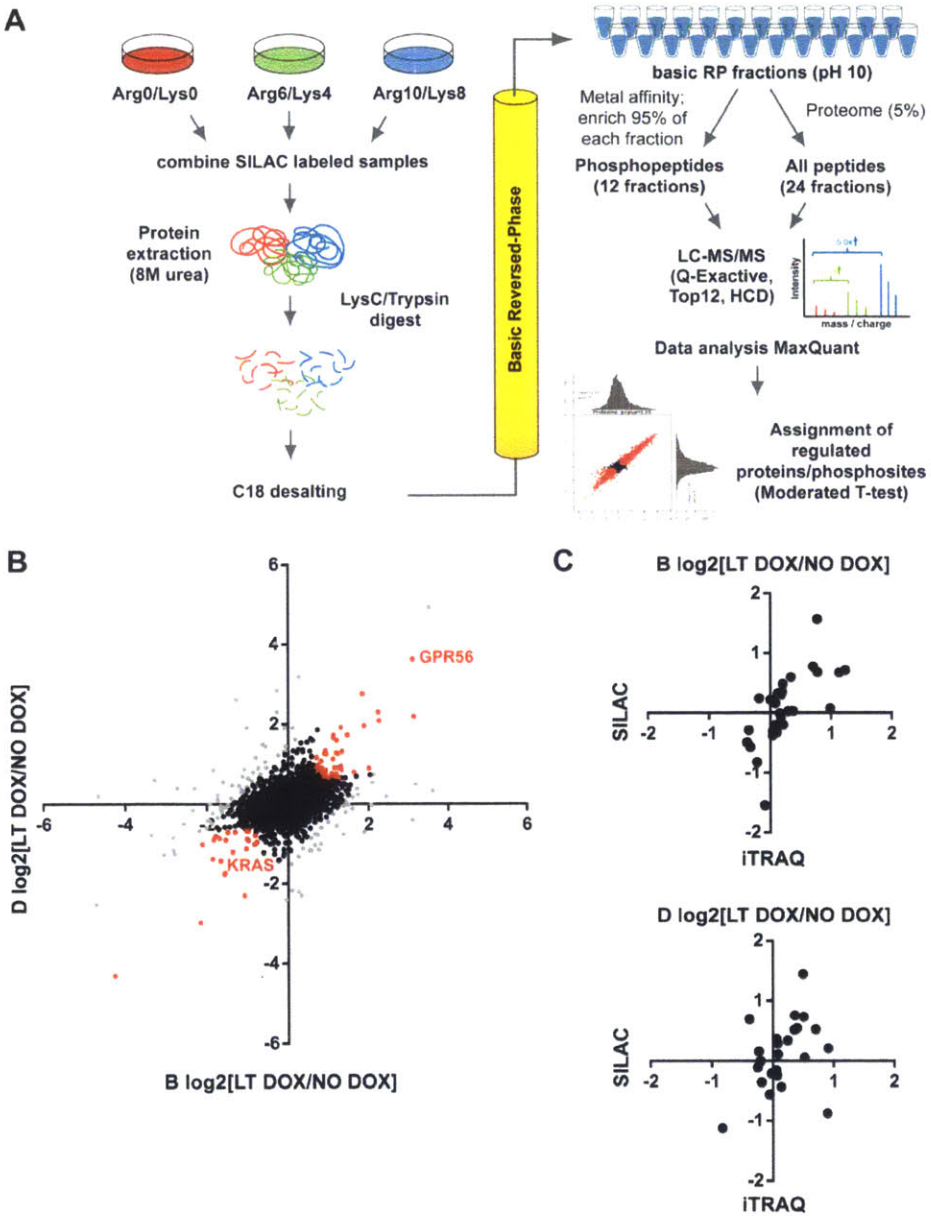

Supplementary Figure 5: SILAC-based proteomic and phosphoproteomic analyses.

A. Schematic of the workflow of SILAC. The light-, medium- and heavy-labeled lysates were combined in a 1:1:1 protein ratio. Samples were processed and separated by basic reversed-phase chromatography. Peptide samples were combined into 24 sub-fractions to be used for proteome analysis. 5% of the volumetric samples were reserved for proteome analysis, and the remaining 95% of the samples were further combined to generate 12 peptide fractions to undergo enrichment for phosphorylated peptides. Iron-chelated IMAC beads were used to enrich for phosphorylated peptides. Samples were analyzed on LC-MS/MS. The mass spectra were analyzed with MaxQuant software and relative quantitation of proteins and phosphosites were determined.

B. Scatter plot of the log2 ratios of total protein abundance in LT DOX/No DOX in B and D lines. Kras and Gpr56 are labeled. Red: significant at FDR<0.05 (47 upregulated proteins in LT DOX and 24

downregulated proteins in LT DOX), black: within confidence interval (7637 proteins), grey: not within confidence interval.

C. Scatter plot showing log2 ratios (LT DOX/No DOX) of the abundance of pY peptides identified in both iTRAQ and SILAC experiments for the B and D lines. The two distinct phosphoproteomic profiling approaches exhibit positive correlations in pY peptide quantitation.

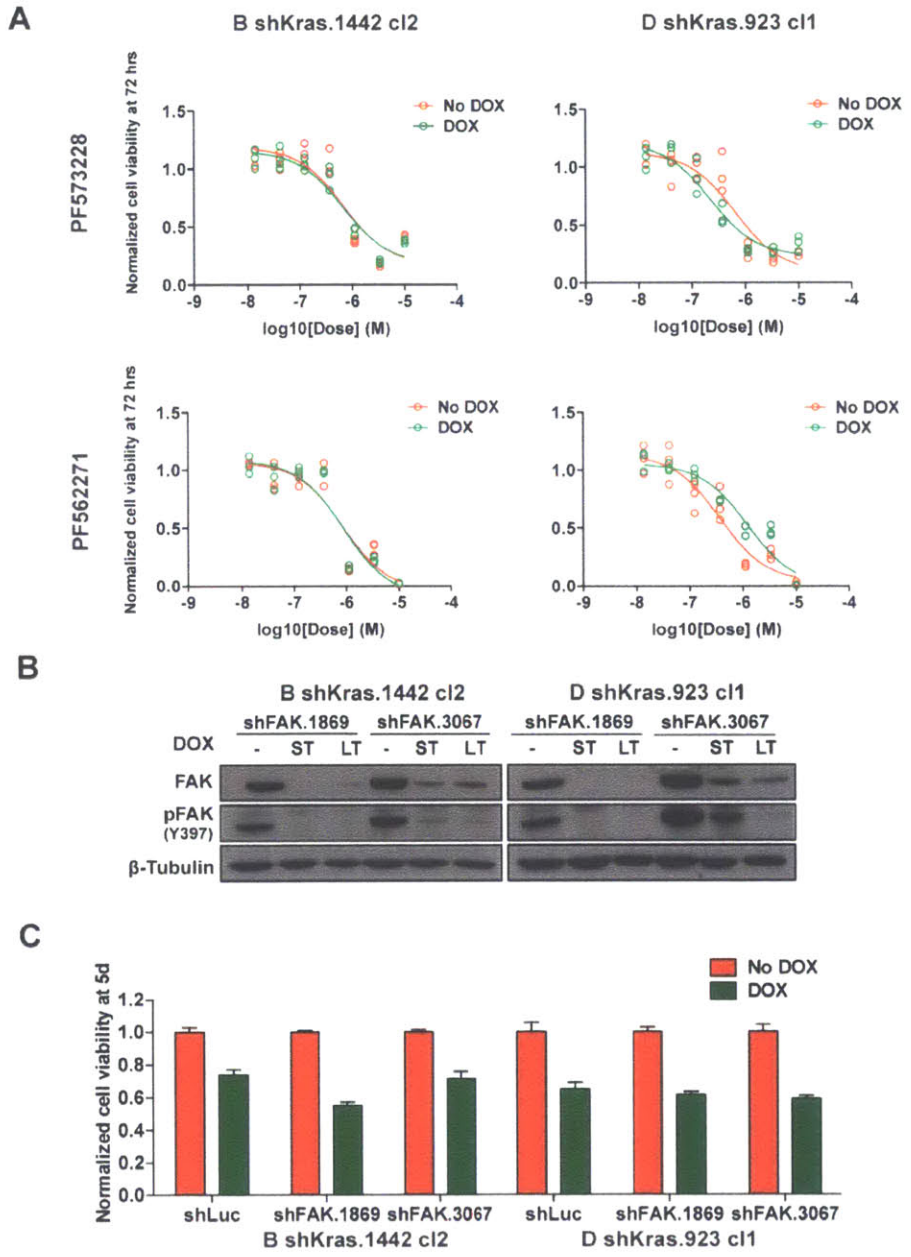

Supplementary Figure 6: Pharmacologic and RNAi-mediated FAK inhibition *in vitro*.

A. Dose response curves of PF573228 or PF562271 treatment on cells treated with LT DOX or No DOX. Shown are cell viability +/- SEM (n=3 replicates) at each dose. Curve represents best line-to-fit.

B. Western blot shows effective short-term and long-term knockdown of FAK proteins and phosphorylated FAK by two different shRNAs (1869 and 3067). shFAK.1869 is more effective than shFAK.3067 as shown by a greater decrease in protein levels, and thus is used for all of the *in vitro* and *in vivo* experiments.

C. Cell viability following short-term (5 days) DOX treatment compared to No DOX condition of cell lines in (B). Average cell viability +/- SEM (n=5 replicates per condition) is shown and demonstrates that FAK knockdown does not synergize with Kras knockdown to diminish cell viability.

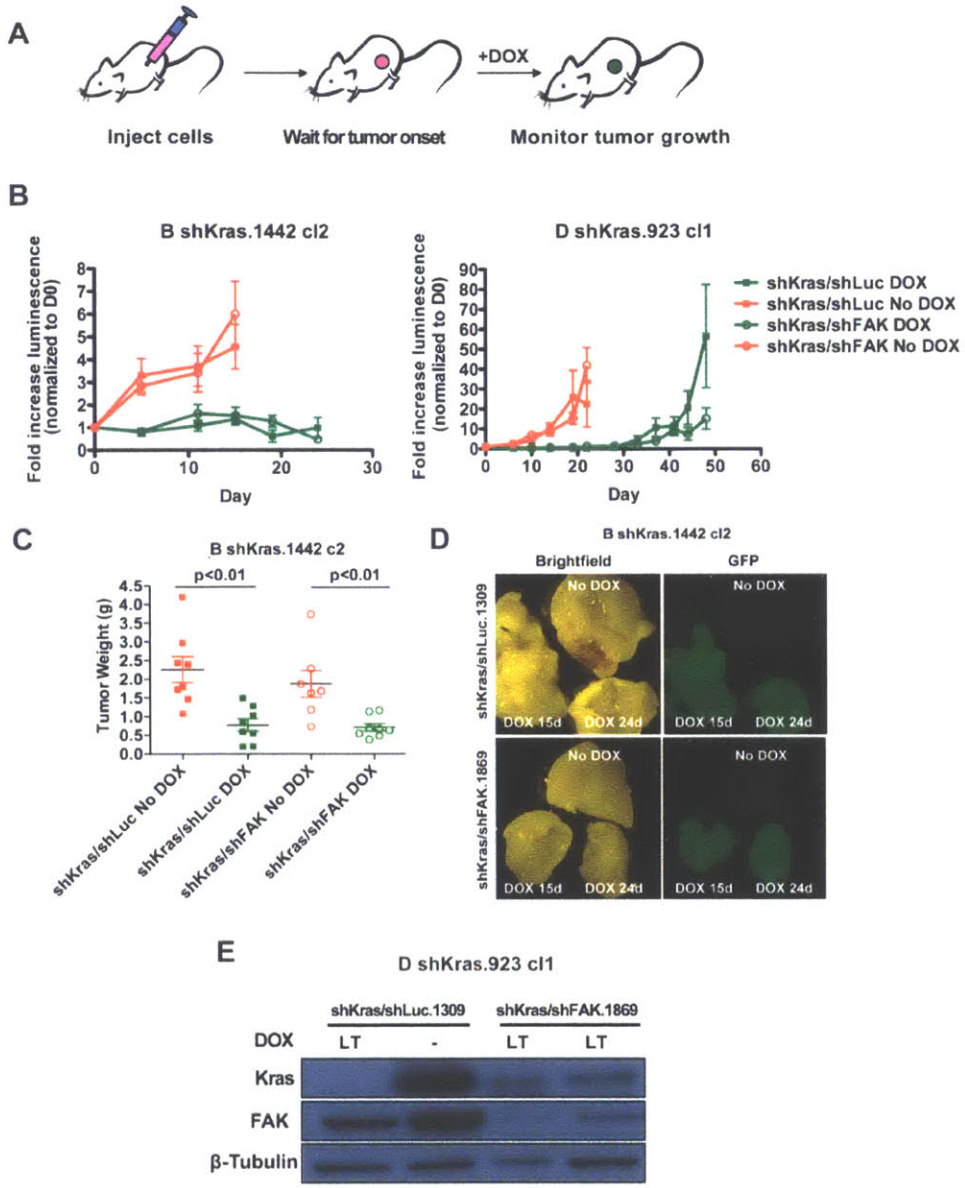

Supplementary Figure 7: Combined Kras and FAK inhibition *in vivo*.

A. Schematic of the *in vivo* subcutaneous transplant experiment. Cells are injected and allowed to form tumors prior to treatment with or without DOX to monitor tumor growth following hairpin induction.
B. Fold increase in luminescence (as a surrogate for tumor growth) with or without DOX treatment of shKras-transduced cells co-transduced with shFAK.1869 or shLuc.1309 control. Simultaneous knockdown of FAK and Kras does not exhibit a greater inhibitory effect compared to Kras knockdown alone.
C. Final tumor weights (in grams) at 15 days following DOX treatment of tumors in (B). Line represents mean of tumor weights. $p<0.01$, two-tailed student's t-test.
D. Tumors that are harvested from mice on DOX diet continue to express GFP, suggesting that shRNA is stably expressed and maintained *in vivo* for prolonged periods (15 and 24 days).
E. Western blot analysis on lysates of tumors from (B) indicates effective and maintained knockdown of Kras and FAK *in vivo*.

Supplementary Table 1: RTKs in the phospho-RTK array

Coordinate	Receptor Family	RTK/Control	Coordinate	Receptor Family	RTK/Control
A1, A2	Reference	--	C17, C18	Tie	Tie-1
A23, A24	Reference	--	C19, C20	Tie	Tie-2
B1, B2	EGFR	EGFR	C21, C22	NGFR	TrkA
B3, B4	EGFR	ErbB2	C23, C24	NGFR	TrkB
B5, B6	EGFR	ErbB3	D1, D2	NGFR	TrkC
B7, B8	EGFR	ErbB4	D3, D4	VEGFR	VEGFR1
B9, B10	FGFR	FGFR2 (IIIc)	D5, D6	VEGFR	VEGFR2
B11, B12	FGFR	FGFR3	D7, D8	VEGFR	VEGFR3
B13, B14	FGFR	FGFR4	D9, D10	MuSK	MuSK
B15, B16	Insulin R	Insulin R	D11, D12	EphR	EphA1
B17, B18	Insulin R	IGF-1R	D13, D14	EphR	EphA2
B19, B20	Axl	Axl	D15, D16	EphR	EphA3
B21, B22	Axl	Dtk	D17, D18	EphR	EphA6
B23, B24	Axl	Mer	D19, D20	EphR	EphA7
C1, C2	HGFR	HGFR	D21, D22	EphR	EphA8
C3, C4	HGFR	MSPR	D23, D24	EphR	EphB1
C5, C6	PDGFR	PDGFRα	E1, E2	EphR	EphB2
C7, C8	PDGFR	PDGFRβ	E3, E4	EphR	EphB4
C9, C10	PDGFR	SCFR	E5, E6	EphR	EphB6
C11, C12	PDGFR	Flt-3	E7, E8	Control (-)	PBS
C13, C14	PDGFR	M-CSFR	F1, F2	Reference	--
C15, C16	RET	c-Ret			

**Table and coordinate key are adapted from the Appendix of R&D Proteome Profiler™ Array: Mouse Phospho-RTK Array Kit product data sheet (Catalogue #ARY014, 2012).*

Coordinate key:

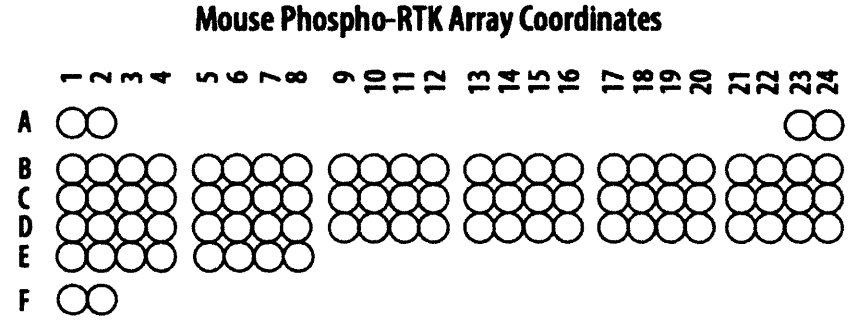

Supplementary Table 2: shRNA and primer sequences

shKras.1442	5'-ACAGACCCAGTATGAAATAGTA-3'
shKras.923	5'-CGGAAACCTTCTTTTTTCTAAG-3'
shLuc.1309	5'-TTAATCAGAGACTTCAGGCGGT-3'
shFAK.1869	5'-CCCTGGCATCTTTGATATTATA-3'
shFAK.3067	5'-ACGGTCCAATGACAAGGTATAT-3'
shGpr56.1247	5'- CGAGGTAGAAGCCACTCACAAA-3'
5' miR30-XhoI primer	5'-TACAATACTCGAGAAGGTATATTGCTGTTGACAGTGAGCG-3'
3' miR30-EcoRI primer	5'-ACTTAGAAGAATTCCGAGGCAGTAGGCA-3'
MSCV 5' sequencing primer	5'-CCCTTGAACCTCCTCGTTCGACC-3'

Listed are the sequences of 22-mers for shRNA design and the primers used for shRNA cloning. The 5' and 3' miR30 primers were used to clone the shRNAs, and the MSCV 5' sequencing primer was used to confirm the sequence of the shRNA that were cloned.

Supplementary Table 3: Comparison of protein pathways between LT DOX/No DOX in B and D lines analyzed by SILAC (ssGSEA for MSigDB pathways; upregulated in LT DOX; FDR<0.05)

Pathway Name	Normalized Enrichment Score (B)	Normalized Enrichment Score (D)
KEGG_LYSOSOME	9.94	9.01
REACTOME_MITOCHONDRIAL_PROTEIN_IMPORT	9.38	7.77
REACTOME_SPHINGOLIPID_METABOLISM	7.93	5.30
REACTOME_GLYCOSPHINGOLIPID_METABOLISM	7.17	5.56
REACTOME_METABOLISM_OF_LIPIDS_AND_LIPOPROTEINS	7.77	4.92
KEGG_PEROXISOME	6.06	4.27
REACTOME_FORMATION_OF_ATP_BY_CHEMIOSMOTIC_COUPLING	5.95	4.25
REACTOME_IRON_UPTAKE_AND_TRANSPORT	6.20	3.87
REACTOME_BRANCHED_CHAIN_AMINO_ACID_CATABOLISM	6.49	3.36
REACTOME_PHOSPHOLIPID_METABOLISM	6.09	3.76
REACTOME_CHONDROITIN_SULFATE_DERMATAN_SULFATE_METABOLISM	4.59	4.96
REACTOME_INSULIN_RECEPTOR_RECYCLING	5.89	3.62
KEGG_SPHINGOLIPID_METABOLISM	6.20	3.29
REACTOME_MITOCHONDRIAL_FATTY_ACID_BETA_OXIDATION	5.75	3.49
REACTOME_PEROXISOMAL_LIPID_METABOLISM	5.30	3.67
KEGG_FATTY_ACID_METABOLISM	5.45	3.46
REACTOME_HEPARAN_SULFATE_HEPARIN_HS_GAG_METABOLISM	4.98	3.65
REACTOME_A_TETRASACCHARIDE_LINKER_SEQUENCE_IS_REQUIRED_FOR_GAG_SYNTHESIS	3.95	4.41
KEGG_RETINOL_METABOLISM	3.34	4.88
KEGG_N_GLYCAN_BIOSYNTHESIS	2.89	5.11
REACTOME_GLYCOSAMINOGLYCAN_METABOLISM	4.44	3.47
PID_INTEGRIN5_PATHWAY	4.18	3.69
PID_INTEGRIN3_PATHWAY	3.40	4.21

Supplementary Table 4: Comparison of protein pathways between LT DOX/No DOX in B and D lines analyzed by SILAC (ssGSEA for MSigDB pathways; downregulated in LT DOX; FDR<0.05)

Pathway Name	Normalized Enrichment Score (B)	Normalized Enrichment Score (D)
REACTOME_METABOLISM_OF_MRNA	-9.55	-8.84
REACTOME_3_UTR_MEDIATED_TRANSLATIONAL_REGULATION	-9.40	-8.03
REACTOME_NONSENSE_MEDIATED_DECAY_ENHANCED_BY_THE_EXON_JUNCTION_COMPLEX	-9.19	-7.87
REACTOME_METABOLISM_OF_RNA	-7.88	-8.54
REACTOME_TRANSLATION	-9.05	-7.18
REACTOME_PEPTIDE_CHAIN_ELONGATION	-8.64	-7.18
KEGG_RIBOSOME	-8.39	-7.18
REACTOME_CELL_CYCLE_MITOTIC	-3.02	-6.25
REACTOME_MITOTIC_G1_G1_S_PHASES	-4.68	-4.44
REACTOME_NUCLEAR_EVENTS_KINASE_AND_TRANSCRIPTION_FACTOR_ACTIVATION	-4.74	-4.25
PID_RAC1_PATHWAY	-5.27	-3.68
PID_LKB1_PATHWAY	-4.58	-4.27
REACTOME_MAPK_TARGETS_NUCLEAR_EVENTS_MEDIATED_BY_MAP_KINASES	-4.98	-3.72
REACTOME_G1_PHASE	-5.13	-3.57

Supplementary Table 5: Comparison of phospho-protein pathways between LT DOX/No DOX in B and D lines analyzed by SILAC (ssGSEA for MSigDB pathways; phosphosite abundance normalized to protein abundance; FDR < 0.1)

Pathway Name	Normalized Enrichment Score (B)	Normalized Enrichment Score (D)
PSP:KinaseSubstrate:DYRK2	-3.34	-4.41
REACTOME_CLASS_A1_RHODOPSIN_LIKE_RECEPTORS	-4.16	-4.40
KEGG_NEUROACTIVE_LIGAND_RECEPTOR_INTERACTION	-3.87	-4.40
REACTOME_TOLL_RECEPTOR_CASCADES	4.72	3.76
REACTOME_NFKB_AND_MAP_KINASES_ACTIVATION_MEDIATED_BY_TLR4_SIGNALING_REPERTOIRE	4.31	3.87
REACTOME_TRAF6_MEDIATED_INDUCTION_OF_NFKB_AND_MAP_KINASES_UPON_TLR7_8_OR_9_ACTIVATION	4.38	3.91
REACTOME_PLATELET_ACTIVATION_SIGNALING_AND_AGGREGATION	5.20	4.11
PID_HNF3APATHWAY	4.54	4.47
REACTOME_IMMUNE_SYSTEM	4.49	4.48
REACTOME_INNATE_IMMUNE_SYSTEM	4.95	4.87

MATERIALS AND METHODS

Cell lines and culture conditions

A, B, and D parental cells were derived from three distinct primary pancreatic tumors from *Kras*$^{LSL\text{-}G12D/+}$; *p53*$^{flox/flox}$; *Pdx1-CreER* mice treated with tamoxifen (Sigma) to induce oncogenic *Kras*^{G12D} activation and biallelic *p53* inactivation in the pancreas[13]. All cell lines were maintained in DMEM (Corning Cellgro) supplemented with 10% fetal bovine serum (Hyclone) and penicillin/streptomycin. For inducible-shRNA experiments, doxycycline (DOX, Sigma) was used at 1 μg/mL in culture media and replaced every 2-3 days. Cell viability was analyzed after 4-5 days of DOX treatment using the CellTiter-Glo luminescence assay (Promega), which measures cellular ATP levels as a surrogate for cell number and growth. Luminescence was read on a Tecan M2000 Infinite Pro plate reader. Cells were imaged with a Nikon Eclipse TE2000-U light microscope and SPOT RT3 camera. For iTRAQ, cells were grown on 15-cm plates and harvested when 70-80% confluent for lysis. For SILAC labeling, cells were passaged in heavy, medium, or light media for 7-8 population doublings, and carefully maintained at optimal confluence (70-80%) during passaging before lysis.

Inducible shRNA retroviral constructs

A, B, and D cell lines were sequentially transduced with retroviral constructs for rtTA3 (MSCV-rtTA3-hygro; **Fig. 1A**) and constructs for inducible shKras[38] and shLuc expression, adapted from the TGMP (TRE-GFP-miR30-PGK-Puro^R) inducible knockdown system previously described by G. Hannon and S. Lowe and colleagues[39]. For double knockdown experiments, shFAK and shGpr56 were cloned into a TGMB (TRE-GFP-miR30-PGK-Blast^R) vector. mir30-based shRNA 97-mers were synthesized (Life Technologies) for cloing. The

individual shRNAs were cloned into the TGMP and TGMB vectors using XhoI and EcoRI restriction enzyme sites. High-fidelity restriction enzymes and T4 ligase (New England BioLabs) were used in recommended buffers. The sequences of the shRNA 22-mers and primers used for shRNA cloning are listed in **Supplementary Table 2**. *MSCV-IRES-GFP* and *MSCV-KrasG12D-IRES-GFP* retroviral vectors were used for overexpression studies to confirm on-target Kras knockdown.

Retroviral transduction

For retroviral infections, retroviral backbone, and pCL-Eco (for mouse cells) were transfected into 293T cells with TransIT-LT1 (Mirus Bio). Supernatant was collected at 48 and 72 hours and applied to target cells with 8 μg/mL polybrene for transduction. Transduced cells were treated with 2 μg/mL puromycin (Life Technologies), 400 μg/mL hygromycin B (Roche), or 10 μg/mL blasticidin S (Life Technologies) for 3-7 days, as appropriate, for antibiotic selection. To generate single cell clones from the transduced cells, we sorted one cell per well into 96-well plates using a FACSAria II (Becton Dickinson) FACS sorter.

***In vitro* growth and adherence assays**

For growth curves, 1000 cells were plated on day 0 and grown for five days in culture. 4-5 replicates for each cell line per day were assessed for cell viability by CellTiter-Glo (Promega). Cell viability results were normalized to luminescence at day 0. For growth curves measured in cell number rather than luminescence, 10,000 cells per well were plated in 6-well plates on day 0 in five replicates, and cells were trypsinized and counted every day. Low-density colony forming assays were performed by plating 1000 cells into 6-well plates in triplicate and staining

with 0.5% crystal violet 7-10 days after plating. Cells for clonal efficiency assay were grown in 96-well dishes for 21 days with media supplementation with or without DOX every 2-3 days. Clones were stained with crystal violet and absorbance at 540 nm quantified following solubilization with Sorensen's buffer. 3D cultures were established by plating 250-500 cells onto a growth factor-reduced matrigel (Corning) layer, allowing cell migration into matrigel for 4-6 hours. Cells were grown in complete media for 12 days prior to analysis. For adherence assay, single cell suspensions were generated and 5000-10,000 cells were plated in 100 uL media into 96-well plates. After one hour, media was aspirated, and cell viability of remaining adhered cells was analyzed by CellTiter-Glo and compared to cell viability of suspension cells immediately at time of plating. To disrupt actin cytoskeleton, cells were treated with latrunculin B (632 nM) for 1 hour prior to imaging. For anoikis assay, cells were grown as single cell suspension for 48 hours on poly-HEMA coated plates prior to protein collection for immunoblotting. To determine response to matrigel, suspension cells were assessed for cell viability using CellTiter-Glo.

Immunoblotting

Cells were lysed with ice-cold RIPA buffer (Pierce), supplemented with 0.5 μM EDTA and Halt protease and phosphatase inhibitors (Thermo Scientific), rotated at 4°C for 15-30 minutes to mix, and centrifuged at maximum speed for 15 minutes to collect whole cell lysates. For total pY analysis, cells were lysed by freezing the cell pellet in RIPA buffer (with EDTA and inhibitors) at -80°C overnight to best preserve phosphorylation. Protein concentration was measured with the BCA protein assay (Pierce). 30 μg of total protein per sample was loaded into 4-12% Bis-Tris gradient gels (Life Technologies) and separated by SDS-PAGE. Proteins were

transferred to nitrocellulose (for fluorescence detection) or PVDF (for chemiluminescent detection) membranes. The following antibodies were used for immunoblotting: mouse anti-HSP90 (BD #610418, 1:10,000), rabbit anti-β-tubulin (CST 2128, 1:1000), mouse anti-KRAS (SCBT sc-30, 1:200), mouse anti-phosphotyrosine (Millipore 4G10, 1:1000), mouse anti-paxillin (BD #610052, 1:1000), mouse anti-vinculin (Sigma-Aldrich V9131, 1:800), rabbit anti-FAK (Millipore 06-543, 1:1000), rabbit anti-FAK pY397 (Invitrogen 44-624G, 1:1000), rabbit anti-pERK1/2(T202/Y204) (CST 4370, 1:1000), mouse anti-ERK1/2 (CST 9107, 1:1000), and rabbit anti-CC3(Asp175) (CST 9664, 1:1000). HSP90 and β-tubulin were used as loading controls. Primary antibodies were detected with fluorescent-conjugated (LI-COR) or HRP-conjugated (BioRad) secondary antibodies for fluorescent (LI-COR) or chemiluminescent detection (Amersham), respectively. For the phospho-RTK array, 500 μg protein in 250 μl lysis buffer for each sample was incubated with the membrane, and experiment was performed following the protocol provided (R&D mouse proteome profiler phospho-RTK array kit #ARY014).

Immunofluorescence

For immunofluorescent staining of focal adhesion structures, 50,000 (for D line) or 100,000 (for B line) cells were plated on cover slips in 6-well plates, and were grown for 2 days before fixation. The fixed cells were then stained with mouse anti-paxillin (BD #610052, 1:500) or mouse anti-vinculin (Sigma-Aldrich V9131, 1:800), along with DAPI (Life Technologies) and Alexa Fluor 555 Phalloidin (ThermoFisher Scientific). The secondary antibody used was donkey anti-mouse IgG (H+L) Alexa Fluor 488 conjugate (ThermoFisher Scientific, 1:250). The stained cells were imagined with Applied Precision DeltaVision Spectris Imaging microscope, and images were deconvoluted with the Softworx deconvolution software. The percentage of

cells containing focal adhesion plaques were quantified by counting cells under high power fields (hpf). Only the hpf that contained at least 10 cells were included and graphed in the final quantitation.

RNA isolation and RNA-sequencing (RNA-Seq) analysis

RNA was isolated from PDAC cells using TRIzol (Life Technologies). cDNA libraries were prepared using an Illumina TruSeq sample preparation kit with indexed adaptor sequences and polyA selection. Sequencing was performed on an Illumina HiSeq 2000 instrument to obtain single-end 40-nt reads. All reads that passed quality metrics were mapped to the UCSC mm9 mouse or hg19 human genome build (http://genome.ucsc.edu/) using RSEM. For pairwise differential expression analyses, data normalization (MedianNorm) and differential analyses between experimental conditions were performed using EBSeq v1.4.0. All RNA-Seq analyses were conducted in the R Statistical Programming language (http://www.r-project.org/). Unsupervised clustering was performed using a Pearson correlation based pairwise distance measure. Heat maps were generated using the Heatplus package in R.

High-resolution signature analyses between clones within each cell line were performed using a blind source separation methodology based on Independent Component Analysis (ICA) (A.B. et al., in preparation). RSEM generated estimated expression counts were upper-quartile normalized to a count of 1000. The R implementation of the core JADE algorithm (Joint Approximate Diagonalization of Eigenmatrices) was used along with custom R utilities. Signatures were visualized using the sample-to-signature correspondence schematic afforded by Hinton plots where colors represent directionality of gene expression (red upregulated, green downregulated) and the size of each rectangle quantifies the strength of a signature (column) in a

given sample (row). Each signature is two-sided, allowing for identification of upregulated and downregulated genes for each signature within each sample. Biologically relevant and statistically significant signatures were identified using a Mann-Whitney U test. Heat maps were plotted with the top and bottom 2% genes in each signature.

Gene Set Enrichment Analyses (GSEA) were carried out using the pre-ranked mode using log2 fold-change values (for pairwise analyses) or standardized signature correlation scores (for ICA signatures) with default settings. Network representations of GSEA results were generated using EnrichmentMap for Cytoscape v3.2.1 using $p<0.05$ and $FDR<0.25$ as cut-offs. Each circle represents a gene set with circle size corresponding to gene set size and intensity corresponding to enrichment significance. Red is upregulated and blue is downregulated. Each line corresponds to minimum 50% mutual overlap with line thickness corresponding to degree of overlap.

Candidate point mutations in RNA-Seq datasets were called using a pipeline based on the GATK Toolkit. Transcriptomic reads were mapped (to mm9, hg19) using the Tophat spliced aligner and subjected to local realignment and score recalibration using the GATK Toolkit. Mutations were called in KO samples (individual and pooled) against WT samples (individual and pooled) with a minimum base quality threshold of 30. Genomic annotations were performed using ANNOVAR.

Quantitative RT-PCR

RNA was reverse transcribed using High-Capacity cDNA Reverse Transcription Kit (Applied Biosystems). Quantitative PCR (qPCR) was performed using Taqman probes (Applied

Biosystems). C_t values were measured by a LightCycler 480 Real-Time PCR System (Roche) and relative expression (normalized to TBP) was calculated using the $\Delta\Delta C_t$ method.

Drug treatments

PF562271 and PF573228 were purchased from Selleck Chemical. All compounds were diluted to 10 mM stock concentration in DMSO. To generate dose-response curves, cells (250-500 for D clones, 750-1000 for B clones) were plated in 96-well white plates (Perkin Elmer) in 100 μL of media and incubated overnight. 100 μL of drug at 2X final concentration was added to each well in triplicate for each cell line and dose. Cell viability was determined at 72 hours using CellTiter-Glo (Promega). Percent viability was calculated for each dosed well compared to solvent controls (DMSO) and plotted against log10[Dose] (M). For dose-response curves, each replicate for each cell line and dose was plotted along with curve-fit regression for three-component inhibitor response (Prism).

Subcutaneous tumor transplant in immunocompromised mice

All animal studies were approved by the MIT Institutional Animal Care and Use Committee. Cells were transplanted to form tumors in NOD/SCID mice (Taconic) via subcutaneous injections. 100 μL of cell suspensions of varying concentrations in cold PBS were injected per tumor to determine tumor-forming capacity and tumor growth kinetics in the context of gene kncokdown. Tumor formation was monitored over time by visual observation. Tumor-initiating cell number was calculated based on limiting dilutions of transplanted cells using web-based ELDA software (http://bioinf.wehi.edu.au/software/elda/).

Tumor growth was followed by caliper measurement or luciferase imaging. Caliper measurement was done in 3-4 day intervals. Tumor volume was calculated from caliper measurements using the modified ellipsoid formula: (length)x(width)^2/2. Because the PDAC cells are engineered to express *MSCV-Luciferase-IRES-GFP* (plasmids were retrovirally transduced like the inducible shRNA constructs), tumors were measured based on luminescence using IVIS spectrum optical imaging (Xenogen corporation). Bioluminescence imaging by IVIS was done in 3-4 day intervals by injecting 100µl of 30mg/ml luciferin per mouse and imaging 10 minutes post-injection. The level of bioluminescence in radiance was analyzed by Living Image software (Perkin Elmer). Cell lines were made from subcutaneous tumors by dissociation using a collagenase IV (Worthington), dispase, trypsin, and DNAse cocktail in HEPES-buffered HBSS.

Phosphotyrosine analysis via LC-MS/MS (iTRAQ)

Cells were lysed in 8M urea (Sigma) and were quantified using BCA assay (Pierce). Proteins were reduced with 10mM dithiothreitol (Sigma) for 1h at 56°C and then alkylated with 55mM iodoacetamide (Sigma) for 1h at 25°C in the dark. Proteins were then digested with modified trypsin (Promega) at an enzyme/substrate ratio of 1:50 in 100mM ammonium acetate, pH 8.9 at 25°C overnight. Trypsin activity was halted by addition of acetic acid (99.9%, Sigma) to a final concentration of 5%. After desalting using a C18 Sep-Pak Plus cartridge (Waters), peptides were lyophilized and store at -80°C. Peptides were labeled with iTRAQ 4plex (AB Sciex) as previously described[30]. Lyophilized samples (400ug) were labeled with 1 aliquot of iTRAQ label per peptide sample. Peptides were dissolved in 30µL of 500mM triethylammonium bicarbonate, pH 8.5, and each iTRAQ reagent was dissolved in 70µL of

isopropanol. Each peptide sample was combined with one of four iTRAQ labels, vortexed, and incubated for 1h at 25°C. The labeled peptides were then combined and concentrated to completion.

For immunoprecipitation, protein G agarose (60μL, Millipore) was incubated with anti-phosphotyrosine antibodies (12μg 4G10 (Millipore), 12μg PT66 (Sigma), and 12μg PY100 (CST)) in 400μL of IP buffer (100mM Tris, 100mM NaCl, and 1% Nonidet P-40, pH 7.4) for 8h at 4°C with rotation. The antibody conjugated protein G was washed with 400μL of IP buffer. The iTRAQ labeled peptides were dissolved in 400μL IP buffer and the pH was adjusted to 7.4. The iTRAQ labeled peptides were then incubated with the antibody conjugated protein G overnight at 4°C with rotation. The agarose was washed with 400μL IP buffer followed by four rinses with 400μL rinse buffer (100mM Tris, pH 7.4). Peptides were eluted with 70μL of 100mM glycine, pH 2 for 30 minutes at 25°C. Offline immobilized metal affinity chromatography (IMAC) was used to further enrich for phosphotyrosine peptides[30].

Peptides were then loaded on a precolumn and separated by reverse phase HPLC using an EASY- nLC1000 (Thermo) over a 140 minute gradient before nanoelectrospray using a QExactive mass spectrometer (Thermo). The mass spectrometer was operated in a data-dependent mode. The parameters for the full scan MS were: resolution of 70,000 across 350-2000 *m/z*, AGC $3e^6$, and maximum IT 50 ms. The full MS scan was followed by MS/MS for the top 10 precursor ions in each cycle with a NCE of 32 and dynamic exclusion of 30 s. Raw mass spectral data files (.raw) were searched using Proteome Discoverer (Thermo) and Mascot version 2.4.1 (Matrix Science). Mascot search parameters were: 10 ppm mass tolerance for precursor ions; 0.8 Da for fragment ion mass tolerance; 2 missed cleavages of trypsin; fixed modification were carbamidomethylation of cysteine and iTRAQ 4plex modification of lysines and peptide N-

termini; variable modifications were methionine oxidation, tyrosine phosphorylation, and serine/threonine phosphorylation. Only peptides with a Mascot score greater than or equal to 25 and an isolation interference less than or equal to 25 were included in the quantitative data analysis. The average false discovery rate was 0.0029 (ranging from 0.0013-0.0041). iTRAQ quantification was obtained using Proteome Discoverer and isotopically corrected per manufacturer's instructions. The iTRAQ values were normalized to the mean relative protein quantification ratios obtained from a total protein analysis. For the total protein analysis, 0.2% of the supernatant from the phosphotyrosine peptide immunoprecipitation was analyzed via LC-MS/MS. This analysis serves as a loading control as it gives quantitation for the most abundant non-phosphorylated peptides. The phosphortyrosine LC-MS/MS analysis was performed three times with different sample preparations. Only tyrosine phosphorylation sites that were detected in at least two independent experiments were considered for further analysis.

SILAC analysis

Preparation of SILAC-labeled murine PDAC cells.

SILAC-labeled cells were cultured at a concentration of 10^6 cells/mL in DMEM medium supplemented with 10% FBS and penicillin/streptomycin, and either normal L-lysine (K0) and L-arginine (R0), or medium-labeled D_4- lysine (K4) and $^{13}C_6$- arginine (R6), or heavy-labeled $^{13}C_6$-$^{15}N_2$ lysine (K8) and $^{13}C_6$-$^{15}N_4$ arginine (R10). Lysine and arginine were supplemented at concentrations of 40 mg/L and 120 mg/L, respectively. Labeled murine PDAC cells (LT DOX or No DOX) were harvested after 7-8 cell doublings.

Cell lysis and peptide digestion.

Cells were washed once with PBS and lysed for 30 min in ice-cold lysis urea buffer (8 M urea; 75 mM NaCl, 50 mM Tris HCl pH 8.0, 1 mM EDTA, 2 μg/mL aprotinin (Sigma, A6103), 10 μg/mL leupeptin (Roche, #11017101001), 1 mM PMSF (Sigma, 78830), 10 mM NaF, 5 mM sodium butyrate, 5 mM iodoacetamide (Sigma, A3221), Phosphatase Inhibitor Cocktail 2 (1:100, Sigma, P5726), Phosphatase Inhibitor Cocktail 3 (1:100, Sigma, P0044). Lysates were centrifuged at 20,000*g* for 10 min, and protein concentrations of the clarified lysates were measured via BCA assay (Pierce, 23227). A total of 5 mg total proteins per SILAC channel were combined for a total of 15 mg proteins per SILAC experiment.

Protein disulfide bonds of the combined lysates were reduced for 45 min with 5 mM dithiothreitol (Thermo Scientific, 20291) and alkylated for 45 min with 10 mM iodoacetamide. Samples were then diluted 1:4 with 50 mM Tris HCl, pH 8.0, to reduce the urea concentration to 2 M. Lysates were digested for 2 h using 1:50 enzyme-to-substrate ratio LysC (Wako, 129-02541) and trypsin (Promega, V511X) was added in a 1:50 enzyme-to-substrate ratio for digest at room temperature overnight. Peptide mixtures were acidified to a final volumetric concentration of 1% formic acid (Fluka, 56302) and centrifuged at 2,000*g* for 5 min to pellet urea that had precipitated out of solution. Peptide mixtures were desalted on tC18 SepPak columns (Waters, 500 mg WAT036790). Columns were conditioned with 1 × 5 ml 100% acetonitrile and 1 × 5 ml 50% acetonitrile/0.1% formic acid washes, and equilibrated with 4 × 5 ml 0.1% trifluoroacetic acid (Fluka, TX1276-6). After loading the sample onto the column, samples were desalted with 3× 5 ml 0.1% trifluoroacetic acid washes and 1 × 5 ml 1% formic acid wash. Peptides were eluted from the column with 2 × 3 ml 50% acetonitrile/0.1% formic acid. Eluted peptide samples were placed in a vacuum concentrator to evaporate the elution solvent and produce purified peptide samples.

Basic reversed-phase separation of peptides and generation of proteome samples for analysis.

To reduce peptide complexity, samples were separated by basic reversed-phase chromatography. For basic RP separation, desalted peptides were reconstituted in 1.8 mL 20 mM ammonium formate, pH 10, and centrifuged at 10,000*g* to clarify the mixture before it was transferred into autosampler tubes. Basic reversed-phase chromatography was conducted on a 9.4 mm × 250 mm column Zorbax 300 Å Extend-C18 column (Agilent, 5 μm bead size), using an Agilent 1100 Series HPLC instrument. Solvent A (2% acetonitrile, 5 mM ammonium formate, pH 10), and a nonlinear increasing concentration of solvent B (90% acetonitrile, 5 mM ammonium formate, pH 10) were used to separate peptides by their hydrophobicity at a high pH. We used a flow rate of 3 ml/min and increased the percentage of solvent B in a nonlinear gradient with 4 different slopes (0% for 2 min; 0% to 10% in 5 min; 10% to 27% in 34 min; 27% to 31% 4 min; 31% to 39% in 4 min; 39% to 60% in 7 min; 60% for 8 min). Eluted peptides were collected in 96 × 2 mL deepwell plates (Whatman, #7701-5200) with 1 min (= 1 ml) fractions for the 4.6 mm column and 40 s (= 2 ml) fractions for the 9.4 mm column. Early eluting peptides were collected in fraction "A", which is a combined sample of all fractions collected before any major UV-214 signals were detected.

Peptide samples were combined into 24 subfractions, respectively, to be used for proteome analysis. Subfractions were achieved by combining every 24th fraction (1,25,49; 2,26,50; ...). Subfractions were acidified to a final concentration of 1% formic acid, and 5% of the volumetric samples were reserved for proteome analysis.

The remaining 95% of each of the original 72 subfractions from bRP (above) were further combined before enrichment for PTM analyses as follows: every 12th fraction was combined (1,13; 2,14; ...) to generate 12 fractions. Peptide fractions were subsequently dried by

vacuum sublimation in a vacuum concentrator. We have also analyzed an early eluting hydrophilic fraction labeled fraction A which contains a large number of multiply phosphorylated peptides.

IMAC phospho-enrichment of peptides.

As described previously[29], iron-chelated IMAC beads were prepared from Ni-NTA superflow agarose beads (Qiagen, #1018611) that were stripped of nickel with 100 mM EDTA and incubated in an aqueous solution of 10 mM $FeCl_3$ (Sigma, 451649). Dried phosphopeptide fractions were reconstituted in 50% acetonitrile/0.1% trifluoroacetic acid and then diluted 1:1 with 100% acetonitrile/0.1% trifluoroacetic acid to obtain a final 80% acetonitrile/0.1% TFA peptide solution at a concentration of 0.5 μg/μl. Peptide mixtures were enriched for phosphorylated peptides with 10 μL IMAC beads for each sample for 30 min. Enriched IMAC beads were loaded on Empore C18 silica-packed stage tips (3M, 2315). Stage tips were equilibrated with 2 × 100 μL washes of methanol, 2 × 50 μL washes of 50% acetonitrile/0.1% formic acid, and 2 × 100 μL washes of 1% formic acid. Samples were then loaded onto stage tips and washed twice with 50 μL of 80% acetonitrile/0.1% trifluoroacetic acid and 100 μL of 1% formic acid. Phosphorylated peptides were eluted from IMAC beads with 3 × 70 μL washes of 500 mM dibasic sodium phosphate, pH 7.0, (Sigma, S9763) and washed twice with 100 μL of 1% formic acid before being eluted from stage tips with 60 μL 50% acetonitrile/0.1% formic acid. All washes were performed on a tabletop centrifuge at a maximum speed of 3,500*g*.

LC-MS/MS analysis.

All peptide samples were separated on an online nanoflow EASY-nLC 1000 UHPLC system (Thermo Fisher Scientific) and analyzed on a benchtop Orbitrap Q Exactive mass spectrometer (Thermo Fisher Scientific). Ten percent of each proteome (containing ~1 μg) and

fifty percent of each phosphopeptide, K(GG) peptide, and K(Ac) peptide sample were injected onto a capillary column (Picofrit with 10 μm tip opening / 75 μm diameter, New Objective, PF360-75-10-N-5) packed in-house with 20 cm C18 silica material (1.9 μm ReproSil-Pur C18-AQ medium, Dr. Maisch GmbH, r119.aq). The UHPLC setup was connected with a custom-fit microadapting tee (360 μm, IDEX Health & Science, UH-753), and capillary columns were heated to 50 °C in column heater sleeves (Phoenix-ST) to reduce backpressure during UHPLC separation. Injected peptides were separated at a flow rate of 200 nL/min with a linear 80 min gradient from 100% solvent A (3% acetonitrile, 0.1% formic acid) to 30% solvent B (90% acetonitrile, 0.1% formic acid), followed by a linear 6 min gradient from 30% solvent B to 90% solvent B. Each sample was run for 150 min, including sample loading and column equilibration times. Data-dependent acquisition was obtained using Xcalibur 2.2 software in positive ion mode at a spray voltage of 2.00 kV. MS1 Spectra were measured with a resolution of 70,000, an AGC target of 3e6 and a mass range from 300 to 1800 *m/z*. Up to 12 MS2 spectra per duty cycle were triggered at a resolution of 17,500, an AGC target of 5e4, an isolation window of 2.5 *m/z*and a normalized collision energy of 25. Peptides that triggered MS2 scans were dynamically excluded from further MS2 scans for 20 s.

Identification and quantification of proteins.

All mass spectra were analyzed with MaxQuant software version 1.3.0.5 using a mouse UniProt database. MS/MS searches for the proteome data sets were performed with the following parameters: Oxidation of methionine and protein N-terminal acetylation as variable modifications; carbamidomethylation as fixed modification. For IMAC data sets phosphorylation of serine, threonine and tyrosine residues were searched as additional variable modifications. Trypsin/P was selected as the digestion enzyme, and a maximum of 3 labeled

amino acids and 2 missed cleavages per peptide were allowed. The mass tolerance for precursor ions was set to 20 p.p.m. for the first search (used for nonlinear mass re-calibration) and 6 p.p.m. for the main search. Fragment ion mass tolerance was set to 20 p.p.m. For identification we applied a maximum FDR of 1% separately on protein, peptide and PTM-site level. We required 2 or more unique/razor peptides for protein identification and a ratio count of 2 or more for protein quantification per replicate measurement. PTM-sites were considered to be fully localized when they were measured with a localization probability >0.75 in each of the three replicates. To assign regulated proteins and PTM-sites we used the Limma package in the R environment to calculate moderated *t*-test *P*values corrected by the Benjamini Hochberg method, as described previously[40]. Bland-Altman filtering was applied at 99.9% (+/-3.29 sigma).

ACKNOWLEDGEMENTS

We thank E. Vasile for training and technical support with microscopy and imaging of the immunofluorescence-based analysis, and F. Gertler and D. Riquelme for insightful discussions and protocols on focal adhesion cell biology experiments. We appreciate F. White for his help with setting up the collaborative iTRAQ analysis with the Proteomics Core Facility, and we thank M. Yaffe, B. Joughin, and K. Krismer for their consultation and help with iTRAQ and SILAC data analysis (specifically, kinase-substrate interactions and motif analyses). Additionally, we thank members in the Jacks lab, especially W. Xue, K. Mercer, and H. Jenq, for many helpful discussions and for their generosity in sharing experimental reagents and protocols.

This work was supported by the Howard Hughes Medical Institute, Lustgarten Foundation Consortium grant, Blum-Kovler Pancreatic Cancer Action Network-AACR Innovative grant, Department of Defense Congressionally-Directed Medical Research Program grant (W81XWH-12-043), and in part by the Cancer Center Support (core) grant P30-CA14051 from the National Cancer Institute. M.D.M. is supported by a KL2/Catalyst Medical Research Investigator Training award (an appointed KL2 award) from Harvard Catalyst | The Harvard Clinical and Translational Science Center (National Center for Research Resources and the National Center for Advancing Translational Sciences, National Institutes of Health Award KL2 TR001100). T.J. is a Howard Hughes Medical Institute Investigator, the David H. Koch Professor of Biology, and a Daniel K. Ludwig Scholar.

REFERENCES

1. Ryan, D.P., Hong, T.S. & Bardeesy, N. Pancreatic adenocarcinoma. *N Engl J Med* **371**, 2140-2141 (2014).
2. Cancer Facts & Figures 2016. (American Cancer Society, Atlanta, 2016).
3. Conroy, T., *et al.* FOLFIRINOX versus gemcitabine for metastatic pancreatic cancer. *N Engl J Med* **364**, 1817-1825 (2011).
4. Von Hoff, D.D., *et al.* Increased survival in pancreatic cancer with nab-paclitaxel plus gemcitabine. *N Engl J Med* **369**, 1691-1703 (2013).
5. Bardeesy, N. & DePinho, R.A. Pancreatic cancer biology and genetics. *Nat Rev Cancer* **2**, 897-909 (2002).
6. Jones, S., *et al.* Core signaling pathways in human pancreatic cancers revealed by global genomic analyses. *Science* **321**, 1801-1806 (2008).
7. Waddell, N., *et al.* Whole genomes redefine the mutational landscape of pancreatic cancer. *Nature* **518**, 495-501 (2015).
8. Cox, A.D., Fesik, S.W., Kimmelman, A.C., Luo, J. & Der, C.J. Drugging the undruggable RAS: Mission possible? *Nat Rev Drug Discov* **13**, 828-851 (2014).
9. Collins, M.A., *et al.* Oncogenic Kras is required for both the initiation and maintenance of pancreatic cancer in mice. *J Clin Invest* **122**, 639-653 (2012).
10. Collins, M.A., *et al.* Metastatic pancreatic cancer is dependent on oncogenic Kras in mice. *PLoS ONE* **7**, e49707 (2012).
11. Hingorani, S.R., *et al.* Trp53R172H and KrasG12D cooperate to promote chromosomal instability and widely metastatic pancreatic ductal adenocarcinoma in mice. *Cancer Cell* **7**, 469-483 (2005).
12. Ying, H., *et al.* Oncogenic Kras maintains pancreatic tumors through regulation of anabolic glucose metabolism. *Cell* **149**, 656-670 (2012).
13. Gidekel Friedlander, S.Y., *et al.* Context-dependent transformation of adult pancreatic cells by oncogenic K-Ras. *Cancer Cell* **16**, 379-389 (2009).
14. Hingorani, S.R., *et al.* Preinvasive and invasive ductal pancreatic cancer and its early detection in the mouse. *Cancer Cell* **4**, 437-450 (2003).
15. Singh, A., *et al.* A gene expression signature associated with "K-Ras addiction" reveals regulators of EMT and tumor cell survival. *Cancer Cell* **15**, 489-500 (2009).
16. Collisson, E.A., *et al.* Subtypes of pancreatic ductal adenocarcinoma and their differing responses to therapy. *Nature Medicine* **17**, 500-503 (2011).
17. Kapoor, A., *et al.* Yap1 activation enables bypass of oncogenic Kras addiction in pancreatic cancer. *Cell* **158**, 185-197 (2014).
18. Viale, A., *et al.* Oncogene ablation-resistant pancreatic cancer cells depend on mitochondrial function. *Nature* **514**, 628-632 (2014).
19. Hata, A.N., *et al.* Tumor cells can follow distinct evolutionary paths to become resistant to epidermal growth factor receptor inhibition. *Nature Medicine* **22**, 262-269 (2016).
20. Sun, C., *et al.* Reversible and adaptive resistance to BRAF(V600E) inhibition in melanoma. *Nature* **508**, 118-122 (2014).
21. Burrell, R.A. & Swanton, C. Tumour heterogeneity and the evolution of polyclonal drug resistance. *Molecular Oncology* **8**, 1095-1111 (2014).
22. Pribluda, A., de la Cruz, C.C. & Jackson, E.L. Intratumoral Heterogeneity: From Diversity Comes Resistance. *Clin Cancer Res* **21**, 2916-2923 (2015).

23. Sharma, S.V., *et al.* A chromatin-mediated reversible drug-tolerant state in cancer cell subpopulations. *Cell* **141**, 69-80 (2010).
24. Glasspool, R.M., Teodoridis, J.M. & Brown, R. Epigenetics as a mechanism driving polygenic clinical drug resistance. *Br J Cancer* **94**, 1087-1092 (2006).
25. Kurata, T., *et al.* Effect of re-treatment with gefitinib ('Iressa', ZD1839) after acquisition of resistance. *Annals of oncology : official journal of the European Society for Medical Oncology / ESMO* **15**, 173-174 (2004).
26. Yano, S., *et al.* Retreatment of lung adenocarcinoma patients with gefitinib who had experienced favorable results from their initial treatment with this selective epidermal growth factor receptor inhibitor: a report of three cases. *Oncol Res* **15**, 107-111 (2005).
27. Bailey, P., *et al.* Genomic analyses identify molecular subtypes of pancreatic cancer. *Nature* **531**, 47-52 (2016).
28. Wang, M.T., *et al.* K-Ras Promotes Tumorigenicity through Suppression of Non-canonical Wnt Signaling. *Cell* **163**, 1237-1251 (2015).
29. Mertins, P., *et al.* Integrated proteomic analysis of post-translational modifications by serial enrichment. *Nature Methods* **10**, 634-637 (2013).
30. Zhang, Y., *et al.* Time-resolved mass spectrometry of tyrosine phosphorylation sites in the epidermal growth factor receptor signaling network reveals dynamic modules. *Mol Cell Proteomics* **4**, 1240-1250 (2005).
31. Hofmann, I., *et al.* K-RAS mutant pancreatic tumors show higher sensitivity to MEK than to PI3K inhibition in vivo. *PLoS ONE* **7**, e44146 (2012).
32. Mitra, S.K., Hanson, D.A. & Schlaepfer, D.D. Focal adhesion kinase: in command and control of cell motility. *Nat Rev Mol Cell Biol* **6**, 56-68 (2005).
33. Kanteti, R., Batra, S.K., Lennon, F.E. & Salgia, R. FAK and paxillin, two potential targets in pancreatic cancer. *Oncotarget* (2016).
34. McLean, G.W., *et al.* The role of focal-adhesion kinase in cancer - a new therapeutic opportunity. *Nat Rev Cancer* **5**, 505-515 (2005).
35. Sulzmaier, F.J., Jean, C. & Schlaepfer, D.D. FAK in cancer: mechanistic findings and clinical applications. *Nat Rev Cancer* **14**, 598-610 (2014).
36. Zheng, Y., *et al.* FAK phosphorylation by ERK primes ras-induced tyrosine dephosphorylation of FAK mediated by PIN1 and PTP-PEST. *Molecular Cell* **35**, 11-25 (2009).
37. Hochwald, S.N., *et al.* A novel small molecule inhibitor of FAK decreases growth of human pancreatic cancer. *Cell Cycle* **8**, 2435-2443 (2009).
38. Shao, D.D., *et al.* KRAS and YAP1 converge to regulate EMT and tumor survival. *Cell* **158**, 171-184 (2014).
39. Premsrirut, P.K., *et al.* A rapid and scalable system for studying gene function in mice using conditional RNA interference. *Cell* **145**, 145-158 (2011).
40. Udeshi, N.D., *et al.* Methods for quantification of in vivo changes in protein ubiquitination following proteasome and deubiquitinase inhibition. *Mol Cell Proteomics* **11**, 148-159 (2012).

CHAPTER 3

Survival of pancreatic cancer cells lacking KRAS function

Mandar Deepak Muzumdar[1,2,3*], Pan-Yu Chen[1,4*], Kimberly Judith Dorans[1],

Katherine Minjee Chung[1], Arjun Bhutkar[1], Erin Hong[1],

and Tyler Jacks[1,4,5]

Author Affiliations:
[1] David H. Koch Institute for Integrative Cancer Research, Massachusetts Institute of Technology, Cambridge, MA 02139, USA
[2] Dana-Farber Cancer Institute, Boston, MA 02215, USA
[3] Harvard Medical School, Boston, MA 02215, USA
[4] Department of Biology, Massachusetts Institute of Technology, Cambridge, MA 02139, USA
[5] Howard Hughes Medical Institute, Massachusetts Institute of Technology, Cambridge, MA 02139, USA

[*]M.D.M. and P-Y.C. contributed equally to this work.

M.D.M., P-Y.C., and T.J. designed the study; M.D.M., P-Y.C., K.J.D., K.M.C., and E.H. performed all the molecular biology, *in vitro*, and *in vivo* experiments in the laboratory of T.J.; A.B. conducted bioinformatics analyses; a large part of this Chapter is adapted from a manuscript that was written by M.D.M., P-Y.C., and T.J., with comments from other co-authors.

ABSTRACT

Activating mutations in the proto-oncogene *KRAS* are a hallmark of pancreatic ductal adenocarcinoma (PDAC), an aggressive malignancy with few effective therapeutic options. Despite efforts to develop KRAS-targeted drugs, the absolute dependence of PDAC cells on KRAS remains incompletely understood. Here we modeled complete KRAS inhibition using CRISPR/Cas-mediated genome editing. While *KRAS* knockout led to decreased *in vitro* proliferation and impaired *in vivo* tumorigenic growth, KRAS was dispensable in a subset of human and mouse PDAC cells. *KRAS* knockout cells exhibited hyperactivation of the PI3K pathway and induced sensitivity to phosphoinositide 3-kinase (PI3K) inhibitors. Mechanistically, PI3K inhibition in *KRAS* knockout cells led to transient mitogen-activated protein kinase (MAPK) blockade while impeding AKT-dependent 4EBP1 phosphorylation and cap-dependent translation. Furthermore, comparison of gene expression profiles of cells retaining or lacking KRAS revealed a novel functional role of KRAS in the suppression of metastasis-related genes. Accordingly, *KRAS* knockout gene expression signatures correlated with PDAC circulating tumor cell (CTC) signatures, and human PDAC tumors with gene expression patterns enriched in signatures from *KRAS* knockout cells were associated with worse survival in patients. Together, these data underscore the potential for resistance of PDAC to even the very best of KRAS inhibitors and suggest combination therapies with PI3K inhibitors as a viable strategy to circumvent resistance.

INTRODUCTION

Pancreatic ductal adenocarcinoma (PDAC) is the fourth leading cause of cancer death in the United States and a major cause of morbidity and mortality worldwide[1,2]. While advances in combination chemotherapy have improved median survival[3,4], long-term survival remains poor at 7%[1,2], highlighting the need for the development of novel therapeutic approaches.

Genomic studies have identified mutations in the proto-oncogene *KRAS,* occurring in >90% of cases[5–8], as a hallmark of PDAC. KRAS is a small GTPase that acts as a molecular switch to regulate proliferation, differentiation, metabolism, and survival[9]. Oncogenic forms of *KRAS* harboring mutations in codons 12, 13, and 61 are insensitive to GTPase activating protein (GAP)-induced GTP hydrolysis, leading to constitutive activation[10]. Studies in animal models have confirmed an important role of oncogenic KRAS in tumor initiation[11], making KRAS an attractive therapeutic target.

Unfortunately, the development of effective KRAS inhibitors has been made challenging by several unique features of oncogenic KRAS: 1) its high affinity for GTP, impeding the identification of GTP-competitive inhibitors; 2) the difficulty of inducing gain-of-function hydrolytic activity with small molecules; and 3) redundant pathways for membrane localization required for KRAS activity[9,10]. New approaches to directly inhibit KRAS through covalent binding of specific mutant variants (e.g. G12C)[12], interference with guanine-exchange factor (GEF) association to prevent initial GTP loading[13,14], and destabilization of additional membrane localization complexes[15] continue to be developed. Furthermore, the success of a recent effort spearheaded by the National Cancer Institute of the United States to develop novel RAS-targeted therapies[16,17] requires a better understanding of the dependency of PDAC cells on KRAS as well as predicting resistance mechanisms that can develop upon KRAS inhibition.

Given the lack of KRAS inhibitors, genetic tools have been used to evaluate the requirement of KRAS in PDAC maintenance. Acute knockdown of KRAS by RNA interference (RNAi) decreased cell proliferation and/or induced apoptosis in a series of human PDAC (hPDAC) cancer cell lines[18–20]. Variability in apoptotic response to KRAS knockdown led to the classification of some cells as "KRAS-dependent" and others as "KRAS-independent"[19,20]. Based on these studies, it was unclear whether the "KRAS-independent" phenotype was a consequence of the incomplete inhibitory effects of RNAi such that residual KRAS protein was sufficient to sustain cell survival and proliferation. Recent evidence for PDAC cell survival in the absence of oncogenic KRAS expression derived from a doxycycline (DOX)-inducible oncogenic *KRAS* transgenic mouse model[21]. In this model, DOX treatment led to oncogenic KRAS expression in the pancreas to initiate tumorigenesis, while DOX withdrawal halted transgene expression and induced tumor regression. Interestingly, a subset of PDAC tumors recurred lacking *KRAS* transgene expression[21]. Despite these findings, the absolute dependence of hPDAC and mouse PDAC (mPDAC) cells on endogenous KRAS remains unknown, a prerequisite for the successful translation of novel KRAS inhibitors.

Here, we investigated the consequence of complete endogenous KRAS ablation in PDAC cells using the Clustered Regularly Interspaced Short Palindromic Repeats (CRISPR)/Cas system. The bacterial CRISPR/Cas adaptive immune system, modified for genome editing in mammalian cells, utilizes a single guide RNA (sgRNA) to direct the Cas9 nuclease to cleave matching double-stranded DNA (dsDNA) sequences, resulting in insertions and deletions via error-prone non-homologous end joining (NHEJ) repair mechanisms[22]. By inducing loss-of-function mutations in *KRAS*, we modeled the cellular effects of complete inhibition to predict potential resistance mechanisms to KRAS inhibition and to uncover important KRAS-regulated

pathways in PDAC.

RESULTS

KRAS is dispensable in a subset of PDAC cells

To evaluate the absolute dependence of PDAC cells on endogenous *KRAS*, we employed CRISPR/Cas technology[22] to completely eliminate KRAS function. We transduced or transfected *KRAS* mutant hPDAC and mPDAC cell lines with Cas9 and a panel of sgRNAs targeting various *KRAS* exons (**Supplementary Fig. 1a, Supplementary Table 1**) to identify sgRNAs that effectively induced *KRAS* protein loss (**Supplementary Fig. 1b**). Given the lack of unique protospacer adhesion motifs (PAM) encompassing mutant codon 12, our sgRNAs did not discriminate between wild-type and mutant forms of *KRAS*, modeling a non-selective KRAS inhibitor. The consequence of short-term CRISPR/Cas-mediated KRAS knockout mimicked the effect of short hairpin RNA (shRNA)-mediated KRAS knockdown on cell viability (**Supplementary Figs. 1c,d**). Consistent with published results[19], previously-defined "KRAS-independent" cells (8988T, PANC-1) were largely insensitive to sgRNA transduction, while "KRAS-dependent" cells (8902) exhibited significantly decreased viability (**Supplementary Fig. 1e**).

We further generated single cell subclones to evaluate whether PDAC cells could survive in the complete absence of KRAS expression. We successfully isolated *KRAS* knockout subclones from 8988T hPDAC (**Fig. 1a, Supplementary Fig. 2a**), PANC-1 hPDAC (**Supplementary Fig. 2e**), and A13 mPDAC cells (**Fig. 1a**). We confirmed decreased overall RAS activity in knockout cells as evident by dramatically reduced RAS-GTP levels (**Fig. 1b**). Sanger sequencing revealed indels in the *KRAS* locus leading to premature stop codons or in-

frame deletions of important functional domains[23] (**Figs. 1c,d**), likely perturbing protein folding and stability. Notably, the capacity to generate knockout clones differed between cell lines (**Supplementary Fig. 3a**). The greatest determinant of knockout clone isolation appeared to be intrinsic dependence of the cell lines to KRAS inhibition, as those cell lines most affected by RNAi knockdown (**Supplementary Fig. 1c** and previous studies[19]) generated clones that all retained KRAS protein (8902 hPDAC, **Supplementary Fig. 3b**) or did not form recoverable clones at all (YAPC hPDAC) due to apoptosis.

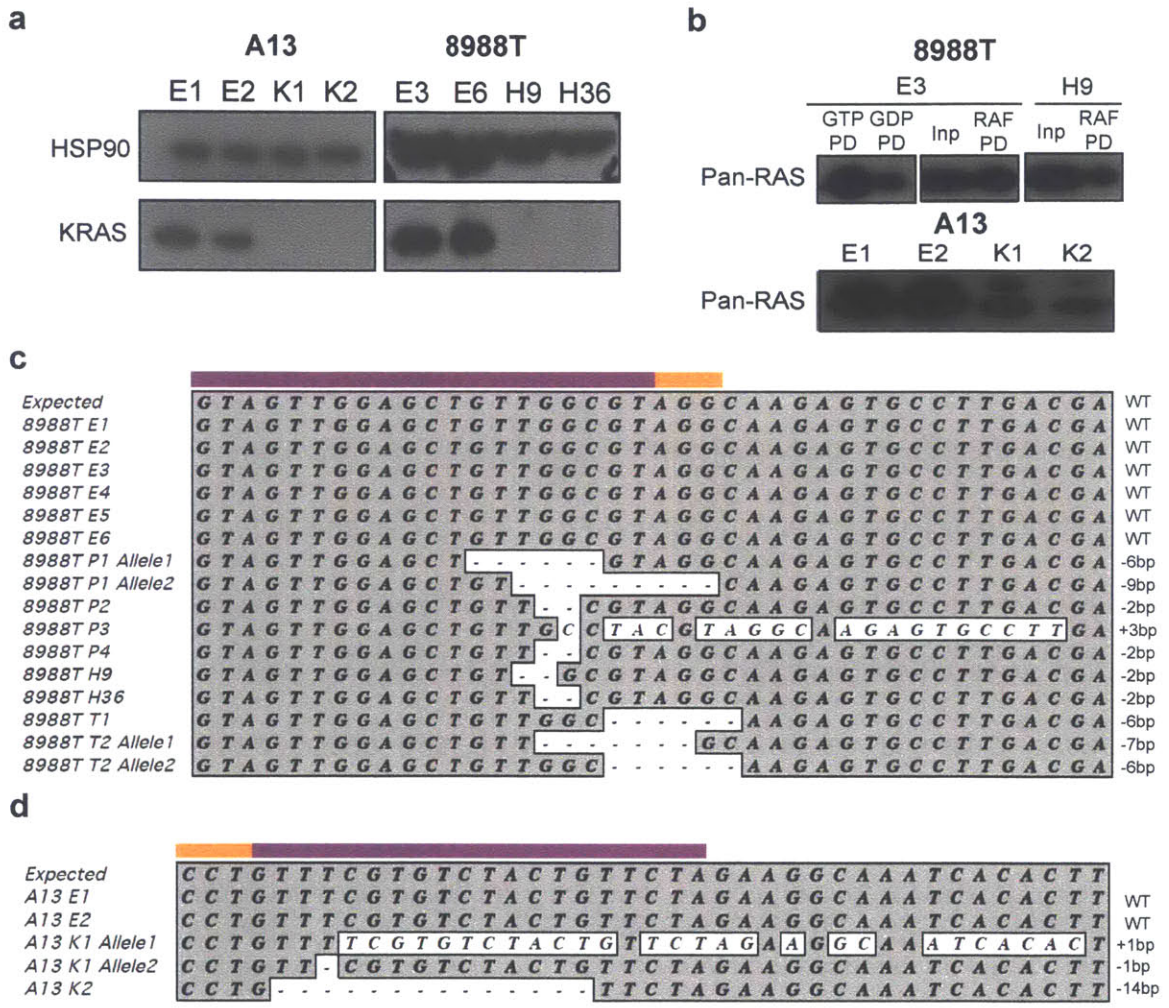

Figure 1. CRISPR/Cas9-mediated *KRAS* knockout in PDAC cells.

(a) Western blot confirmed loss of KRAS protein in knockout clones (A13-K1 and K2, 8988T- H9 and H36) compared to intact clones (A13-E1 and E2, 8988T-E3 and E6).

(b) RAS-GTP levels were decreased in knockout (8988T H9 and A13 K1-2) compared to intact (8988T E3 and A13 E1-2) clones. GTPγS (non-hydrolysable)-treated positive control (GTP PD) and GDP-treated negative control (GDP PD) for 8988T E3 are shown. PD = pull-down. Inp = input before pull-down.

(c) DNA alleles from 8988T clones show indels in knockout clones. Expected sequence corresponds to reference from UCSC hg19 and was observed in all intact clones (E1-E6). Mutations are homozygous except for P1 and T2 for which two different alleles were identified. Clones with one detectable allele likely generated an indel in one allele followed by homology-directed repair of the other allele using the indel allele as a template. Alternatively, the second allele may represent a large deletion encompassing an entire exon and evading the PCR reaction used for sequencing. Both out-of-frame (P2, P4, H9, H36, T2 allele 1) and in-frame indels compromising essential codons 12 or 13 (P1, P3, T1, and T2 allele 2) were observed in sequenced knockout clones. The purple and orange bars denote the sgRNA and PAM sequences, respectively.

(d) DNA alleles from A13 clones showed indels in knockout clones. Expected sequence corresponds to reference from UCSC mm9 and was observed in intact clones (E1, E2). K2 harbored a homozygous 14bp out-of-frame deletion, while K1 carried a heterozygous 1bp insertion and deletion.

PDAC cells that survived KRAS loss exhibited perturbations of several growth characteristics. Knockout cells exhibited altered morphology (**Fig. 2a, Supplementary Figs. 2b,e**) comparable to that observed with KRAS knockdown (**Supplementary Fig. 1d**), significantly diminished anchorage-independent colony formation (**Fig. 2b, Supplementary Figs. 2c,e**), and slower proliferation in 2D and 3D culture (**Fig. 2c, Supplementary Figs. 2d,e**). Knockout cells retained the ability to form subcutaneous tumors in immunocompromised mice, though tumors grew more slowly (**Fig. 2d**). Together, these data demonstrate that loss of KRAS has a significant impact on proliferation *in vitro* and tumorigenic growth *in vivo*, confirming the importance of KRAS in the maintenance of PDAC cells. Furthermore, the proportional relationship between KRAS protein levels and cellular phenotypes (morphology, proliferation, and anchorage-independent growth (**Supplementary Fig. 2e**)) supports the notion that greater KRAS inhibition would lead to greater tumor suppressive effect.

To ensure that the phenotypes we observed were due to on-target *KRAS* mutagenesis, we assessed off-target mutations in the closest exonic matches and found no mutations in these loci (**Supplementary Figs. 4a,b**). Furthermore, expression of NRAS or HRAS in our knockout subclones was unaltered, consistent with KRAS specificity of the sgRNAs (**Supplementary Fig. 4c**). Additionally, mutation analysis of RNA-Sequencing (RNA-Seq) from 8988T and A13 (data not shown) subclones did not reveal recurrent protein-coding single nucleotide polymorphisms (SNPs) in expressed genes that distinguished all intact and knockout clones. Finally, we re-expressed oncogenic KRAS in knockout clones (**Supplementary Fig. 4d**), and observed a reversal in cell morphology (**Supplementary Fig. 4e**), *in vitro* proliferation (**Supplementary Fig. 4f**), and soft agar colony formation (**Supplementary Fig. 4g**).

Based on the absence of recurrent clonal mutations in knockout cells and the reversibility of phenotypes with re-expression of oncogenic *KRAS*, we hypothesized that PDAC cells underwent adaptation to a state of tolerance to KRAS loss rather than clonal selection. Consistent with this hypothesis, we have used a doxycycline-inducible short hairpin RNA (shRNA) system (**Supplementary Fig. 1c)** and observed a reversible state of adaptive resistance to KRAS knockdown in PDAC cells (**Chapter 2**). We also detected high efficiency *KRAS* knockout in 8988T *KRAS.22V* cells in nearly all clones analyzed (23/24), suggesting that survival in the absence of KRAS is not an isolated phenomenon in this cell line (**Supplementary Fig. 3a**). Given lower clonal efficiencies with other cell lines and sgRNAs, we cannot definitively exclude the possibility that these additional clones are rare cells inherently resistant to *KRAS* knockout.

Notably, several factors affected the efficiency of knockout clone generation, including 1) the efficacy of different sgRNAs to induce loss-of-function mutations; 2) transduction efficiency and Cas9 expression level in individual cells; 3) the ability of cell lines to form single cell clones irrespective of KRAS modulation (8988T and A13 grew more efficiently as single cell clones than PANC-1 cells); and 4) ploidy (PANC-1 is hypertriploid while 8988T and A13 are not). Individual sgRNAs had different efficiencies in inducing KRAS loss-of-function in the same cell lines (**Supplementary Fig. 3a**, e.g. 8988T *KRAS.22V* versus *KRAS.165*). We quantified the mutation efficiency of all potential sgRNAs (based on PAM sequence availability) across the entire human *KRAS* locus. We transduced Cas9-expressing 8902 cells with a bicistronic lentiviral vector permitting simultaneous sgRNA and green fluorescent protein (GFP) expression (**Supplementary Fig. 3c**) and performed competition assays between transduced (GFP+) and untransduced (GFP-) cells within the population. sgRNAs with significant effects

on cell viability (corresponding to KRAS loss-of-function mutagenesis) would be expected to more rapidly deplete in the population. While most sgRNAs had an effect on cell viability, there were marked differences in the degree and rate of depletion (**Supplementary Fig. 3c** and data not shown), with greater efficacy of sgRNAs targeting exons 1 and 2, likely due to the presence of essential functional domains[23] (such as GTP-binding residues). Despite these limitations, our results demonstrate that endogenous KRAS is dispensable in a subset of human and mouse pancreatic cancer cells, underscoring the potential for resistance to even the very best of KRAS inhibitors.

***KRAS* knockout cells exhibit PI3K pathway activation and dependence**

While previous work reported that marked overexpression of YAP1 could support the growth of a subset of PDAC tumors following loss of KRAS expression[21,24], we did not observe similar elevations in YAP1 RNA or protein levels in *KRAS* knockout cells (**Supplementary Figs. 5a,b**). Moreover, *KRAS* knockout cell lines did not exhibit increased sensitivity to verteporfin, a YAP-TEAD interaction inhibitor, compared to *KRAS* intact cells (**Supplementary Fig. 5c**). To identify essential pathways that support the proliferation and survival of PDAC cells in the absence of KRAS function in an unbiased manner, we employed high-throughput drug screening and evaluated unique dependencies in *KRAS* knockout cells. We screened 8988T intact and knockout clones against a compound library comprised of kinase inhibitors, epigenetic modifiers, and chemotherapeutic agents, many of which are being tested in clinical trials or are FDA-approved. While no compound uniquely decreased cell viability in *KRAS* intact cells, knockout cells exhibited increased sensitivity to pan-PI3K and mTOR inhibitors (**Supplementary Fig. 6a**). As dose-response curves and direct observation suggested a cytotoxic effect of pan-PI3K inhibitors rather than the cytostatic effect of mTOR inhibition (**Supplementary Figs. 6b-d**), we chose to further characterize the effect of PI3K inhibition on knockout cells.

We confirmed increased sensitivity to the pan-PI3K inhibitors GDC-0941 and BAY80-6946 in additional 8988T *KRAS* knockout clones (**Fig. 3a, Supplementary Fig. 7a**) and in A13 knockout clones (**Fig. 3b**). Moreover, GDC-0941 increased apoptosis in knockout cells (**Fig. 3c**) and selectively inhibited knockout tumor growth *in vivo* (**Fig. 3d**). Treatment with combinations of PI3K class I isoform-specific inhibitors revealed a synergistic effect of p110α inhibition with p110β- or p110δ-specific inhibitors (**Supplementary Fig. 7b,c**), suggesting the need for pan-

class I PI3K inhibition for full effect. Biochemically, we observed relatively stable MAPK activity but significantly increased PI3K/AKT pathway activation in knockout cells at steady state (**Fig. 3e, Supplementary Fig. 7d**), possibly due to feedback stimulation by upregulated receptor tyrosine kinases (RTKs)[25–27], as activating PI3K pathway mutations and changes in the protein levels of the phosphoinositide phosphatases PTEN and INPP4B (**Supplementary Fig. 7e)** were not observed in knockout cells.

In order to recapitulate the therapeutic effect of combined KRAS and PI3K inhibition in established PDAC tumors, we engineered A13 cells to stably express Cas9 and a DOX-inducible Kras-targeting sgRNA. We identified two clones (clone 7 and clone 31) that displayed efficient ablation of Kras proteins assayed after 7 days of *in vitro* DOX treatment (**Fig. 3f inset**). To minimize clonal and animal differences, we subcutaneously transplanted clones 7 and 31 on the right and left flanks, respectively, of immunocompromised mice. Notably, there was minimal variation in tumor growth rate between the two clones. Administration of DOX feed led to sgKras expression in established tumors and acute suppression of tumor growth (started on day 0 in **Fig. 3f**). Subsequent daily dosing of GDC-0941 selectively suppressed the growth of *Kras* knockout tumors (started on day 4 in **Fig. 3f**). Importantly, Kras inhibition alone was insufficient to suppress tumor growth beyond day 9, possibly due to selection of escapers that harbor non-frameshift mutations or cells that bypassed the requirement of Kras by PI3K/AKT activation. These observations demonstrate that combined Kras and PI3K inhbition can be a useful therapeutic strategy in established PDAC tumors.

Interestingly, we observed that PDGFRβ and FGFR2 were both upregulated in knockout cells (**Supplementary Fig. 7f**), but inhibition of PDGFR or FGFR alone or in combination did not alter PI3K/AKT activation or show greater sensitivity in *KRAS* knockout cells

(**Supplementary Figs. 7g**). Similarly, RTK array profiling of A13 intact and knockout clones did not reveal significant differences in phosphorylation across a broader array of RTKs (**Supplementary Fig. 7h**). In contrast, stimulation with any of the RTK ligands EGF, PDGF-BB, or FGF1 decreased sensitivity of knockout cells to PI3K inhibition (**Supplementary Figs. 7i,j**). Together, these data suggest that individual RTKs may be sufficient but not necessary to support the PI3K pathway in knockout cells, indicating compensatory mechanisms exist. However, activation of PI3K represents a convergent targetable node in PDAC cells lacking KRAS function.

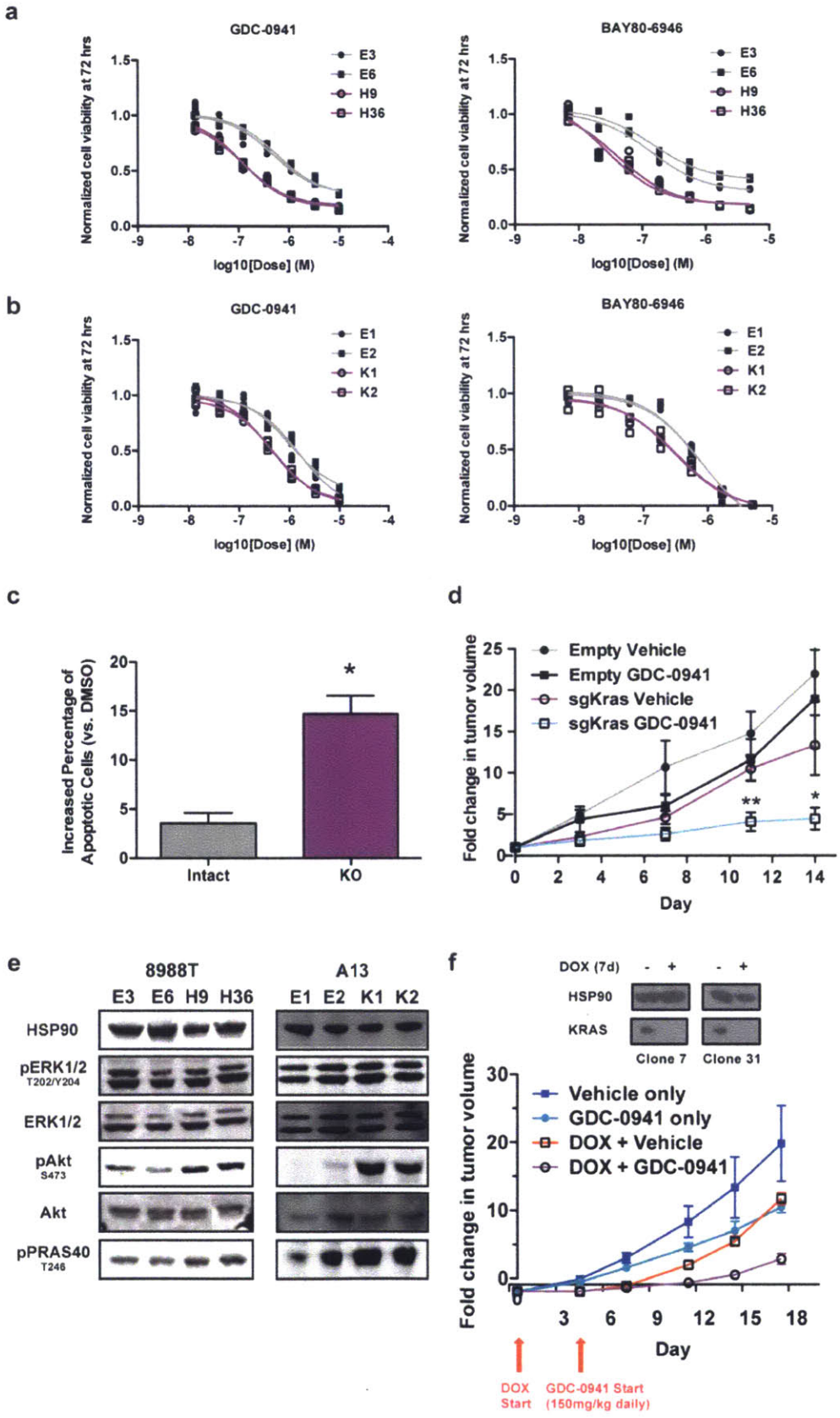
a
GDC-0941
BAY80-6946
Normalized cell viability at 72 hrs
log10[Dose] (M)
E3
E6
H9
H36
b
E1
E2
K1
K2
c
Increased Percentage of Apoptotic Cells (vs. DMSO)
Intact
KO
d
Fold change in tumor volume
Empty Vehicle
Empty GDC-0941
sgKras Vehicle
sgKras GDC-0941
Day
e
8988T
A13
HSP90
pERK1/2
T202/Y204
ERK1/2
pAkt
S473
Akt
pPRAS40
T246
f
DOX (7d)
KRAS
Clone 7
Clone 31
Vehicle only
GDC-0941 only
DOX + Vehicle
DOX + GDC-0941
DOX Start
GDC-0941 Start (150mg/kg daily)

Figure 3. Increased PI3K pathway activation and dependence of *KRAS* knockout cells *in vitro* and *in vivo*.

(a) Dose-response curves of 8988T intact (grey) and knockout (purple) cells to pan-PI3K inhibitors GDC-0941 and BAY80-6946.

(b) Dose-response curves of A13 cells to pan-PI3K inhibitors.

(c) Increased apoptosis (change in percentage Annexin V-positive cells vs. DMSO) in *KRAS* knockout cells 48 hours after 2μM GDC-0941 treatment. Average +/- SEM is plotted (n=2 clones per group). *p<0.05, Student's t-test.

(d) GDC-0941 significantly decreased the tumorigenic growth of knockout but not intact A13 cells transplanted in nude mice. Average tumor volume +/- SEM (n=8 tumors per group) is plotted. *p<0.05, **p<0.01, two-tailed Student's t-test for measurements at each time point comparing GDC-0941 to vehicle.

(e) Western blot showed stable pERK1/2 but increased pAKT and pPRAS40 levels in knockout cells consistent with PI3K/AKT pathway activation.

(f) Combined Kras (by DOX-inducible sgKras) and PI3K (by GDC-0941) inhibition in established subcutaneous tumors effectively inhibited tumor growth, whereas inhibition of Kras or PI3K alone was insufficient to suppress tumor growth long-term. Shown is a composite of tumors generated by clones 7 and 31. Average tumor volume fold increase +/- SEM is plotted (n=10 tumors per group). Inset: western blot showed complete Kras protein ablation after 7 days of DOX treatment *in vitro*.

Simultaneous MAPK and AKT blockade by PI3K inhibition in *KRAS* knockout cells

To understand the mechanism underlying PI3K inhibitor sensitivity in *KRAS* knockout cells, we evaluated the effect of AKT inhibition on cell viability *in vitro*. Surprisingly, AKT inhibition did not recapitulate the differential sensitivity observed with PI3K inhibition (**Supplementary Figs. 8a,b**). However, overexpression of constitutively active myristoylated (*myr*) forms of *AKT1* or *AKT2* [but not the kinase-dead mutant *AKT1* (*K179M*)] prevented GDC-0941-induced AKT pathway inhibition and markedly decreased PI3K inhibitor sensitivity (**Figs. 4a,b, Supplementary Figs. 8c-f**). These data suggested that PI3K inhibitor-mediated AKT blockade was necessary but insufficient for its effect on cell viability.

Recent work indicated that PI3K inhibitors can transiently inactivate the MAPK pathway in cells harboring PI3K pathway mutations to induce apoptosis[28,29]. Indeed, while GDC-0941 sustainably suppressed pAKT in both *KRAS* knockout and intact cells, a transient decrease in pERK1/2 levels lasting minutes to hours only occurred in knockout cells (**Figs. 4c,d, Supplementary Figs. 9a,b**). The effect of GDC-0941 appeared to be due to inhibition of wild-type RAS activity upstream of the MAPK pathway, as RAS-GTP, pCRAF, and pMEK1/2 (**Figs. 4e,f**) levels were transiently diminished in *KRAS* knockout cells. Consistent with this observation, GDC-0941 also induced a decline in pERK levels in the *KRAS* wild-type hPDAC cell line BxPC3 (**Supplementary Fig. 9c**).

Several lines of evidence support the hypothesis that simultaneous MAPK and AKT inhibition by GDC-0941 may underlie its therapeutic effect in the absence of KRAS. First, the MEK inhibitor AZD6244 synergized with the AKT inhibitor MK2206 in both intact and knockout cells (**Supplementary Fig. 9d**). However, while AZD6244 enhanced the effect of GDC-0941 on intact cells, such synergy was absent in knockout cells (**Supplementary Fig. 9e**),

likely due to the MAPK inhibitory effect already provided by GDC-0941. Second, overexpression of constitutively active MEK (*MEK-DD*) or sgRNA-resistant oncogenic *KRAS* in knockout cells prevented the transient pERK1/2 decline and reduced drug sensitivity to GDC-0941 (**Figs. 4g,h, Supplementary Fig. 9f**). Finally, in PANC-1 knockout cells, which do not exhibit PI3K inhibitor sensitivity, GDC-0941 effectively suppressed AKT and downstream targets without affecting pERK1/2 levels (**Supplementary Fig. 9g**).

Prior research has suggested that the MAPK and AKT pathways may converge on the 4EBP1-EIF4E axis to regulate cap-dependent translation in cancer cells[30,31]. Interestingly, oncogenic gene signatures associated with the cap-dependent translation mediators MYC and EIF4E[32,33] were enriched in gene expression analysis of 8988T *KRAS* intact cells (data not shown), suggesting that *KRAS* may also regulate this process in this cell line. While we did not observe a difference in MYC protein levels (**Supplementary Fig. 7e**), we did see a decrease in baseline phospho-4EBP1 levels in 8988T knockout cells (**Supplementary Fig. 7d**), which would be expected to permit 4EBP1 sequestration of EIF4E and limit cap-dependent translation. We hypothesized that GDC-0941 treatment might further decrease 4EBP1 phosphorylation in these knockout cells, pushing them beyond a threshold to functionally impair cap-dependent translation. To test this, we transduced 8988T *KRAS* intact and knockout cells with a *mCherry-IRES-GFP* translation reporter (**Supplementary Fig. 10a**). *KRAS* knockout cells exhibited a more marked decrease in cap-dependent translation when treated with GDC-0941 or the mTORC1/2 inhibitor AZD8055 than intact cells (**Supplementary Fig. 10b**). Moreover, the effects of GDC-0941 on cell viability, 4EBP1 phosphorylation, and cap-dependent translation were rescued by overexpression of *myr-AKT1* but not *myr-AKT1 K179M* (**Supplementary Figs. 8e,f, Supplementary Fig. 10c**). These data highlight cap-dependent translation as a potential

MAPK and AKT convergent node that mediates sensitivity to GDC-0941 in *KRAS* knockout cells.

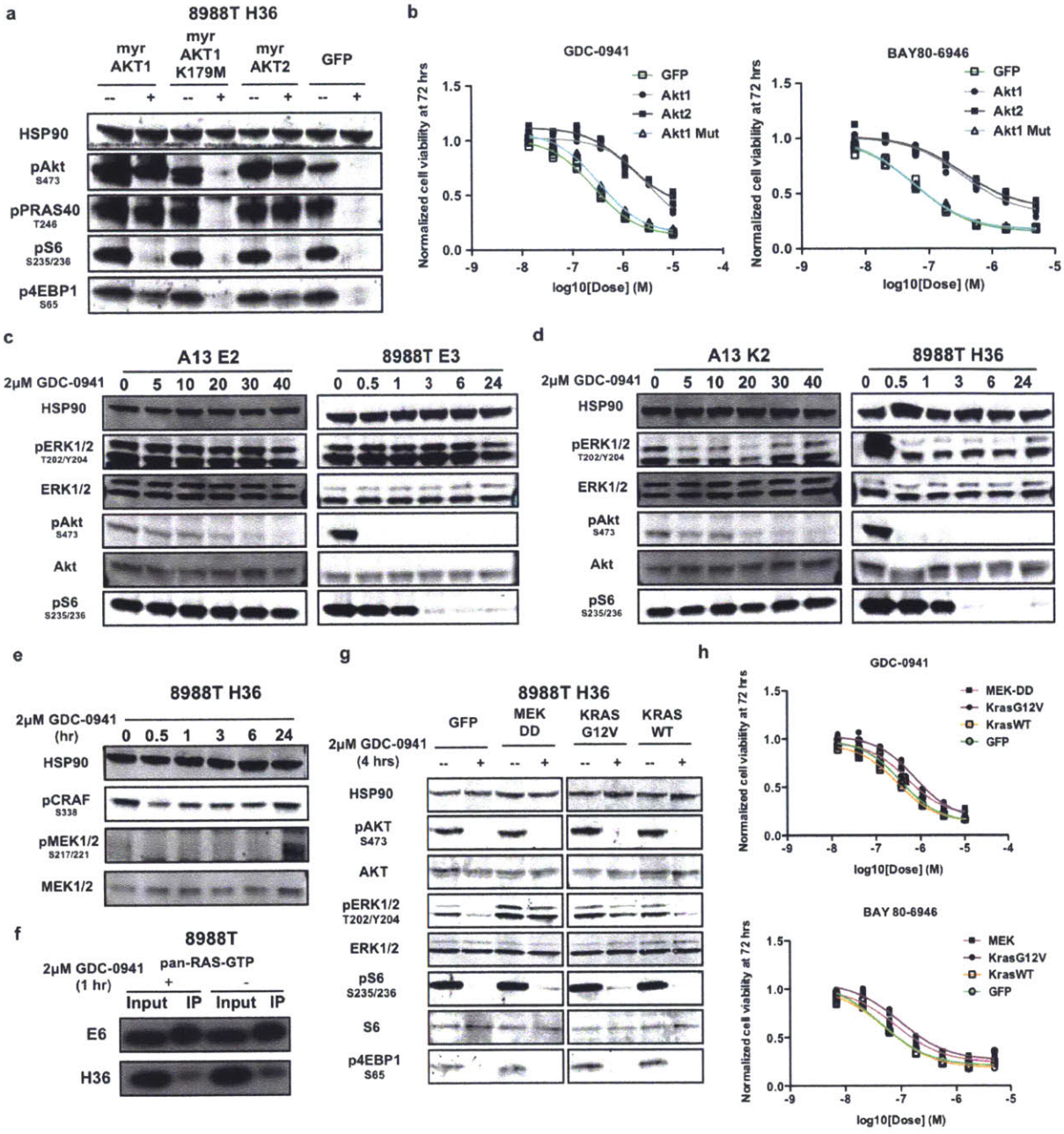

Figure 4. Transient MAPK blockade following PI3K inhibition in *KRAS* knockout cells.

(a) Western blot showing the effects of 4-hour treatment with 2μM GDC-0941 on H36 knockout cells revealed sustained phosphorylation of AKT and downstream targets (PRAS40, S6, and 4EBP1) only in *myr-AKT1*- and *myr-AKT2*-expressing cells but not in *myr-AKT1 (K179M)*- or control *GFP*-expressing cells.

(b) Dose-response curves of cell lines in (a) treated with GDC-0941 and BAY80-6946 demonstrated a marked decrease in PI3K sensitivity with *AKT1* or *AKT2* overexpression.

(c) Western blot showed no change in pERK1/2 levels in A13 and 8988T intact cells at designated times (minutes for A13, hours for 8988T) following 2μM GDC-0941 treatment.

(d) Western blot showed transient decrease in pERK1/2 levels in A13 and 8988T knockout cells at designated times (minutes for A13, hours for 8988T) following 2μM GDC-0941 treatment.
(e) Western blot showed transient decrease in phosphorylation of the MAPK regulators CRAF and MEK1/2 following 2μM GDC-0941 treatment in knockout cells.
(f) Western blot of RAS-GTP levels in intact (E6) and knockout (H36) clones following 1-hour treatment with 2μM GDC-0941 showed a specific decline in knockout cells.
(g) Overexpression of constitutively active MEK (*MEK-DD*) or oncogenic *KRAS-G12V*, but not *KRAS-WT* or *GFP*, blocked pERK1/2 inhibition by a 4-hour treatment with 2μM GDC-0941.
(h) *MEK-DD* and *KRAS-G12V*-transduced cells show modestly decreased sensitivity to PI3K inhibition compared to control *GFP*- and *KRAS-WT*-transduced cells.

Identification of KRAS-regulated pathways in PDAC cells

In addition to elucidating mechanisms of resistance to KRAS inhibition, we uncovered key biological processes regulated by KRAS in PDAC cells by comparing the gene expression profiles of isogenic *KRAS* intact and knockout cells. Specifically, we performed RNA sequencing (RNA-Seq) on multiple 8988T and A13 clones. Unsupervised hierarchical clustering cleanly segregated intact from knockout clones (**Fig. 5a**), and pairwise differential expression analysis identified a large number of genes with significantly altered expression. We performed independent component analysis (ICA), a blind-source separation approach (see Methods), to generate high-resolution gene signatures associated with *KRAS* knockout (**Supplementary Figs. 11a,b**). To gain insight into the knockout signature, we performed gene-set enrichment analysis (GSEA)[34,35] across gene expression datasets in MSigDB[35]. As internal validation of our analysis, GSEA revealed anti-correlation of the knockout signatures with genes upregulated by expression of oncogenic *KRAS* in primary epithelial cells (data not shown). We further compared our gene signatures to datasets generated using the DOX-inducible *KRAS* transgene mouse model to modulate KRAS levels[21,36,37]. Given the high degree of heterogeneity observed between tumors and conditions in these datasets, we used ICA to identify KRAS-ON and KRAS-OFF signatures associated with acute (24-hour) KRAS withdrawal[8] (**Supplementary Fig. 11c**), surviving cells following longer-term KRAS withdrawal[13] (**Supplementary Fig. 11d**), and KRAS-independent relapsed tumors in mice[9] (**Supplementary Fig. 12a**). The KRAS-OFF signatures from these datasets were strongly enriched in our knockout signatures (**Supplementary Fig. 12b**), supporting the robustness of our *KRAS* knockout signatures across species and model systems.

We next examined GSEA results more broadly to identify key pathways regulated by KRAS in PDAC cells. A13 knockout cells showed statistically significant enrichment of a

limited number of curated gene sets in pathways previously associated with KRAS, including EMT, integrin and receptor tyrosine kinase (RTK) signaling, and redox metabolism[19,38,39] (**Fig. 5b**). In contrast, 8988T cells exhibited alterations in a large number of biologic processes (**Fig. 5c**). Consistent with cellular phenotypes, 8988T knockout cells showed decreased expression of genes related to cell cycle progression, nucleotide metabolism, and oxidative phosphorylation (**Fig. 5c**). Importantly, we uncovered novel roles of KRAS including the regulation of genes involved in ribosomal biogenesis and protein translation as well as the suppression of interferon response genes (IRGs).

KRAS-relevant signatures predict survival in PDAC patients

Recent data from mouse models demonstrated an inverse relationship between proliferation and metastatic capacity in PDAC[40]. Interestingly, we observed a similar inverse relationship in the expression of genes associated with cell proliferation (cell cycle progression, nucleotide metabolisms, and protein translation) and those associated with the metastatic process (EMT and invasion and integrin pathways) based on KRAS status in GSEA analyses. Moreover, our knockout signatures were strongly enriched in gene expression signatures derived from circulating tumor cells (CTCs) (compared to primary tumors) in a *Kras; p53* mutant PDAC model[41] (**Supplementary Figs. 13a,b**). Therefore, we hypothesized that the *KRAS* knockout signatures may predict worse patient survival.

We analyzed data from The Cancer Genome Atlas (TCGA) and ranked early-stage (mostly resected) primary human PDAC tumors based on gene expression correlation to the knockout signatures. As predicted, we observed that tumors highly correlated with either the 8988T or A13 knockout signatures were associated with poor survival in multivariate analysis

(**Supplementary Figs. 14a,b**). These tumors enriched in gene sets associated with EMT, invasion, focal adhesion/integrin signaling, and metastasis (**Supplementary Figs. 14c,d**). Despite their poor prognosis, these tumors anti-correlated with gene sets associated with ribosomal biogenesis, protein translation, oxidative phosphorylation, and cell cycle progression (**Supplementary Figs. 14c,d**). In these survival analyses, we noticed that tumors independently correlating with the 8988T or A13 knockout signatures had minimal overlap ($p=0.44$, hypergeometric test). In contrast, tumors anti-correlated with the knockout signatures were largely the same regardless of the cell line from which the signature was derived ($p=1.04 \times 10^{-7}$). This suggests that loss of oncogenic KRAS function leads to the expression of genes that promote a more aggressive phenotype. Consistent with this hypothesis, the murine CTC signature exhibited enrichment of gene sets downregulated by oncogenic KRAS expression in various cell types (**Supplementary Fig. 13c**).

We next integrated our hPDAC and mPDAC gene expression profiles to define a core set of KRAS-regulated genes with greater prognostic value. We jointly analyzed the 8988T and A13 signatures to generate a 32-gene knockout signature (see Methods, **Fig. 5d**). While the downregulated genes in this set relate to MAPK signaling (*DUSP4, DUSP9, SPRY4, ETV1, ETV4, ETV5*), the upregulated genes support pathways involved in the metastatic cascade, including EMT (*TGFB2, PBX1, FGFBP1*), cell adhesion (*FLRT3, ICAM1*), and extracellular matrix breakdown (*MMP19, MMP28*). Strikingly, ranking tumors by expression of just the 16 upregulated genes was sufficient to improve the prediction of PDAC survival (**Fig. 5e, Supplementary Fig. 14b**). We confirmed the prognostic capability of this 16-gene signature for survival in a separate PDAC cohort from the International Cancer Genome Consortium (**Fig. 5f**). Collectively, these data offer an independent prognostic gene signature to predict survival in

early-stage patients with PDAC and implicate loss of KRAS-related transcriptional suppression as a potential mechanism towards PDAC metastasis.

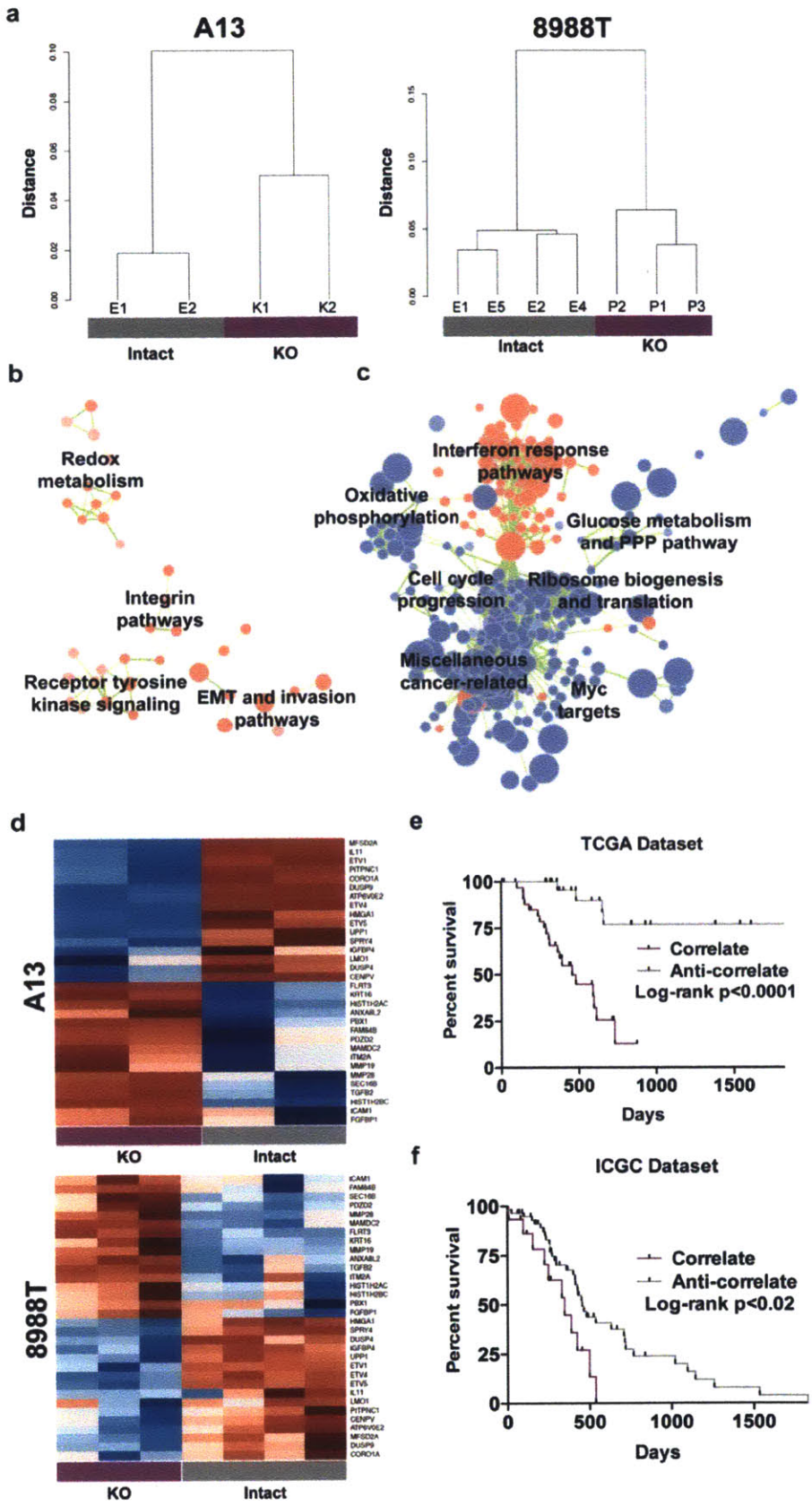
a
A13
Distance
E1
E2
K1
K2
Intact
KO
8988T
Distance
E1
E5
E2
E4
P2
P1
P3
Intact
KO
b
Redox metabolism
Integrin pathways
Receptor tyrosine kinase signaling
EMT and invasion pathways
c
Interferon response pathways
Oxidative phosphorylation
Glucose metabolism and PPP pathway
Cell cycle progression
Ribosome biogenesis and translation
Miscellaneous cancer-related
Myc targets
d
A13
KO
Intact
8988T
KO
Intact
e
TCGA Dataset
Percent survival
Correlate
Anti-correlate
Log-rank p<0.0001
Days
f
ICGC Dataset
Percent survival
Correlate
Anti-correlate
Log-rank p<0.02
Days

Figure 5. Gene expression analysis reveals multiple dysregulated cellular processes in *KRAS* knockout cells.

(a) Unsupervised hierarchical clustering dendrograms of 8988T and A13 clones indicated clean segregation between intact and knockout cells.

(b) Network representation of overlapping enriched GSEA/MSigDB gene sets in the A13 knockout signature ($p<0.05$, FDR<0.25). Each circle represents a gene set with circle size corresponding to gene set size and intensity corresponding to enrichment significance. Red is upregulated and blue is downregulated. Each line corresponds to minimum 50% mutual overlap with line thickness corresponding to degree of overlap. Cellular processes associated with related gene sets are listed.

(c) Network representation of overlapping enriched GSEA/MSigDB gene sets in the 8988T knockout signature ($p<0.005$, FDR<0.1).

(d) Heatmaps of a 32-gene combined knockout signature generated through ICA analysis of A13 and 8988T gene expression data sets. Row normalized gene expression values are shown where red designates relative upregulation and blue designates relative downregulation.

(e) Kaplan-Meier plots of survival in human tumors from TCGA PDAC dataset correlated (top quintile) and anti-correlated (bottom quintile) with the combined knockout signature (UP genes only). Log-rank (Mantel-Cox) p-value is shown.

(f) Kaplan-Meier plots of survival in human tumors from ICGC PDAC dataset correlated (top quintile) and anti-correlated (remaining tumors) with the combined knockout signature (UP genes only). Log-rank (Mantel-Cox) p-value is shown.

DISCUSSION

In this study, we examined the consequence of *KRAS* knockout in PDAC cells using CRISPR/Cas technology. While we confirmed the variable dependence of hPDAC cell lines based on prior RNAi studies[19,20], we isolated a subset of hPDAC and mPDAC cells that can survive and proliferate despite lacking endogenous KRAS function. Using an unbiased chemical screen, we identified an induced sensitivity to PI3K inhibition in *KRAS* knockout cells, offering a potential pharmacologically-tractable method to subvert resistance to KRAS blockade. Furthermore, we provide mechanistic insight into how PI3K inhibition simultaneously blocks the MAPK and AKT pathways to impair cap-dependent translation and cell viability in the context of *KRAS* ablation. Finally, gene expression profiling has defined novel KRAS-regulated pathways in PDAC cells and identified KRAS-relevant gene signatures that strongly predict survival in PDAC patients, offering a novel molecularly-guided prognostic tool in early-stage PDAC.

Given the significant adverse effects of *KRAS* knockout on *in vitro* proliferation and *in vivo* tumorigenic growth even in knockout-tolerant cells, our study adds to the growing body of evidence supporting the continued development of KRAS-directed therapies[10,17]. Furthermore, the dose-response relationship between KRAS levels and the cellular phenotypes observed (**Supplementary Fig. 2e**) highlight the therapeutic benefit of developing the most potent inhibitor possible. With the significant public and private investment towards the generation of novel KRAS-targeted drugs[16,17], elucidation of potential resistance mechanisms concurrent with the development of these inhibitors will facilitate their effectiveness in the clinic. Recent studies have implicated YAP1 overexpression as a means to escape KRAS inhibition in a subset of tumors and cell lines[21,24]. Our *KRAS* knockout cells revealed an alternative bypass mechanism

supported by canonical and non-canonical PI3K signaling. Given the variety of resistance mechanisms observed for tyrosine-kinase inhibitor therapy in RTK-mutated cancers, it is not surprising that multiple pathways could maintain PDAC cell survival following KRAS inhibition in various contexts.

While PI3K signaling has been implicated in mouse models to contribute to PDAC development, its role in PDAC maintenance has been less clear. Expression of oncogenic *PIK3CA* in the developing pancreas phenocopies pancreatic cancer initiation and progression observed in *KRAS* mutant mice[42,43]. In contrast, PI3K inhibitor therapy alone has only marginal benefit in preclinical mouse PDAC models, whereas combination therapies with MEK inhibition demonstrate significantly greater therapeutic effects[44–46]. Consistent with these observations, the combined MAPK and AKT blockade exhibited by single-agent PI3K inhibitors in PDAC cells is only evident when oncogenic KRAS is absent. Although the MAPK pathway dependence on PI3K has been demonstrated previously[28,29,47,48], we reveal a novel induced dependency to PI3K inhibition due to loss of oncogenic KRAS expression. Furthermore, we provide evidence that this rewiring occurs at the level of wild-type RAS. Though the precise nature of this association remains unclear, we speculate that this could be due to alterations in GAP activity or recruitment via Gab1/Shp2[49]. Nonetheless, we show that PI3K transitions to an upstream regulator of not only the canonical AKT pathway but also the RAS-MAPK pathway when oncogenic KRAS is lost.

In our study, we also took advantage of isogenic *KRAS* intact and knockout cell lines to identify novel KRAS-regulated pathways in PDAC. These include the upregulation of genes associated with ribosomal biogenesis and protein translation and the downregulation of genes associated with interferon response and the metastatic cascade. Moreover, we have developed a

16-gene signature, suppressed by KRAS, with independent prognostic value in PDAC validated in two different cohorts (TCGA and ICGC). Finally, we have demonstrated that our *KRAS* knockout signatures are enriched in PDAC CTCs relative to primary tumors. Given our data and evidence that CTCs displayed expression of genes downregulated by oncogenic KRAS, we propose that decreased KRAS activity may promote gene expression changes that drive metastasis. While further work is needed in primary human specimens to confirm the relationship between KRAS activity and metastasis, our work highlights KRAS-relevant gene signatures as independent prognostic factors in PDAC.

In summary, we have provided evidence to suggest that *KRAS*, the hallmark mutated gene in PDAC, is dispensable in a subset of PDAC cells. We have identified novel functions of KRAS in altering gene expression balancing proliferation and metastasis. Finally, our data demonstrate that canonical and non-canonical PI3K pathway activation may bypass the requirement for *KRAS* in PDAC and that simultaneous inhibition of KRAS and PI3K may be a viable combinatorial therapeutic strategy for this disease.

SUPPLEMENTARY FIGURES AND TABLES

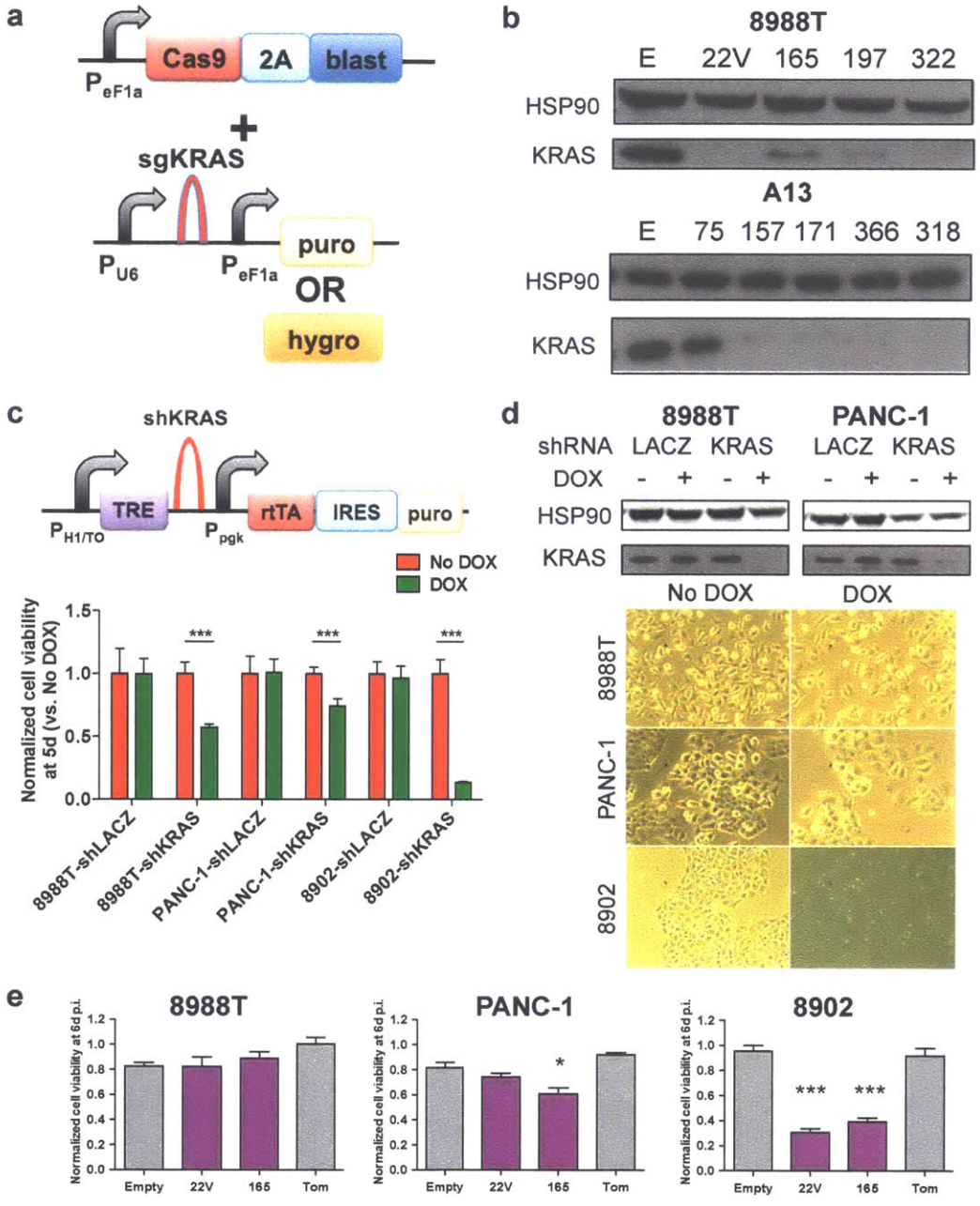

Supplementary Figure 1. CRISPR/Cas-mediated *KRAS* knockout in PDAC cells.

(a) Schematic of lentiviral constructs used to express Cas9 nuclease and sgRNAs in PDAC cells. P_{eF1a} = ubiquitously expressed elongation factor 1a promoter. P_{U6} = RNA polymerase III human U6 promoter. 2A = self-cleaving peptide. Blast = blasticidin resistance gene. Puro = puromycin resistance gene. Hygro = hygromycin resistance gene.

(b) Western blot of KRAS levels assayed 7 days after sgRNA transduction in Cas9-expressing 8988T and A13 cells at population levels. Residual protein is likely due to inefficient cutting or in-frame mutagenesis in some cells of the population. See Supplementary Table 1 for sgRNA sequences.

(c) Schematic of doxycycline (DOX)-inducible shRNA lentiviral construct pLKO-Tet-On. TRE = tetracycline-responsive element. P_{pgk} = ubiquitously expressed phosphoglycerate kinase promoter. rtTA = reverse tetracycline transactivator. IRES = internal ribosomal entry site. 8988T and PANC-1 (KRAS-independent) cell lines exhibited a modest but significant decrease in cell viability after 5 days of shKRAS induction with DOX, while 8902 (KRAS-dependent) cells showed a marked decrease in viability. Average cell viability +/- SD (n=5 replicates per condition) is plotted. ***p<0.001, two-tailed Student's t-test comparing shKRAS to shLACZ.

(d) Western blot of KRAS levels following 7 days of DOX treatment with 8988T and PANC-1 cell lines transduced with shLACZ or shKRAS. KRAS knockdown induced alterations in cell morphology in 8988T and PANC-1 cells and apoptosis in 8902 cells.

(e) Cell viability 6 days following transduction of empty vector, *hsKRAS.G12V*, *hsKRAS.165*, or *sgTomato* control vector. Cells were maintained in puromycin following transduction to ensure sgRNA transduction and viability was normalized to unselected cells. Average cell viability +/- SD (n=4 replicates per condition) is plotted. *p<0.05, ***p<0.001, two-tailed Student's t-test comparing sgRNA with empty vector control.

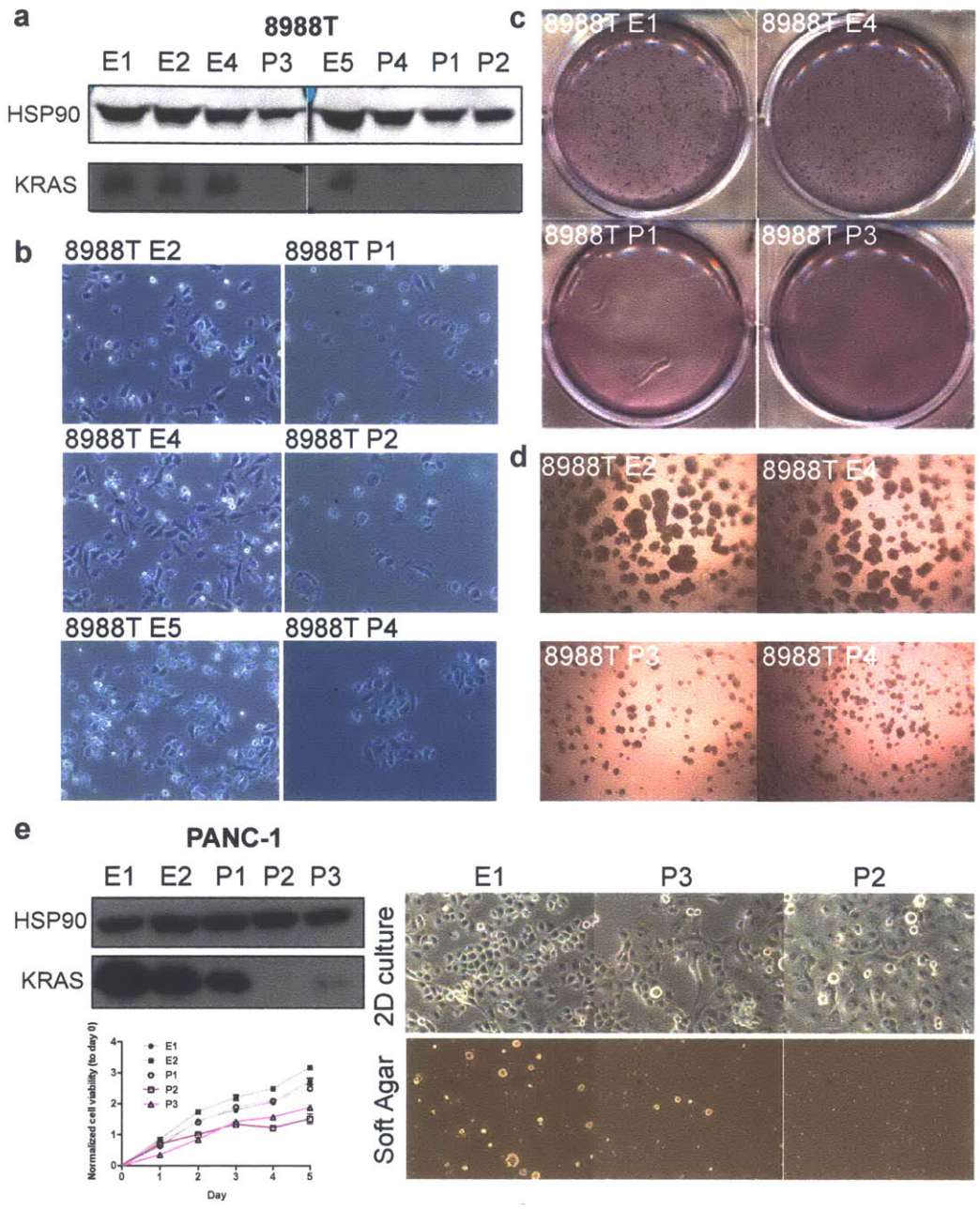

Supplementary Figure 2. *KRAS* is dispensable in additional PDAC cells.

(a) Western blot showed loss of KRAS protein in additional 8988T knockout clones (P1-P4) compared to intact clones (E1-2, E4-5).

(b) Additional knockout clones exhibited altered cell morphology, characterized by increased cell size, cytoplasmic translucency, and smooth edges.

(c) Additional knockout clones showed decreased anchorage-independent growth in soft agar.

(d) Knockout clones were capable of growing in 3D culture in matrigel but grew at a slower rate than intact clones, exhibiting smaller spheres 7 days after single cell suspension plating.

(e) PANC-1 knockout clone (P2) and partial knockout clone (P3) exhibit a dose-dependent effect of KRAS expression on proliferation, morphology, and capacity to form colonies in soft agar compared to intact clones (E1, E2, P1).

a

8988T	Wells Plated	Grown Out	Screened for KO by WB	Confirmed KO by WB
Empty	480	28	9	0
KRAS.22V	480	36	24	23 complete*
KRAS.165	480	39	39	8 partial, 2 complete

*one clone retained protein and lacked mutagenesis due to loss of Cas9 expression (designated E1)

PANC-1	Wells Plated	Grown Out	Screened for KO by WB	Confirmed KO by WB
Empty	288	16	4	0
KRAS.165	288	2	2	1 partial
KRAS.322	288	4	4	1 partial, 1 complete

8902	Wells Plated	Grown Out	Screened for KO by WB	Confirmed KO by WB
Empty	288	>30	4	0
KRAS.22V	288	8	8	0
KRAS.322	288	7	7	0

A13	Wells Plated	Grown Out	Screened for KO by WB	Confirmed KO by WB
Empty	384	201	20	0
Kras.366	384	157	60	8 partial, 2 complete

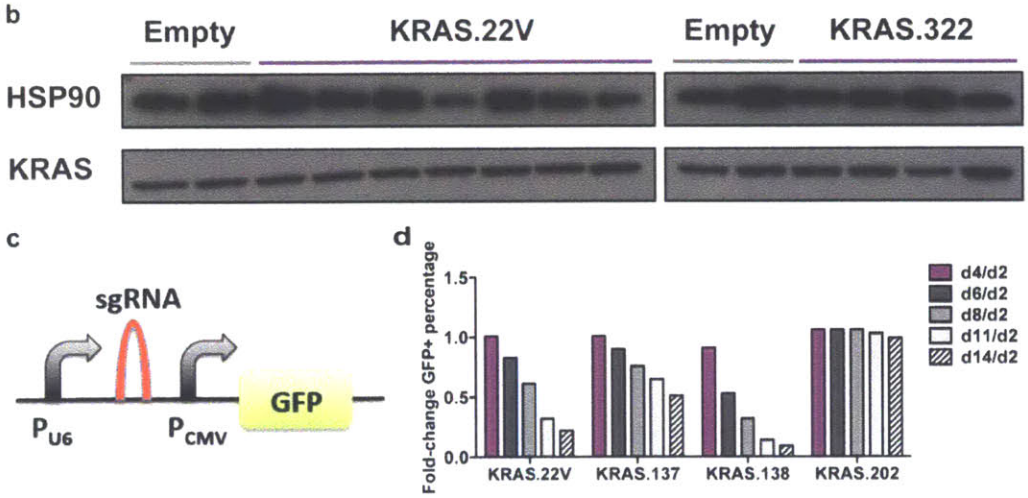

Supplementary Figure 3. Variable efficiency of *KRAS* knockout clone generation.

(a) Table of efficiency of knockout (KO) clone generation for 8988T, PANC-1, 8902, and A13 cell lines based on sgRNAs tested. Single cells were plated in 96-well plates (3-5 plates per cell line per sgRNA) and the number of clones that grew out was quantitated. Numbers of clones screened for KO by western blot (WB) and those confirmed to have no protein are listed.

(b) All 8902 subclones that grew out retained baseline levels (compared to empty vector controls) of KRAS protein. A subset of cells was sequenced and verified baseline sequence of *KRAS* locus consistent with lack of cutting (e.g. "technical escapers").

(c) Schematic of pUSCG vector that permits bicistronic expression of sgRNA from hU6 promoter (P_{U6}) and GFP from CMV promoter (P_{CMV}) for competition assays.

(d) Graphical representation of GFP-positive cell depletion over time following transduction of different sgRNAs targeting human *KRAS*.

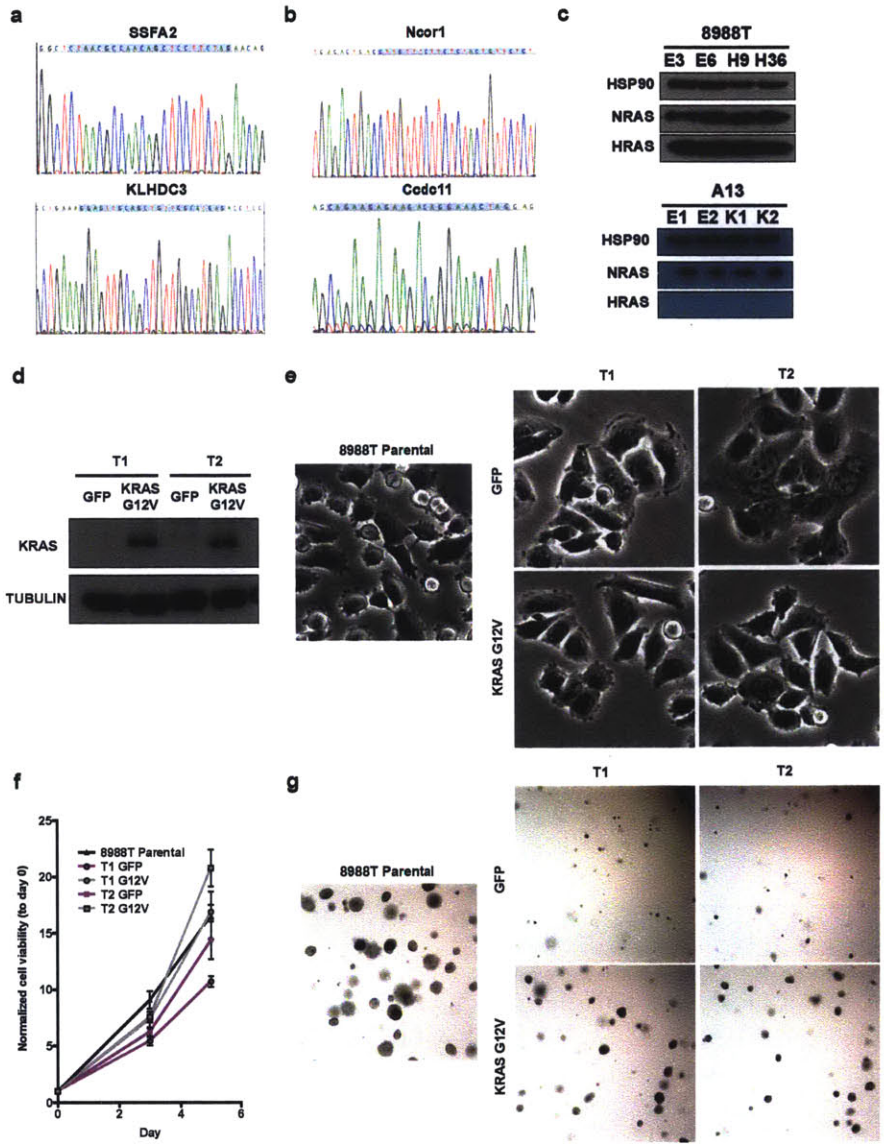

Supplementary Figure 4. On-target effects of sgRNAs targeting *KRAS*.

(a) Representative Sanger sequencing results of top two exonic mismatch genes for human sgRNA *hsKRAS.22V* revealed no mutational changes in knockout clones.

(b) Representative Sanger sequencing results of top two exonic mismatch genes for mouse sgRNA *mmKras.366* showed no mutational changes in knockout clones.

(c) HRAS and NRAS levels are not significantly changed in *KRAS* knockout clones. A13 cells did not express detectable levels of HRAS protein.

(d) Western blot showing re-expression of oncogenic *KRAS-G12V* in knockout clones (T1 and T2). Tubulin is loading control.

(e) Re-expression of oncogenic *KRAS-G12V* reverted cell morphology similar to what was observed in 8988T parental cells.

(f) Re-expression of oncogenic *KRAS-G12V* enhanced proliferation rate *in vitro* comparable to 8988T parental cells. Normalized cell viability (compared to day 0) +/- SD (n=5 replicates per cell line per time point) is shown.

(g) Re-expression of oncogenic *KRAS-G12V* increased soft agar colony formation similar to what was observed with 8988T parental cells.

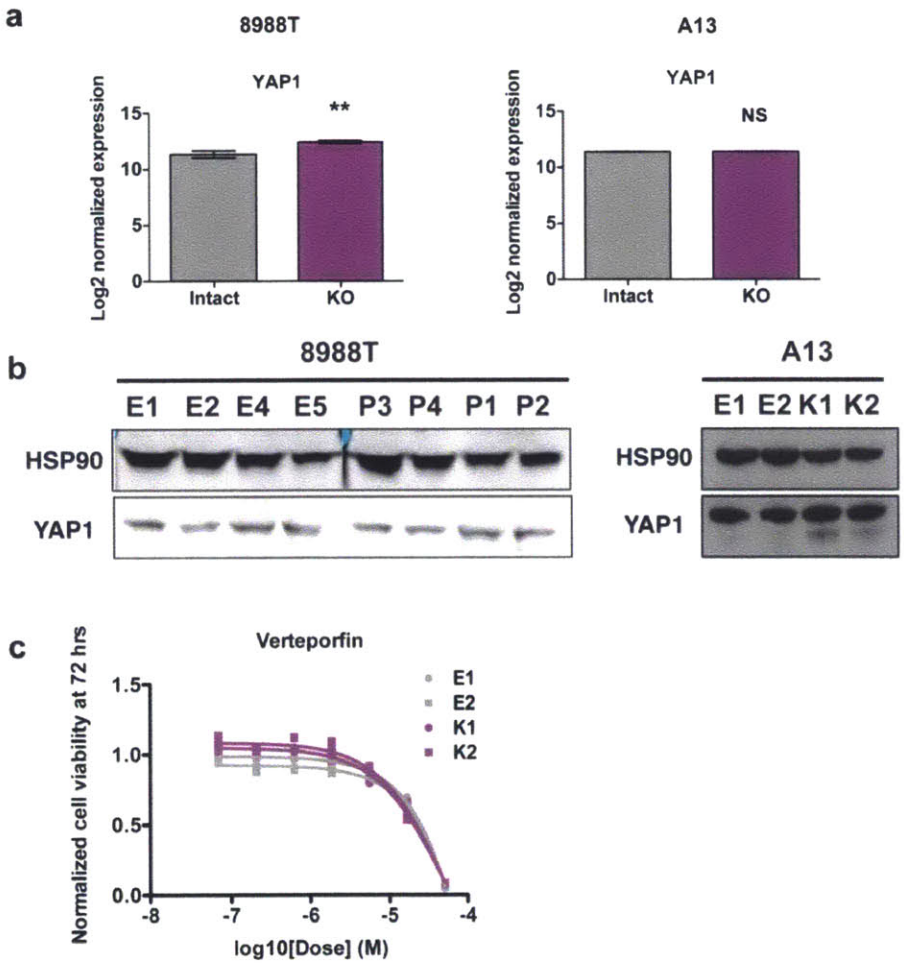

Supplementary Figure 5. YAP1 levels and sensitivity to YAP inhibition in *KRAS* knockout cells.

(a) Normalized YAP1 gene expression (log2) +/- SD by RNA-Seq in 8988T (n=3-4 clones in each group) and A13 cells (n=2 clones in each group). ** $p<0.01$, two-tailed Student's t-test.

(b) Western blot of YAP1 levels in *KRAS* intact (8988T E1, E2, E4, E5, A13 E1 and E2) and *KRAS* knockout (8988T P3, P4, P1, P2, and A13 K1 and K2) cells. HSP90 is loading control.

(c) Dose-response curves of A13 *KRAS* intact (grey) and knockout (purple) cells demonstrate comparable sensitivity to verteporfin treatment.

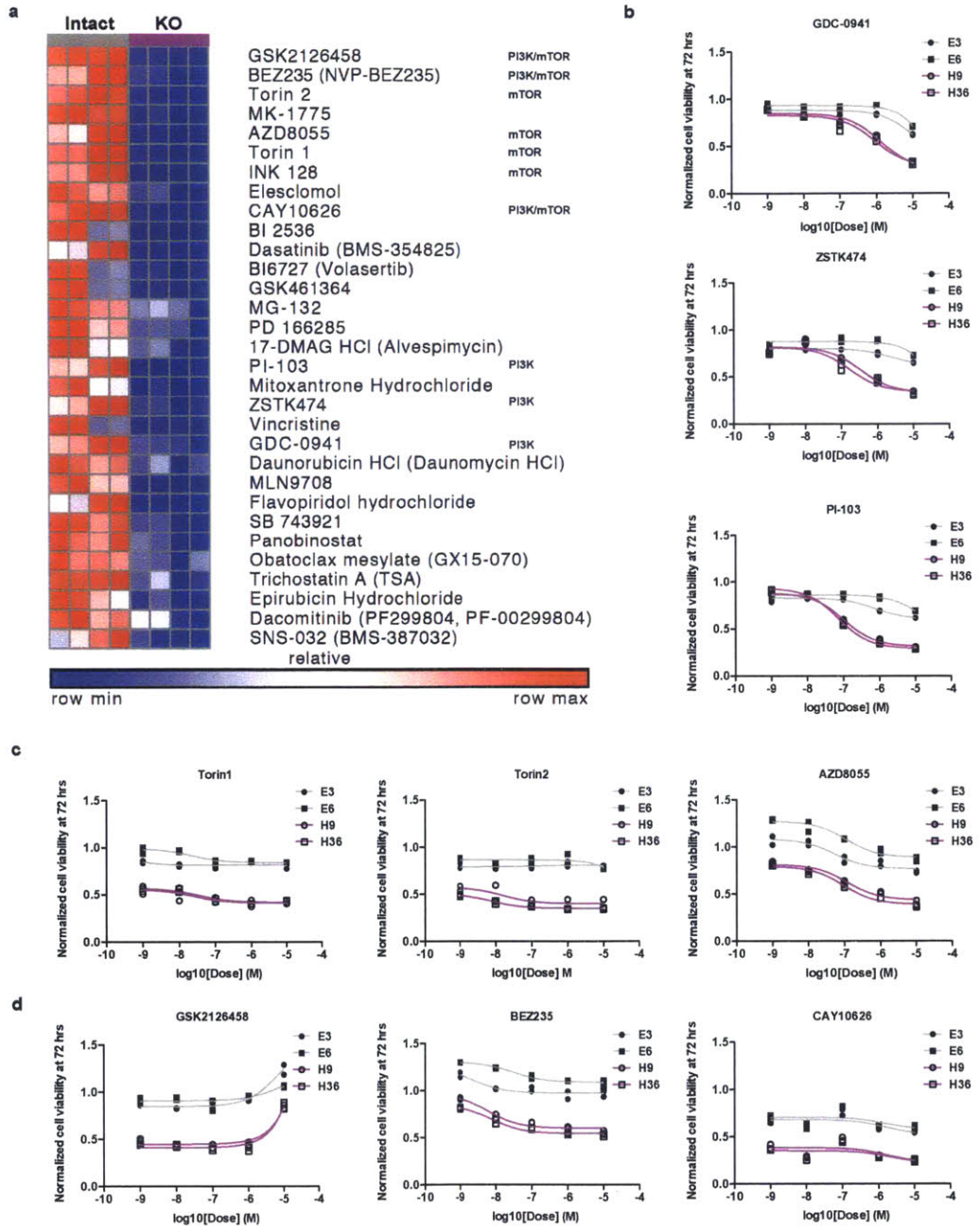

Supplementary Figure 6. High-throughput drug screen to identify unique dependencies in *KRAS* intact and knockout cells.

(a) Heat map of area under the curve (AUC) for *KRAS* intact and knockout clones treated with various compounds. Row normalized data is presented with red designating high AUC (less sensitive) and blue denoting lower AUC (more sensitive). Shown are hit compounds (see Methods) exhibiting greater sensitivity in knockout cells listed in order of ΔAUC from highest to lowest. PI3K and mTOR inhibitors are noted.

(b) Dose-response curves for pan-PI3K inhibitors in compound library on intact and knockout cells.

(c) Dose-response curves for mTOR inhibitors in compound library.

(d) Dose-response curves for PI3K/mTOR inhibitors in compound library.

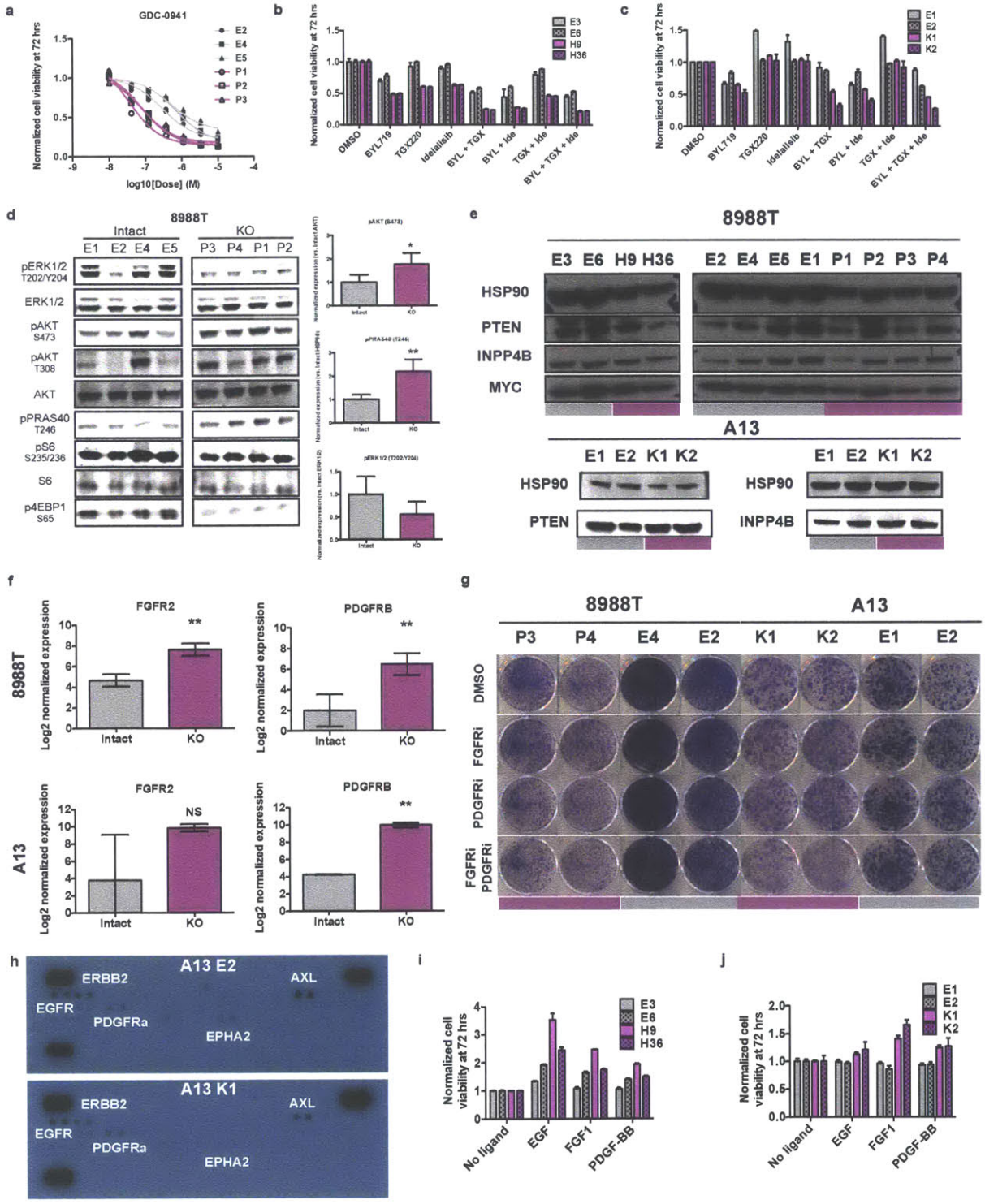

Supplementary Figure 7. Additional data on PI3K pathway activation and dependence in *KRAS* knockout cells.

(a) Dose-response curves of additional 8988T intact (grey) and knockout (purple) clones to GDC-0941.

(b) Normalized cell viability +/- SEM (compared to DMSO solvent, n=3 replicates per cell line per condition) of 8988T *KRAS* intact (E3 and E6) and knockout (H9 and H36) clones after treatment with various combinations of p110α (BYL719 = BYL), p110β (TGX220 = TGX), and p110δ (Idelalisib = Ide) inhibitors for 72 hours. All inhibitors alone or in combination were given at 5 μM concentration.
(c) Normalized cell viability +/- SEM (compared to DMSO solvent, n=3 replicates per cell line per condition) of A13 *KRAS* intact (E1 and E2) and knockout (K1 and K2) clones after treatment with isoform-specific p110 inhibitors for 72 hours.
(d) Western blot of MAPK (pERK1/2) and PI3K/AKT (pAKT, pPRAS40, pS6, p4EBP1) pathways in additional 8988T clones. Quantitation of pAKT, pPRAS40, and pERK1/2 levels is shown (n=5-6 clones per group). *$p<0.05$, **$p<0.01$, Mann-Whitney U-Test.
(e) Western blot showed no significant consistent change in PTEN, INPP4B, and MYC levels between *KRAS* intact (grey) and knockout (purple) clones.
(f) Normalized FGFR2 and PDGFRβ gene expression (log2) +/- SD by RNA-Seq in 8988T (n=3-4 clones in each group) and A13 cells (n=2 clones in each group). ** $p<0.01$, two-tailed Student's t-test.
(g) Crystal violet staining of 8988T and A13 *KRAS* intact (grey) and knockout (purple) clones following 10 days of treatment with designated inhibitors showed no significant differences. FGFRi = 100 nM BGJ398, PDGFRi = 100 nM crenolanib. Control is DMSO solvent.
(h) RTK array profiling of *KRAS* intact (A13 E2) and knockout (A13K1) clones showed no differential activation of RTKs. Similar results were observed for comparison of A13 E1 and A13 K2.
(i) Normalized cell viability +/- SEM (n=3 replicates per cell line per condition) after 72 hours of treatment with 2 μM GDC-0941 and designated recombinant human ligands: 20 nM epidermal growth factor (EGF), 100 ng/mL fibroblast growth factor 1 (FGF1), or 100 ng/mL platelet-derived growth factor BB (PDGF-BB).

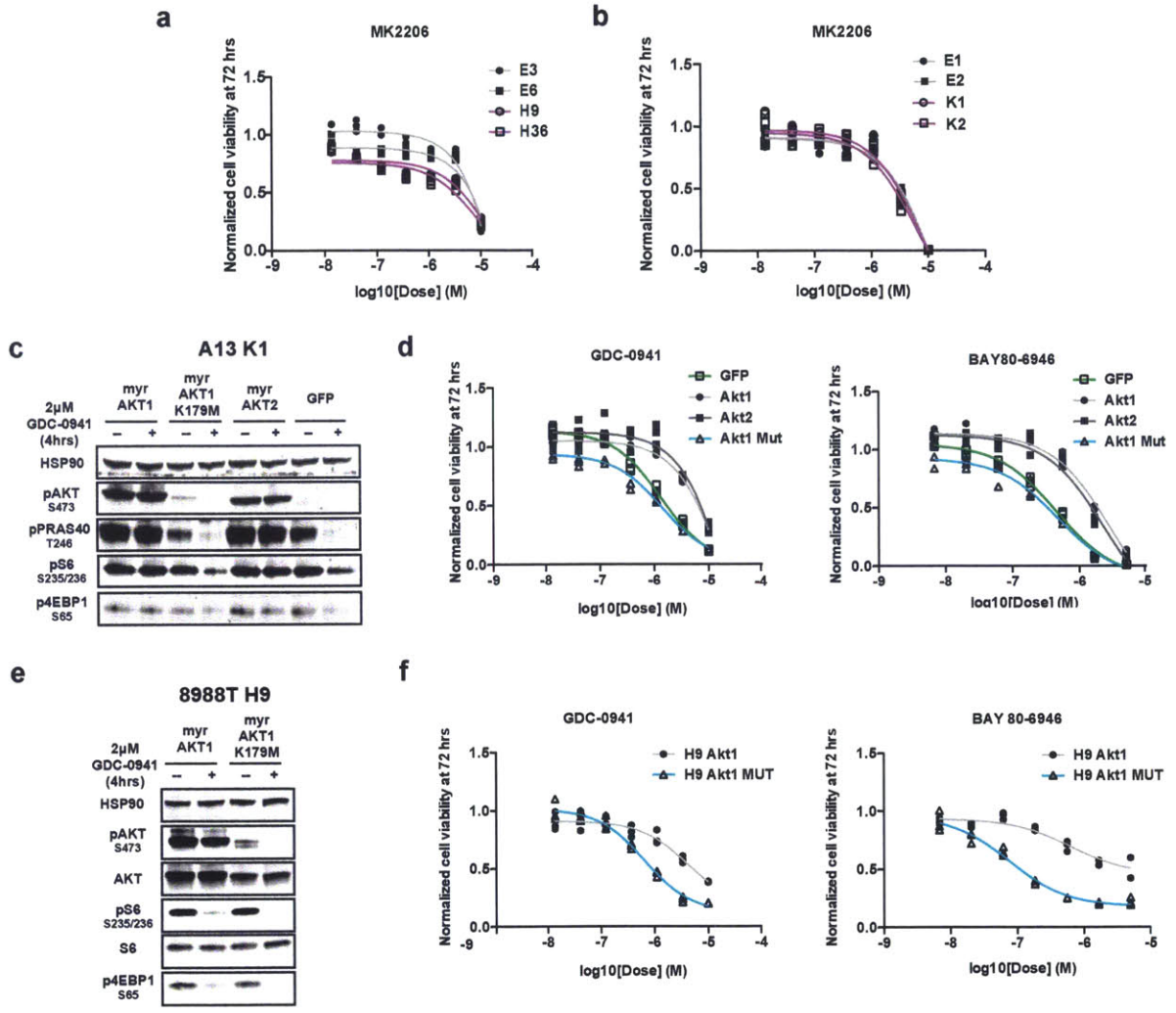

Supplementary Figure 8. AKT inhibition is necessary but insufficient for the cell viability effect of PI3K inhibitors on *KRAS* knockout cells.

(a) Dose-response curves of 8988T intact (grey) and knockout (purples) clones to AKT inhibitor MK2206.

(b) Dose-response curves of A13 clones to AKT inhibitor MK2206.

(c) Western blot of the effects of 4-hour treatment with 2μM GDC-0941 on A13 K1 knockout cells overexpressing *myr-AKT1* or *myr-AKT2* revealed sustained phosphorylation of AKT and downstream targets (PRAS40, S6, and 4EBP1) not seen in cells overexpressing kinase-dead *myr-AKT1 (K179M)* (Akt1 Mut) or *GFP*.

(d) Dose-response curves of cell lines in (c) treated with GDC-0941 and BAY80-6946 showed a marked decrease in PI3K sensitivity with *myr-AKT1* or *myr-AKT2* overexpression but not with *myr-AKT1 (K179M)* compared to *GFP* control.

(e) Western blot of the effects of 4-hour treatment with 2μM GDC-0941 on H9 knockout cells overexpressing *myr-AKT1* or *myr-AKT1 (K179M)*. Only *myr-AKT1* expression sustained phosphorylation of AKT and downstream targets (PRAS40, S6, and 4EBP1) post-treatment.

(f) Dose-response curves of cell lines in (e) treated with GDC-0941 and BAY80-6946 reveal a marked decrease in PI3K sensitivity with *myr-AKT1* overexpression.

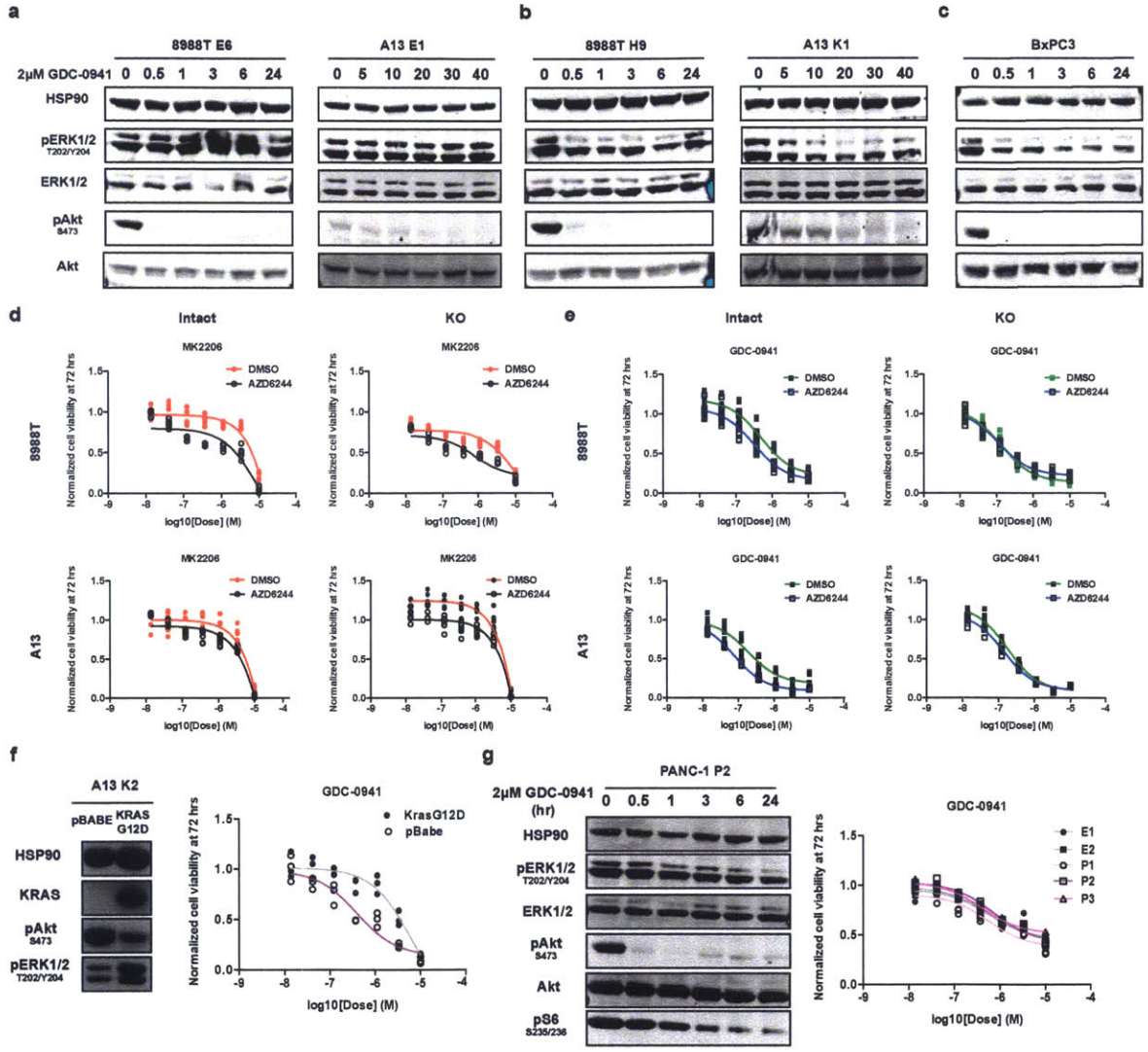

Supplementary Figure 9. Transient MAPK pathway inhibition mediates anti-growth effects of PI3K inhibition in knockout cells.

(a) Western blot showed no change in pERK1/2 levels in additional A13 and 8988T intact cells at designated times (minutes for A13, hours for 8988T) following 2μM GDC-0941 treatment.

(b) Western blot demonstrated transient decrease in pERK1/2 levels in additional A13 and 8988T knockout cells at designated times (minutes for A13, hours for 8988T) following 2μM GDC-0941 treatment.

(c) Western blot showed transient decrease in pERK1/2 levels in *KRAS* wild type cell line BxPC3 knockout cells at designated times (hours) following 2μM GDC-0941 treatment.

(d) Dose-response curves of intact or knockout (KO) cell lines treated with the AKT inhibitor MK2206 and the MEK inhibitor AZD6244 (2μM) (black) or DMSO (red).

(e) Dose-response curves of intact or knockout (KO) cell lines treated with GDC-0941 and 2μM AZD6244 (blue) or DMSO (green).

(f) Western blot of A13 K2 cells transduced with *pBABE-KRAS-G12D* (*sgKRAS*-resistant form of mouse *KRAS-G12D*) or *pBABE* empty vector control revealed overexpression of KRAS, upregulation of pERK1/2, and downregulation of pAKT in *KRAS-G12D*-expressing cells. Dose-response curve showed mutant *KRAS* overexpression decreased GDC-0941 sensitivity.

(g) Western blot of MAPK (pERK1/2) and AKT signaling (pAKT, pS6) following 2μM GDC-0941 treatment at designated times showed no significant effect on pERK1/2 levels in PANC-1 knockout clone (P2) and KRAS levels do not correlate with GDC-0941 sensitivity.

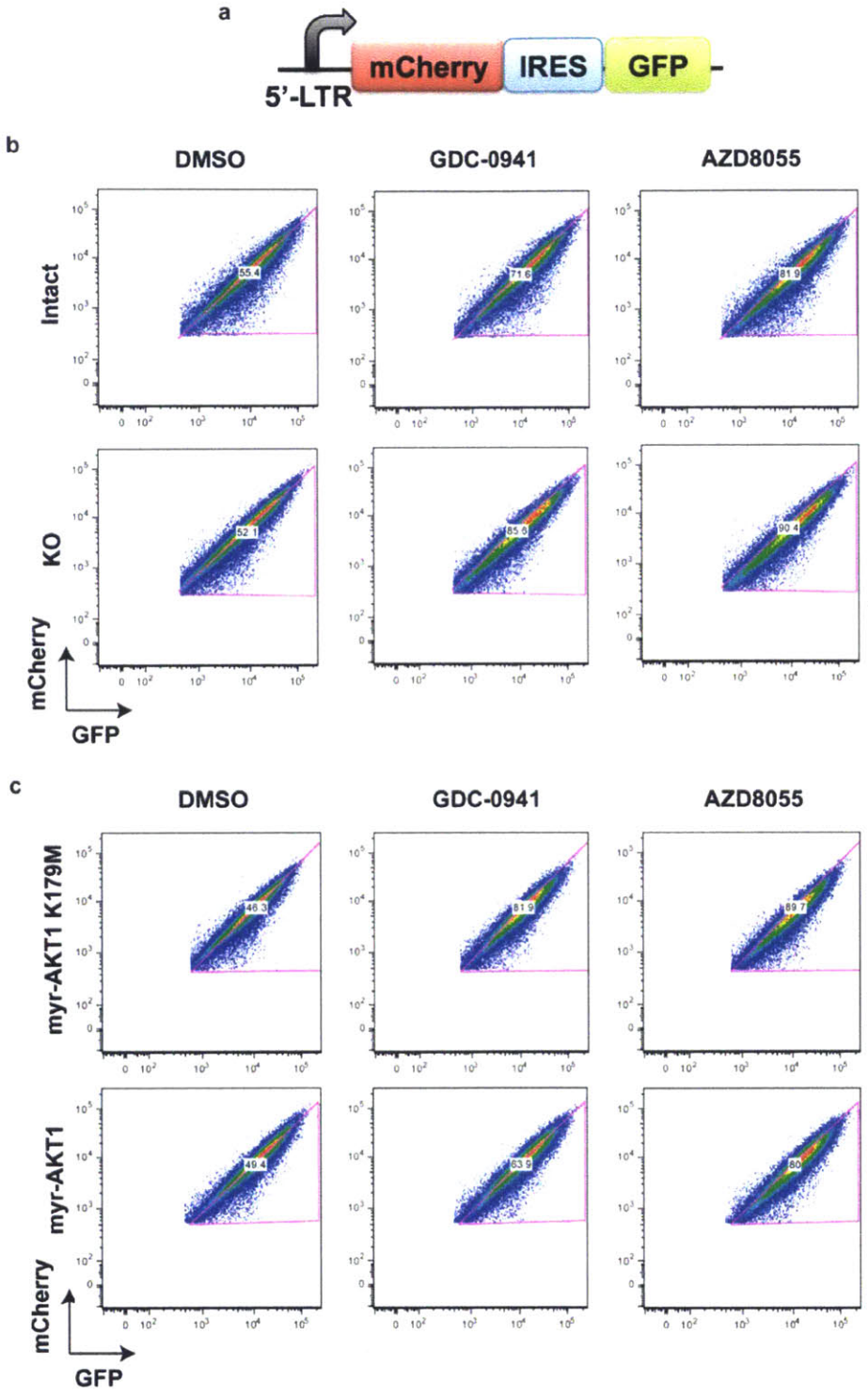

Supplementary Figure 10. PI3K inhibition enhances cap-dependent translation inhibition in *KRAS* knockout cells.

(a) Schematic of cap-dependent translation reporter construct. 5'-LTR = 5' long terminal repeat of MSCV virus with promoter activity. In transduced cells, mCherry expression correlates with cap-dependent translation and GFP expression correlates with cap-independent translation initiated via an internal ribosomal entry site (IRES).

(b) FACS plots of GFP and mCherry fluorescence in intact and knockout cells. *KRAS* knockout cells exhibited a greater decrease in mCherry (relative to GFP) expression when treated for 24 hours with GDC-0941 (2μM) or the mTORC1/2 inhibitor AZD8055 (100 nM) than intact cells. Triangle gates were drawn along the midline diagonal of the FACS plots of DMSO-treated cells and maintained in plots of drug treatment. Numbers denote percentages of cells within gate and is inversely proportional to cap-dependent translation of reporter

(c) FACS plots of GFP and mCherry fluorescence knockout cells transduced with *myr-AKT1* or *myr-AKT1 (K179M)*. Wild-type *AKT1* expression decreased the effect of GDC-0941 on cap-dependent translation compared to its kinase-dead variant.

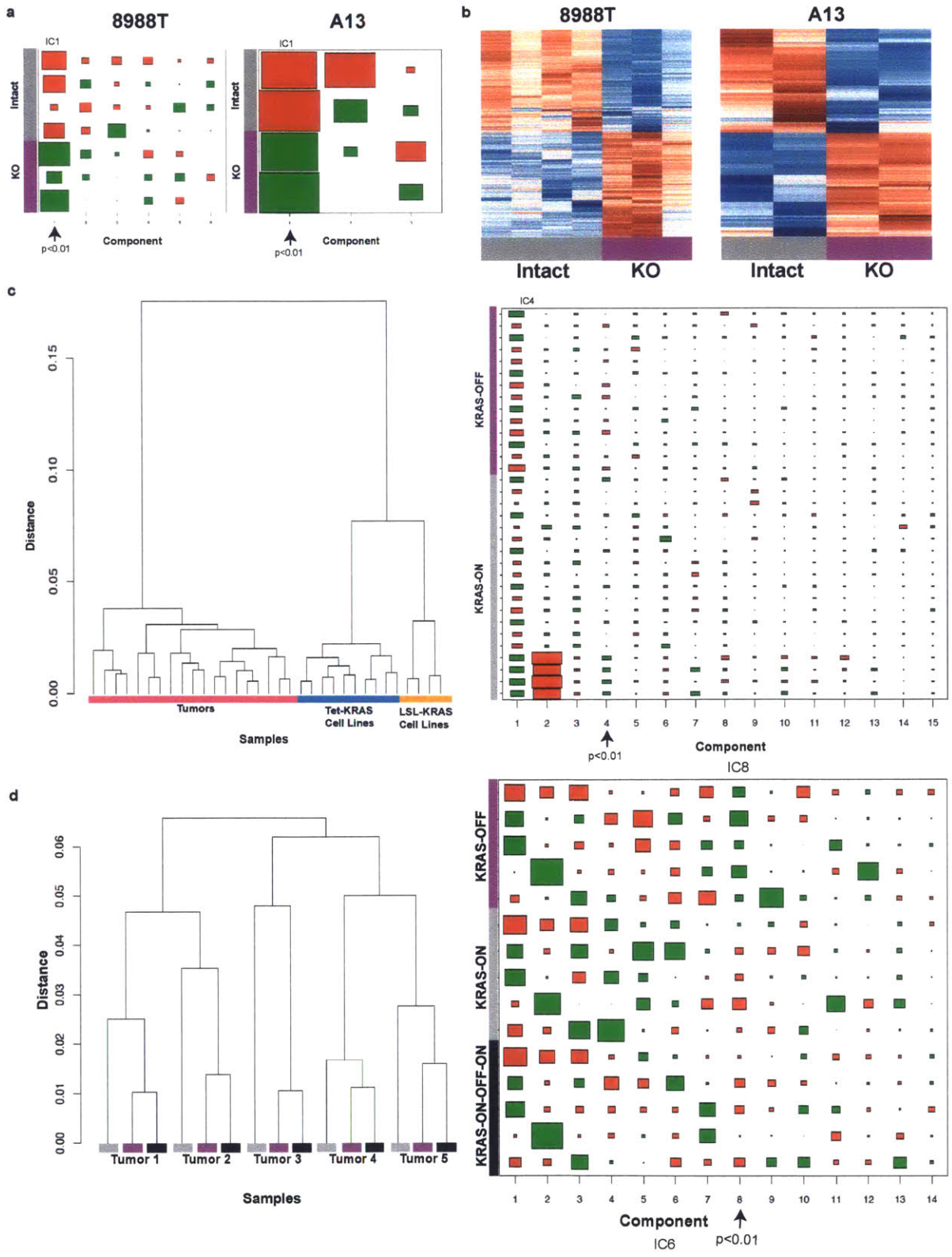
a
8988T
A13
IC1
Intact
KO
p<0.01
Component
b
8988T
A13
Intact
KO
c
Distance
0.00
0.05
0.10
0.15
Tumors
Tet-KRAS Cell Lines
LSL-KRAS Cell Lines
Samples
IC4
KRAS-OFF
KRAS-ON
Component
d
Distance
0.00
0.01
0.02
0.03
0.04
0.05
0.06
Tumor 1
Tumor 2
Tumor 3
Tumor 4
Tumor 5
Samples
IC8
KRAS-OFF
KRAS-ON
KRAS-ON-OFF-ON
IC6

Supplementary Figure 11. ICA-derived gene expression signatures from 8988T and A13 cells and external datasets derived from a *KRAS* transgenic model.

(a) Hinton diagrams of ICA analyses of 8988T and A13 cells. Columns represent distinct gene expression patterns (signatures) where colors encode directionality of gene expression (red upregulated, green downregulated). Sizes of individual boxes correlate with strength of association between each signature and a given sample (row). Independent component 1 (IC1) distinguished intact and knockout clones ($p<0.01$, Mann-Whitney U-Test) in each case.

(b) Heatmaps of ICA-derived signatures comprising the top 2% upregulated and top 2% downregulated genes (FC>2) in A13 and 8988T intact and knockout clones. Row normalized gene expression values are shown where red designates upregulation and blue designates downregulation.

(c) Unsupervised hierarchical clustering of microarray data from Ying et al.[36] from tumors and cell lines in which oncogenic *KRAS* expression was acutely withdrawn in transgenic animals. Samples segregated based on origin (tumors vs. cell lines) and model system (transgenic Tet-KRAS cell lines vs. *LSL-KRAS* cell lines) and not on KRAS-OFF or KRAS-ON state. ICA analysis identified a signature (component 4 (IC4) in Hinton diagram) that distinguished KRAS-OFF and KRAS-ON cells ($p<0.01$, Mann-Whitney U-Test).

(d) Unsupervised hierarchical clustering of microarray data from Viale et al.[37] using cells derived from tumors following *KRAS* transgene withdrawal. Samples segregated on tumors and not on KRAS-OFF or KRAS-ON state. ICA analysis identified a signature (component 8 (IC8) in Hinton diagram) that distinguished KRAS-OFF and KRAS-ON or KRAS-ON-OFF-ON (KRAS withdrawn and then re-expressed) tumor cells ($p<0.01$, Mann-Whitney U-Test).

a

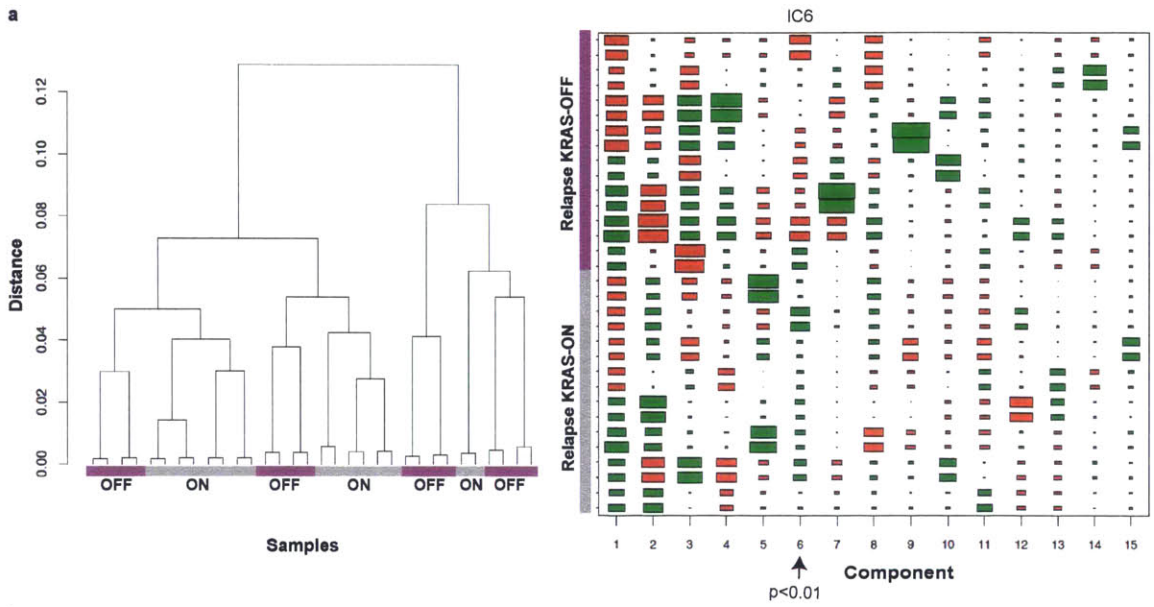

b

8988T KO signature

Gene Set	NES	p-value
YING IC4 KRAS OFF	1.94	0
KAPOOR IC6 KRAS ON	1.57	0.009
KAPOOR IC6 KRAS OFF	1.53	0.02
VIALE IC8 KRAS OFF	1.50	0.03
YING IC4 KRAS ON	1.33	0.08
VIALE IC8 KRAS ON	-1.35	0.07

A13 KO signature

Gene Set	NES	p-value
YING IC4 KRAS OFF	2.28	0
VIALE IC8 KRAS OFF	2.17	0
KAPOOR IC6 KRAS OFF	1.96	0
VIALE IC8 KRAS ON	-2.16	0
KAPOOR IC6 KRAS ON	-2.16	0
YING IC4 KRAS ON	-1.57	0.006

Supplementary Figure 12. Comparison of *KRAS* knockout gene signatures with external datasets derived from a *KRAS* transgenic model.

(a) Unsupervised hierarchical clustering of microarray data from Kapoor et al.[21] using cell lines derived from relapsed tumors following *KRAS* withdrawal, which continued to express oncogenic *KRAS* (KRAS-ON) or did not (KRAS-OFF). Samples did not cleanly segregate based on KRAS-ON or KRAS-OFF status. ICA analysis identified a signature (component 6 (IC6) in Hinton diagram) that distinguished relapsed KRAS-OFF and relapsed KRAS-ON tumor cell lines ($p<0.01$, Mann-Whitney U-Test).

(b) GSEA revealed enrichment of KRAS-OFF signatures from Supplementary Figures 11c,d and 12a in 8988T and A13 knockout signatures. A13 also exhibited statistically significant anti-correlation with KRAS-ON signatures from these external datasets.

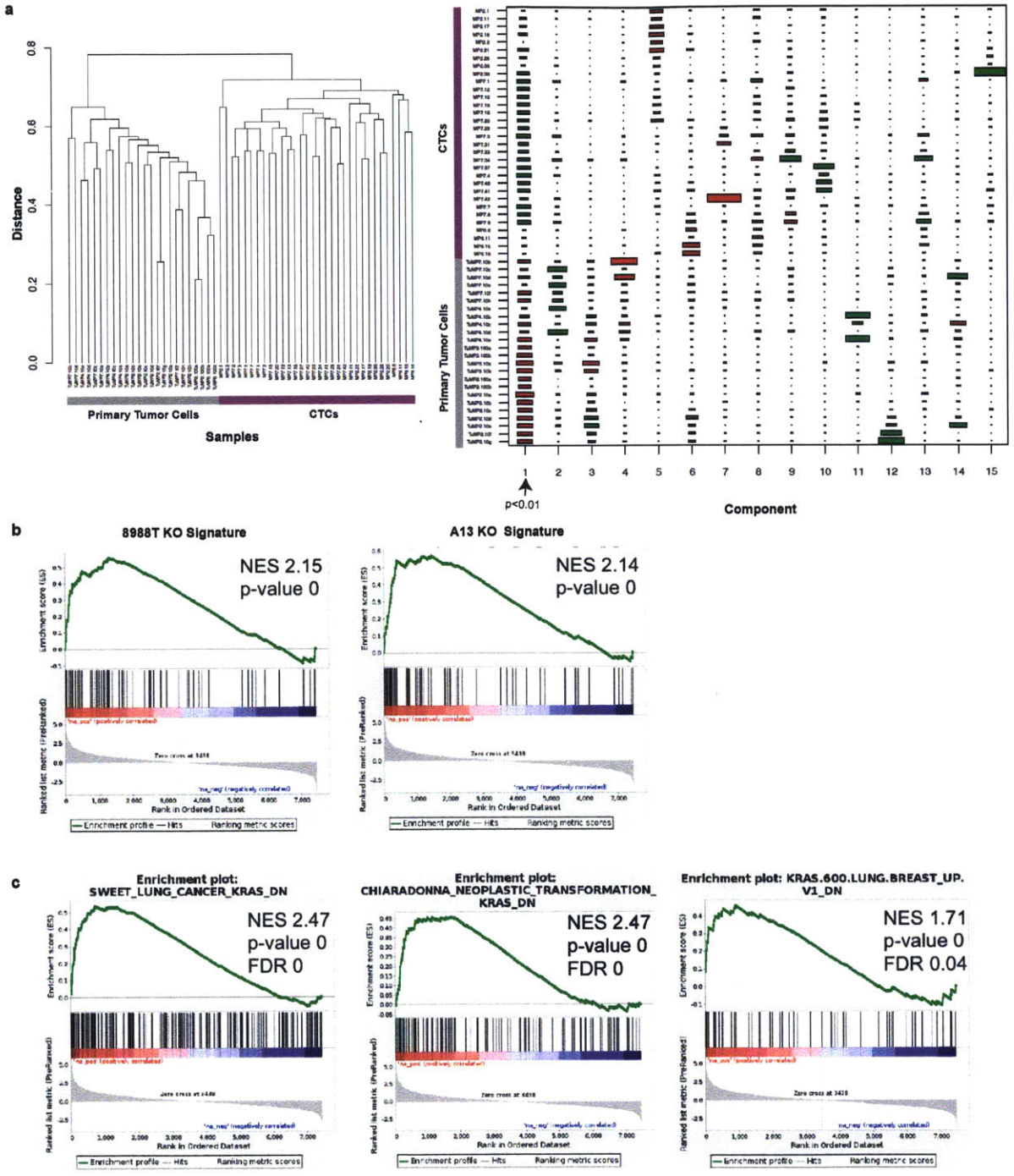

Supplementary Figure 13. *KRAS* knockout signatures correlate with CTC gene expression.

(a) Unsupervised hierarchical clustering and ICA analysis of single cell RNA-Seq data from Ting et al.[41] using circulating tumor cells (CTCs) and primary tumor cells from a *Kras;p53* mutant mouse model. ICA analysis identified a signature (component 1 (IC1) in Hinton diagram) that distinguished CTCs from primary tumors ($p<0.01$, Mann-Whitney U-Test).

(b) GSEA plots of 8988T and A13 knockout signatures (top/bottom 2% genes) enriched in ICA-derived CTC signature shown above. Normalized enrichment scores (NES) and p-values are listed for each gene set.
(c) Significantly enriched MSigDB gene sets in CTCs include genes downregulated (DN) following KRAS expression in the *KrasLA2* lung cancer mouse model (Sweet), mouse fibroblasts (Chiaradonna), and in primary human lung and breast epithelial cells (KRAS.600). NES, p-values, and FDR are listed for each gene set.

a

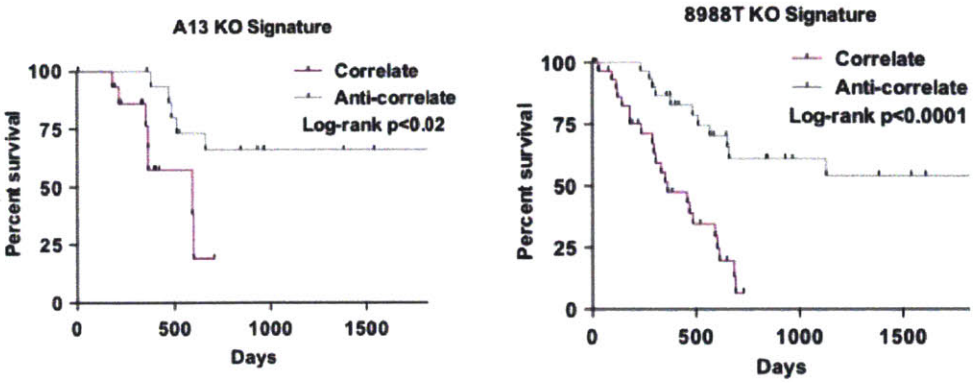

b

Signature	HR	P value
8988T KO signature (top vs. bottom quintiles n=33 tumors per group)	5.83	0.00394
A13 KO signature (top vs. bottom deciles, n=16-17 tumors per group)	29.34	0.01392
Combined signature (top vs. bottom quintiles, n=33 tumors per group)	23.53	0.00108

Variables in multivariate model include: age, gender, T stage, N stage, resection, lymph node number

c

d

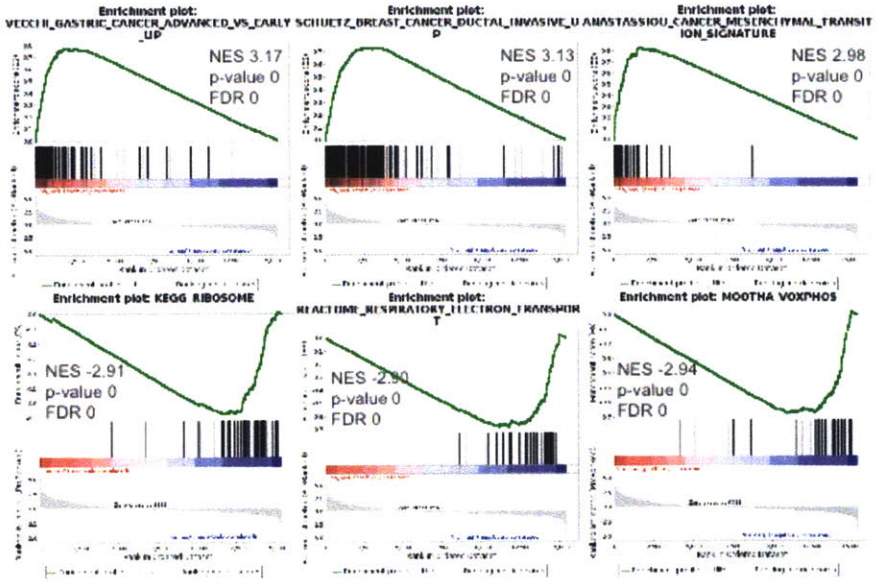

Supplementary Figure 14. Human PDAC tumors correlated with *KRAS* knockout signatures are associated with worse survival.

(a) Kaplan-Meier plots of survival in human PDAC tumors from TCGA correlated and anti-correlated with the A13 (n=16 correlated and n=17 anti-correlated tumors) and 8988T (n=33 correlated and n=33 anti-correlated tumors) knockout signatures. Log-rank (Mantel-Cox) p-values are shown.

(b) Multivariate analysis of survival based on 8988T, A13, and combined knockout signatures controlling for listed variables. Hazard ratios (HR) and p-values (Cox regression) are reported.

(c) Network representation of overlapping enriched GSEA/MSigDB gene sets in human tumors from TCGA most correlated with the A13 and 8988T knockout signature ($p<0.05$, FDR<0.25).

(d) Significantly enriched GSEA/MSigDB gene sets in human tumors from TCGA correlating with the 8988T and A13 knockout signatures include those associated with advanced disease, EMT, and invasion. Anti-correlated gene sets associated with the ribosome and oxidative phosphorylation are also shown. Normalized enrichment scores (NES) and p-values are listed with relation to the 8988T knockout signature.

Supplementary Table 1: sgRNA sequences for human and mouse

sgRNA name	20bp Guide Sequence	PAM	Orientation	Exon	Protein decrease	Source
hsKRAS.22V	GTAGTTGGAGCTGTTGGCGT	AGG	Sense	1	Y	D
hsKRAS.22V	GTAGTTGGAGCTGATGGCGT	AGG	Sense	1	N	D
hsKRAS.75	GTAGTTGGAGCTGATGGCGT	AGG	Antisense	1	N	C
hsKRAS.165	TCTCGACACAGCAGGTCAAG	AGG	Sense	2	Y	G
hsKRAS.197	CAATGAGGGACCAGTACATG	AGG	Sense	2	Y	G
hsKRAS.312	GGACTCTGAAGATGTACCTA	TGG	Sense	3	N	C
hsKRAS.322	GATGTACCTATGGTCCTAGT	AGG	Sense	3	Y	G
hsKRAS.391	GATGTACCTATGGTCCTAGT	TGG	Sense	3	N	G
hsKRAS.486	TTCTCGAACTAATGTATAGA	AGG	Antisense	4	N	G
mmKras.75	CTGAATTAGCTGTATCGTCA	AGG	Antisense	1	N	C
mmKras.157	TTGGATATTCTCGACACAGC	AGG	Sense	2	Y	C
mmKras.171	GTCGAGAATATCCAAGAGAC	AGG	Antisense	2	Y	C
mmKras.366	TAGAACAGTAGACACGAAAC	AGG	Sense	3	Y	C
mmKras.318	TAGAACAGTAGACACGAAAC	TGG	Sense	3	Y	C
sgTomato	GGCCACGAGTTCGAGATCGA	GGG	Sense	N/A	Y	D

sgRNA name species key:

hs = human

mm = mouse

Source key:

D = self-designed based on available PAM sequences

C = sequences outputted from Feng Zhang lab CRISPR design tool (crispr.mit.edu)

G = sequences from GeCKO v2 library from Feng Zhang lab

Supplementary Table 2: Primers for cDNA amplification and cloning

cDNA	Template	Species	F/R	Sequence
eGFP	MSCV-Luciferase-IRES-GFP	Jellyfish	F	ACCATGGTGAGCAAGGGCGAG
eGFP	MSCV-Luciferase-IRES-GFP	Jellyfish	R	TTACTTGTACAGCTCGTCCATGCC
myr-HA-AKT1	pLNCX myr HA Akt1 (Addgene #9005)	Human	F	ACCATGGGGTCTTCAAAATCTAAAC
myr-HA-AKT1	pLNCX myr HA Akt1 (Addgene #9005)	Human	R	TCAGGCCGTGCCGCTG
myr-HA-AKT1-K179M	pLNCX myr HA Akt1 K179M (Addgene #9006)	Human	F	ACCATGGGGAGCAGCAAGAGC
myr-HA-AKT1-K179M	pLNCX myr HA Akt1 K179M (Addgene #9006)	Human	R	TCAGGCCGTGCCGCTG
myr-HA-AKT2	pBabe puroL Myr HA Akt2 (Addgene #9018)	Human	F	ACCATGGGGAGCAGCAAGAGC
myr-HA-AKT2	pBabe puroL Myr HA Akt2 (Addgene #9018)	Human	R	TCACTCGCGGATGCTGGC
MEK-DD	pBabe-Puro-MEK-DD (Addgene #15268)	Mouse	F	ACCATGCCCAAGAAGAAGCCGAC
MEK-DD	pBabe-Puro-MEK-DD (Addgene #15268)	Mouse	R	TCAGATGCTGGCAGCGT
KrasG12V sgRNA-resistant	pLX304-KrasG12V	Human	F	TCAGATGCTGGCAGCGT
KrasG12V	pLX304-KrasG12V	Human	R	TTACATAATTACACACTTTGTCT
KrasG12D sgRNA-resistant Part 1	MSCV-KrasG12D-IRES-GFP	Mouse	F	ACCATGACTGAGTATAAGCTTGTGGT
KrasG12D sgRNA-resistant Part 1	MSCV-KrasG12D-IRES-GFP	Mouse	R	TGCTAACTCCTGAGCTTGCTTGGTATCTACTGTTCTAGAAGG
KrasG12D sgRNA-resistant Part 2	MSCV-KrasG12D-IRES-GFP	Mouse	F	CCTTCTAGAACAGTAGATACCAAGCAAGCTCAGGAGTTAGCA
KrasG12D sgRNA-resistant Part 2	MSCV-KrasG12D-IRES-GFP	Mouse	R	TCACATAACTGTACACCTTGT
Hygromycin	MSCV-Luciferase-PGK-Hygro	N/A	F	ATGAAAAAGCCTGAACTCACC
Hygromycin	MSCV-Luciferase-PGK-Hygro	N/A	R	CTATTCCTTTGCCCTCGGAC
mCherry	pBS-imCherry	Coral	F	ACCATGGCAAGCAAGGGCGAGGAGGATAAC
mCherry	pBS-imCherry	Coral	R	TCAAGACTTGTACAGCTCGTCCATG

Key: F/R = Forward or reverse

Notes:

1. **ACC Kozak sequence was added to each forward primer**
2. **sgRNA-resistant constructs were made by including silent mutations in the guide sequence**
3. **KrasG12D sgRNA-resistant cDNA was cloned as two parts joined by Gibson assembly (NEB)**

Supplementary Table 3: PCR amplification primers for sequencing

Gene	Species	Exon	F/R	Sequence
KRAS	Human	1	F	AAGTACAGTTCATTACGATACACGTCTGC
KRAS	Human	1	R	TGTTGAGAAGAAGATAGGAAAATACTGCTG
KRAS	Human	2	F	TAGTGGCCATTTGTCCGTCA
KRAS	Human	2	R	GCAGTCTGGAGCAAGTTACTC
KRAS	Human	3	F	TTTGGTGTAGTGGAAACTAGGAA
KRAS	Human	3	R	CATGGACACTGGATTAAGAAGCA
KRAS	Human	4	F	CCTGTACACATGAAGCCATCG
KRAS	Human	4	R	CACCAAAAGCCCCAAGACAG
Kras	Mouse	1	F	TGGCTGTTTAGATCAACAAGCTAAATGATAG
Kras	Mouse	1	R	AGCCTTGGAACTAAAGGACATCACATATAA
Kras	Mouse	2	F	TTTGTCCACCTCCTTCTCCC
Kras	Mouse	2	R	AAAGAAAGCCCTCCCCAGTT
Kras	Mouse	3	F	AGATGTGCCTATGGTCCTGG
Kras	Mouse	3	R	AGCTGGAGTACACAGAGAGAC
SSFA2	Human	16	F	GCCTGGGACTTGGAGAAATG
SSFA2	Human	16	R	AGTCATACGGGAGGTGGGTA
KLHDC3	Human	10	F	AGGTGTTCTCTGTGCTGTGA
KLHDC3	Human	10	R	CTCCAGCCTTCTCCACCATA
Ncor1	Mouse	4	F	ACCCAGAAATGCAGGTACCA
Ncor1	Mouse	4	R	CACTGCTGCCAAATGTTAGGA
Ccdc11	Mouse	6	F	GCTCCACTTTCATAGCCCCT
Ccdc11	Mouse	6	R	CCTCTGGCCTTCTCGTCTAG

Key: F/R = Forward or reverse

Notes:

1. **All PCR reactions were performed at 60°C annealing temperature**
2. **Forward primer for each pair was used for sequencing reaction except for exon 3 of Kras (mouse), for which reverse primer was used, and exon1 for KRAS (human) and Kras (mouse), which are as follows:**

Gene	Species	Exon	F/R	Sequence
KRAS	Human	1	F	GGCCTGCTGAAAATGACTGA
Kras	Mouse	1	R	CGCAGACTGTAGAGCAGCG

MATERIALS AND METHODS

Cell lines and culture conditions

PA-TU-8988T (8988T), PA-TU-8902 (8902), PANC-1, YAPC, and BxPC3 cells were obtained from the Broad Institute Cancer Cell Line Encyclopedia and sourced from DSMZ-Germany and American Type Culture Collection (ATCC). 8988T, 8902, and YAPC cells harbor *KRAS-G12V* mutations, PANC-1 cells have a *KRAS-G12D* mutation, and BxPC3 cells are *KRAS* wild type. A13 cells were derived from a pancreatic tumor in a *LSL-Kras^{G12D}; p53$^{flox/flox}$; Pdx1-CreER* mouse treated with tamoxifen (Sigma) to induce oncogenic *Kras^{G12D}* activation and biallelic *p53* inactivation in the pancreas[50]. All cell lines were maintained in DMEM (Corning Cellgro) supplemented with 10% fetal bovine serum (Hyclone) and penicillin/streptomycin. For inducible-shRNA experiments, doxycycline (DOX, Sigma) was used at 1 μg/mL in culture media and replaced every 2-3 days. Cell viability was analyzed after 5 days of DOX treatment using the CellTiter-Glo (CTG) luminescence assay (Promega), which measures cellular ATP levels as a surrogate for cell number and growth. Luminescence was read on a Tecan M2000 Infinite Pro plate reader. Cells were imaged with a Nikon Eclipse TE2000-U light microscope and SPOT RT3 camera.

Lentiviral constructs and cloning of sgRNAs and overexpression constructs

Lentiviral constructs for CRISPR/Cas-mediated genome editing from the dual-vector lentiviral GeCKOv2 system, *lentiCas9-Blast* and *lentiGuide-Puro*[51] (**Supplementary Fig. 1a**), were provided by Dr. Feng Zhang. sgRNAs targeting various human and mouse *KRAS* exons were designed (**Supplementary Table 1**) and ligated into the BsmBI site with compatible annealed oligos. *lentiGuide-Hygro* (**Supplementary Fig. 1a**) was generated following sgRNA

ligation by subcloning a hygromycin resistance gene PCR amplified from *MSCV-Luciferase-pPGK-hygro* (Addgene #18782) into the BsiWI and MluI sites. pUSCG was constructed by Gibson assembly and sgRNAs were cloned into the BsmBI site with compatible annealed oligos. pLKO-Tet-On constructs (**Supplementary Fig. 1c**) targeting KRAS (shKRAS.407) and LACZ (shLACZ.1650) were provided by Dr. William Hahn. *sgKras.366* targeting mouse Kras was cloned into a lentiviral vector for DOX-inducible sgRNA expression provided by Dr. Marco Herold[52]. To generate lentiviral constructs for overexpression, we first produced *LV-pSV40-mCherry-pPGK-FlpO* and *LV-pSV40-puro-pPGK-eGFP* by assembling four parts with overlapping DNA ends into a 5.7 kb lentiviral backbone using Gibson assembly (NEB). PCR amplified cDNAs (**Supplementary Table 2**) were subcloned into AfeI and AscI sites to replace FlpO and GFP and verified by sequencing and restriction digest. Alternatively, cDNAs were subcloned into the EcoRI and BamHI of *pBABE-zeo* (Addgene #1766) or *pBABE-puro* (Addgene #1764) retroviral vectors. The translation reporter construct *MSCV-mCherry-IRES-GFP* was generated by subcloning PCR amplified mCherry into the XhoI and EcoRI sites of *MSCV-IRES-GFP* (Addgene #9044).

Lentiviral and retroviral production and transduction

For lentiviral infections, lentiviral backbone, packaging vector (delta8.2 or psPAX2), and envelope (VSV-G) were transfected into 293T cells with TransIT-LT1 (Mirus Bio). Supernatant was collected at 48 and 72 hours and applied to target cells with 8 μg/mL polybrene (EMD Millipore) for transduction. Transduced cells were treated with 10 μg/mL blasticidin S (Life Technologies), 2-4 μg/mL puromycin (Life Technologies), 400 μg/mL hygromycin B (Roche), or 400 μg/mL zeocin (Life Technologies) for 3-7 days, as appropriate, for antibiotic selection.

Alternatively, *Cas9-Blast*-expressing cells were transfected with *lentiGuide-Puro* harboring sgKRAS to induce *KRAS* knockout (8988T T1 and T2 cells) using the Amaxa Nucleofector Kit for Mammalian Epithelial Cells (Lonza). To generate single cell clones from *sgKRAS*-transduced cells, we sorted one cell per well into 96-well plates using a FACSAria II (Becton Dickinson) or MoFlo (Beckman Coulter) FACS sorter. Intact clones were derived from *lentiGuide-Puro*- or *lentiGuide-Hygro*-transduced cells without inserted guide sequence (empty vector) except for 8988T E1, which was derived from *hsKRAS.22V*-transduced cells but exhibited loss of Cas9 protein expression, no mutagenesis, and *KRAS* intact cell properties. 8988T knockout clones were derived from *hsKRAS.22V*-transduced cells. The PANC-1 knockout clone was derived from *hsKRAS.322*-transduced cells. A13 knockout clones were derived from *mmKras.366*-transduced cells. 8902 and YAPC knockout clones transduced with *hsKRAS.22V* were not recoverable. For overexpression constructs harboring mCherry, fluorescent cells were sorted using a FACSAria II sorter. For retroviral infections, the retroviral backbone and pCL-Eco (for mouse cells) or pUVMC and VSV-G (for human cells) were transfected into 293T cells. For the translational reporter experiments, fluorescence was assessed using an LSR II FACS analyzer (Becton Dickinson) and data were analyzed using FlowJo software.

In vitro Growth Assays

Anchorage-independent growth was assessed by plating 10,000 cells in 0.4% low melting temperature agarose (Seaplaque) in complete media on top of a 0.8% preformed agarose layer. Cells were grown for 10-14 days and colonies were stained with 0.5% crystal violet and destained with water. Microscopic images of the colonies were taken pre- and post-crystal violet

staining. For growth curves, 250-1000 cells were plated on day 0 and grown for five days in culture. 4-5 replicates for each cell line per day were assessed for cell viability by CTG assay. Cell viability results were normalized to luminescence at day 0. 3D culture was established by plating 250-500 cells form a single-cell suspension onto a growth factor-reduced matrigel (Corning) layer, allowing cell migration into matrigel for 4-6 hours. Cells were grown in complete media for 7-10 days prior to analysis. Apoptosis was measured using the Guava Nexin Reagent per manufacturer's instructions and analyzed on a Guava flow cytometry system (Millipore). Competition assays using pUSCG were performed by measuring GFP-positive cells on a Guava flow cytometer every other day for two weeks starting on day 2 after transduction of 8902 cells expressing *Cas9-Blast*. Untransduced cells were used for negative gating.

Immunoblotting

Cells were lysed with ice-cold RIPA buffer (Pierce), supplemented with 0.5 μM EDTA and Halt protease and phosphatase inhibitors (Thermo Scientific), rotated at 4°C for 15-30 minutes to mix, and centrifuged at maximum speed for 15 minutes to collect whole cell lysates. Protein concentration was measured with the BCA protein assay (Pierce). 20-30 μg of total protein per sample was loaded into 4-12% Bis-Tris gradient gels (Life Technologies) and separated by SDS-PAGE. Proteins were transferred to nitrocellulose (for LI-COR) or PVDF (for ECL) membranes. The following antibodies were used for immunoblotting: mouse anti-HSP90 (BD #610418, 1:10,000), rabbit anti-beta-Tubulin (CST 2128, 1:1000), mouse anti-KRAS (SCBT sc-30, 1:200), mouse anti-NRAS (SCBT sc-31, 1:200), mouse anti-HRAS (SCBT sc-29, 1:200), rabbit anti-pERK1/2(T202/Y204) (CST 4370, 1:1000), mouse anti-ERK1/2 (CST 9107, 1:1000), rabbit anti-pAKT(S473) (CST 4060, 1:2000), rabbit anti-pAKT(T308) (CST 2965,

1:1000), mouse anti-AKT (CST 2966, 1:2000), rabbit anti-pPRAS40(T246) (CST 2997, 1:1000), rabbit anti-PTEN (CST 9559, 1:1000), rabbit anti-INPP4B (Abcam ab81269, 1:1000), rabbit anti-pS6(S235/236) (CST 4858, 1:2000), mouse anti-S6 (CST 2317, 1:1000), rabbit anti-4EBP1(S65) (CST 9451, 1:1000), rabbit anti-pCRAF(S338) (CST 9427, 1:1000), rabbit anti-pMEK1/2(S217/221) (CST 9154, 1:1000), mouse anti-MEK1/2 (CST 4694, 1:1000), rabbit-anti-c-MYC (Abcam ab32072, 1:1000), rabbit anti-c-MYC (CST 5605, 1:1000), rabbit anti-YAP1 (CST 4912, 1:1000). HSP90 and beta-Tubulin were used as loading controls. RAS-GTP assays were performed using an Active RAS Pull-Down and Detection Kit (Thermo Scientific) per manufacturer's instructions using *in vitro* GTPγS (non-hydrolysable) and GDP pull-down controls and the provided pan-RAS antibody (1:200). Mouse RTK arrays (R&D Systems) were assayed per manufacturer's instructions. Primary antibodies were detected with fluorescent DyLight-conjugated (CST) or HRP-conjugated (BioRad) secondary antibodies for fluorescent (LI-COR) or chemiluminescent detection (Amersham), respectively. Quantification of protein levels from western blots was performed using Image Studio Lite (LI-COR).

Genomic DNA isolation for sequencing of mutations

Genomic DNA from cell lines was collected using QuickExtract DNA extraction solution (Epicentre) or the QiaAMP DNA Mini Kit (Qiagen). PCR products for sequencing were amplified using a Herculase II Fusion DNA polymerase kit (Agilent) and primers described in **Supplementary Table 3**. PCR products were gel purified and sequenced (Quintara Biosciences). For subclones with multiple *KRAS* mutant alleles, we cloned the PCR product into a TOPO vector (Life Technologies) and sequenced at least 10-20 bacterial colonies. The most probable off-target genes for sgRNAs were identified using CRISPR Design

(http://crispr.mit.edu) and no gene had fewer than 3 exonic mismatches. All sequences and chromatograms were analyzed using MacVector software.

High-throughput drug screen

High-throughput screening was performed as previously described[53]. To determine the optimal plating density during assay development, 8988T E3, E6, H9, and H36 cells were plated at either 500, 1000, or 1500 cells per well into 384-well opaque, white assay plates (Corning), 50 μL per well, and incubated overnight at 37°C/5% CO2. The next day, cells were treated with MG-132 (Enzo Bioscience) starting at a high concentration of 40 μM, in a 14-pt, 2-fold dilution series, 16 replicates/concentration, for 72 hours. 0.1% DMSO (solvent for all compounds) was used as a negative control. Sensitivity was assayed using CTG. Luminescence was measured using a M1000 Infinite Pro plate reader (Tecan). The Z' factor at each concentration point was calculated and compared between each cellular density to determine the largest dynamic detection window for subsequent screening. Estimated Z' factors were calculated using the following formula: $1-(3x(\sigma_p+\sigma_n)/(\mu_p-\mu_n))$ where σ (standard deviation) and μ (mean) were determined from the positive (p) and negative (n) controls. For the screen, cells were plated at a density optimized during assay development as above. A modified version of the Selleck Cambridge Cancer Compound Library (http://www.selleckchem.com/screening/cambridge-cancer-compound-library.html) containing 384 structurally diverse, medicinally active, and cell permeable cancer-relevant compounds was used for screening. Compounds were plated in 384-well format in 5-pt, 10-fold concentration ranges, starting at 10 mM. 50 nL of compounds were pin-transferred (V&P Scientific pin tool mounted onto a Tecan Freedom Evo 150 MCA96 head) into duplicate assay plates and incubated for 72 hours. The DMSO content was 0.1% within

each well. 32 wells of DMSO vehicle control and 32 wells of positive control MG-132 were included on each plate. After three days of incubation, 10 μL of CellTiter-Glo was added to each well, incubated for 10 minutes, and luminescence output was read as a surrogate for cell viability. Z' factors were >0.5 for all plates in the screen. Percent viability (PV) compared to DMSO control was calculated for each compound well and plotted against log10[Dose] (M). Area under the curve (AUC) was calculated using the trapezoidal rule: $((PV_1+PV_2)/2)x(dose_1-dose_2)$. AUCs were averaged for intact (AUC_i) and knockout (AUC_{KO}) cells across replicates. Compounds were considered hits if 1) AUC_i or AUC_{KO} were <4; 2) ΔAUC ($AUCi–AUC_{KO}$) was >0.5 or <-0.5; and 3) AUC_i and AUC_{KO} were significantly different ($p<0.05$, Student's t-test).

Drug treatments

GDC-0941, BAY80-6946, AZD6244, MK2206, AZD8055, BYL719, TGX220, Idelalisib, BGJ-398, and Crenolanib were purchased from Selleck Chemical. Verteporfin was purchased from Sigma. All compounds were diluted to 10-20 mM stock concentration in DMSO except for BAY80-6946, which was diluted to 5 mM in DMSO with 10 mM trifluoroacetic acid. To generate dose-response curves, cells (500-1000 for A13 clones, 1000-2000 for 8988T clones, 2000-4000 for PANC-1 clones) were plated in 96-well white plates (Perkin Elmer) in 100 μL of media and incubated overnight. 100 μL of drug at 2X final concentration was added to each well in triplicate for each cell line and dose. Cell viability was determined at 72 hours using CellTiter-Glo. For ligand treatments, cells were treated with recombinant EGF, FGF1, or PDGF-BB when initially plated. Percent viability was calculated for each dosed well compared to solvent controls (DMSO or DMSO with trifluoroacetic acid at 0.1-0.2%) and plotted against log10[Dose] (M). For dose-response curves, each replicate for each cell line and dose was

plotted along with curve-fit regression for three-component inhibitor response (Prism). For long-term drug treatments, cells were plated at low-density in 6-well plates, treated with drugs for 10-14 days (media was refreshed with drug every 2 days), and stained with 0.5% crystal violet when control cells became confluent.

Subcutaneous tumor transplant and GDC-0941 dosing in immunocompromised mice

All animal studies were approved by the MIT Institutional Animal Care and Use Committee. A13 mouse clones were transplanted to form tumors in nude mice (Taconic) via subcutaneous injections. $5x10^5$ cells suspended in 100 μL of cold PBS were injected per tumor to determine tumor-forming capacity. For drug treatment *in vivo*, a higher number of knockout cells ($2x10^6$) was injected to synchronize tumor formation between intact and knockout clones, as $5x10^5$ cells of K1 and K2 give rise to subcutaneous tumors but at significantly slower rates than E1 and E2. Tumor formation was monitored over time by direct observation, caliper measurement, and IVIS spectrum optical imaging (Xenogen Corporation). When subcutaneous tumors grew to 0.5 cm in diameter (approximate bioluminescent radiance of $1x10^{10}$ photons/s/cm2/sr), mice were dosed with 150 mg/kg of GDC-0941 (LC Laboratories) or vehicle alone (10% DMSO and 5% Tween-20 in nuclease-free water) daily for 14 days by oral gavage. For the transplant of A13 cells harboring DOX-inducible sgKras, $5x10^5$ cells suspended in 100 μL of cold PBS were injected per tumor subcutaneously. Clone 7 was injected to the left flank and clone 31 to the right flank of each immunocompromised mouse. DOX feed (Harlan-Teklad) was administered after all the tumors were 0.5 cm in diameter as monitored by caliper measurements. After 4 days of DOX feed, 150 mg/kg of GDC-0941 or vehicle alone was dosed daily for 14 days by oral gavage. Caliper measurements and bioluminescence imaging by IVIS

was done in 3-4 day intervals by injecting 100μl of 30mg/ml luciferin per mouse and imaging 10 minutes post-injection. The level of bioluminescence in radiance was analyzed by Living Image software (Perkin Elmer). Tumor volume was calculated from caliper measurements using the modified ellipsoid formula: (length)x(width)^2/2.

RNA isolation and RNA-sequencing (RNA-Seq) analysis

RNA was isolated from PDAC cells using TRIzol (Life Technologies). cDNA libraries were prepared using an Illumina TruSeq sample preparation kit with indexed adaptor sequences and polyA selection. Sequencing was performed on an Illumina HiSeq 2000 instrument to obtain single-end 50-nt reads. All reads that passed quality metrics were mapped to the UCSC mm9 mouse or hg19 human genome build (http://genome.ucsc.edu/) using RSEM[54]. For pairwise differential expression analyses, data normalization (MedianNorm) and differential analyses between experimental conditions were performed using EBSeq v1.4.0[55]. All RNA-Seq analyses were conducted in the R Statistical Programming language (http://www.r-project.org/). Unsupervised clustering was performed using a Pearson correlation based pairwise distance measure. Heat maps were generated using the Heatplus package in R. RNA-Seq data has been deposited into the publically available Gene Expression Omnibus (GEO) under accession GSE71876.

High-resolution signature analyses between clones within each cell line were performed using a blind source separation methodology based on Independent Component Analysis (ICA) (A.B. et al., in preparation). RSEM generated estimated expression counts were upper-quartile normalized to a count of 1000[56]. The R implementation of the core JADE algorithm (Joint Approximate Diagonalization of Eigenmatrices)[57–59] was used along with custom R utilities.

Signatures were visualized using the sample-to-signature correspondence schematic afforded by Hinton plots where colors represent relative directionality of gene expression (red upregulated, green downregulated) and the size of each rectangle quantifies the strength of a signature (column) in a given sample (row). Each signature is two-sided, allowing for identification of upregulated and downregulated genes for each signature within each sample. Biologically relevant and statistically significant signatures were identified using a Mann-Whitney U test. Signature correlation scores (Z-scores) for each gene in the statistically significant signatures are included as supplementary tables. Heat maps were plotted with the top and bottom 2% genes in each signature. Additionally, genes with standardized signature correlation scores $z > 3$ (alternatively $z < -3$) were used as gene sets to score TCGA (https://tcga-data.nci.nih.gov/tcga/) Pancreatic Adenocarcinoma (PAAD) tumors using ssGSEA[60]. Tumors were stratified using standardized scores and top and bottom percentile buckets were compared for a difference in survival times. Significance of overlap between tumor buckets scored using 8988T and A13 signatures was determined using the Hypergeometric test. Survival analyses were conducted using the survival package in R.

In order to derive a combined knockout signature, the top and bottom 2% genes in the human signature were analyzed in the mouse expression dataset and ICA analysis revealed a WT/KO signature. The up and down gene sets were determined using a standardized signature correlation score of $z > 0.5$ (alternatively, $z < -0.5$). These were used in survival analyses similar to those described above for TCGA and also for ICGC Pancreatic Cancer Australia (PACA-AU) tumors (https://icgc.org/icgc/cgp/68/304/798).

Publicly available microarray datasets were used to generate KRAS-ON and KRAS-OFF signatures from a mouse model of DOX-regulated *KRAS* transgene expression[21,36,37]. Array CEL

files were retrieved from GEO (GSE32277, GSE 53169, and GSE 58307) and processed using Affymetrix Power Tools v. 1.15.0 (rma-sketch). Probes were collapsed (max. value) to yield per gene expression estimates. Genes with upper quartile log2 expression value less than 5 across all samples were dropped from further analysis. The resulting datasets was used for signature analysis with ICA.

Publicly available RNA-Seq datasets were used to generate the CTC signature[41]. Read counts for the sample set (number of raw reads mapped per gene) were downloaded from GEO for record GSE51372. Entries with duplicate symbols or missing gene names were dropped from further consideration. Samples with less than 5 million total mapped reads were dropped from the dataset in order to eliminate expression noise from low coverage. Only samples identified as tumor or classical CTC were retained for downstream analyses. Read counts for the remaining samples were normalized using quartile normalization with the upper quartile set to 1000. In the resulting expression dataset, genes with an upper quartile of expression count less than 1000 across all samples were tagged as lowly expressed genes and dropped. Normalized expression values were log2 transformed and used as input for signature analysis using ICA.

Gene Set Enrichment Analyses (GSEA) were carried out using the pre-ranked mode using log2 fold-change values (for pairwise analyses) or standardized signature correlation scores (for ICA signatures) with default settings[35]. Network representations of GSEA results were generated using EnrichmentMap (http://www.baderlab.org/Software/EnrichmentMap) for Cytoscape v3.2.1 (http://www.cytoscape.org).

Candidate point mutations in RNA-Seq datasets were called using a pipeline based on the GATK Toolkit (https://www.broadinstitute.org/gatk/). Transcriptomic reads were mapped (to mm9, hg19) using the Tophat[61] spliced aligner and subjected to local realignment and score

recalibration using the GATK Toolkit. Mutations were called in KO samples (individual and pooled) against WT samples (individual and pooled) with a minimum base quality threshold of 30. Genomic annotations were performed using ANNOVAR (http://www.openbioinformatics.org/annovar/).

Statistical analyses

P-values for comparisons of two groups were determined by Student's t-test (for normally distributed data) or Mann-Whitney U-test (for non-normally distributed data) as noted in the figure legends. Log-rank (for univariate analysis) and Cox regression (for multivariate analysis) tests were used for survival analyses. A p-value of <0.05 was used to denote statistical significance. All error bars denote standard error of mean (SEM) or standard deviation (SD) as noted in the figure legends.

ACKNOWLEDGEMENTS

We thank J. Settleman for critical reading of contents presented in this chapter; A. Li, V. Gocheva, N. Dimitrova, F. Sanchez-Rivera, C. Li, K. Chung, B. Wagner, A. Aguirre, and O. Shalem for technical assistance and reagents; J. Cheah and C. Soule from the Koch Institute (KI) Genomics Core/HTS Facility for screening assistance; K. Cormier and C. Condon from the Hope Babette Tang (1983) Histology Facility for histology assistance; M. Jennings, M. Griffin, G. Paradis, and S. Malstrom from the Swanson Biotechnology Center for technical support; S. Levine and A. Perez from the MIT BioMicroCenter for RNA-Seq support; and W. Hahn, M. Herold, S. Lowe, W. Sellers, R. Weinberg, and F. Zhang for constructs. We acknowledge that all experimental and analytical work done in the KI Genomics Core/HTS Facility is funded by the NIH and must be made available through the NIH's public access policy when published (https://publicaccess.nih.gov/).

This work was supported by the Howard Hughes Medical Institute, Lustgarten Foundation Consortium Grant and Research Investigator Award, Blum-Kovler Pancreatic Cancer Action Network-AACR Innovative grant, Department of Defense Congressionally-Directed Medical Research Program grant (W81XWH-12-043), and in part by the Cancer Center Support (core) grant P30-CA14051 from the National Cancer Institute. M.D.M. is supported by a KL2/Catalyst Medical Research Investigator Training award (an appointed KL2 award) from Harvard Catalyst | The Harvard Clinical and Translational Science Center (National Center for Research Resources and the National Center for Advancing Translational Sciences, National Institutes of Health Award KL2 TR001100). T.J. is a Howard Hughes Medical Institute Investigator, the David H. Koch Professor of Biology, and a Daniel K. Ludwig Scholar.

REFERENCES

1. American Cancer Society. Cancer Facts & Figures 2015. **Atlanta: American Cancer Society,** (2015).

2. Ryan, D. P., Hong, T. S. & Bardeesy, N. Pancreatic Adenocarcinoma. *NEJM* **371,** 1039–1049 (2014).

3. Conroy, T. *et al.* FOLFIRINOX versus gemcitabine for metastatic pancreatic cancer. *N. Engl. J. Med.* **364,** 1817–1825 (2011).

4. Von Hoff, D. D. *et al.* Increased Survival in Pancreatic Cancer with nab-Paclitaxel plus Gemcitabine. *N. Engl. J. Med.* **369,** 1691–1703 (2013).

5. Hezel, A. F., Kimmelman, A. C., Stanger, B. Z., Bardeesy, N. & DePinho, R. a. Genetics and biology of pancreatic ductal adenocarcinoma. *Genes Dev.* **20,** 1218–1249 (2006).

6. Jones, S. *et al.* Core signaling pathways in human pancreatic cancers revealed by global genomic analyses. *Science* **321,** 1801–1806 (2008).

7. Biankin, A. V. *et al.* Pancreatic cancer genomes reveal aberrations in axon guidance pathway genes. *Nature* **491,** 399–405 (2012).

8. Waddell, N. *et al.* Whole genomes redefine the mutational landscape of pancreatic cancer. *Nature* **518,** 495–501 (2015).

9. Karnoub, A. E. & Weinberg, R. a. Ras oncogenes: split personalities. *Nat. Rev. Mol. Cell Biol.* **9,** 517–531 (2008).

10. Stephen, A. G., Esposito, D., Bagni, R. G. & McCormick, F. Dragging ras back in the ring. *Cancer Cell* **25,** 272–281 (2014).

11. Hingorani, S. R. *et al.* Preinvasive and invasive ductal pancreatic cancer and its early detection in the mouse. *Cancer Cell* **4,** 437–450 (2003).

12. Ostrem, J. M., Peters, U., Sos, M. L., Wells, J. a & Shokat, K. M. K-Ras(G12C) inhibitors allosterically control GTP affinity and effector interactions. *Nature* **503,** 548–51 (2013).

13. Maurer, T. *et al.* Small-molecule ligands bind to a distinct pocket in Ras and inhibit SOS-mediated nucleotide exchange activity. *Proc. Natl. Acad. Sci.* **109,** 5299–5304 (2012).

14. Sun, Q. *et al.* Discovery of small molecules that bind to K-Ras and inhibit Sos-mediated activation. *Angew. Chemie - Int. Ed.* **51,** 6140–6143 (2012).

15. Zimmermann, G. *et al.* Small molecule inhibition of the KRAS-PDEδ interaction impairs oncogenic KRAS signalling. *Nature* **497,** 638–42 (2013).

16. Ledford, H. The ras renaissance. *Nature* **520,** 278–280 (2015).

17. Cox, A. D., Fesik, S. W., Kimmelman, A. C., Luo, J. & Der, C. J. Drugging the

undruggable RAS: Mission Possible? *Nat. Rev. Drug Discov.* **13,** 828–51 (2014).

18. Brummelkamp, T. R., Bernards, R. & Agami, R. Stable suppression of tumorigenicity by virus-mediated RNA interference. *Cancer Cell* **2,** 243–247 (2002).

19. Singh, A. *et al.* A Gene Expression Signature Associated with 'K-Ras Addiction' Reveals Regulators of EMT and Tumor Cell Survival. *Cancer Cell* **15,** 489–500 (2009).

20. Collisson, E. a *et al.* Subtypes of pancreatic ductal adenocarcinoma and their differing responses to therapy. *Nat. Med.* **17,** 500–503 (2011).

21. Kapoor, A. *et al.* Yap1 activation enables bypass of oncogenic KRAS addiction in pancreatic cancer. *Cell* **158,** 185–197 (2014).

22. Ran, F., Hsu, P., Wright, J. & Agarwala, V. Genome engineering using the CRISPR-Cas9 system. *Nat. Protoc.* **8,** 2281–308 (2013).

23. Shi, J. *et al.* Discovery of cancer drug targets by CRISPR-Cas9 screening of protein domains. *Nat. Biotechnol.* **33,** 661–667 (2015).

24. Shao, D. D. *et al.* KRAS and YAP1 converge to regulate EMT and tumor survival. *Cell* **158,** 171–184 (2014).

25. Turke, A. B. *et al.* MEK inhibition leads to PI3K/AKT activation by relieving a negative feedback on ERBB receptors. *Cancer Res.* **72,** 3228–3237 (2012).

26. Ebi, H. *et al.* Receptor tyrosine kinases exert dominant control over PI3K signaling in human KRAS mutant colorectal cancers. *J. Clin. Invest.* **121,** 4311–4321 (2011).

27. Lee, H. J. *et al.* Drug resistance via feedback activation of stat3 in oncogene-addicted cancer cells. *Cancer Cell* **26,** 207–221 (2014).

28. Ebi, H. *et al.* PI3K regulates MEK/ERK signaling in breast cancer via the Rac-GEF, P-Rex1. *Proc. Natl. Acad. Sci. U. S. A.* **110,** 21124–9 (2013).

29. Will, M. *et al.* Rapid induction of apoptosis by PI3K inhibitors is dependent upon their transient inhibition of RAS-ERK signaling. *Cancer Discov.* **4,** 334–348 (2014).

30. She, Q., Halilovic, E., Ye, Q., Zhen, W. & Shirasawa, S. and ERK Signaling Pathways That Integrates Their Function in. **18,** 39–51 (2012).

31. Martineau, Y. *et al.* Pancreatic tumours escape from translational control through 4E-BP1 loss. *Oncogene* **33,** 1367–74 (2014).

32. Ilic, N., Utermark, T., Widlund, H. R. & Roberts, T. M. PI3K-targeted therapy can be evaded by gene amplification along the MYC-eukaryotic translation initiation factor 4E (eIF4E) axis. *Proc. Natl. Acad. Sci. U. S. A.* **108,** E699–E708 (2011).

33. Wendel, H.-G. *et al.* Survival signalling by Akt and eIF4E in oncogenesis and cancer therapy. *Nature* **428,** 332–337 (2004).

34. Mootha, V. K. *et al.* PGC-1alpha-responsive genes involved in oxidative phosphorylation are coordinately downregulated in human diabetes. *Nat. Genet.* **34,** 267–273 (2003).

35. Subramanian, A., Tamayo, P., Mootha, V. K., Mukherjee, S. & Ebert, B. L. Gene set enrichment analysis : A knowledge-based approach for interpreting genome-wide. *Proc Natl Acad Sci U S A* **102,** 15545–15550 (2005).

36. Ying, H. *et al.* Oncogenic kras maintains pancreatic tumors through regulation of anabolic glucose metabolism. *Cell* **149,** 656–670 (2012).

37. Viale, A. *et al.* Oncogene ablation-resistant pancreatic cancer cells depend on mitochondrial function. *Nature* **514,** 628–632 (2014).

38. Seguin, L. *et al.* An integrin β3-KRAS-RalB complex drives tumour stemness and resistance to EGFR inhibition. *Nat. Cell Biol.* **16,** 457–68 (2014).

39. DeNicola, G. M. *et al.* Oncogene-induced Nrf2 transcription promotes ROS detoxification and tumorigenesis. *Nature* **475,** 106–109 (2011).

40. Whittle, M. C. *et al.* RUNX3 Controls a Metastatic Switch in Pancreatic Ductal Adenocarcinoma. *Cell* **161,** 1345–1360 (2015).

41. Ting, D. T. *et al.* Single-Cell RNA Sequencing Identifies Extracellular Matrix Gene Expression by Pancreatic Circulating Tumor Cells. *Cell Rep.* **8,** 1905–1918 (2014).

42. Eser, S. *et al.* Selective requirement of PI3K/PDK1 signaling for kras oncogene-driven pancreatic cell plasticity and cancer. *Cancer Cell* **23,** 406–420 (2013).

43. Payne, S. N. *et al.* PIK3CA mutations can initiate pancreatic tumorigenesis and are targetable with PI3K inhibitors. *Oncogenesis* **4,** e169 (2015).

44. Hofmann, I. *et al.* K-RAS Mutant Pancreatic Tumors Show Higher Sensitivity to MEK than to PI3K Inhibition In Vivo. *PLoS One* **7,** (2012).

45. Junttila, M. R. *et al.* Modeling Targeted Inhibition of MEK and PI3 Kinase in Human Pancreatic Cancer. *Mol. Cancer Ther.* **14,** 40–47 (2014).

46. Alagesan, B. *et al.* Combined MEK and PI3K Inhibition in a Mouse Model of Pancreatic Cancer. *Clin. Cancer Res.* **21,** 396–404 (2015).

47. Wells, V., Downward, J. & Mallucci, L. Functional inhibition of PI3K by the betaGBP molecule suppresses Ras-MAPK signalling to block cell proliferation. *Oncogene* **26,** 7709–7714 (2007).

48. Carracedo, A. *et al.* Inhibition of mTORC1 leads to MAPK pathway activation through a PI3K-dependent feedback loop in human cancer. *J. Clin. Invest.* **118,** 3065–3074 (2008).

49. Sampaio, C. *et al.* Signal strength dictates phosphoinositide 3-kinase contribution to Ras/extracellular signal-regulated kinase 1 and 2 activation via differential Gab1/Shp2 recruitment: consequences for resistance to epidermal growth factor receptor inhibition. *Mol. Cell. Biol.* **28,** 587–600 (2008).

50. Friedlander, S. Y. G. *et al.* Context-Dependent Transformation of Adult Pancreatic Cells by Oncogenic K-Ras. *Cancer Cell* **16,** 379–389 (2009).

51. Sanjana, N. E., Shalem, O. & Zhang, F. Improved vectors and genome-wide libraries for CRISPR screening. *Nat. Protoc.* **11,** 783–784 (2014).

52. Aubrey, B. J. *et al.* An Inducible Lentiviral Guide RNA Platform Enables the Identification of Tumor-Essential Genes and Tumor-Promoting Mutations In Vivo. *Cell Rep.* **10,** 1422–1432 (2015).

53. Basu, A. *et al.* An interactive resource to identify cancer genetic and lineage dependencies targeted by small molecules. *Cell* **154,** 1151–1161 (2013).

54. Li, B. & Dewey, C. N. RSEM: accurate transcript quantification from RNA-Seq data with or without a reference genome. *BMC Bioinformatics* **12,** 323 (2011).

55. Leng, N. *et al.* EBSeq: An empirical Bayes hierarchical model for inference in RNA-seq experiments. *Bioinformatics* **29,** 1035–1043 (2013).

56. Bullard, J. H., Purdom, E., Hansen, K. D. & Dudoit, S. Evaluation of statistical methods for normalization and differential expression in mRNA-Seq experiments. *BMC Bioinformatics* **11,** 94 (2010).

57. Nordhausen, K. *et al.* JADE: JADE and other BSS methods as well as some BSS performance criteria. *R Packag. version 1.1* (2012).

58. Rutledge, D. N. & Jouan-Rimbaud Bouveresse, D. Independent Components Analysis with the JADE algorithm. *Trends Anal. Chem.* **50,** 22–32 (2013).

59. Biton, A. *et al.* Independent Component Analysis Uncovers the Landscape of the Bladder Tumor Transcriptome and Reveals Insights into Luminal and Basal Subtypes. *Cell Rep.* **9,** 1235–1245 (2014).

60. Barbie, D. a *et al.* Systematic RNA interference reveals that oncogenic KRAS-driven cancers require TBK1. *Nature* **462,** 108–112 (2009).

61. Trapnell, C., Pachter, L. & Salzberg, S. L. TopHat: Discovering splice junctions with RNA-Seq. *Bioinformatics* **25,** 1105–1111 (2009).

CHAPTER 4

CONCLUSIONS AND DISCUSSION

KRAS is the most frequently mutated proto-oncogene in solid tumors. The high prevalence of activating *KRAS* mutations in pancreatic, lung, and colorectal adenocarcinomas makes oncogenic KRAS an extremely attractive therapeutic target. In particular, *KRAS* mutations are considered the defining genetic feature of pancreatic cancer[1,2]. Unfortunately, attempts to directly or indirectly inhibit KRAS have been largely unsuccessful, and there are no effective KRAS-specific pharmacological inhibitors to date (Chapter 1). A deeper understanding of the functions of oncogenic KRAS signaling in mediating cancer progression may open up new avenues to the development of KRAS-directed therapeutic strategies. The work presented in this thesis aimed to investigate the requirement of KRAS function in maintaining pancreatic cancer cell viability, which is critical to understand for the development of KRAS-directed therapies. Whereas the role of oncogenic KRAS in tumor initiation has been well defined and demonstrated in various *in vitro* and *in vivo* cancer models of the pancreas, lung, and colon[3-10], the function of oncogenic KRAS signaling in tumor maintenance and how it contributes to the progression of malignant transformation remained relatively unresolved.

Previous studies have employed various model systems and experimental techniques to interrogate the requirement of KRAS for PDAC maintenance. In contrary to what one might expect based on the high frequency of activating *KRAS* mutations in human PDAC, the results from these studies suggest that *KRAS* dependency is cancer cell- and tumor-dependent. RNAi-mediated *KRAS* knockdown in a panel of human PDAC cell lines and gene expression profiling of human PDAC tumors suggest that human PDAC cells exhibit variable dependency on *KRAS* expression for survival[11,12], with cells displaying a more mesenchymal gene expression profile being more resistant to KRAS inhibition. On the other hand, mouse models engineered to express an inducible oncogenic *Kras* transgene demonstrates that the withdrawal of oncogenic

Kras expression leads to rapid pancreatic tumor regression initially, but relapse via both *Kras*-dependent and *Kras*-independent mechanisms develop after a period of dormancy[3,10,13]. Further characterization of cancer cells and relapse tumors that escape *Kras* addiction reveals that upregulation and amplification of YAP can bypass *Kras* dependency[13], which is in accordance with analysis of *Kras*-mutant cancer cell lines[14]. Additionally, the remaining cells that survive the loss of oncogenic *Kras* show an increased dependency on mitochondrial oxidative phosphorylation[15]. Observations from these studies provide invaluable insights into how KRAS may function to mediate PDAC progression and maintenance, but care must be taken into extrapolating findings using overexpression systems to explain biological activities of endogenous KRAS. Sensitivity of mammalian cells to the levels of *Kras* expression has been reported previously, which demonstrated that overexpression of oncogenic *Kras* and expression of oncogenic *Kras* at endogenous levels lead to distinct phenotypes[9].

Recent advances in molecular biology that enable perturbation of gene expression in mammalian cells[16,17] allow us to leverage inducible miR30-based shRNA and CRISPR/Cas-based systems to elucidate the degree of endogenous *KRAS* dependency in human and murine PDAC cells. These two systems offer unique advantages despite having certain limitations. Importantly, comparison of the consequences of partial and complete inhibition of endogenous *Kras* (Chapter 2 describes partial Kras inhibition and Chapter 3 describes KRAS ablation) provides insight into the degree of KRAS inhibition required to effectively impair PDAC cell survival. Furthermore, thorough analyses of transcriptional and signaling changes in cell clones that tolerate Kras inhibition uncovered possible resistance mechanisms to Kras inhibition distinct from those previously reported. As presented in Chapter 2, murine PDAC cells appear to tolerate acute and sustained, partial but significant, Kras inhibition by adapting to a reversible

cell state. In Chapter 3, we demonstrate a unique dependency on canonical and non-canonical PI3K signaling in human and murine PDAC cells that experience complete KRAS ablation. This Chapter begins with a discussion on the therapeutic implications of our interesting observations, specifically the degree of KRAS inhibition required to achieve clinical benefits and diverse resistance mechanisms to oncogene inhibition. Finally, this Chapter concludes with a discussion on how our results support the emerging roles of oncogenic KRAS in mediating cancer progression, which can provide novel therapeutic opportunities for inhibiting *KRAS*-driven cancers.

4.1 Significant inhibition of KRAS may be required to impair PDAC cell survival

Combining the results from Chapter 2 and Chapter 3, it appears that the majority of murine PDAC cells can adapt to a partially Kras-inhibited state, whereas only a fraction of human and murine PDAC cells can tolerate complete KRAS ablation. Moreover, the ability of human PDAC cells to tolerate complete loss of KRAS is in accordance with previous RNAi-based classification of KRAS dependency[12]. The stark contrast between the ease to isolate single cell clones that survive partial Kras inhibition and those that survive complete KRAS inhibition suggests that a near complete inhibition of KRAS may be required to impair *KRAS*-mutant cancer cell survival. This implies that for a pharmacological inhibitor targeting KRAS to exhibit therapeutic efficacy, a high degree of inhibition of KRAS function may need to be achieved. Alternatively, combinations of multiple agents that will result in a more complete inhibition of KRAS function may be useful. This section compares and contrasts the strengths and limitations of the knockdown and knockout systems, which should be taken into consideration when interpreting the results.

Strengths and limitations of the inducible Kras knockdown system

The inducible miR30-based shRNA knockdown system provides a powerful toolkit that enables the toggling of the endogenous expression of a gene to study its function[16]. We employed this toolkit to generate an *in vitro* system that reversibly and partially inhibits endogenous wild-type and oncogenic Kras, which mimics the effect of a pharmacological inhibitor that is not mutant-specific. We selected for cells that highly express the GFP reporter, a surrogate for shKras expression, and confirmed that these cells experience significant Kras mRNA and protein knockdown at more than 70% upon DOX treatment. The major strength of this reversible Kras knockdown system is that it allows us to distinguish between the selection for pre-existing resistance-conferring mutations and an adaptive cell state change as a resistance mechanism to partial Kras inhibition (Chapter 2). As *Kras* expression can easily be restored by simply withdrawing DOX treatment, we are able to examine reversal of the Kras-inhibited state by visible morphological changes and proliferative rates that occur within a few days.

Despite being a powerful system, the inducible Kras knockdown system has a few limitations that should be taken into consideration when interpreting the results. First, the Kras hairpins do not distinguish between wild-type and mutant alleles of *Kras*. As mentioned in Chapter 1, it has been postulated that wild-type Kras may have tumor suppressive effects in lung carcinogenesis[18]. If this were true in PDAC, then an ideal therapeutic strategy is to target only the mutant allele and spare the wild-type allele. However, the only currently available mutant-specific Kras inhibitors target $Kras^{G12C}$[19,20], which is not a common *Kras* mutation in PDAC. $Kras^{G12C}$ can be effectively inhibited mainly because of the reactive thiol group on cysteine, and these $Kras^{G12C}$-specific inhibitors are currently effective in laboratory but not clinical settings. Therefore, our results are important as most novel pharmacological inhibitors will likely target

both wild-type and mutant forms of Kras. A second limitation of our analysis is that we analyzed transcriptional, signaling, and adherent properties at steady-state, assuming that stead-state Kras inhibition is equivalent to acute Kras inhibition based on similarities in morphology and proliferation rates. The rationale for analyzing PDAC cells at steady-state Kras inhibition is that there is technical difficulty in determining an acute time point at which all of the cells exhibit Kras knockdown but have not yet undergone a selection process or cell state change. Based on our observation that the majority (at least 70%) of PDAC cells analyzed can adapt to the stably Kras-inhibited state, analysis of the steady state should still provide relevant information on how most cells respond to Kras inhibition. Additionally, concerns associated with the potential off-target effects of RNAi and DOX treatment will be discussed in more details in a later section below. Finally, although our analysis indicates that PDAC cells can tolerate acute and sustained Kras inhibition, it is unclear whether incomplete Kras inhibition is simply insufficient to impair cell survival. It is possible that a near complete inhibition of Kras will have to be achieved to have a significant clinical impact. Therefore, this limitation led us to explore the effects of CRISPR/Cas-mediated Kras ablation on PDAC cells.

Strengths and limitations of the CRISPR/Cas-based KRAS knockout system

In order to determine whether a greater degree of inhibition (more than 70%) is required to impair PDAC cell survival, we employed the CRISPR/Cas9 technology[17] to knockout endogenous KRAS in a panel of human and murine PDAC cell lines. We found that human PDAC cell lines previously characterized as "*KRAS*-dependent"[12] underwent massive apoptosis upon *KRAS* ablation. In contrast, "*KRAS*-independent" cell lines gave rise to a small number of stably KRAS-knockout cell clones. This small number can be due to the poor tolerance of human PDAC cells to KRAS ablation or possible technical limitations, including the inability to

strongly express both Cas9 and sgKRAS or abundance of mutations that are non-frameshift or do not occur at functionally important domains[21]. Nevertheless, along with Kras-knockout clones derived from murine PDAC cell lines, these cell clones allowed us to thoroughly compare the effects of partial and complete KRAS inhibition in PDAC cells.

One of the biggest advantages of this stable knockout system is that after selection of clones that contain only alleles with frameshift mutation, a true null phenotype rather than the hypomorphic phenotype created by knockdown, can be studied. Chapter 3 shows that complete KRAS inhibition leads to strong transcriptional and signaling changes, which allows the identification of a gene expression signature that is not parental clone-dependent. Furthermore, the signaling changes that occur in KRAS knockout cells can easily be detected by western blots, although a mass spectroscopy analysis may be more sensitive. Another advantage of this system is that it is not dependent on DOX treatment, which can be a confounding factor in gene expression and signaling analyses in the inducible shKras system. Example of a gene whose expression is strongly induced by DOX is *Gpr56*, as shown in Chapter 2.

Since the stable knockout system does not allow reversal of endogenous KRAS ablation (although expression of an exogenous *KRAS* cDNA can achieve reversal), it is relatively difficult to determine whether the increased dependency on PI3K signaling of KRAS knockout cells is an adaptive and reversible state. At least based on mutation analysis using RNA sequencing data, no enrichment of PI3K-associated mutations is observed in knockout cells. Another limitation with this system is the challenge to determine the percentage of PDAC cells that are able to tolerate complete KRAS knockout. A few factors contribute to the difficulty to perform a similar experiment using the stable knockout system as the one we have designed to test the percentage of cell clones that can tolerate sustained Kras knockdown: the efficacy of sgRNA to produce

loss-of-function mutations is dependent on cutting efficiency and the targeting site containing an important functional domain; transduction efficiency and Cas9 expression in individual cells; the ability of cell lines to form single cell clones irrespective of *KRAS* modulation; ploidy; and intrinsic dependence on *KRAS*. In order to overcome this issue with the stable knockout system, we adapted an inducible CRISPR/Cas-based knockout system[22] to induce DOX-dependent KRAS knockout in human and murine PDAC cells. Not only does this system allow near complete KRAS inhibition (based on the number of cells that harbor frameshift mutations upon DOX induction, which is an analysis we are currently pursuing) in established subcutaneous tumors to mimic a therapeutic effect, but it also allows us to analyze the percentage of cells that can tolerate KRAS ablation. We plan to identify the sgRNA that most effectively knockout *KRAS*, and compare the number of single cell clones that are able to grow in the presence or absence of DOX treatment. This information will allow us to better understand the nature of resistance to KRAS ablation.

A graded effect on gene expression is observed in cells that tolerate partial or complete Kras inhibition

Comparison between the RNA-sequencing analyses on Kras knockdown and Kras knockout cells that are derived from the same parental cell line (murine PDAC clone A) revealed an interesting graded effect on gene expression. First, in contrast to gene expression profiles of cells in the Kras knockdown study that segregate based on the origin of the parental clone rather than Kras status, unsupervised hierarchical clustering clearly segregates Kras knockout and from Kras intact clones (**Fig. 1A**). ICA derived a component (IC1) that clusters cells that are partially or completely Kras-inhibited apart from Kras intact cells (**Fig. 1B**). This IC1 signature represents genes that are enriched in murine PDAC cells that are Kras-inhibited (**Fig. 1C**),

suggesting that these genes might mediate important functions that are required for the survival of PDAC cells in response to Kras inhibition. As shown in Chapter 2, partial Kras inhibition does not result in significant transcriptional changes, and thus the IC1 signature is only mildly enriched in Kras knockdown cells. However, this signature is strongly enriched in Kras knockout cells, indicating that the significant transcriptional profile changes of Kras knockout cells help drive the identification of IC1. Importantly, the graded effect on gene expression demonstrates that the phenotypes we have observed in Kras knockdown cells are not due to off-target effects. We have previously validated the effect is on-target by showing that expression of an exogenous *Kras* cDNA, but not *GFP*, can rescue the morphological and proliferative changes induced by Kras knockdown (Chapter 2). The comparison of transcriptional changes between Kras knockdown and knockout cells further corroborates these results. Network association analysis reveals that within this signature, genes associated with RTK signaling and redox metabolism are upregulated whereas genes associated with interferon response are downregulated (**Fig. 1D**). It is possible that RTK signaling and redox metabolism are upregulated as resistance mechanisms to compensate for the loss of Kras. Interestingly, based on RNA sequencing data, we have observed increased expression of RTKs like PDGFRβ and FGFR2 in human KRAS knockout cells. We therefore hypothesized that upregulation of these RTKs may be responsible for PI3K/AKT activation. However, pharmacological inhibition of PDGFRβ or FGFR alone or in combination did not alter PI3K/AKT activation or show greater sensitivity in KRAS knockout cells, suggesting that these kinases alone do not play a role in distinguishing intact and knockout cells. The upregulation of redox metabolism genes is interesting because a separate study analyzing remaining cells that survive the withdrawal of oncogenic *Kras* expression exhibit an increased dependency on oxidative phosphorylation[15].

Taken together, genes associated with RTK signaling and redox metabolism pathways can be considered as drug targets that may be useful to inhibit in combination with KRAS-directed therapies. On the other hand, expression of interferon response genes is possibly regulated by Kras activity. However, in Chapter 3 we showed that interferon response pathways are downregulated based on gene expression in human KRAS knockout cells. It is unresolved why such discrepancy exists, but we hypothesize that this may be a species difference. Finally, ICA derived a DOX signature, IC5, which includes the *Gpr56* gene (**Fig. 1E**). This signature can be extremely useful for future analysis on data generated by DOX-dependent systems to filter out off-target effects of DOX treatment.

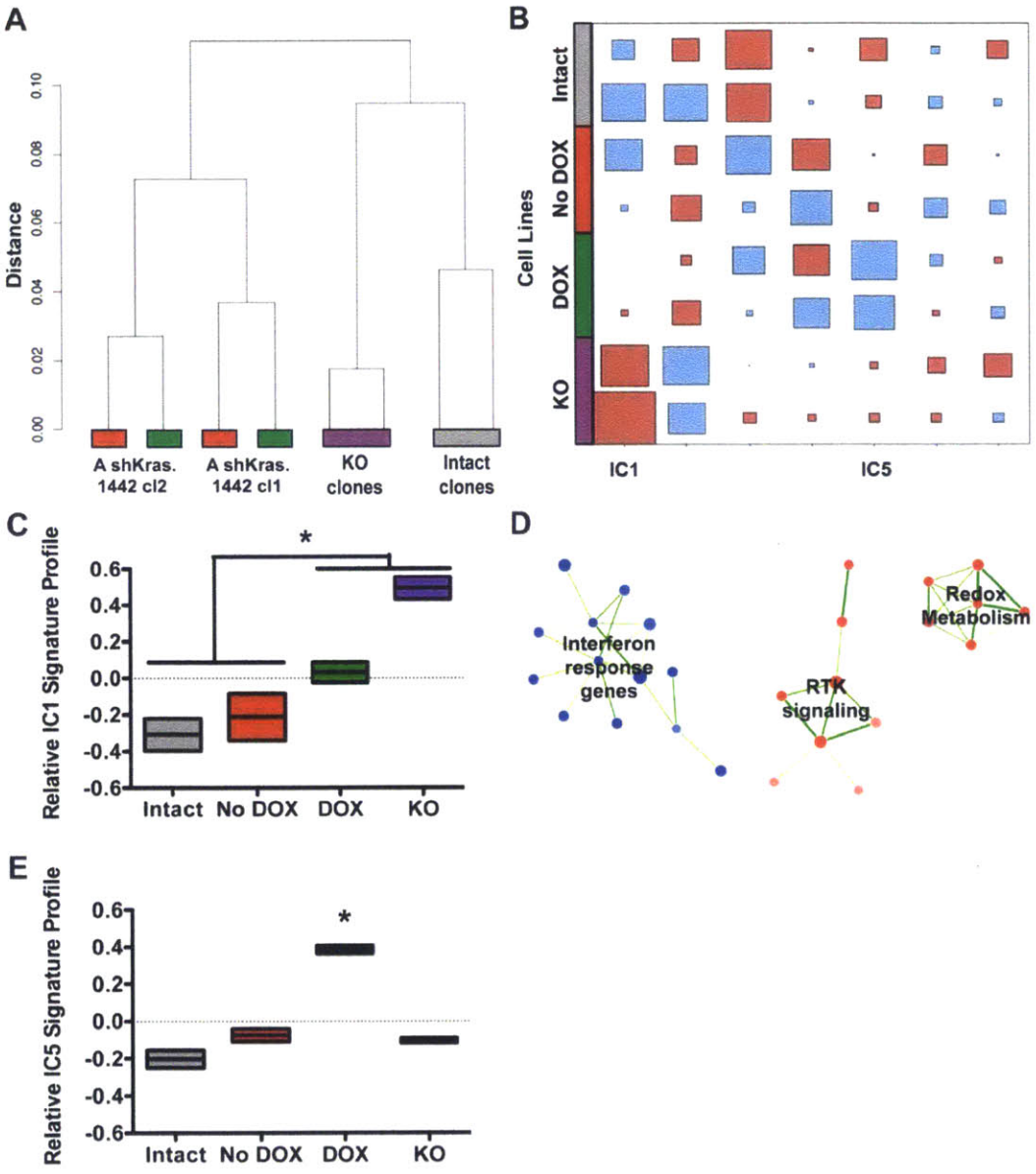

Figure 1: A graded effect on gene expression is observed in Kras knockdown and Kras knockout cells.

A. Unsupervised clustering of murine PDAC A13-derived cell clones. Whereas Kras knockdown cells segregate based on the origin of the parental clone, Kras knockout cells segregate based on Kras status.

B. ICA derived a signature associated with response to Kras inhibition (IC1) and a DOX signature (IC5).

C. IC1 is mildly enriched in Kras knockdown cells (DOX) and strongly enriched in Kras knockout cells (KO).

D. Network representation of IC1 signature indicates that genes associated with RTK signaling and redox metabolism are upregulated (red), while genes associated with interferon response are downregulated (blue).

E. The IC5 DOX signature is significantly and strongly enriched in DOX-treated cells only.

4.2 Resistance mechanisms to KRAS inhibition are adaptive and reversible

An improved understanding of the molecular basis of cancer and oncogene addiction[23] have led to the development of successful molecularly targeted therapies, which have transformed cancer care in the last decade. Targeting the specific molecular defects of individual tumors significantly enhances the therapeutic window to selectively kill cancer cells over normal cells[24]. However, the duration of response and efficacy of single-agent targeted therapies have been limited by the rapid emergence of acquired drug resistance. As such, some single-agent targeted therapies lead to prolonged progression-free survival but only similar overall survival compared to standard of care chemotherapies[25]. Examples include crizotinib treatment in *ALK*-rearranged NSCLC and gefitinib treatment in *EGFR*-mutant NSCLC[26,27]. These limited clinical benefits underscore the need to elucidate possible resistance mechanisms that arise in response to therapies, so that rational combination therapies or appropriate treatment schedules can be preemptively designed to induce long-lasting responses. Work described in this thesis adds to the growing body of evidence that support the importance and relevance of non-genetic and even non-transcriptional resistance mechanisms, which must be taken into consideration when designing cancer therapeutic strategies.

The Kras-inhibited murine PDAC cells are similar to previously described persister cells that survive targeted therapies

It is thought that resistance to cancer therapies comes in two forms. The first type is an early intrinsic resistance, which is due to the presence of pre-existing resistant subclones that quickly expand after therapy. The second type is a late acquired resistance, which arises from an acquired response to environmental factors and the subsequent clonal evolution of resistant variants[25,28]. Although these two forms of resistance seem to represent two sides to the debate

over the origins of drug resistance[28], recent studies show that they are actually not mutually exclusive within a cancer cell population[29,30]. While a subpopulation of cancer cells intrinsically resistant to therapy by genetic mechanisms can grow out quickly upon treatment, a different and possibly larger subpopulation of drug-tolerant "persister" cells that exhibit negligible growth can survive initial treatment and undergo further evolution to acquire a variety of possible resistance mechanisms[29,30]. These observations suggest that early treatment with therapies aimed to overcome resistance can steer tumor evolution towards an alternative, and possibly more difficult to target, resistance mechanism. Accordingly, we found that a large fraction of murine PDAC cells survived sustained Kras inhibition and continue to proliferate at a decreased rate *in vitro* (Chapter 2), similar to the relatively quiescent persister cells. Furthermore, these cells retain tumorigenic abilities and lead to subcutaneous tumor outgrowth *in vivo* (Chapter 2), providing additional evidence that persister cells can be the key to resistance to therapy.

Non-mutational and non-transcriptional mechanisms underlie the resistance to Kras inhibition

Early characterization of cancer drug resistance mostly focused on genetic mechanisms. A classic example of a secondary mutation that alters the binding kinetics of ATP-competitive inhibitors to the target is the T790M gatekeeper mutation in mutant *EGFR*, which explains approximately half of the resistance observed in *EGFR*-mutant NSCLCs treated with EGFR inhibitors[31-33]. Furthermore, downstream pathway activation by *PIK3CA* mutation or parallel pathway activation via *MET* amplification has also been found in resistant human *EGFR*-mutant tumors[34]. Similarly, studies using a human *EGFR*-mutant lung cancer cell line PC9 to identify acquired resistance mechanisms in persister cells after prolonged exposure to EGFR inhibitor demonstrated that ultimate outgrowth of persister cells depends on the acquisition of secondary

T790M mutation or *MET* amplification[29,30], among others. Other examples of genetic mechanisms of resistance include secondary *ALK* mutations or mutations in *EGFR* or *KRAS* in *EML4-ALK*-positive NSCLC[35,36].

More recently, several studies have suggested that non-genetic mechanisms of resistance are possible. In *BRAF*-mutant melanomas, resistance to vemurafenib can occur via secondary mutations in $BRAF^{V600E}$ but also through aberrantly spliced $BRAF^{V600E}$ that enables RAS-independent $BRAF^{V600E}$ dimerization[37] or activation of alternative pro-survival pathways via enhanced PDGFRβ signaling[38]. Interestingly, analysis of BRAF inhibitor- and MEK inhibitor-resistant *BRAF*-mutant melanoma tumors revealed an adaptive resistant state associated with enhanced TGFβ signaling that leads to increased *EGFR* and *PDGFRB* expression[39]. Importantly, this adaptive state is reversible, suggesting that melanoma patients whose tumors acquire *EGFR* expression and exhibit resistance to treatment can benefit from drug holidays. Another recent study discovered a drug-tolerant state that is not dependent on genetic alterations in human cancer cell lines from different tissue origins[40]. These drug-tolerant persister cells exhibit significantly reduced drug sensitivity to targeted inhibition or chemotherapy by engaging IGF-1 receptor signaling and an altered chromatin state, and can be selectively eliminated by treatment with IGF-1 receptor inhibitors or chromatin-modifying agents[40]. Our description of the adaptive and reversible Kras-inhibited state (Chapter 2) adds to the emerging understanding of non-genetic mechanisms of resistance to cancer therapies, and supports the notion that intermittent dosing of an inhibitor can re-sensitize cancer cells to show a treatment response.

Another important aspect of our finding is that the tolerance to Kras inhibition not only is independent of additional mutational events, but also is independent of significant transcriptional changes (Chapter 2). However, it is also important to note that our mutation analysis is not

comprehensive, as we did not examine copy number variations or changes in non-coding regions. We did not analyze epigenetic changes because the conversion between Kras-uninhibited and Kras-inhibited states happens rapidly, as evident by morphological and proliferative changes that take place within 3-5 days of DOX administration or withdrawal (Chapter 2). Based on this observation and the lack of significant transcriptional changes at steady-state, we postulated that the cell state change is mediated by rewiring of signaling rather than epigenetic alterations. However, this does not necessarily have to be true. Characterization of chromatin changes may provide further insight into the Kras-inhibited state and reveal more potential drug targets. Based on unbiased phosphoproteomic analysis, we have identified that increased focal adhesion signaling at least in part contributes to the tolerance to Kras inhibition. Moreover, activation of this pathway likely underlies the key morphological and adherent features that characterize the Kras-inhibited state (Chapter 2), suggesting that it may be functionally important. On the other hand, we have yet to determine whether the dependency on PI3K activation associated with Kras ablation is reversible (Chapter 3), and this is a topic we are interested in exploring.

Characterization of PDAC subclones that tolerate partial or complete KRAS inhibition contributes to the understanding of tumor heterogeneity

As cancer researchers are only beginning to understand the full extent of tumor heterogeneity, how tumor microenvironment contributes to tumor heterogeneity, which aspects of tumor heterogeneity are relevant in a clinical setting, and how to exploit tumor heterogeneity for therapeutic gain[41], our in-depth analyses of human and murine PDAC cell clones contribute to the emerging understanding of tumor heterogeneity and its therapeutic implications. Since there is not a perfect preclinical model for tumor heterogeneity, a variety of models such as

genetically engineered mouse models, patient-derived xenografts (PDX), organoids, and *in silico* models are being used to gain insight into tumor evolution in patients.

In Chapter 2, we used murine cells derived from the primary PDAC tumors of a genetically engineered autochthonous mouse model to avoid confounding our analysis due to the vast difference in genetic backgrounds of human cancer cell lines. This method allows cost-effective and controlled manipulation of gene expression and facilitates the characterization of a cell state in multiple facets, including cell biological features, tumorigenic ability, transcriptional, mutational, proteomic, and signaling. In Chapter 3, we expanded our analysis to include both murine and human PDAC cell lines to enhance the generalizability of our observations, as murine tumors tend to harbor less genetic alterations than human tumors and can be polyclonal in contrast to the monoclonal nature of many human cancers. Although our analyses of both partial and complete Kras inhibition are limited to a few subclones, we aimed to understand mechanisms of resistance that can arise regardless of the number of cells within a tumor that exhibit resistant behavior. Therefore, irrespective of the percentage of cells that are able to tolerate KRAS inhibition, the key to achieving long-term therapeutic efficacy is to simultaneously target sensitive cells and inhibit outgrowth of resistant cells. The cells we analyzed represent a subset of cells in a heterogeneous population in a tumor that could contribute to possible disease relapse to the inhibition of a driver oncogene. Interestingly, among the cells we analyzed, we observed more variability in KRAS dependency in human cell lines than murine cell lines, possibly attributable to a greater extent of heterogeneity among human cell lines than murine cell lines.

An improved model for understanding how resistance to KRAS inhibition may arise within a heterogeneous tumor would be to induce shRNA- or CRISPR/Cas-mediated KRAS

inhibition in PDX models to recapitulate the genetic complexity accumulated during human tumor evolution, and then inhibit KRAS with an inducible shRNA or sgRNA targeting KRAS. Both of these methods will generate a greater diversity in genetic and epigenetic backgrounds of cancer cells, allowing us to gain a more comprehensive view of how cancer cells may respond to KRAS inhibition. However, in addition to the technical hurdles in introducing inducible shRNA and sgRNA systems into PDX models, the reliable detection of epigenetic, genetic, transcriptional, and especially proteomic and phosphoproteomic changes of cancer cells isolated from dissociated tumors can be challenging.

Collectively, our work provides evidence for possible mechanisms of resistance to KRAS inhibition. Under partial Kras inhibition, which is insufficient to impair the survival of the majority of murine PDAC cells, presister cells adapt to a reversible Kras-inhibited state that is mediated by increased focal adhesion signaling (Chapter 2). Complete KRAS ablation is more detrimental at least in cells previously classified as *KRAS*-dependent, but a subset of human and murine PDAC cells are able to survive by PI3K activation (Chapter 3). These observations suggest that inhibition of components of the focal adhesion pathway or PI3K inhibition in combination with KRAS inhibition could be a viable therapeutic strategy for PDAC.

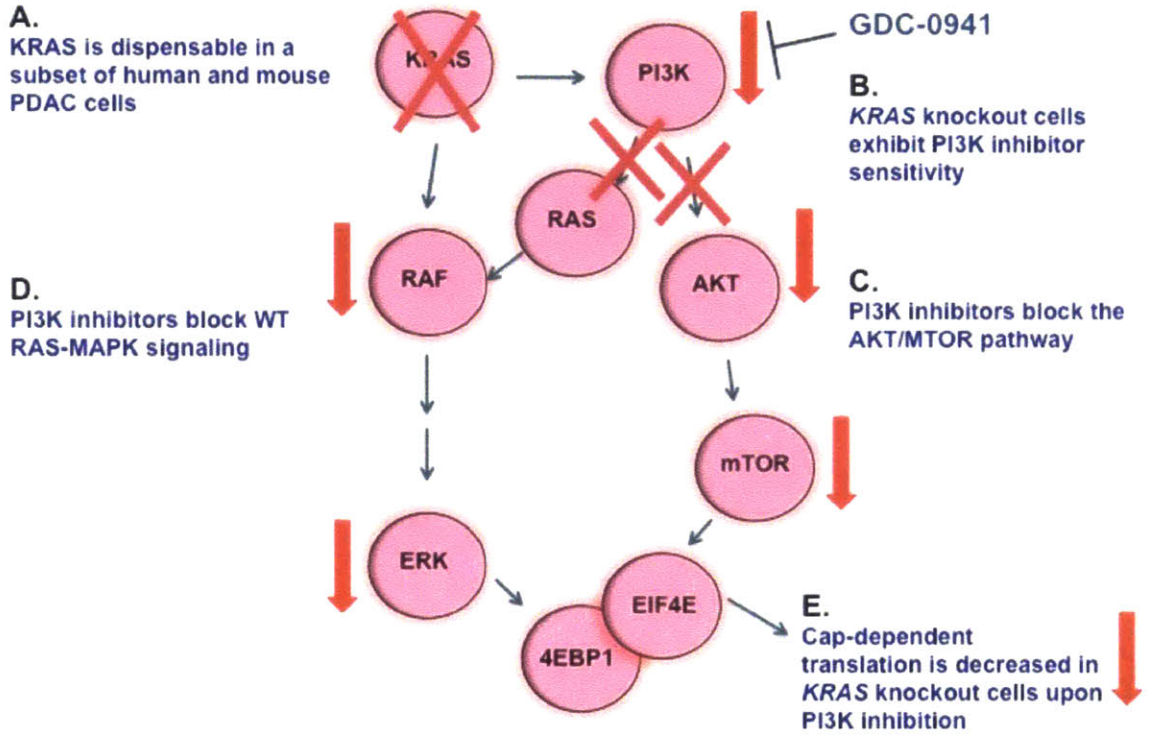

Figure 2. Proposed model of the underlying mechanism of unique PI3K dependency in *KRAS* knockout cells.

A. In Chapter 3, we have shown that KRAS is dispensable in a subset of human and mouse PDAC cells.
B. *KRAS* knockout cells exhibited increased PI3K inhibitor sensitivity.
C. PI3K inhibitor treatment led to sustained inhibition of the AKT/MTOR pathway.
D. PI3K inhibition transiently inhibited the wild-type RAS-MAPK signaling axis uniquely in *KRAS* knockout cells.
E. We have demonstrated that PI3K inhibition had a significantly greater effect on cap-dependent translation, a potential convergent node downstream of the MAPK and AKT pathways, in *KRAS* knockout cells. We hypothesize that this led to an enhanced cytotoxic effect of PI3K inhibition in *KRAS* knockout compared to *KRAS* intact cells.

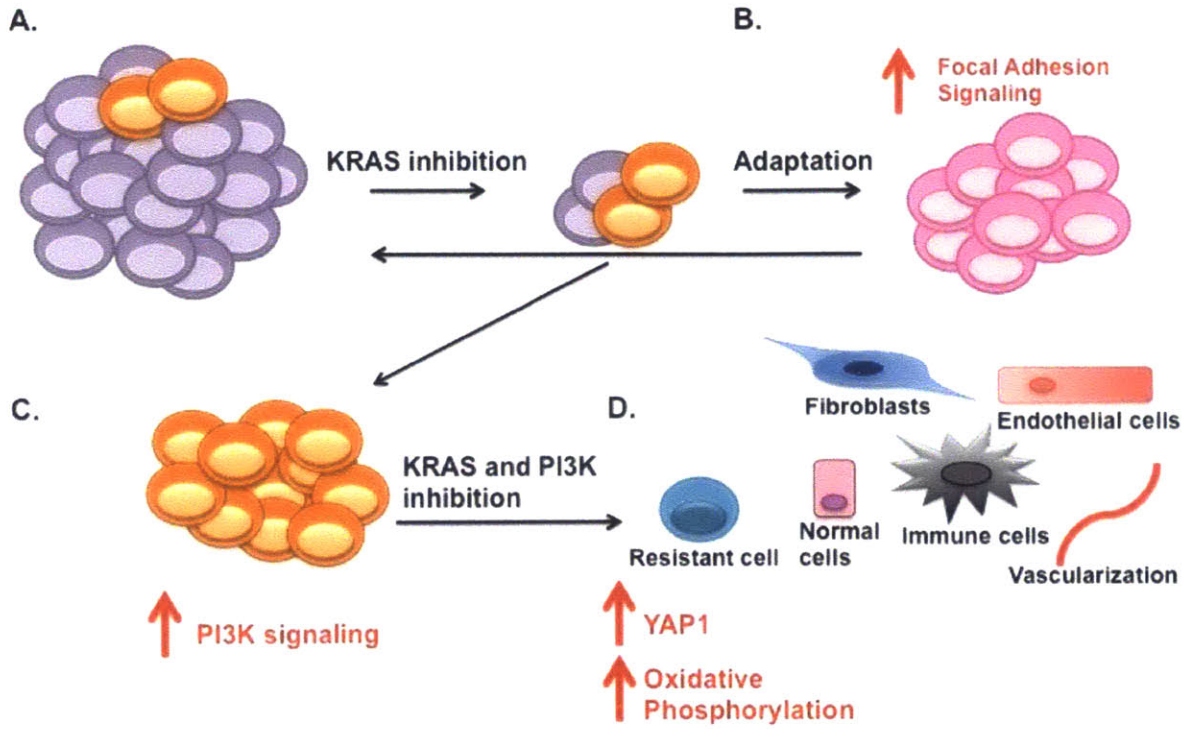

Figure 2. Therapeutic implications of our findings.

A. In Chapters 2 and 3, we have demonstrated that a subset of human and murine PDAC cells can survive KRAS inhibition. Orange: cancer cells that can survive KRAS inhibition. Purple: cancer cells that cannot survive KRAS inhibition.

B. In our inducible RNAi-mediated knockdown studies, we saw that a large number of PDAC cells can tolerate sustained and partial KRAS inhibition via an adaptive response. This suggests that in a bulk tumor, some cells are sensitive to inhibition while others can persist through an adaptive process. One possible mechanism for adaptation is to upregulate alternative pro-survival pathways such as focal adhesion signaling (Chapter 2). As the withdrawal of KRAS inhibition fully reverted the Kras-inhibited phenotypes, we hypothesize that withdrawal of drug treatment can re-create a tumor that may be re-sensitized to KRAS inhibition, indicating that intermittent dosing of a KRAS inhibitor may be useful. Pink: cancer cells that have adapted to a reversible Kras-inhibited state.

C. In our KRAS ablation study (Chapter 3) that mimics the effects of the very best of KRAS inhibitors, we saw that canonical and non-canonical PI3K activation is a possible resistance mechanism, suggesting that combined inhibition of KRAS and PI3K could be a viable therapeutic strategy to overcome resistance in some contexts.

D. Alternative mechanisms of acquired resistance can be possible. Data from other groups suggested that YAP1 overexpression or induced dependence on oxidative phosphorylation could lead to resistance. Importantly, interaction between tumor cells and the tumor microenvironment could potentially alter response to KRAS inhibitors to lead to unexpected resistance mechanisms. Since PI3K inhibitors are already being evaluated in clinical trials for cancer treatment, we have uncovered a more rapidly translatable resistance mechanism. Further work is required to identify the biomarkers that will allow us to classify tumors and predict therapeutic response and possible resistance.

4.3 Emerging roles of oncogenic KRAS in PDAC progression and maintenance offer therapeutic opportunities

The hallmarks of cancer comprise eight major biological capabilities that are acquired, largely due to genomic instability, during the multistep development of human tumors: sustaining proliferative signaling, evading growth suppressors, resisting cell death, enabling replicative immortality, inducing angiogenesis, activating invasion and metastasis, reprogramming of energy metabolism, and evading immune destruction[42]. Importantly, oncogenic RAS is known to contribute to multiple hallmark capabilities by altering the signaling of effector cascades, including proliferative signaling, survival, angiogenesis, invasion, and energy metabolism[42,43]. Our analyses of KRAS knockdown and ablation have led to the identification of signaling pathways that compensate for the loss of KRAS, as well as transcriptional programs and cell functions that may be regulated by KRAS in PDAC. These results contribute to the emerging understanding of possible roles of oncogenic KRAS in cancer progression and maintenance.

KRAS maintains a balance between proliferative and invasive properties in PDAC cells

In addition to elucidating mechanisms of resistance to KRAS inhibition, our analysis of KRAS ablation in human and murine PDAC cells uncovered key biological processes regulated by KRAS by comparing the gene expression profiles of isogenic *KRAS* intact and knockout cells (Chapter 3). While the Kras knockout signature of murine Kras knockout cells showed statistically significant enrichment of a limited number of curated gene sets in pathways previously associated with KRAS, including EMT, integrin, and RTK signaling, human KRAS knockout cells exhibited alterations in a large number of biological processes. Interestingly, human PDAC KRAS knockout cells showed decreased expression of genes related to cell cycle

progression, nucleotide metabolism, and protein translation. The increased invasive properties are consistent with increased expression of genes associated with integrin signaling and possibly related to enhanced focal adhesion signaling in murine Kras knockdown cells (Chapter 2). Moreover, decreased expression of ribosome-related genes is also observed in murine Kras knockdown cells, which will be discussed in detail in the following section.

Taken together, we observed an inverse relationship between the expression of genes associated with proliferation and those associated with metastatic properties, which may be regulated by KRAS. A similar inverse relationship between proliferative and metastatic properties has been reported in a recent study using a $Kras^{G12D/+};p53^{R172H/+}$ PDAC mouse model[44]. These interesting results suggest that increased proliferative ability does not necessarily facilitate the metastatic process. In contrary, decreased proliferation may allow cancer cells to better migrate, invade, and secrete proteins that favor distant colonization. KRAS possibly maintains an intricate balance between proliferative and invasive potentials of PDAC cells, and mediate their appropriate up- and down-regulation at different stages of cancer progression.

KRAS regulates ribosome biogenesis and translation in PDAC cells

As described above, both murine Kras knockdown and human KRAS knockout cells exhibit a decrease in the expression of genes associated with translation and ribosome biogenesis (Chapters 2 and 3). Additionally, our unbiased proteomic analysis indicated a similar decrease in the abundance of translation-associated proteins in murine Kras knockdown cells (data not shown). Regulation of these genes by KRAS has not been described before. It is possible that regulation of these genes are mediated by the convergence of PI3K and MAPK signaling on 4E-BP1, which is a cap-dependent translation repressor and has been implicated in integrating AKT and ERK signaling in human cancer cell lines to promote translation and survival[45].

Dephosphorylation of 4E-BP1 allows it to bind to the eIF4E-mRNA cap complex and prevents cap-dependent translation[46].

In the context of KRAS inhibition, decreased signaling input from ERK (as we observe an upregulation of the PI3K/AKT signaling axis in response to KRAS inhibition) may result in overall decrease of 4E-BP1 phosphorylation, which in turn leads to dampened translation in PDAC cells. Decreased translation and ribosome biogenesis may not have adverse effects on PDAC cell survival, as AKT activation maintains basal levels of translation and at the same time proliferative rates are reduced. However, this may provide a therapeutic opportunity, as further inhibition on translation may push KRAS-inhibited cells beyond a basal translation threshold and impair cell survival.

An emerging role of oncogenic KRAS in metabolic reprogramming and maintaining redox balance

In order to meet the increased biosynthetic demands of a growing tumor, cancer cells frequently alter their metabolism[47]. Recently, several studies have implicated oncogenic KRAS in driving metabolic reprogramming in tumors to promote cancer progression. Importantly, many of the metabolic changes are critical for tumor maintenance but less crucial for normal cells, which makes targeting these metabolic alterations a favorable therapeutic strategy. It has been demonstrated that oncogenic *KRAS*-expressing human PDAC cells use macropinocytosis to take up extracellular albumin, which is then degraded into amino acids and used to fuel the tricarboxylic acid (TCA) cycle[48]. Importantly, macropinocytosis and autophagy, another process that has been suggested to be required for *KRAS*-mutant cancer maintenance[49], both depend on lysosomal acidification, which can be inhibited by chloroquine and its derivative hydroxychloroquine[50]. It is thought that treatment with hydroxychloroquine may have anti-

tumor effects in oncogenic *KRAS*-driven cancers, although this is still a subject of debate[51]. Furthermore, a PDAC mouse model showed that oncogenic Kras controls glucose metabolism by promoting a transcriptional program that leads to alterations of key rate-limiting enzymes of anabolic glucose metabolism[10]. This leads to an increased flux of glycolytic intermediates through the hexosamine biosynthesis pathway (HBP) and the non-oxidative arm of the pentose phosphate pathway (PPP), which then results in increased production of precursors used for glycosylation and ribose used for nucleic acid biosynthesis. Importantly, shRNA-mediated inhibition of either of these pathways also inhibits PDAC cell proliferation and tumor xenograft growth. Interestingly, a recent study using $Kras^{G12D}$-transformed mouse embryonic fibroblasts (MEFs) and lung cancer cells suggested that oncogenic Kras is responsible for channeling glucose-derived metabolites into the TCA cycle and glutathione biosynthesis, which results in glutathione-mediated detoxification[52]. This study further links this metabolic reprogramming to the frequently observed mutant *KRAS* amplification in human and mouse NSCLC tumors.

Another related and emerging role of oncogenic KRAS in PDAC maintenance is its ability to maintain a redox balance. This may be through a shift in glutamine metabolism that leads to increased NADPH production, which maintains the reduced glutathione pools for redox balance[53]. Alternatively, it can occur through the upregulation of NRF2, a master regulator of cellular defense against reactive oxygen species (ROS). It was shown that endogenous levels of oncogenic $Kras^{G12D}$ leads to decreased ROS levels through the induction of the NRF2 antioxidant program[54]. Accordingly, analysis of cells that survive removal of oncogenic *Kras* expression in PDAC has demonstrated that these cells exhibit an increased dependency on oxidative phosphorylation[15]. Together, these studies imply that oncogenic KRAS may help maintain a controlled level of ROS that is beneficial for tumor growth, and disruption in this

balance can impair cancer cell survival. Consistent with a role of KRAS in metabolic rewiring and redox control, we observed an increased expression of genes associated with redox metabolism in mouse Kras knockout cells, but a decreased expression of genes associated with oxidative phosphorylation, glucose metabolism and PPP pathway in human KRAS knockout cells (Chapter 3). It is difficult to decipher the optimal state of metabolic reprograming and redox balance that is required for maintaining survival of cells in response to KRAS ablation, but our results add to the growing body of evidence that implicate oncogenic KRAS as a regulator of these processes in cancer. Importantly, targeting the metabolic and redox alterations associated with oncogenic KRAS may be useful in selectively killing *KRAS*-mutant cancer cells.

REFERENCES

1. Bardeesy, N. & DePinho, R.A. Pancreatic cancer biology and genetics. *Nat Rev Cancer* **2**, 897-909 (2002).
2. Ryan, D.P., Hong, T.S. & Bardeesy, N. Pancreatic adenocarcinoma. *N Engl J Med* **371**, 2140-2141 (2014).
3. Collins, M.A., *et al.* Oncogenic Kras is required for both the initiation and maintenance of pancreatic cancer in mice. *J Clin Invest* **122**, 639-653 (2012).
4. Haigis, K.M., *et al.* Differential effects of oncogenic K-Ras and N-Ras on proliferation, differentiation and tumor progression in the colon. *Nature Genetics* **40**, 600-608 (2008).
5. Hingorani, S.R., *et al.* Preinvasive and invasive ductal pancreatic cancer and its early detection in the mouse. *Cancer Cell* **4**, 437-450 (2003).
6. Hingorani, S.R., *et al.* Trp53R172H and KrasG12D cooperate to promote chromosomal instability and widely metastatic pancreatic ductal adenocarcinoma in mice. *Cancer Cell* **7**, 469-483 (2005).
7. Jackson, E.L., *et al.* Analysis of lung tumor initiation and progression using conditional expression of oncogenic K-ras. *Genes & Development* **15**, 3243-3248 (2001).
8. Johnson, L., *et al.* Somatic activation of the K-ras oncogene causes early onset lung cancer in mice. *Nature* **410**, 1111-1116 (2001).
9. Tuveson, D.A., *et al.* Endogenous oncogenic K-ras(G12D) stimulates proliferation and widespread neoplastic and developmental defects. *Cancer Cell* **5**, 375-387 (2004).
10. Ying, H., *et al.* Oncogenic Kras maintains pancreatic tumors through regulation of anabolic glucose metabolism. *Cell* **149**, 656-670 (2012).
11. Collisson, E.A., *et al.* Subtypes of pancreatic ductal adenocarcinoma and their differing responses to therapy. *Nature Medicine* **17**, 500-503 (2011).
12. Singh, A., *et al.* A gene expression signature associated with "K-Ras addiction" reveals regulators of EMT and tumor cell survival. *Cancer Cell* **15**, 489-500 (2009).
13. Kapoor, A., *et al.* Yap1 activation enables bypass of oncogenic Kras addiction in pancreatic cancer. *Cell* **158**, 185-197 (2014).
14. Shao, D.D., *et al.* KRAS and YAP1 converge to regulate EMT and tumor survival. *Cell* **158**, 171-184 (2014).
15. Viale, A., *et al.* Oncogene ablation-resistant pancreatic cancer cells depend on mitochondrial function. *Nature* **514**, 628-632 (2014).
16. Premsrirut, P.K., *et al.* A rapid and scalable system for studying gene function in mice using conditional RNA interference. *Cell* **145**, 145-158 (2011).
17. Ran, F.A., *et al.* Genome engineering using the CRISPR-Cas9 system. *Nature Protocols* **8**, 2281-2308 (2013).
18. Zhang, Z., *et al.* Wildtype Kras2 can inhibit lung carcinogenesis in mice. *Nature Genetics* **29**, 25-33 (2001).
19. Lito, P., Solomon, M., Li, L.S., Hansen, R. & Rosen, N. Allele-specific inhibitors inactivate mutant KRAS G12C by a trapping mechanism. *Science* **351**, 604-608 (2016).
20. Ostrem, J.M., Peters, U., Sos, M.L., Wells, J.A. & Shokat, K.M. K-Ras(G12C) inhibitors allosterically control GTP affinity and effector interactions. *Nature* **503**, 548-551 (2013).
21. Shi, J., *et al.* Discovery of cancer drug targets by CRISPR-Cas9 screening of protein domains. *Nature Biotechnology* **33**, 661-667 (2015).

22. Aubrey, B.J., *et al.* An inducible lentiviral guide RNA platform enables the identification of tumor-essential genes and tumor-promoting mutations in vivo. *Cell Rep* **10**, 1422-1432 (2015).
23. Weinstein, I.B. Cancer. Addiction to oncogenes--the Achilles heal of cancer. *Science* **297**, 63-64 (2002).
24. Berns, K. & Bernards, R. Understanding resistance to targeted cancer drugs through loss of function genetic screens. *Drug Resist Updat* **15**, 268-275 (2012).
25. Groenendijk, F.H. & Bernards, R. Drug resistance to targeted therapies: deja vu all over again. *Molecular Oncology* **8**, 1067-1083 (2014).
26. Maemondo, M., *et al.* Gefitinib or chemotherapy for non-small-cell lung cancer with mutated EGFR. *N Engl J Med* **362**, 2380-2388 (2010).
27. Shaw, A.T., *et al.* Crizotinib versus chemotherapy in advanced ALK-positive lung cancer. *N Engl J Med* **368**, 2385-2394 (2013).
28. Oxnard, G.R. The cellular origins of drug resistance in cancer. *Nature Medicine* **22**, 232-234 (2016).
29. Hata, A.N., *et al.* Tumor cells can follow distinct evolutionary paths to become resistant to epidermal growth factor receptor inhibition. *Nature Medicine* **22**, 262-269 (2016).
30. Ramirez, M., *et al.* Diverse drug-resistance mechanisms can emerge from drug-tolerant cancer persister cells. *Nat Commun* **7**, 10690 (2016).
31. Pao, W., *et al.* Acquired resistance of lung adenocarcinomas to gefitinib or erlotinib is associated with a second mutation in the EGFR kinase domain. *PLoS Med* **2**, e73 (2005).
32. Yun, C.H., *et al.* The T790M mutation in EGFR kinase causes drug resistance by increasing the affinity for ATP. *Proc Natl Acad Sci U S A* **105**, 2070-2075 (2008).
33. Godin-Heymann, N., *et al.* The T790M "gatekeeper" mutation in EGFR mediates resistance to low concentrations of an irreversible EGFR inhibitor. *Mol Cancer Ther* **7**, 874-879 (2008).
34. Sequist, L.V., *et al.* Genotypic and histological evolution of lung cancers acquiring resistance to EGFR inhibitors. *Sci Transl Med* **3**, 75ra26 (2011).
35. Doebele, R.C., *et al.* Mechanisms of resistance to crizotinib in patients with ALK gene rearranged non-small cell lung cancer. *Clin Cancer Res* **18**, 1472-1482 (2012).
36. Katayama, R., *et al.* Mechanisms of acquired crizotinib resistance in ALK-rearranged lung Cancers. *Sci Transl Med* **4**, 120ra117 (2012).
37. Poulikakos, P.I., *et al.* RAF inhibitor resistance is mediated by dimerization of aberrantly spliced BRAF(V600E). *Nature* **480**, 387-390 (2011).
38. Nazarian, R., *et al.* Melanomas acquire resistance to B-RAF(V600E) inhibition by RTK or N-RAS upregulation. *Nature* **468**, 973-977 (2010).
39. Sun, C., *et al.* Reversible and adaptive resistance to BRAF(V600E) inhibition in melanoma. *Nature* **508**, 118-122 (2014).
40. Sharma, S.V., *et al.* A chromatin-mediated reversible drug-tolerant state in cancer cell subpopulations. *Cell* **141**, 69-80 (2010).
41. Alizadeh, A.A., *et al.* Toward understanding and exploiting tumor heterogeneity. *Nature Medicine* **21**, 846-853 (2015).
42. Hanahan, D. & Weinberg, R.A. Hallmarks of cancer: the next generation. *Cell* **144**, 646-674 (2011).
43. Pylayeva-Gupta, Y., Grabocka, E. & Bar-Sagi, D. RAS oncogenes: weaving a tumorigenic web. *Nat Rev Cancer* **11**, 761-774 (2011).

44. Whittle, M.C., *et al.* RUNX3 Controls a Metastatic Switch in Pancreatic Ductal Adenocarcinoma. *Cell* **161**, 1345-1360 (2015).
45. She, Q.B., *et al.* 4E-BP1 is a key effector of the oncogenic activation of the AKT and ERK signaling pathways that integrates their function in tumors. *Cancer Cell* **18**, 39-51 (2010).
46. Richter, J.D. & Sonenberg, N. Regulation of cap-dependent translation by eIF4E inhibitory proteins. *Nature* **433**, 477-480 (2005).
47. Cox, A.D., Fesik, S.W., Kimmelman, A.C., Luo, J. & Der, C.J. Drugging the undruggable RAS: Mission possible? *Nat Rev Drug Discov* **13**, 828-851 (2014).
48. Commisso, C., *et al.* Macropinocytosis of protein is an amino acid supply route in Ras-transformed cells. *Nature* **497**, 633-637 (2013).
49. Guo, J.Y., *et al.* Activated Ras requires autophagy to maintain oxidative metabolism and tumorigenesis. *Genes & Development* **25**, 460-470 (2011).
50. Mancias, J.D. & Kimmelman, A.C. Targeting autophagy addiction in cancer. *Oncotarget* **2**, 1302-1306 (2011).
51. Eng, C.H., *et al.* Macroautophagy is dispensable for growth of KRAS mutant tumors and chloroquine efficacy. *Proc Natl Acad Sci U S A* **113**, 182-187 (2016).
52. Kerr, E.M., Gaude, E., Turrell, F.K., Frezza, C. & Martins, C.P. Mutant Kras copy number defines metabolic reprogramming and therapeutic susceptibilities. *Nature* **531**, 110-113 (2016).
53. Son, J., *et al.* Glutamine supports pancreatic cancer growth through a KRAS-regulated metabolic pathway. *Nature* **496**, 101-105 (2013).
54. DeNicola, G.M., *et al.* Oncogene-induced Nrf2 transcription promotes ROS detoxification and tumorigenesis. *Nature* **475**, 106-109 (2011).

APPENDIX 1

Investigating the synthetic lethal interaction between *Stk33* and oncogenic *Kras*

Pan-Yu Chen[1, 2], Kim Mercer[1], Amy Li[1, 2, 3], Tuomas Tammela[1], Arjun Bhutkar[1], Mandar Deepak Muzumdar[1, 3, 4*], and Tyler Jacks[1, 2, 5*]

Author Affiliations:
[1] David H. Koch Institute for Integrative Cancer Research, Massachusetts Institute of Technology, 500 Main Street, Cambridge, MA 02139, USA
[2] Department of Biology, Massachusetts Institute of Technology, 77 Massachusetts Avenue, Cambridge, MA 02139, USA
[3] Harvard Medical School, 25 Shattuck Street, Boston, MA 02115, USA
[4] Dana-Farber Cancer Institute, 450 Brookline Avenue, Boston, MA 02115, USA
[5] Howard Hughes Medical Institute, Massachusetts Institute of Technology, Cambridge, MA 02139, USA

P-Y.C., M.D.M. and T.J. designed the study; P-Y.C. and K.M. performed all of the molecular biology, *in vitro*, and *in vivo* experiments in the laboratory of T.J.; A.L. and T.T. provided technical assistance with critical *in vivo* experiments; A.B. conducted bioinformatics analyses on the MiSeq data.

ABSTRACT

Activating mutations of *KRAS* are highly prevalent in human cancers, especially in cancers of the pancreas, lung, and colon. The critical role of oncogenic KRAS in tumor initiation has been demonstrated in numerous mouse models, and there is an emerging understanding of the requirement of oncogenic KRAS for tumor maintenance. Although KRAS remains an extremely appealing therapeutic target in human cancers, various properties of KRAS contribute to the challenges associated with its direct pharmacological inhibition. Therefore, there is a strong interest in uncovering alternative therapeutic targets in *KRAS*-mutant cancers. The serine/threonine kinase STK33 has been identified to be a putative synthetic lethal target in *KRAS*-mutant cancers. However, genetic and pharmacological inhibitions of STK33 in various contexts had exhibited inconsistent results. Given that the utility of STK33 inhibition in *KRAS*-mutant cancers remains a controversy, we interrogated the requirement of Stk33 expression in $Kras^{G12D}$-driven *in vitro* and *in vivo* cancer models. Due to technical limitations, we are unable to definitively conclude whether *Stk33* exhibits synthetic lethal interactions with $Kras^{G12D}$. However, based on our preliminary results, it appeared that at least the kinase activity of Stk33 is dispensable in an autochthonous mouse model of $Kras^{G12D}$-drven pancreatic cancer. Furthermore, the requirement of Stk33 may be context-dependent.

INTRODUCTION

KRAS is the most frequently mutated proto-oncogene in human solid tumors, making it an extremely attractive therapeutic target for cancer. However, efforts to develop pharmacological inhibitors that directly target KRAS have been largely unsuccessful to date. Since the direct inhibition of KRAS is challenging and simultaneous inhibition of multiple KRAS effectors may have a narrow therapeutic window, an alternative and more favorable therapeutic approach to increase selectivity and reduce toxicity is to inhibit synthetic lethal interactions with oncogenic *KRAS*. Targeting genes whose loss of function is lethal only in the presence of mutant *KRAS* will specifically eliminate *KRAS*-mutant cancer cells and spare *KRAS* wild-type normal cells. Additionally, the protein products of genes synthetically lethal to *KRAS* mutations may be more amenable to pharmacological attack and present excellent targets for anti-cancer therapy[1].

Taking advantage of *KRAS* oncogene addiction, several studies have applied RNAi-based screens in human cancer cell lines to identify genes that exhibit synthetic lethal interactions with mutant *KRAS*. Employing a variety of siRNA and shRNA libraries, a wide range of candidate genes have been identified[2]. These candidate genes encode proteins that are involved in diverse cellular processes, including cell cycle and mitosis, senescence, apoptosis, and the regulation of transcriptional programs[3-8]. Identification of these candidates suggests that even though oncogenic *KRAS* plays a critical role in promoting cancer cell proliferation, survival, and genomic instability, additional cellular pathways are involved in supporting the survival of *KRAS*-mutant cancer cells.

From a therapeutic standpoint, the main goal of uncovering synthetic lethal interactions with oncogenic *KRAS* is to identify drug targets that are likely to be therapeutically tractable, as

opposed to the undruggable oncogenic KRAS itself. Inhibiting components of the cell cycle machinery can lead to considerable toxicity in normal tissues, whereas transcription factors are equally difficult to directly target. In 2009, results from three shRNA-based *KRAS* synthetic lethal screens performed in human cancer cell lines elicited great enthusiasm for drug development, because candidate protein kinases, including serine/threonine kinase 33 (STK33), were reported[3,7,9]. It was found that human cancer cells dependent on mutant *KRAS* expression were also dependent on *STK33*, irrespective of the tissue of origin. Furthermore, this study reported that STK33 promotes cancer cell viability in a kinase activity-dependent manner by suppressing mitochondrial apoptosis mediated through S6K1-induced inactivation of pro-apoptotic BAD selectively in mutant *KRAS*-dependent cells. Unfortunately, subsequent studies found that neither genetic nor pharmacological inhibition of STK33 selectively inhibited the growth of *KRAS*-mutant cancer cells[10-12]. Further complication arose when it was demonstrated that STK33 kinase activity is not required for *KRAS*-dependent cancer cell viability[12]. Whether *STK33* is actually a synthetic lethal target of oncogenic *KRAS* remains controversial[13,14].

Other than being a putative synthetic lethal target of oncogenic *KRAS*, little is known about the function of STK33 in cells. Human *STK33* was discovered in 2001 because it resides in human chromosomal region 11p15, which is known to be associated with predispositions to develop various cancers[15]. Mouse *Stk33* is located on chromosome 7, and exhibits a high sequence homology with human *STK33* (84% nucleotide and 85% amino acid identities in the coding region)[15]. Phylogenetic analysis suggested that STK33, a 57.8kDa protein, belongs to the calcium/calmodulin-dependent protein kinase (CAMK) group, although it lacks the calcium/calmodulin-binding domain[15]. Both human and mouse STK33 contain a serine/threonine kinase active site and an ATP-binding domain, indicating that they have kinase

activities[15]. Gene expression analysis of human and mouse *STK33* demonstrated that it is non-ubiquitously expressed and displays only low levels of expression in most tissues[16]. The only tissue that shows high *STK33* expression is the testis, particularly in the spermatogenic epithelium[16]. cDNA dot-blot hybridization showed that human *STK33* is also expressed in the fetal lung and heart, pituitary gland, kidney, pancreas, trachea, and thyroid gland[16]. Additionally, *Stk33* is expressed in mouse embryos. It is speculated that STK33 may have a role in spermatogenesis and organ ontogenesis, although its precise functions are not elucidated[16].

In order to understand the therapeutic value of *STK33* inhibition in oncogenic *KRAS*-driven cancers, we investigated whether *Stk33* exhibits synthetic lethality with oncogenic *Kras*. Utilizing various $Kras^{G12D}$-driven pancreatic and lung adenocarcinoma *in vitro* and *in vivo* models, we interrogated the requirement of *Stk33* expression for $Kras^{G12D}$ -mediated *in vitro* transforming and *in vivo* tumorigenic abilities. While our conclusions are limited by technical complications, our preliminary observations indicate that the kinase activity of Stk33 is dispensable for $Kras^{G12D}$-driven pancreatic cancer. Moreover, the requirement for Stk33 may be context-dependent.

RESULTS

Preliminary characterization of an $Stk33^{flox}$ allele

In order to determine whether *Stk33* exhibits synthetic lethal interactions with oncogenic *Kras*, we sought to perform an *in vivo* genetic experiment to analyze the requirement of *Stk33* expression for $Kras^{G12D}$-driven tumorigenesis. An $Stk33^{flox}$ allele ($Stk33^{fl}$) has been designed and made by Ronald DePinho's group. As it has been suggested that the kinase activity of Stk33 underlies its requirement for the survival of *Kras*-mutant cancer cells[9], the LoxP sites were

designed to flank exon 7 of *Stk33* in the *Stk33^{fl}* allele because exon 7 contains the kinase domain (**Fig. 1A**). Cre recombinase-mediated recombination of LoxP sites is supposed to result in a premature STOP codon, and consequently the complete loss of Stk33 protein expression (**Fig. 1A**). There has been no published characterization of this *Stk33^{fl}* allele, so we first tested the efficiency of recombination by crossing this allele into a *deleter-Cre (CMV-Cre)* mouse strain (JAX mouse strain 006054). Since the mouse testis displays the highest mRNA expression of *Stk33* (**Supplementary Fig. 1A**) and allows reliable detection of Stk33 protein levels by immunohistochemistry (IHC) (**Supplementary Fig. 1B**), we confirmed loss of Stk33 proteins upon recombination in the testis of *CMV-Cre; Stk33$^{fl/fl}$* and *CMV-Cre; Stk33$^{fl/+}$* mice (**Fig. 1B**).

After confirming the utility of the *Stk33^{fl}* allele in leading to loss of Stk33 proteins in the mouse testis, we set out to investigate the effect of Stk33 loss in *Kras^{G12D}*-driven cancer mouse models. We employed an autochthonous pancreatic ductal adenocarcinoma (PDAC) mouse model (*Pdx1-Cre; Kras$^{LSL\text{-}G12D/+}$; p53$^{fl/fl}$; Rosa26$^{TdTomato/\,TdTomato}$*, or *Pdx1-Cre;KPT*)[17,18], in which *Pdx1*-driven expression of *Cre* in the mouse pancreas leads to activation of *Kras^{G12D}* and biallelic inactivation of *p53*, leading to the development of PDAC. In addition, Cre-mediated recombination leads to the expression of the red fluorescent *Tomato* reporter. If Stk33 were required for *Kras^{G12D}*-driven tumorigenesis, then we would expect the *Pdx1-Cre;KPT* mice harboring *Stk33^{fl}* alleles to show prolonged survival compared to *Stk33* wild-type mice. We first confirmed the recombination of *Stk33^{fl}* allele upon *Cre* expression in the pancreas (**Fig. 1C**) and ensured that *Stk33* expression is dispensable for normal pancreatic development by demonstrating Tomato fluorescence in all compartments of the pancreas of *Pdx1-Cre; Stk33$^{f/fll}$;T/T* mice (**Fig. 1D**). Importantly, incomplete recombination of *Stk33^{fl}* was observed due to mosaic expression of *Pdx1* in the pancreas[19]. We found that the survival of *Pdx1-Cre;KPT*

mice was unaffected by Stk33 status (**Fig. 1G**). Moreover, *Kras*-mutant mouse embryonic fibroblasts (MEFS) displayed the same partially transformed morphology[20] *in vitro* regardless of Stk33 status. MEFs derived from $Kras^{LSL\text{-}G12D/+}$; $Stk33^{fl/+}$ and $Kras^{LSL\text{-}G12D/+}$; $Stk33^{fl/fl}$ mice were administered with AdCMVCre, an adenoviral vector driving the expression of Cre recombinase from the Cytomegalovirus promotor, or AdCMVEmpty, which contains the CMV promoter but lacks any protein expression as a control. Recombination of *Kras* and *Stk33* was confirmed (**Fig. 1E**), but the absence of STK33 did not prevent the transformed Kras mutant morphology (**Fig. 1F**). Collectively, these preliminary observations appeared to suggest that the *in vitro* transforming ability and *in vivo* tumorigenicity of $Kras^{G12D}$ are not dependent on *Stk33* expression, indicative of a lack of synthetic lethal interaction between *Stk33* and oncogenic *Kras*.

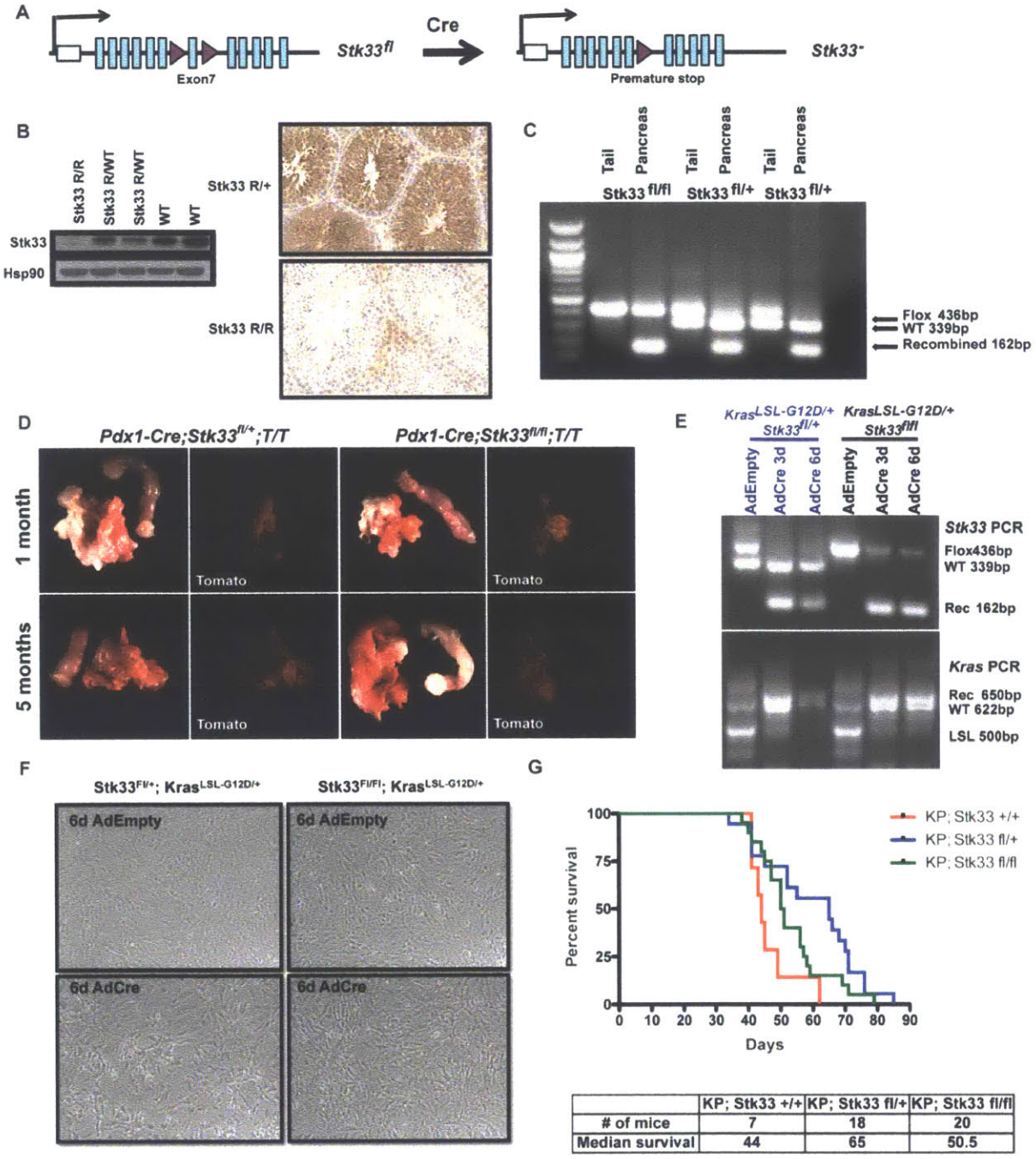

	KP; Stk33 +/+	KP; Stk33 fl/+	KP; Stk33 fl/fl
# of mice	7	18	20
Median survival	44	65	50.5

Figure 1. Basic characterizations of the *Stk33-flox (Stk33^{fl})* allele.

A. The LoxP sites of the *Stk33^{fl}* allele flank exon 7 of *Stk33*. Exon 7 contains the kinase domain. Cre-mediated recombination results in a premature stop codon and leads to loss of Stk33 protein expression.

B. Western blot shows Stk33 protein deletion in the testis of *CMV-Cre (deleter Cre); STK33$^{fl/fl}$* mice. Immunohistochemical analysis similarly shows loss of Stk33 expression in *CMV-Cre; Stk33$^{R/R}$* testis. WT or +: wild-type, R: recombined allele.

C. DNA analysis shows that recombination of *Stk33* occurs in the pancreas of *Pdx1-Cre; Stk33-flox* mice. Recombination is incomplete due to mosaic expression of *Pdx1* in the pancreas. Tail DNA samples are included as controls. Rec: recombined, WT: wild-type, LSL: lox-stop-lox cassette.
D. Expression of Stk33 in the pancreas is not required, as *Pdx1-Cre;Stk33$^{fl/fl}$;T/T (Rosa26-TdTomato)* and *Pdx1-Cre;Stk33$^{fl/+}$;T/T* mice showed normal pancreatic development. Shown are pancreas and duodenum (as control). Pancreas exhibits *Tomato* expression upon recombination of *Stk33*.
E. Confirmation of recombination of *Stk33* and *Kras* induced by AdCre (or control AdEmpty) infections in mouse embryonic fibroblasts (MEFs).
F. AdCre-mediated recombination of *Stk33^{fl}* does not impair the ability of *Kras^{G12D}* expression to partially transform MEFs (recombination confirmed as shown in E) based on morphology.
G. Stk33 status does not affect the survival of *Pdx1-Cre; Kras$^{LSL\text{-}G12D/+}$; p53$^{fl/fl}$* mice.

Alternatively spliced transcripts of *Stk33* are made upon Cre-mediated *Stk33^{fl}* recombination

Since *Stk33* is only expressed at low levels in many tissues (**Supplementary Fig. 1A**), one limitation with our analysis was that we could not reliably detect Stk33 protein or mRNA (data not shown) in the *Stk33* wild-type pancreas. Therefore, it was not possible to confirm the loss of Stk33 proteins in *Stk33$^{fl/fl}$* animals after recombination by IHC or western blot analyses. However, even in the lung, where *Stk33* mRNA levels are relatively high and Stk33 protein detection is possible (**Supplementary Fig. 1A**), IHC showed ambiguous Stk33 protein status in *CMV-Cre; Stk33$^{R/R}$* (R denotes recombined *Stk33$^{fl/fl}$*) animals (**Supplementary Fig. 1C**). We observed high levels of Stk33 background staining in the bronchial epithelium of the *Stk33$^{R/R}$* lung, and unlike in the testis (**Supplementary Fig. 1B**), the levels of Stk33 protein expression were not significantly different between *Stk33* wild-type animals and *Stk33$^{R/R}$* animals. These observations suggested the possibility that recombination of the *Stk33^{fl}* allele might not have led to actual Stk33 protein loss in tissues other than the testis.

Communications with Claudia Scholl, who has been characterizing the *Stk33^{fl}* allele in a *KP* lung adenocarcinoma mouse model, led us to investigate the possibility of an alternative splicing event that skips exons 7 and 8 of *Stk33* to generate an in-frame *Stk33* transcript upon recombination of *Stk33^{fl}* in the pancreas. If this were true, then recombination did not result in loss of Stk33 proteins, but rather the expression of a kinase-dead form of Stk33. We utilized primers that flank different exons of *Stk33* cDNA to amplify various *Stk33* open reading frames (ORFs), and found that exons 7 and 8 skipping occurred in all tissues examined except for the testis (**Fig. 2A**). While we were unable to detect cDNA of normal pancreas that was harvested from a *CMV-Cre; Stk33$^{R/R}$* mouse, we observed exons 7 and 8 skipping in multiple PDAC

tumors harvested from a *Pdx1-Cre; KPT; Stk33*$^{fl/fl}$ mouse (**Fig. 2B**). These surprising findings suggested that the *Stk33*^{fl} allele we characterized is not ideal for analyzing whether total Stk33 protein loss impairs oncogenic *Kras*-driven tumorigenesis, as recombination of this allele in most tissues lead to the expression of a kinase-dead Stk33. However, it can be a useful allele for analyzing the requirement of Stk33 kinase activity in different tissues. Therefore, the lack of impact on the *in vitro* transforming ability (**Fig. 1E**) and *in vivo* tumorigenicity of Kras^{G12D} (**Fig. 1F**) upon *Stk33*^{fl} recombination demonstrated that the kinase activity of Stk33 is not required for *Kras*^{G12D}-mediated tumorigenesis.

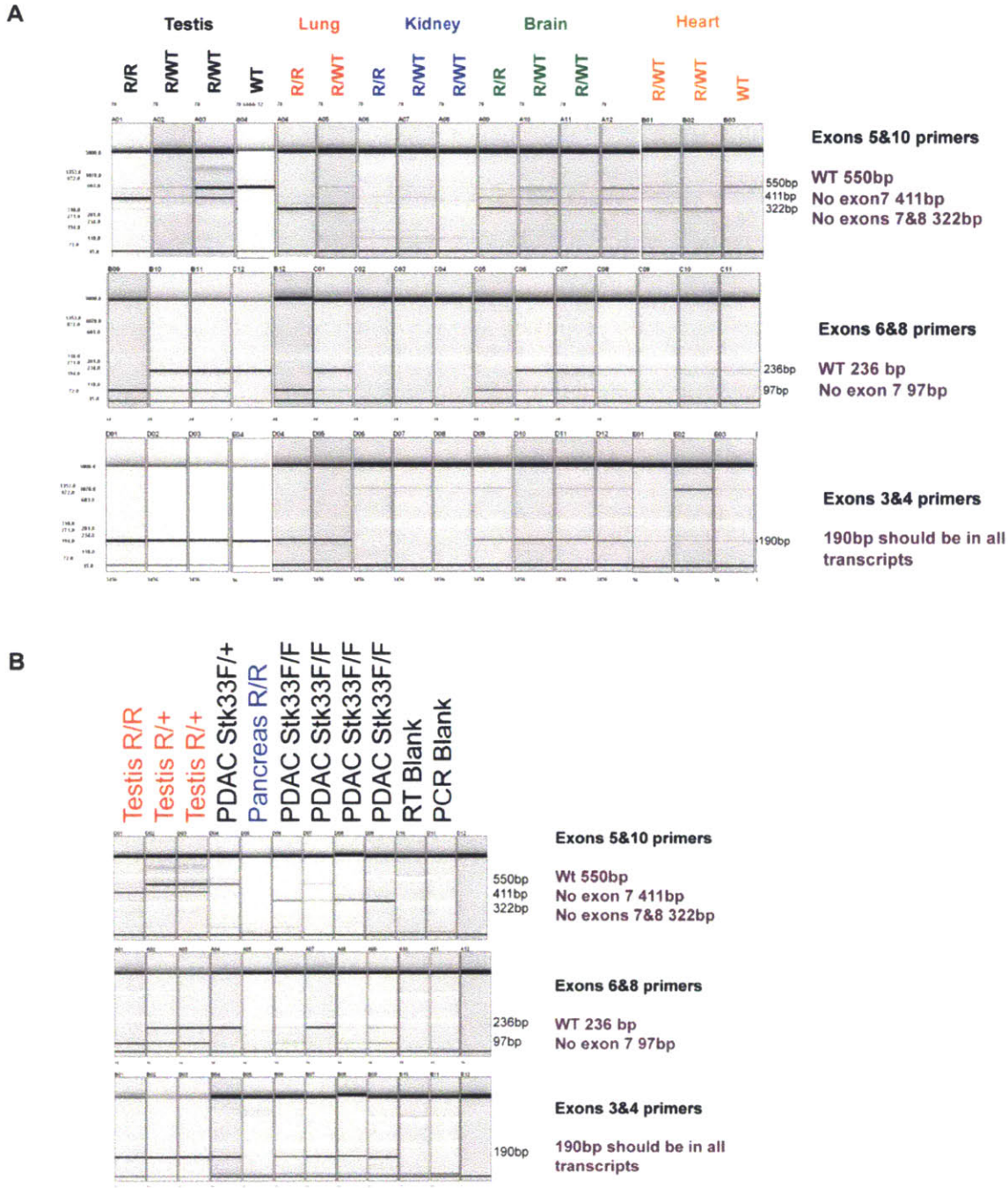

Figure 2. Alternatively spliced transcripts of *Stk33* are made upon recombination of the *Stk33^{flox}* allele.

A. Using primers that amplify different open reading frames (ORFs) of the *Stk33* cDNA, it is evident that exons 7 and 8 are skipped in lung, brain, and heart. The testis is the only tissue in which exon 8 is not skipped. *Stk33* expression in the kidney is undetectable. R: recombined, WT: wild-type.

B. *Stk33* expression is detectable in PDAC. Exons 7 and 8 are skipped in PDAC but not in testis. Both R and F denote recombined *Stk33^{fl}*, while R indicates the tissues are harvested from a *CMV-Cre* mouse and F indicates the tissues are harvested from a *Pdx1-Cre; KPT* mouse. +: wild-type.

CRISPR/Cas9-mediated genome editing of *Stk33* in an autochthonous *Kras^{G12D}*-driven lung cancer mouse model

Limitations of the *Stk33^{fl}* allele as well as the difficulty to reliably detect *Stk33* mRNA and protein in the pancreas led us to employ a different strategy to interrogate synthetic lethal interactions between *Stk33* and oncogenic *Kras*. Since the expression of *Stk33* mRNA and protein in the lung is relatively high (**Supplementary Figs. 1A, 1C, and Fig. 2A**), and our lab has recently developed a pSECC lentiviral vector[21] that allows CRISPR/Cas9-mediated somatic gene editing in a *KP* autochthonous lung cancer mouse model, we tested the requirement of *Stk33* for *Kras^{G12D}*-driven lung tumorigenesis using the pSECC system. We identified two sgRNAs targeting exon 2 of *Stk33* (sgStk33 2-1 and sgStk33 2-2) that most effectively resulted in Cas9-mediated editing of the *Stk33* locus *in vitro* (**Fig. 3A**). The 373T1 cell line we tested these sgRNAs in was derived from a primary *KP* lung tumor that exhibited metastatic ability[22]. This cell line was chosen because it is the only lung cancer cell line we tested in which we could consistently detect *Stk33* mRNA (data not shown), although we were unable to detect Stk33 proteins by western blot (**Figs. 3B, 3C**). Overall, we found that lysates made from primary pancreatic or lung tumors allowed *Stk33* mRNA and protein detection by RT-PCR and western blotting, respectively. However, as cells were passaged in culture, then it became more difficult, if not impossible, to detect *Stk33* mRNA and protein by these assays (data not shown).

Leveraging the pSECC lentiviral system, we intratracheally infected *KP* mice to induce lung tumorigenesis and analyzed lung tumor histology, Stk33 protein expression and *Stk33* mutational status in tumors, and tumor burden of the infected mice. Histology analysis showed minimal tumor grade differences between pSECC-sgStk33 lentivirus infected mice and pSECC-sgTomato lentivirus infected mice. Most tumors were a mixture of grade 2 and 3 (based on

histology) irrespective of treatment group (data not shown). IHC analysis of Stk33 expression in tumors in cross sections of the lung or microdissected lung tumors that were taken upon euthanasia showed strong Stk33 protein expression in tumors of pSECC-sgStk33 lentivirus infected mice (**Supplementary Fig. 2A**). Furthermore, western blot analysis also showed high levels of Stk33 protein expression in microdissected pSECC-sgStk33 lung tumors, and phospho-S6 levels (phosphorylation of both S6 kinase and S6 was suggested to be modulated by Stk33 kinase activity[9]) did not correlate with Stk33 protein levels (**Supplementary Fig. 2B**). Sequencing of the *Stk33* exon 2 regions spanning the sgStk33-targeting sites showed a high allelic fraction of wild-type *Stk33* in the majority of the tumors analyzed (**Supplementary Fig. 2C**), suggesting that at least one wild-type *Stk33* allele was retained in all tumors analyzed. Only one tumor contained a loss-of-function *Stk33* allele (tumor sgStk33 2-1 120A), and another tumor contained an *Stk33* allele with an in-frame mutation (tumor sgStk33 2-2 123D) (**Supplementary Fig. 2C**). Additionally, tumor burden quantitation of the different treatment groups showed that mice infected with different pSECC-based lentiviruses displayed minimal tumor burden differences (**Supplementary Fig. 2D**), possibly due to inefficient induction of loss-of-function mutations in *Stk33*. Together, these results indicated that either the loss of Stk33 function was selected against in lung tumors, or the *in vivo* CRISPR/Cas9-mediated genome editing of *Stk33* was inefficient due to technical limitations. Due to the difficulty to distinguish between these two possibilities, our results were inconclusive in determining whether *Stk33* is a synthetic lethal target of oncogenic *Kras*.

Isolation and characterization of 373T1 *Stk33* knockout single cell clones

Since the induction of loss-of-function mutations in *Stk33* by pSECC-based lentivirus in autochthonous *KP* lung cancer model proved to be challenging, we sought to analyze the effects of *Stk33* ablation on the oncogenic abilities of 373T1 cells by isolating single cell clones of 373T1 that were confirmed to be *Stk33* knockout. We FACS-sorted a population of 373T1 cells harboring Cas9- and sgRNA-expressing lentiviral vectors (**Fig. 3B**) into single cell clones in 96-well tissue culture plates. Overall, approximately 13% of the sorted cells were able to grow out as single cell clones (**Supplementary Fig. 3A**). We identified one sgStk33 2-1 lentivirus transduced clone (clone #4) and one sgStk33 2-2 lentivirus transduced clone (clone #7) that each contained two loss-of-function *Stk33* alleles (**Supplementary Fig. 3B**). Additionally, we isolated sgTomato lentivirus transduced clones of 373T1 as *Stk33* intact controls (**Fig. 3C, Supplementary Figs. 3A, 3B**). However, we were unable to confirm Stk33 protein loss in these clones because baseline Stk33 protein was undetectable by western blot in 373T1 cells, and phospho-S6 levels did not correlate with the predicted Stk33 status so could not serve as a surrogate for Stk33 expression (**Fig. 3C**). Additionally, Stk33 ablation (based on DNA sequencing analysis) did not result in reduced proliferative kinetics (**Fig. 3D**) or diminished ability for anchorage-independent growth in soft agar (**Fig. 3E**). These results suggested that if Stk33 protein expression were completely inhibited as predicted by DNA sequencing analysis in these two 373T1 *Stk33* knockout clones, then Stk33 is not required for the proliferative or oncogenic abilities of *Kras*-mutant cancer cells *in vitro*.

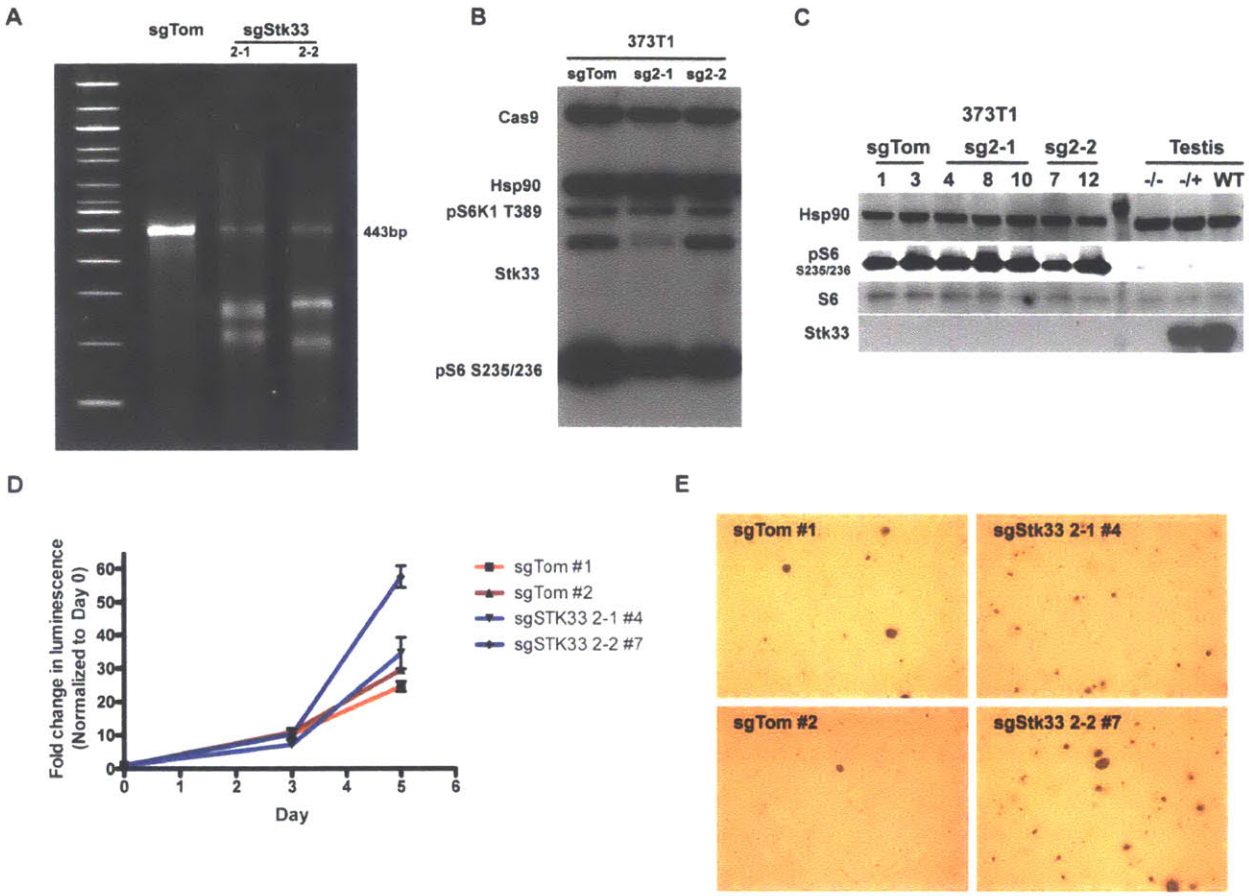

Figure 3. CRISPR/Cas-mediated *Stk33* knockout does not result in decreased proliferative or tumorigenic abilities of *Kras*-mutant lung cancer cells *in vitro*.

A. In 373T1 KP Tmet cell line, sgRNAs (2-1 and 2-2) targeting exon 2 of *Stk33* led to Cas9-mediated genome editing at the *Stk33* locus, as shown by the smaller bands as results of a surveyor assay. sgTomato (control) does not result in Cas9-mediated cutting at the *Stk33* locus, so only an intact 443bp band amplified by *Stk33* PCR primers is detected.

B. Western blot shows that Cas9 is expressed in 373T1. pS6K1 T389 and pS6 S235/236 levels are not significantly altered in cells expressing sgStk33. Stk33 proteins are undetectable. The bands just below the pS6K1 T389 bands are thought to be nonspecific bands (because they are not 53-58kDa, the expected size of mouse Stk33). Hsp90 serves as the loading control.

C. Stk33 protein levels are undetectable in 373T1 single cell clones although we do detect cDNA (data not shown). Stk33 proteins are detected in the testis (lysates were used as controls to confirm that the Stk33 antibody works well). Hsp90 serves as the loading control.

D. 373T1 *Stk33* knockout single cell clones do not proliferate differently *in vitro* compared to *Stk33* intact single cell clones (sgTomato). Average fold increase in luminescence signal (n=5) +/-SEM is plotted here.

E. Anchorage-independent growth in soft agar is not impaired by *Stk33* knockout in 373T1 cells.

373T1 *Stk33* knockout clones exhibited impaired ability to transplant lung tumors in immunocompromised mice

In order to investigate the requirement of Stk33 for *in vivo* tumorigenic ability of *Kras*-mutant lung cancer cells, we intratracheally transplanted the two 373T1 *Stk33* knockout clones and two 373T1 *Stk33* intact clones and assayed the ability of these individual clones to form tumors in the lungs of immunocompromised mice. Interestingly, histological analyses and quantitation of lung tumor burden revealed that the *Stk33* knockout clones exhibited an impaired ability to transplant lung tumors. While lungs from mice transplanted with *Stk33* intact clones had approximately 40% of their lung area taken up by tumor, there was minimal tumor burden in lungs transplanted with *Stk33* knockout clones (**Fig. 4A, 4C**). Despite the striking difference in tumor burden, there was no significant difference in histology between lung tumors formed by *Stk33* knockout and *Stk33* intact clones (**Fig. 4B**). If the effects we observed were due to Stk33 ablation, then our results would suggest that while the loss of Stk33 does not impair proliferation or tumorigenicity *in vitro*, Stk33 is required for *Kras*-mutant lung cancer cells to transplant orthotopic tumors *in vivo*. Importantly, 373T1 *Stk33* knockout and intact clones transplanted subcutaneously had comparable abilities in forming tumors in immunocompromised mice (data not shown), suggesting the differential tumorigenic effect was specific to orthotopic transplants. Unfortunately, we were unable to confirm Stk33 protein loss in *Stk33* knockout clone-transplanted lung tumors by western blot assays, as the antibody we employed exhibited cross-reactivity with non-specific targets (data not shown). To further characterize the requirement of Stk33 for orthotopic tumorigenesis by *Kras*-mutant cancer cells, we plan to test the ability of exogenous expression of *Stk33* to rescue the impaired tumorigenic ability of *Stk33* knockout clones.

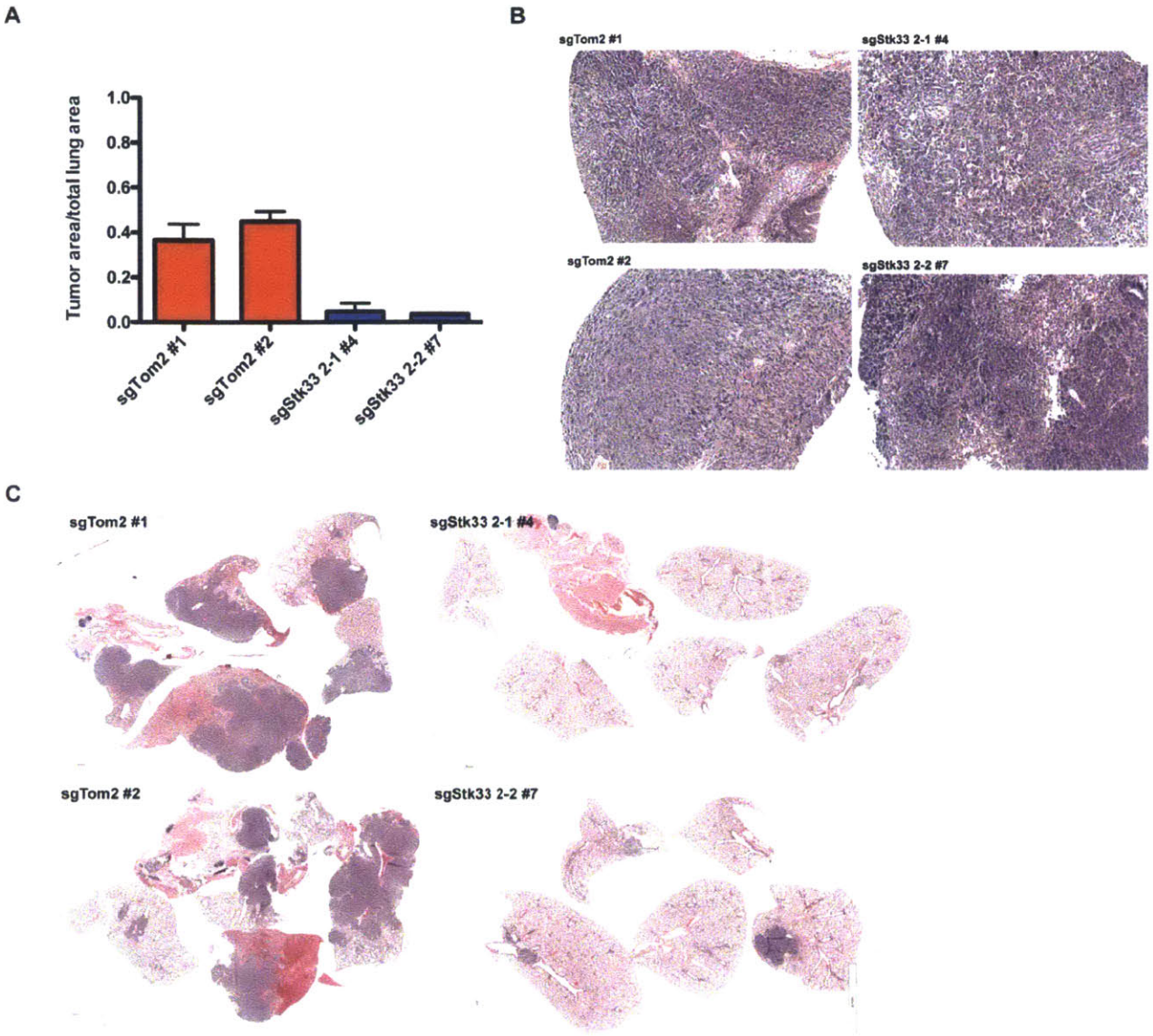

Figure 4. The ability of 373T1 *Stk33* knockout cells to form intratracheally transplanted lung tumors is diminished.

A. Tumor burden (total tumor area/total lung area measured with Aperio ImageScope software) is significantly decreased in mice that received intratracheal transplant of 373T1 *Stk33* knockout cells. Average tumor burden (n=4 for all except for sgStk33 2-2 #7, which has n=2) +/- SEM. $p<0.05$ between all pairs of sgTom and sgStk33, unpaired student's t-test.

B. There is no significant difference in histology between lung tumors formed by the different cell clones. The samples are H&E stained.

C. Examples of the histology of whole lungs are shown. The samples are H&E stained.

DISCUSSION

Utilizing Cre/LoxP- and CRISPR/Cas-based approaches in various *in vitro* and *in vivo* cancer models, we investigated the requirement of Stk33 for $Kras^{G12D}$-driven murine cancers. First, we made the surprising finding that a previously designed $Stk33^{fl}$ allele meant to result in Stk33 protein loss actually led to exons 7 and 8 skipping of $Stk33^{fl}$ upon recombination, creating a kinase-dead Stk33 protein. Based on the lack of impact of Stk33 status on the survival of *Pdx1-Cre;* $Kras^{G12D/+}$*;* $p53^{fl/fl}$ mice, our results suggested that the kinase activity of Stk33 is not required for $Kras^{G12D}$-driven murine PDAC initiation and progression. Second, our attempt to induce *Stk33* biallelic loss-of-function mutations in the lung via the pSECC lentiviral system was extremely inefficient, but this could be due to either *Stk33* loss-of-function mutations were selected against during $Kras^{G12D}$-driven lung tumor initiation and progression or simply technical limitations. Finally, we generated 373T1 *Stk33* knockout single cell clones, whose *Stk33* knockout status was confirmed by DNA sequencing but not by protein analysis due to the lack of a clean and reliable Stk33 antibody. If these clones were truly *Stk33* knockout, then our results demonstrated that while Stk33 loss did not affect proliferation *in vitro*, Stk33 might be required for the formation of orthotopic lung tumors *in vivo*. Importantly, Stk33 loss did not impair the ability of 373T1 cells to transplant subcutaneous tumors *in vivo*, suggesting a context-dependent Stk33 requirement.

Although the $Stk33^{fl}$ allele we characterized was not an ideal allele for analyzing the consequences of Stk33 protein deletion, it can be utilized to investigate the importance of the kinase activity of Stk33. Initially, it was thought that Stk33 kinase activity was required *Kras*-mutant cancer cell survival[9]. However, follow-up studies of the initial shRNA-based screen results suggested otherwise. Kinase inhibitors of Stk33 failed to impair cancer cell survival[10,12],

but instead it was suggested that non-kinase functions of Stk33 appeared to be important[13]. Our preliminary results were consistent with the previous findings that Stk33 kinase activity may not be required for oncogenic *Kras*-mediated tumor initiation and progression. Whether Stk33 protein itself is critical for cancer cell survival remains to be elucidated.

Appropriate controls are required for us to understand the underlying reason for inefficient CRISPR/Cas-mediated editing of *Stk33 in vivo*. A few possible technical limitations exist: the viral titer was too low; the mice were euthanized too early (16 weeks post-infection) so that the tumor burden in the control group was too low for a possible decrease in tumor burden to be detectable; and Cas9 cannot induce double strand breaks at the *Stk33* locus as efficiently as it does at other genetic loci. Before we can exclude these technical limitation possibilities, we cannot conclude that *Stk33* loss-of-function mutations are selected against during $Kras^{G12D}$-mediated lung tumorigenesis based on our data.

To further investigate whether the strikingly impaired tumorigenic ability of 373T1 *Stk33* knockout clones to form orthotopic lung tumors were due to Stk33 ablation, we will have perform more thorough analyses to confirm that the effects were on-target. We plan to express exogenous cDNA of wild-type or kinase-dead *Stk33* that are sgStk33-resistant (by introducing silent mutations in the sgStk33-targeting sites) in these 373T1 *Stk33* knockout clones to determine if exogenous *Stk33* expression would rescue their tumorigenic ability in the lung. Furthermore, we would generate more knockout clones from other *KP* lung cancer cell lines to determine whether the effect was cell line-specific. Before we pursue these analyses, we cannot definitively conclude that there is synthetic lethal interaction between *Stk33* and oncogenic *Kras*. An important observation we made was that subcutaneous and orthotopic transplant experiments showed completely different results. The tumorigenic ability of subcutaneously transplanted

cells was consistent with the proliferative ability of these cells *in vitro*. This observation demonstrated the importance of leveraging different experimental methods and model systems to parse out context-dependent effects.

In summary, we have characterized the utility of different *in vitro* and *in vivo* genetic tools and models for analyzing possible synthetic lethal interactions between *Stk33* and oncogenic *Kras*. Although we were unable to definitively determine whether Stk33 is an ideal therapeutic target for *Kras*-mutant cancers, we made interesting observations that can provide the basis for further investigations.

SUPPLEMENTARY FIGURES AND TABLES

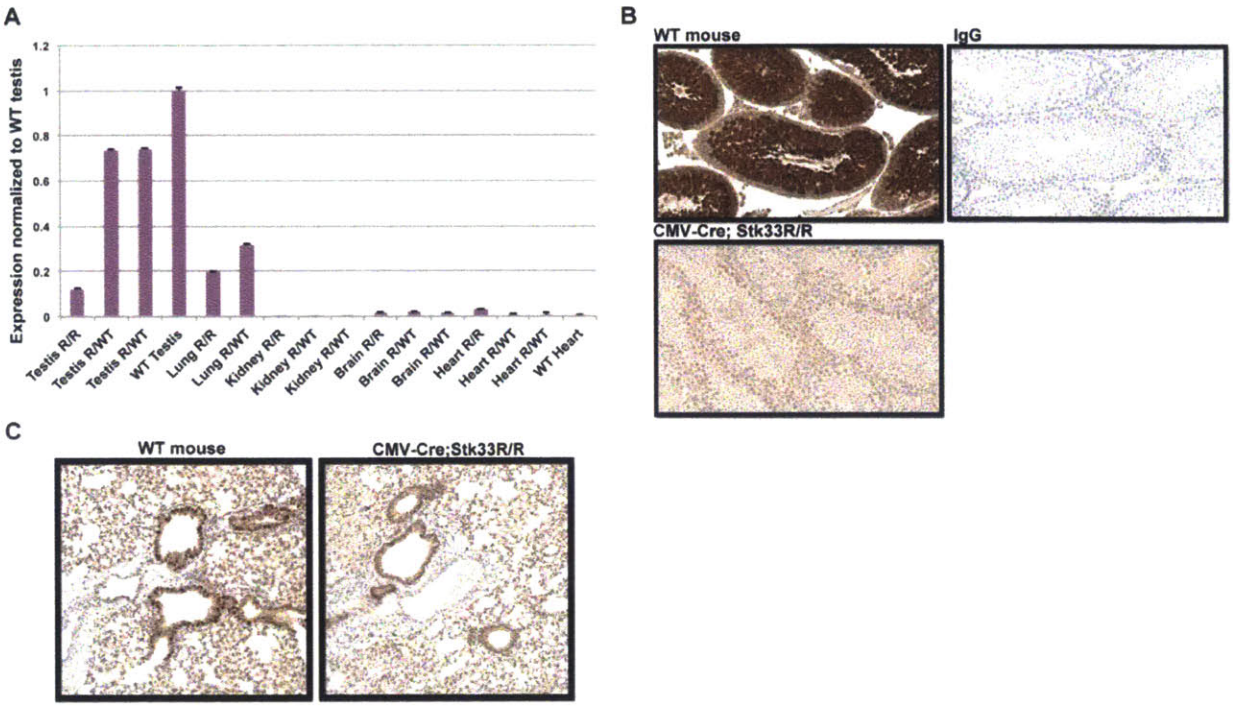

Supplementary Figure 1. Expression of Stk33 in various mouse tissues.

A. *Stk33* mRNA levels in different tissues. Average expression +/- SD (n=3), normalized to expression in WT testis (which is expected to have the highest *Stk33* mRNA levels), is graphed. R: recombined, WT: wild-type.

B. Immunohistochemical staining of Stk33 in the testis of wild-type mouse and *CMV-Cre; Stk33*$^{R/R}$ mouse. IgG staining of wild-type mouse testis is included as negative control.

C. Immunohistochemical staining of Stk33 in the lungs of wild-type mouse and *CMV-Cre; Stk33*$^{R/R}$ mouse. Tissue samples are harvested from the same animals as the ones in (B). Background staining of the bronchial epithelium is observed in animals of different genotypes.

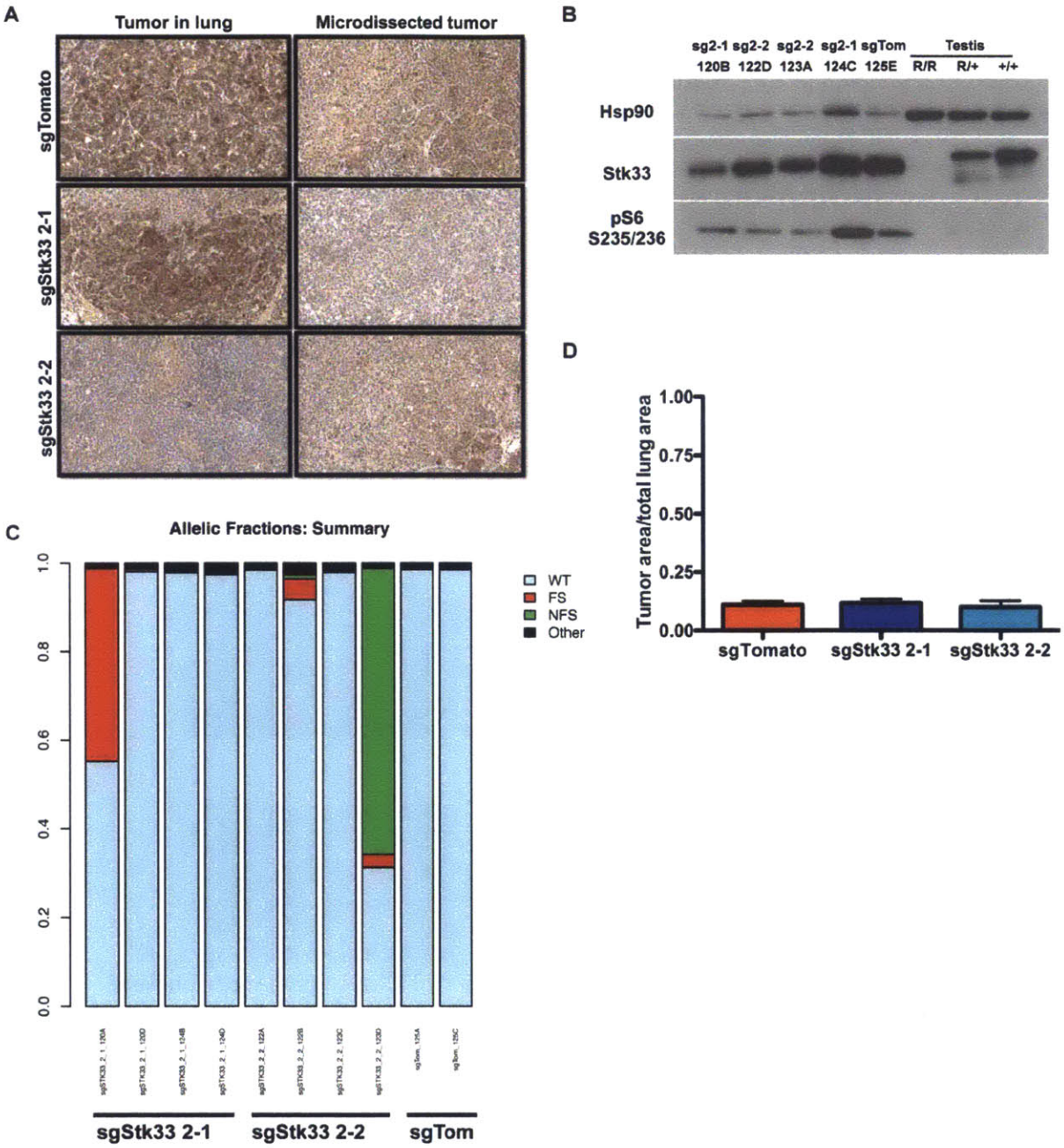

Supplementary Figure 2. CRIPSR/Cas-mediated editing of Stk33 in *Kras*$^{LSL\text{-}G12D/+}$; *p53*$^{fl/fl}$ mice *in vivo* is inefficient in generating loss-of-function Stk33 mutations.

A. Immunohistochemical staining of Stk33 in lung tumors or microdissected lung tumors does not show differences in Stk33 protein expression in mice infected with lentivirus pSECC-sgStk33 or pSECC-sgTomato (control).

B. Western blot on microdissected tumors demonstrates that high levels of Stk33 proteins are expressed in pSECC-sgStk33-induced tumors.

C. DNA sequencing (MiSeq) analysis of microdissected tumors showed that most of the tumors retain wild-type *Stk33* in 80% of the reads per tumor (allelic fraction). WT: wild-type, FS: frameshift mutations, NFS: non-frameshift mutations, others: mutations found in less than 1% of total reads.

D. Average lung tumor burden +/- SEM (n=6-15) of KP pSECC mice. Differences between each sgStk33 group compared to sgTomato group are insignificant based on unpaired student's t-test.

A

sgRNA	# clones that grew	# sent for sequencing	# showed cutting at *Stk33* locus	# with 2 FS alleles
sgTomato	30/192	5	0	0
sgStk33 2-1	24/192	12	3	1
sgStk33 2-2	26/192	12	2	1

B

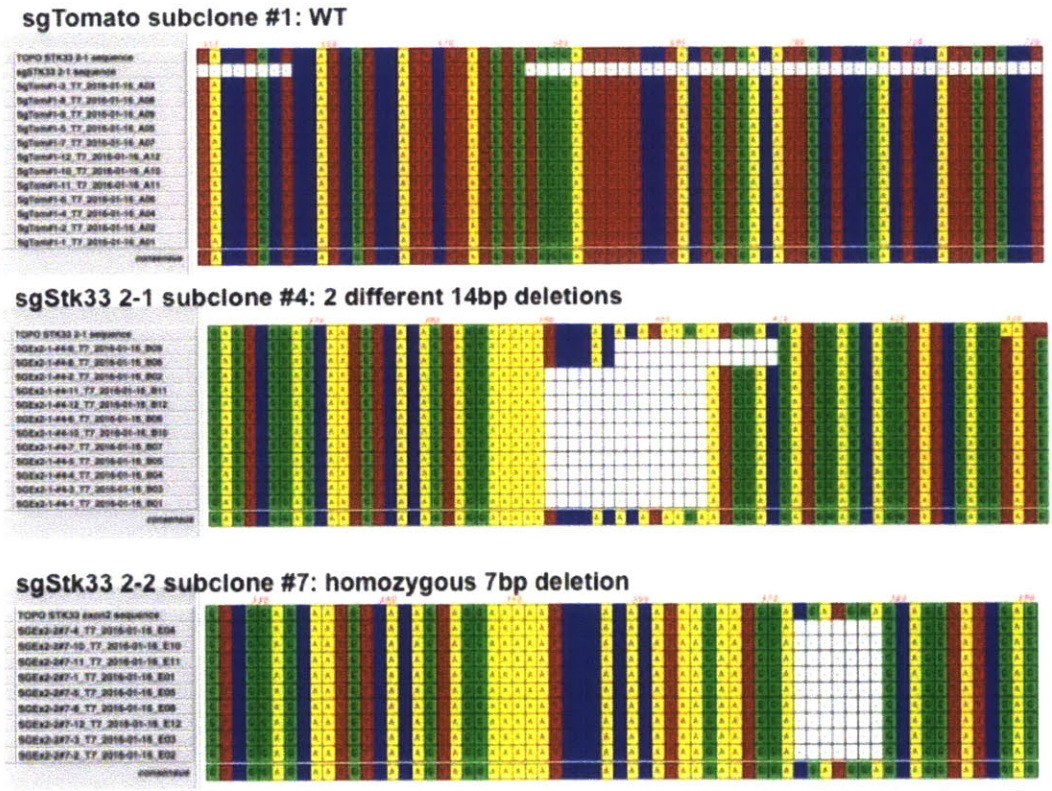

Supplementary Figure 3. 373T1 sgStk33 subclones contain two alleles that have frameshift mutations in Stk33.

A. Efficiency of isolation of CRISPR/Cas-mediated *Stk33* knockout single cell subclones in 373T1 Tmet lung cancer cell line. FS = framshift mutation.

B. Shown are the alignments of TOPO-cloned sequences (based on Sanger sequencing) of 373T1 subclones. The top panel is a 373T1 sgTomato subclone that has wild-type Stk33. The middle and bottom panels are 373T1 sgStk33 subclones that display frameshift mutations near the sgStk33-targeting sites. The top sequence of each panel is the reference wild-type Stk33 sequence, and a blank square indicate a mismatch between the TOPO-cloned sequence and the reference sequence.

Supplementary Table 1: sgRNA sequences

sgRNA name	20bp Guide Sequence	PAM	Orientation	Exon	Source
sgStk33 2-1	CACATAAGAATGGACGATGG	TGG	Sense	2	C
sgStk33 2-2	CCACACATAAGAATGGACGA	TGG	Antisense	2	C
sgTomato	GGCCACGAGTTCGAGATCGA	GGG	Sense	N/A	D

Source key:

D = self-designed based on available PAM sequences

C = sequences outputted from Feng Zhang lab CRISPR design tool (crispr.mit.edu)

Supplementary Table 2: PCR primers for amplification of *Stk33*

Primer	Sequence	Orientation	Exon
Stk33 2-5 F	GCCAGTGACTTGTACTGTACTC	Forward	2
Stk33 2-5 R	GTTGCAGTAATCTGGGAGGAG	Reverse	2
Stk33 exon 7 flanking	GGTGAGCATCCTGAAGACTGT	Forward	6
Stk33 exon 7 flanking	TCCAGCTTTAGATCTCTGTGCA	Reverse	8
Stk33 exon 5	CAGGGGAGCTTTGGAATGGT	Forward	5
Stk33 exon 10	TGTCACACTGCTGGCTGTAG	Reverse	10
Stk33 exon 3	CAGGCAAGTCTCCAGTCCTG	Forward	3
Stk33 exon 4	GTGACATTGCTCCGACTCCA	Reverse	4

Notes:

Stk33 2-5 F and R were also used for sequencing.
Annealing temperature of 60°C was used.

Supplementary Table 3: Genotyping primers

Primer	Sequence	Orientation	Expected band size
Stk33 Geno F	TGCACACACGTTCAGTCTCA	Forward	Flox 436bp
Stk33 Geno R	CTCACAAAGCTCCATCACGA	Reverse	WT 339bp
Stk33 Geno R Recomb	GTTGTGGCCGCTCTAGAACT	Reverse	Recomb 162bp
Kras LSL F	GTCTTTCCCCAGCACAGTGC	Forward	WT 622bp
Kras LSL R	CTCTTGCCTACGCCACCAGCTC	Reverse	LSL 500bp
Kras LSL SD5	AGCTAGCCACCATGGCTTGAGTAAGT	Forward	Recomb 650bp
p53 Flox C	AAGGGGTATGAGGGACAAGG	Forward	WT 431 bp
p53 Flox D	GAAGACAGAAAAGGGGAGGG	Reverse	LoxP 584 bp
Tom 1	AAG GGA GCT GCA GTG GAG TA	Forward	
Tom 2	CCG AAA ATC TGT GGG AAG TC	Reverse	Mut 196 bp
Tom 3	GGC ATT AAA GCA GCG TAT CC	Forward	WT 297 bp
Tom 4	CTG TTC CTG TAC GGC ATG G	Reverse	
Cre 1	CACCCTGTTACGTATAGCCG	Forward	
Cre 2	GAGTCATCCTTAGCGCCGTA	Reverse	WT 500bp
Cre 3	CCTTGAGGCTGTCCAAGTGATTCAGGCCATCG	Forward	Cre 300bp
Cre 4	CCAATCTGCTCACACAGGATAGAGAGGGCAGG	Reverse	

Notes:

Annealing temperature of 60°C was used for all except for the Cre 1-4 primers (58°C).
WT=wild-type, Recomb=recombined, Mut=mutant, LSL=lox-stop-lox cassette.

MATERIALS AND METHODS

Cell lines and culture conditions

373T1 cells were derived from a metastatic primary lung adenocarcinoma tumor (Tmet) in a *Kras*$^{LSL\text{-}G12D/+}$; *p53*$^{flox/flox}$ mouse infected intratracheally with Cre-expressing lentiviral vectors to induce oncogenic *Kras*^{G12D} activation and biallelic *p53* inactivation in the lung[22]. Cells were maintained in DMEM (Corning Cellgro) supplemented with 10% fetal bovine serum (Hyclone) and penicillin/streptomycin.

Lentiviral constructs and cloning of sgRNAs

Lentiviral constructs for CRISPR/Cas-mediated genome editing from the dual-vector lentiviral GeCKOv2 system, *lentiCas9-Blast* and *lentiGuide-Puro*[23], were provided by Dr. Feng Zhang. sgRNAs targeting mouse *Stk33* exon 2 were designed (**Supplementary Table 1**) and ligated into the BsmBI site with compatible annealed oligos.

Lentiviral transduction

Lentiviral backbone, packaging vector (delta8.2 or psPAX2), and envelope (VSV-G) were transfected into 293T cells with TransIT-LT1 (Mirus Bio). Supernatant was collected at 48 and 72 hours and applied to target cells with 8 μg/mL polybrene for transduction. Transduced cells were treated with 2-4 μg/mL puromycin (Life Technologies) or 10 μg/mL blasticidin S (Life Technologies) for 3-7 days, as appropriate, for antibiotic selection. To generate single cell clones from the transduced cells, we sorted one cell per well into 96-well plates using a MoFlo (Beckman Coulter) FACS sorter.

In vitro Growth Assays

For growth curves, 200 cells were plated on day 0 and grown for five days in culture. 5 replicates for each cell line per day were assessed for cell viability by CellTiter-Glo luminescence assay (Promega), which measures cellular ATP levels as a surrogate for cell number and growth. Cell viability results were normalized to luminescence at day 0. For soft agar-based anchorage-independent growth assays, low melting point agarose (Seaplaque) was used and 100,000 cells were plated per well in 6-well tissue culture plates.

Immunoblotting

Cells were lysed with ice-cold RIPA buffer (Pierce), supplemented with 0.5 μM EDTA and Halt protease and phosphatase inhibitors (Thermo Scientific), rotated at 4°C for 15-30 minutes to mix, and centrifuged at maximum speed for 15 minutes to collect whole cell lysates. Protein concentration was measured with the BCA protein assay (Pierce). 30 μg of total protein per sample was loaded into 4-12% Bis-Tris gradient gels (Life Technologies) and separated by SDS-PAGE. Proteins were transferred to nitrocellulose (for fluorescence detection) or PVDF (for chemiluminescent detection) membranes. The following antibodies were used for immunoblotting: mouse anti-HSP90 (BD #610418, 1:10,000), rabbit anti-Stk33 (Proteintech 12857-1-AP, 1:500), rabbit anti-p70 S6 Kinase pT389 (CST9205, 1:1000), rabbit anti-phospho-S6 S235/236 (CST4858, 1:1000), and mouse anti-S6 (CST2317, 1:1000). HSP90 was used as loading control. Primary antibodies were detected with fluorescent DyLight-conjugated (CST) or HRP-conjugated (BioRad) secondary antibodies for fluorescent (LI-COR) or chemiluminescent detection (Amersham), respectively.

Immunohistochemistry

Primary antibodies used were rabbit anti-Stk33 (Proteintech 12857-1-AP, 1:50) and rabbit IgG isotype control (CST3900, 1:200). ImPress (Vector Labs) anti-rabbit secondary antibodies were used.

Quantitative RT-PCR

RNA was isolated from PDAC cells using TRIzol (Life Technologies). RNA was reverse transcribed using High-Capacity cDNA Reverse Transcription Kit (Applied Biosystems). Quantitative PCR (qPCR) was performed using Taqman® Gene Expression assays (Applied Biosystems) mouse Stk33 Taqman probe Mm01277482_m1 and human STK33 probe Hs00294893_m1. C_t values were measured by a LightCycler 480 Real-Time PCR System (Roche) and relative expression (normalized to TBP) was calculated using the $\Delta\Delta C_t$ method.

RT-PCR

RNA was isolated from PDAC cells using TRIzol (Life Technologies). RNA was reverse transcribed using High-Capacity cDNA Reverse Transcription Kit (Applied Biosystems). Primers used to amplify ORFs between Exon 5 and 10, flanking Exon 7, and Exon 3 and 4 are listed in **Supplementary Table 2**.

Intratracheal tumor transplant in immunocompromised mice

All animal studies were approved by the MIT Institutional Animal Care and Use Committee. Cells were transplanted to form tumors in NOD/SCID mice (Taconic). $2x10^5$ cells suspended in 30 μL of cold SMEM with 2mM EDTA were intratracheally transplanted per

mouse to determine tumor-forming capacity in the lung. Tumor formation was monitored over time by body condition of the mice. Mice were euthanized approximately one month after transplant.

In vivo CRISPR/Cas-mediated genome editing of *Stk33* in the lung

The *in vivo* pSECC-based experiments were performed according to the original paper describing the pSECC system[21]. The sgRNAs listed in **Supplementary Table 1** were cloned into the pSECC vector and lentivirus was produced and titered to intratracheally infect 35 $Kras^{LSL\text{-}G12D/+}$; $p53^{fl/fl}$ male and female mice (between 3 to 5 months old).

TOPO Cloning

TOPO cloning was performed with Zero Blunt TOPO PCR Cloning Kit for Sequencing (Thermo Fisher #45-0031).

Tail DNA prep and mouse genotyping

DNA was prepared using the HotSHOT method. Genotyping PCR reactions were performed using 1 μl of tail DNA, 14 μl of GoTaq® Green Master Mix (Promega M7123) containing a final concentration of 0.1 μM of appropriate primers as listed in **Supplementary Table 3**.

Adenoviral infection of MEFs

Adenovirus was from the Viral Vector Core Facility of The University of Iowa and the dose was 10^7 pfu per 10^6 cells. $Stk33^{fl/fl}$; $Kras^{LSL\text{-}G12D/+}$ and $Stk33^{fl/+}$; $Kras^{LSL\text{-}G12D/+}$ MEFs were

thawed and resuspended in 6 ml of DMEM with 10% fetal bovine serum (Hyclone) and penicillin/streptomycin (standard media). The 6 ml suspension was then divided into 2 aliquots of 3 ml in separate tubes. 1 µl of Ad5CMV-Cre (Cat#: VVC-U of Iowa-5) was added to one tube and 1 µl of Ad5CMV-empty (Cat#: VVC-U of Iowa-272) was added to the second control tube and the mixture was gently and briefly agitated. After 5-10 minutes, each sample was plated onto a 10 cm plate with 9 ml of additional fresh media. After 24 hours, the media was removed from the cells and replaced with fresh media and an additional 1 µl of adenovirus was added to each plate. Cells were ready to split 72 hours post infection and were examined at days 3 and 6 post-infection for recombination of *Kras* and *Stk33* and morphology changes. The experiment was performed according to a previously described protocol[20].

ACKNOWLEDGEMENTS

We thank T. Dayton for obtaining the mice harboring the *Stk33*^{flox} allele from R. DePinho's laboratory, our collaborator C. Scholl for generous discussions of experimental data, and the BioMicro Center at MIT for help with MiSeq analysis. We greatly appreciate the tremendous help we received from K. Cormier, C. Condon, R. Bronson, and M. Brown at the Histology Core Facility, and M. Jennings at the Flow Cytometry Core Facility at the Swanson Biotechnology Center of the Koch Institute. Additionally, we thank members in the Jacks lab, especially T. Papagiannakopoulos, R. Romero, M. Bauer and F. Sanchez-Rivera, for many helpful discussions and for their generosity in sharing experimental reagents and protocols.

This work was supported by the PO1 collaboration with R. DePinho. T.J. is a Howard Hughes Medical Institute Investigator, the David H. Koch Professor of Biology, and a Daniel K. Ludwig Scholar.

REFERENCES

1. Kaelin, W.G., Jr. The concept of synthetic lethality in the context of anticancer therapy. *Nat Rev Cancer* **5**, 689-698 (2005).
2. Cox, A.D., Fesik, S.W., Kimmelman, A.C., Luo, J. & Der, C.J. Drugging the undruggable RAS: Mission possible? *Nat Rev Drug Discov* **13**, 828-851 (2014).
3. Luo, J., *et al.* A genome-wide RNAi screen identifies multiple synthetic lethal interactions with the Ras oncogene. *Cell* **137**, 835-848 (2009).
4. Sarthy, A.V., *et al.* Survivin depletion preferentially reduces the survival of activated K-Ras-transformed cells. *Mol Cancer Ther* **6**, 269-276 (2007).
5. Vicent, S., *et al.* Wilms tumor 1 (WT1) regulates KRAS-driven oncogenesis and senescence in mouse and human models. *J Clin Invest* **120**, 3940-3952 (2010).
6. Corcoran, R.B., *et al.* Synthetic lethal interaction of combined BCL-XL and MEK inhibition promotes tumor regressions in KRAS mutant cancer models. *Cancer Cell* **23**, 121-128 (2013).
7. Barbie, D.A., *et al.* Systematic RNA interference reveals that oncogenic KRAS-driven cancers require TBK1. *Nature* **462**, 108-112 (2009).
8. Singh, A., *et al.* TAK1 inhibition promotes apoptosis in KRAS-dependent colon cancers. *Cell* **148**, 639-650 (2012).
9. Scholl, C., *et al.* Synthetic lethal interaction between oncogenic KRAS dependency and STK33 suppression in human cancer cells. *Cell* **137**, 821-834 (2009).
10. Babij, C., *et al.* STK33 kinase activity is nonessential in KRAS-dependent cancer cells. *Cancer Research* **71**, 5818-5826 (2011).
11. Weiwer, M., *et al.* A Potent and Selective Quinoxalinone-Based STK33 Inhibitor Does Not Show Synthetic Lethality in KRAS-Dependent Cells. *ACS Med Chem Lett* **3**, 1034-1038 (2012).
12. Luo, T., *et al.* STK33 kinase inhibitor BRD-8899 has no effect on KRAS-dependent cancer cell viability. *Proc Natl Acad Sci U S A* **109**, 2860-2865 (2012).
13. Azoitei, N., *et al.* Targeting of KRAS mutant tumors by HSP90 inhibitors involves degradation of STK33. *J Exp Med* **209**, 697-711 (2012).
14. Frohling, S. & Scholl, C. STK33 kinase is not essential in KRAS-dependent cells--letter. *Cancer Research* **71**, 7716; author reply 7717 (2011).
15. Mujica, A.O., Hankeln, T. & Schmidt, E.R. A novel serine/threonine kinase gene, STK33, on human chromosome 11p15.3. *Gene* **280**, 175-181 (2001).
16. Mujica, A.O., Brauksiepe, B., Saaler-Reinhardt, S., Reuss, S. & Schmidt, E.R. Differential expression pattern of the novel serine/threonine kinase, STK33, in mice and men. *Febs J* **272**, 4884-4898 (2005).
17. Hingorani, S.R., *et al.* Preinvasive and invasive ductal pancreatic cancer and its early detection in the mouse. *Cancer Cell* **4**, 437-450 (2003).
18. Hingorani, S.R., *et al.* Trp53R172H and KrasG12D cooperate to promote chromosomal instability and widely metastatic pancreatic ductal adenocarcinoma in mice. *Cancer Cell* **7**, 469-483 (2005).
19. Gidekel Friedlander, S.Y., *et al.* Context-dependent transformation of adult pancreatic cells by oncogenic K-Ras. *Cancer Cell* **16**, 379-389 (2009).
20. Tuveson, D.A., *et al.* Endogenous oncogenic K-ras(G12D) stimulates proliferation and widespread neoplastic and developmental defects. *Cancer Cell* **5**, 375-387 (2004).

21. Sanchez-Rivera, F.J., *et al.* Rapid modelling of cooperating genetic events in cancer through somatic genome editing. *Nature* **516**, 428-431 (2014).
22. Winslow, M.M., *et al.* Suppression of lung adenocarcinoma progression by Nkx2-1. *Nature* **473**, 101-104 (2011).
23. Sanjana, N.E., Shalem, O. & Zhang, F. Improved vectors and genome-wide libraries for CRISPR screening. *Nature Methods* **11**, 783-784 (2014).